

Combining top-down and bottom-up analyses of terrestrial dissolved organic carbon export to improve the process representation of a coupled hydrological-biogeochemical model

Dissertation zur Erlangung des akademischen Grades eines Doktors der
Naturwissenschaften (Dr. rer. nat.) an der Fakultät für Biologie, Chemie und
Geowissenschaften der Universität Bayreuth

vorgelegt von

Benedikt Joachim Werner

Geb. am 06. Mai 1988 in Dachau

Bayreuth, 2023

Die vorliegende Dissertation wurde im Zeitraum von September/2016 bis Dezember/2022 in Leipzig am Helmholtz-Zentrum für Umweltforschung unter Betreuung von Herrn Prof. Dr. Jan H. Fleckenstein angefertigt.

Vollständiger Abdruck der von der Fakultät für Biologie, Chemie und Geowissenschaften der Universität Bayreuth genehmigten Dissertation zur Erlangung des akademischen Grades eines Doktors der Naturwissenschaften (Dr. rer. nat.).

Art der Dissertation: Kumulative Dissertation

Dissertation eingereicht am: 06.02.2023

Zulassung durch die Promotionskommission: 01.03.2023

Wissenschaftliches Kolloquium: 30.10.2023

Amtierender Dekan: Prof. Dr. Cyrus Samimi

Prüfungsausschuss:

Prof. Dr. Jan Fleckenstein (Gutachter)

Prof. Dr. Stefan Peiffer (Gutachter)

Prof. Dr. Oliver Sass (Vorsitz)

Prof. Dr. Eva Lehndorff

Acknowledgements

I would like to thank Jan H. Fleckenstein, Oliver J. Lechtenfeld and Gerrit H. de Rooij for the supervision, helpful advice and the always open door for fruitful discussions from various scientific perspectives. Special thanks to Andreas Musolff, who tremendously helped me to stay on track, and for the vast majority of the numerous iterations of the published papers. I always enjoyed your critical, trenchant logic, yet funny comments (as well as the St. Martin's Goose). I consider myself blessed to have had the unique opportunity to do research within so many interdisciplinary expertises.

Many thanks to technicians Toralf Keller – for his excellent, persistent and enthusiastic field work – as well as Jan M. Kaesler and Heidrun Paschke for their reliable work in the laboratory.

I would like to thank the entire department of hydrogeology with providing advice and encouraging discussions. In particular this goes to room 355, who on top of that helped me out with an open ear and sometimes the necessary distraction. This support set up the productive environment to finalize this thesis.

I would like to thank all researchers I cooperated with. In particular I thank for the collaboration with Jie Yang for the provision of his HydroGeoSphere skills and Linus Schauer for the provision of his python skills.

Danke Tina, für Deinen vorbehaltlosen Glauben an mich und meine Arbeit. Danke für Dein immer offenes Ohr und Deine uneingeschränkte Unterstützung, auch und gerade auf den letzten Metern der These.

Auch meiner Familie und meinen Eltern Ingrid und Joachim möchte ich hier für ihre grenzenlose Unterstützung und motivierenden Worte, sowie ihr immer offenes Ohr danken.

Table of Contents

Abstract	1
Zusammenfassung	3
Chapter I – Introduction	6
Chapter II – Research Approach	11
2.1 Research Hypotheses and Objectives.....	11
2.2 Workflow.....	12
Chapter III – Materials and Methods	13
3.1 The Rappbode Catchment.....	13
3.2 Understanding integrated response dynamics of DOC concentration and quality (Study 1)	14
3.3 Delineating functional zones of DOC export (Study 2)	16
3.4 Combining understanding of integrated processes and functional zones to derive a complexity reduced, mechanistic model of DOC export (Study 3)	18
Chapter IV – Results and Discussion	22
4.1 Dynamics of dissolved organic carbon quantity and quality in a headwater catchment (Study 1)	22
4.1.1 Warm and dry conditions.....	23
4.1.2 Intermediate conditions	24
4.1.3 Cold and wet conditions	25
4.2 Small-scale topography explains patterns and dynamics of dissolved organic carbon exports from the riparian zone of a temperate, forested catchment (Study 2)	26
4.2.1 Small-scale topographical heterogeneity delineates DOC source zones in terms of molecular composition and hydrological properties.....	26
4.2.2 Quantifying riparian DOC export to the stream.....	28
4.3 Modelling dissolved organic carbon export from a catchment using a complexity- reduced, mechanistic approach (Study 3).....	29

4.3.1 Finding the right model structure	30
4.3.2 Model performance.....	31
4.3.3 On the value of DOC concentration to constrain the model.....	32
Chapter V – Summary, Conclusions and Outlook.....	34
5.1 Summary	34
5.1.1 Investigation of the hydrological and biogeochemical processes and controls of DOC mobilization and export from riparian soils to the streams.....	34
5.1.2 Adapting a catchment-scale, semi distributed mechanistic model to the recent understanding of DOC export.....	35
5.2 Conclusions and Outlook	36
References.....	38
Study 1: High-frequency measurements explain quantity and quality of dissolved organic carbon mobilization in a headwater catchment.....	45
Study 2: Small-scale topography explains patterns and dynamics of dissolved organic carbon exports from the riparian zone of a temperate, forested catchment.....	74
Study 3: Modelling dissolved organic carbon export from a temperate headwater catchment using a complexity-reduced, mechanistic approach.....	113
List of peer-reviewed publications	149

Abstract

Dissolved organic carbon (DOC) exhibited critical upward concentration trends in headwater streams in the last decades with potentially harmful environmental consequences. So far, the ubiquitous sources of organic material in catchments from which DOC can be derived, together with the complex hydrological flow paths that may deliver it to the streams have impeded to fully understand and quantify DOC fluxes from catchments. Therefore, a broader application of DOC export models to catchments not only is a scientific challenge, but also is important to ultimately manage water quality and related ecological issues. Consequently, a parsimonious DOC export model that adequately captures dominant mechanisms of solute export while being easy to transfer between catchments is required.

This PhD project aims to investigate the hydrological and biogeochemical controls for the mobilization and transport of terrestrial DOC to the Rappbode stream (Harz Mountains, Germany; representative of a typical temperate headwater catchment), to then identify functional zones of terrestrial DOC export and their prevailing export mechanisms, and, ultimately conflate the developed understanding to adapt and refine the export mechanisms of a catchment-scale, semi-distributed model. Hereby, a key hypothesis is that there exists a direct relationship between groundwater dynamics in the riparian zone (RZ) – which is considered the main source zone for DOC in temperate catchments – and DOC export that allows to reproduce and predict DOC flux variability at the catchment outlet.

First, Study 1 analyzes the in-stream DOC concentration and quality dynamics at high frequency ($f = \frac{1}{15} \text{ min}^{-1}$) for their top-down controls (integral catchment-scale processes) at the catchment outlet. Seasonal scale, antecedent hydrometeorological parameters and their interaction turned out to be dominant predictors of in-stream DOC dynamics. Those antecedent parameters suite to describe boundary conditions of riparian DOC export (like the on- and offset of hydrological connectivity to the stream). Implementing respective top-down controls into DOC export models can therefore serve as an anchor point, improving general mechanistic validity and thus transferability to catchments of similar riparian functioning.

The mobilization and transport of riparian DOC to the stream from the bottom-up perspective (plot-scale riparian mechanisms) has been evaluated in Study 2. Results from a chemical and topographical analysis of riparian and stream water samples, combined with fully distributed hydrological modeling indicate that DOC export via surface runoff from the Rappbode RZ accounts

for roughly half (47%) of the catchment's total DOC export. Within the RZ, locations of high topographic wetness (depicted by the high-resolution topographic wetness index; TWI_{HR}) are more prominent in generating surface runoff than locations of low TWI_{HR} . A comparison of DOC from the RZ and in-stream samples indicates that near-surface riparian DOC from high TWI_{HR} zones is transported to the stream mainly during events. Proxies that represent soil moisture variability within the RZ – such as TWI_{HR} – therefore are suitable to link distinct terrestrial DOC sources in the RZ with the temporal variability of the stream water DOC concentrations. The study further confirms that soil moisture content in the RZ directly impacts the magnitude of surface runoff generation, if a threshold value is surpassed (representative of groundwater level reaching to the riparian surface).

In Study 3, a semi-distributed coupled hydrology-biogeochemistry model for DOC export was mechanistically adapted to the above depicted understanding. A main focus was to implement an explicit surface flux mechanism that is threshold-controlled by the prevailing antecedent wetness condition in the catchment. Results from Studies 1 and 2 further indicate that in-stream DOC dynamics have an inherent information content with regard to the location, timing and mechanism of terrestrial DOC mobilization and export. This allows to simultaneously calibrate the hydrological (Kling-Gupta efficiency $KGE = 0.79$) and biogeochemical modules ($KGE = 0.73$) of the adapted model. The comparison with measured riparian groundwater levels and associated DOC samples attests the model to be valid in terms of internal and external flux realization, suggesting that riparian groundwater dynamics can be used to reproduce and predict in-stream DOC flux variability at the catchment outlet. In contrast to the simultaneous calibration, an approach that calibrates DOC consecutively to water fluxes largely overestimated riparian DOC concentrations. The information gain of utilizing DOC as a tracer in a coupled model is therefore a promising alternative to the more expensive application of external tracers for model calibration, which in turn should drastically increase the model's transferability to other catchments.

This thesis highlights the strong interactions of hydrological and biogeochemical functioning in the RZ and catchments in general, which enabled a new approach to reflect DOC export mechanisms in a semi-distributed model. Information gain from a multidimensional dataset allowed to implement proxies that integrate location, timing and mechanisms of mobilization and export behavior. The presented model thus supports a more holistic, yet parsimonious representation of DOC export processes, potentially allowing water quality managers to quantify DOC fluxes and predict hydrometeorological impacts in multiple catchments.

Zusammenfassung

In den letzten Jahrzehnten zeigte die gelöste organische Kohlenstoff (DOC) Konzentration einen kritischen Aufwärtstrend in Flussoberläufen, was mit potenziell schädlichen Konsequenzen für die Umwelt einhergeht. Ein ganzheitlicheres Verständnis von DOC Flüssen in entsprechenden Einzugsgebieten ist deswegen nicht nur aus wissenschaftlicher Sicht interessant, sondern dient auch dem Management von Wasserqualitätsfragen und den damit einhergehenden ökologischen Beeinträchtigungen. Die Omnipräsenz von DOC im Einzugsgebiet sowie die hohe Komplexität von hydrologischen Fließpfaden (die letztendlich terrestrisches DOC in den Fluss transportieren) verhinderten jedoch bisher, dass die dafür benötigten DOC Export Modelle in ausreichendem Maße an die relevanten DOC Exportmechanismen angepasst werden konnten um verlässliche Aussagen für mehrere Einzugsgebiete zu generieren. Deshalb wird ein generischeres Modell benötigt, das die hohe Komplexität der Mechanismen adäquat repräsentiert, gleichzeitig aber auch ohne großen Mehraufwand auf mehrere Einzugsgebiete übertragbar ist.

Die vorliegende Dissertation befasst sich mit den hydrometeorologischen Steuerungsgrößen von terrestrischem DOC Export in die Harzer Rappbode (beispielhaft für ein Quelleinzugsgebiet der gemäßigten Zone) und identifiziert funktionale Zonen sowie deren zugrunde liegenden Mechanismen des terrestrischen DOC Exports. Anschließend wird das so generierte Prozessverständnis genutzt, um die DOC Exportmechanismen in einem semi-verteilten Modell zu verfeinern. Hierfür ist eine Schlüsselhypothese, dass ein direkter Zusammenhang zwischen der Grundwasserdynamik der Aue (die Hauptquelle und Mobilisierungszone für DOC in gemäßigten Einzugsgebieten) und DOC Export besteht, der für die Modellierung von DOC Flüssen im Einzugsgebiet herangezogen werden kann.

Studie 1 befasst sich mit der hoch aufgelösten Dynamik ($f = \frac{1}{15} \text{ min}^{-1}$) von DOC Konzentration und Qualität in der Rappbode hinsichtlich ihrer hydrometeorologischen top-down Steuerungsgrößen (integrale Prozesse auf Einzugsgebietsebene). Hierbei zeigte sich, dass zeitlich vorgelagerte, hydrometeorologische Parameter und deren Interaktion wesentlich zur Erklärung der DOC Dynamiken in der Rappbode beitragen. Die identifizierten Parameter können DOC Export in Einzugsgebieten über hydrologische und biogeochemische Rahmenbedingungen beschreiben und in DOC Export Modellen als Ankerpunkt eine generelle Prozessrepräsentation (z.B. das Ein- bzw. Aussetzen von hydrologischer Konnektivität) gewährleisten, was wiederum die Übertragbarkeit auf ähnliche Einzugsgebiete erhöht.

Die Mobilisierung und der Transport von DOC aus der Aue in den Fluss werden in Studie 2 aus der bottom-up Perspektive untersucht (Mechanismen in der Aue). Ergebnisse aus chemischer und topographischer Analyse von Auen- und Flusswasserproben, kombiniert mit numerischer Modellierung zeigen, dass Oberflächenabfluss in der Aue etwa die Hälfte (47%) des gesamten terrestrischen DOC Exports ausmacht. Im spezifischen wird dabei DOC von Auenflächen mit hoher topographischer Feuchtigkeitswahrscheinlichkeit (repräsentiert durch einen hohen, lokalen topographischen Feuchtigkeitsindex; TWI_{HR}) exportiert, wohingegen Flächen mit niedrigerem TWI_{HR} auch weniger zum oberflächlich generiertem Stoffaustrag beitragen. Darüber hinaus zeigt Studie 2, dass oberflächliche Transportwege vor allem während und nach Niederschlagsereignissen aktiviert werden. Näherungsvariablen, die die lokalen Bodenfeuchtigkeitsunterschiede in der Aue repräsentieren – wie der erwähnte TWI_{HR} – können daher die verschiedenen terrestrischen DOC Quellzonen der Aue mit dem observierten DOC Signal im Fluss verbinden. Die hydrologische Modellierung der Aue konnte außerdem zeigen, dass der Bodenfeuchtegehalt in der Aue direkt mit dem zeitlichen Einsetzen und der Menge des beobachteten DOC Exports zusammenhängt, sofern ein bestimmter Feuchtigkeitsgrenzwert im Boden überschritten wird (also Grundwasser die Oberfläche der Aue erreicht und dort abfließt).

In Studie 3 wurde das hydrologische Modul eines halb-verteiltern DOC Export Modells entsprechend der Erkenntnisse aus den Studien 1 und 2 mechanistisch angepasst (u.a. durch die Implementierung eines grenzwertkontrollierten, dynamischen Oberflächenabflussterms). Die Studien 1 und 2 verdeutlichen, dass die DOC Dynamik im Fluss einen inhärenten Informationsgehalt besitzt, aus dem sich die Art der DOC Quelle sowie der Zeitpunkt und der Mechanismus der DOC Mobilisierung ableiten lässt. Dies wiederum erlaubt es, Fluss-DOC zur simultanen Kalibrierung des hydrologischen (Kling-Gupta Effizienz $KGE = 0.79$) und biogeochemischen Moduls ($KGE = 0.73$) des angepassten Modells heranzuziehen. Der Vergleich mit gemessenen Grundwasserdaten (Wasserstand und DOC Konzentration) deutet auf valide interne und externe Modellkompartimente hin und legt nahe, dass die Dynamik der Grundwässer in der Aue dazu genutzt werden können, die DOC Dynamik in der Rappbode zu modellieren. Wird zuerst das hydrologische Modul und anschließend das biogeochemische Modul kalibriert, kommt es zu einer deutlichen Überschätzung der DOC Konzentrationen in einzelnen Modellkompartimenten. Hieraus schließen wir, dass der inhärente Informationsgehalt von Fluss-DOC einen vielversprechenden Ansatz darstellt um DOC Export Modelle zu kalibrieren, sollte das Ausbringen von externen Tracern nicht möglich sein. Dies sollte die Übertragbarkeit von Modellen auf andere Einzugsgebiete wiederum drastisch erleichtern.

Insgesamt unterstreicht die hier verfasste These die starke Interaktion zwischen hydrologischer und biogeochemischer Funktionalität in der Aue, die zur verbesserten DOC Export Modellierung verwendet werden kann. Der Informationszugewinn durch den hier verwendeten hoch aufgelösten, multidimensionalen Geodatensatz erlaubte das Generieren von Näherungsvariablen, die den Ort sowie das Timing und den Mechanismus der Mobilisierung in sich vereinen. In ein Modell implementiert können solche Näherungsvariablen eine ganzheitlichere Repräsentation von DOC Exportprozessen gewährleisten. Wasserqualitätsmanager können so den Einfluss von sich ändernden hydrometeorologischen Steuerungsgrößen auf die DOC Flüsse mehrerer Einzugsgebiete besser abschätzen.

Chapter I – Introduction

Dissolved organic carbon (DOC) in streams and rivers in itself is of central ecological importance (Cole et al., 2007; Battin et al., 2008), but amount and quality of DOC also shape water quality through interactions and co-export with other chemicals in terrestrial solute source areas (Ledesma et al., 2016; Sherene, 2010), rivers and lakes (Prairie, 2008). Changes in land use and climate shift biogeochemical boundary conditions (Larsen et al., 2011; Chantigny, 2003; Wilson and Xenopoulos, 2008) thus increasing and changing DOC concentrations and quality in surface waters, which puts pressure on drinking water quality and ecohydrology of freshwater ecosystems (Tong and Chen, 2002; Ojima et al., 1994; Whitehead et al., 2009). There is increasing scientific consent that an adequate management of DOC export is needed to fulfill infringed water quality directives (Stanley et al., 2012) and increase cost efficiency of drinking water purification (Matilainen et al., 2011). In this context, predictive modelling is an indispensable tool to understand and explore potential DOC loads under future scenarios of climate and land use change, needed for an efficient management of DOC.

Respective DOC export models primarily target riparian zones (RZs) of lower order streams, because RZs represent one of the main sources of terrestrial DOC export (Ledesma et al., 2015; Musolff et al., 2018) and lower order streams make up a large fraction of river networks worldwide (Raymond et al., 2013). Moreover, the position at the terrestrial-aquatic interface renders the RZ a general control unit for DOC processing such that models that target riparian DOC export from headwater catchments can potentially have high impact on management strategies, because of the achievable transferability to catchments with similar characteristics. However, an application of predictive riparian DOC-export modeling at scales that are relevant for effective DOC management is rare in practice (Stanley et al., 2012). One major reason is that an insufficient conceptual understanding of the dominant mechanisms of DOC export (and nutrients in general) at small (riparian) scales so far inhibits estimating the complete dimension of changes in DOC exports in future climate scenarios (Monteith et al., 2007).

A growing body of literature stresses the point that DOC production is spatially heterogeneous and controlled by hydrological and biogeochemical settings in RZs (Frei et al., 2012; Ledesma et al., 2016; Köhler et al., 2008; Bernhardt et al., 2017; Wen et al., 2020). Large uphill contributing areas deliver a steady supply of water to the RZ, such that DOC production and mineralization of DOC mainly get limited by temperature and redox conditions, but not water content in the soil (Luke et

al., 2007). Thus, DOC accumulation rates are highest during anaerobic conditions at low temperatures due to low mineralization rates, whereas high mineralization rates can be realized in oxygenated soil compartments at higher temperatures. On the other hand, the rate of DOC accumulation and respective export is ultimately dependent on hydrological connectivity of DOC sources to the stream, which in turn is highly dependent on local groundwater levels (Bishop et al., 2004; Köhler et al., 2009). This specific setup can lead to a stronger accumulation of DOC close to the soil surface where water mobilizes existing DOC pools only during hydrological events that saturate those surface near layers (Ledesma et al., 2016), leading to enrichment patterns of stream-DOC with increasing stream runoff. Different hydrological and local geomorphological properties can also facilitate preferential runoff, enabling variably contributing DOC source zones (Dick et al., 2015), when depressions in microtopography collect surficial water (Frei et al., 2010; Scheliga et al., 2019) that is typically rich in DOC. Thus topography of the hillslope-RZ continuum, initial groundwater level and precipitation are the main hydrological drivers for export from these DOC sources.

In summary, interaction of biogeochemical and hydrological processes that control production and export of DOC (Wen et al., 2020) lead to complex nonlinear response signals in the stream. RZs are highly dynamic and interactive at the local scale and the sub-daily temporal scale of events, often leading to a mismatch between the scales of observations and those of the underlying processes (Zarnetske et al., 2018), which in turn constrains models in terms of transferability across spatiotemporal scales. Models therefore are required to properly capture, calibrate and validate the small scale mechanisms and interactions in RZs that are responsible for the observed nonlinear responses in order to make meaningful predictions that could support management at the larger catchment scale. This in turn highlights another bottleneck for applicable models that a proper model validation often is disproportionately costly, but essential for reliable model interpretations (Kirchner, 2006; Birkel et al., 2017).

So far, it still is challenging to balance out and optimize model complexity between the two endmembers model specificity – as in fully distributed models (e.g. Frei et al., 2012), which have high model complexity, site specificity, computational cost and predictive power – and model transferability – as in statistical models (e.g. Seibert et al., 2009), which have reduced complexity, site specificity, computational cost and predictive power. Fully distributed models aim to completely represent catchment heterogeneity, whereas simple conceptualizations for DOC export from RZs rely on statistical (unmechanical) relationships disregarding internal fluxes and integrate over small-scale, spatio-temporal variability in DOC export (Dick et al., 2015; Ledesma et al., 2018a). For example, Seibert et al. (2009) specify a steady vertical distribution of pore water concentrations

and depth-dependent discharge for the whole catchment that is derived from the observed DOC dynamics at the catchment outlet. Hence, simple models have limited predictive power of water and DOC fluxes under changing boundary conditions (Ledesma et al., 2021) for riparian management purposes. In contrast, fully distributed model concepts that explicitly capture the mechanisms of small-scale solute mobilization in RZs (e.g. Frei et al., 2010 and 2012) are able to simulate the complex interactions of biogeochemical processing and hydrological export. However, such model setups typically are computationally expensive with model complexity drastically limiting transferability to other catchments. Consequently, to be appropriate for application, a DOC export model is needed that is mechanistically correct, meaning that it explains the dynamic complexity of internal and external riparian fluxes at the temporal scale of discharge events for “the right reasons” (Kirchner, 2006), while at the same time having reduced overall model complexity to be more readily transferable to other catchments.

In this regard, semi-distributed models are a good compromise, because they balance between a spatial discretization of dominant landscape units in the catchment and a mechanistical representation of integral mechanisms and internal fluxes of those functional units. Spatial discretization to model DOC export in catchments typically consist of hillslope, (deeper) groundwater and riparian zone units (Birkel et al., 2014; Dick et al., 2015). Here, storage outflows are represented with non-linear reservoir equations, e.g. based on power law functions (fast near-surface flux in the RZ unit) or linear functions (slow draining groundwater unit). Additional tracer data (like stable water isotopes) is used to internally calibrate model fluxes. However, if only little data is available for validation, this leaves ample scope for equifinality and uncertainty in model parameterization. Strohmenger et al. (2021) successfully modeled discharge, DOC and Nitrate concentration in a small headwater catchment in northern France using the hydrological FLEX model (Fenicia et al., 2006) and constant DOC concentration two reservoir mixing, but their model has high uncertainty due to the lack of validation of the model functioning. Lessels et al. (2015) combined a modified version of the hydrological HBV model (Lindström et al., 1997) with a modified version of the biogeochemical ECOSSE model (Smith et al., 2007) in a sub-arctic alpine catchment with permafrost influence. However, they could calibrate their model only for the summer months. Birkel et al. (2020) successfully transferred their temperate catchment model (Birkel et al., 2014) to reproduce the periodically running riparian-saturation-area processes of tropical wet dry cycles by implementing a dynamic function that constraints the functioning of the riparian unit, thus underlining the conclusion of Hrachowitz et al. (2014) and Birkel et al. (2017) that, besides the internal calibration, a proper model conceptualization and adequate functional constraints are essential for plausible models.

Recent years have seen significant advances in sensing technologies for high-frequency in situ concentration measurements (Rode et al., 2016; Strohmeier et al., 2013), allowing to more accurately differentiate between single solute fluxes contributing to an integrated response signal of DOC in the stream (Tunaley et al., 2016) and attribute them to different riparian source zones (Hood et al., 2006; Sanderman et al., 2009). Capturing those in-stream DOC dynamics more precisely within hydrological events provides an opportunity to significantly improve our mechanistic understanding of DOC mobilization, transport, and ultimately export from catchments (Berggren and del Giorgio, 2015; Creed et al., 2015; Köhler et al., 2009; Strohmeier et al., 2013), especially for transition periods (e.g. from wet to dry season) which are typically difficult to model (Birkel et al., 2011). A systematic analysis of in-stream data together with their hydroclimatic drivers at high-frequency hence can improve our understanding of the delicate interplay between hydrological (mobilization and transport) and biogeochemical controls (buildup of exportable DOC pools) from the event to seasonal scales that ultimately control the timing of DOC export from catchments (Wen et al., 2020) and the riparian unit in particular.

Moreover tools to assess topographical (drones), biogeochemical (molecular DOC characterization) and hydrological (high-frequency automated pressure transducers, numerical models) heterogeneities in riparian zones have become available over the years, which provides more insight into spatiotemporal small-scale variations in the RZ that can be explicitly connected to riparian DOC sources and export generation processes, respectively (Raeke et al., 2017; Seifert et al., 2016; Wagner et al., 2019; Frei et al., 2012). A coupled hydrological-biogeochemical assessment of the RZ at increased detail resolution will ultimately lead to an improved understanding of the dominant DOC source areas in RZs and their respective DOC export mechanisms from these areas to the stream. The gained knowledge will help to delineate functional zones and export mechanism of DOC export which can help adapt and thus increase the specificity of conceptual units and their dominant export mechanisms in semi-distributed DOC export models.

This thesis hence aims to find optimal complexity of such models using high-resolution data and state of the art methods for DOC-quality characterization, while at the same time improving their functioning and conceptualizations of dominant export mechanisms. As shown, there is a high spatio-temporal variability of local mechanisms that control DOC accumulation, mobilization and transport in RZs (Pinay et al., 2015; Bernhardt et al., 2017; Krause et al., 2014), thus leading to the observed nonlinear DOC export pattern at small spatio-temporal scales that so far inhibits a holistic yet conceptual model representation at the required resolution and complexity. In order to correctly represent the spatio-temporal patterns of DOC export from RZs, the topographic impact and the dynamics of groundwater levels on runoff generation in the RZ have to be better represented in

respective models. By combining a high-frequency temporal analysis of integrated response signals in the stream with a detailed spatio-temporal assessment of the RZ, this will allow to derive a mechanistic framework that provides a more accurate timing and attributable source contribution of DOC export in the RZ. This improvement of knowledge about different DOC fluxes in the RZ and the associated stream will in turn allow for a more specific conceptualization as well as constraint of the functional units in a DOC export model. The more explicit realization of the riparian and catchment functioning will help to improve the predictive power of the model while at the same time increase transferability and scalability to similar catchments at a sufficient level of complexity.

Chapter II – Research Approach

The research in this thesis aims to mechanistically describe the interactions of hydrological and biogeochemical drivers on DOC export from a riparian zone and subsequently implement these mechanisms into a semi-distributed, catchment-scale DOC export model. An overall focus lies in achieving optimal model complexity while at the same time being able to improve internal flux calibration and therefore credibility of the model framework by using both, top-down (focusing on the response signal at the catchment outlet, representative of relevant integrated catchment-scale processes) and bottom-up (focusing on a detailed analysis of plot-scale riparian mechanisms) analysis approaches of DOC export mechanisms.

2.1 Research Hypotheses and Objectives

The thesis is driven by the following overarching hypotheses:

- i. Riparian zones are the main source and mobilization zones for DOC in humid, temperate catchments like the Rappbode catchment
- ii. DOC export from riparian soils shows distinct spatial and temporal variability that affects chemical composition and concentration of DOC exported to the streams
- iii. Groundwater level dynamics in the riparian zones are a first-order control for event-driven runoff generation and associated DOC exports
- iv. There is a direct relationship between riparian groundwater dynamics and DOC export at the catchment outlet, which can be used to reproduce and predict DOC flux variability at the outlet.

The key objectives are

- i. to investigate the hydrological and biogeochemical controls and the impact of their interactions for the mobilization and transport of DOC from riparian soils to the streams,
- ii. to identify functional zones of terrestrial DOC export and their prevailing export mechanisms and,
- iii. based on the results from i and ii, to adapt a catchment-scale, semi distributed mechanistic model to the recent understanding of DOC export

2.2 Workflow

In order to answer the key objectives, three studies (Study 1 – 3) were carried out. Study 1 focuses on describing how interactions of dominant hydroclimatical drivers of DOC export force an integrated DOC response signal in the stream. Therefore, continuous high-frequency in-stream observations of DOC quantity and quality as well as hydroclimatic observations during different seasons were utilized to elucidate the event-scale and longer term effects of hydroclimatical factors on mobilization and export of riparian DOC. This establishes a set of key controlling variables that captures important hydrologic, hydroclimatic and biogeochemical external drivers of the system during different times of the year from a top-down perspective. From a bottom-up perspective, Study 2 delineates explicit DOC source zones within the RZ and consequently quantifies their DOC export at high spatio-temporal resolution by utilizing topographic and chemical analysis as well as a quantitative mechanistical evaluation of the temporally variable hydrological export of DOC from these source areas to the stream by using numerical flow modeling. The temporally variable DOC export from these source areas to the stream is then evaluated and respective export mechanisms are derived. The findings from Study 1 and Study 2 allow for a robust and mechanistical understanding of key internal water fluxes as well as transformation processes and fluxes of DOC and thus an improved conceptualization of the RZ. Study 3 ultimately implements the gained understanding of top-down and bottom-up derived hydrological and biogeochemical interactions that generate DOC export in the RZ into a semi-distributed catchment model of DOC export. Therefore, an existing semi-distributed model of DOC export is adapted to a state of the art, mechanistic conceptualization that includes a representation of surface flux. The model was then calibrated and constraint via the integral information content of high-frequency DOC quality and concentration data that is inherently coupled to the newly gained knowledge on riparian DOC export mechanisms, presented in Study 2. This solution for finding an optimum in the trichotomy between model complexity, transferability and applicability that is demanded for catchment water quality models is proposed.

Chapter III – Materials and Methods

Overall three studies are presented in this thesis. As data basis, a combination of spatio temporal high resolved hydrological, biogeochemical and topographical field investigations was compiled. To address the studies specific research questions, multidimensional data analysis and modeling was applied together with statistical/explorative-, fully-distributed numerical- and semi-distributed lumped modeling.

3.1 The Rappbode Catchment

Measurements were conducted in a headwater catchment of the Rappbode stream (51°39'22.61"N 10°41'53.98"E, Fig. 1) located in the Harz Mountains, Central Germany. After draining into a drinking water reservoir, the Rappbode stream flows into the river Bode, and discharges (through the rivers Saale and the Elbe) into the North Sea. The catchment has an area of 2.58 km² and a drainage density of 2.91 km km⁻¹. The study site is characterized by a temperate climate (Kottek et al., 2006), with a long-term mean air temperature of 6.0 °C and mean annual precipitation of 831 mm (Stiege weather station 12 km away from the study site, data provided by the German Weather Service DWD). The uncultivated and uninhabited catchment is predominantly forested with spruce and pine trees (77 %), 11 % is covered with grass, and 12 % is covered by other vegetation and a few unpaved roads. Elevation ranges from 540 to 620 m above sea level; the mean topographic slope is 3.9°. The 90th percentile of the topographic wetness index (TWI) as a measure for the extent of riparian wetlands in the catchment (Musolff et al., 2018) is 10.10 (median 7.58). The geology at this site consists mainly of graywacke, clay schist and diabase (Wollschläger et al., 2016). Soils in the spring area are dominated by peat and peat formation. Overall, 25 % of the catchment soils are humic and stagnic gleysols that are connected to riparian zones.

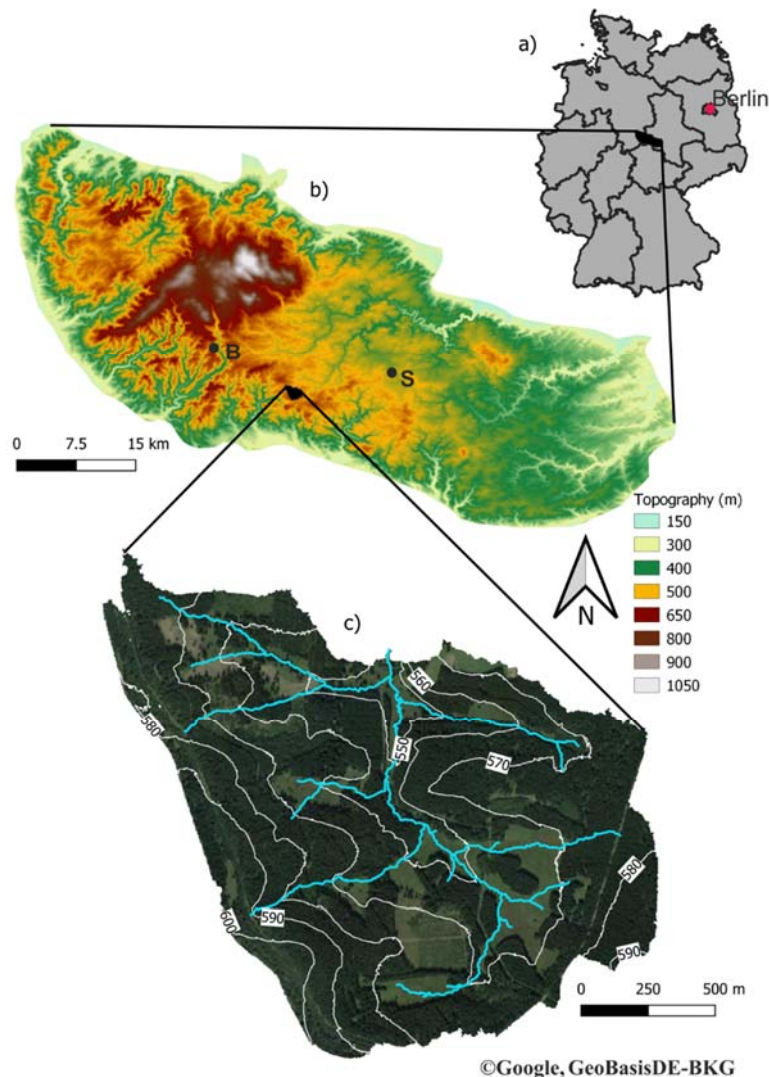


Figure 1. a) Overview map of Germany and the location of the Harz Mountains. b) Topography of the Harz Mountains and the location of the studied catchment. Black dots 'B' and 'S' indicate the location of the weather stations Braunlage and Stiege. c) Altitude and riverine system based on digital elevation data (1 meter resolution). Map data: ©Google, GeoBasisDE-BKG.

3.2 Understanding integrated response dynamics of DOC concentration and quality (Study 1)

We continuously monitored the Rappbode stream's integrated response variables DOC concentration (C_{DOC}) and quality at high frequency ($f = \frac{1}{30} \text{ min}^{-1}$) from April 2013 to October 2014. Quality of DOC can be used as an indicator of the general chemical composition and reactivity of organic carbon (Weishaar et al., 2003) and to distinguish between autochthonous and allochthonous DOC, molecular weights and processing (photobleaching and microbial degradation change aromaticity; Helms et al., 2008). Therefore, patterns of DOC quantity and DOC quality metrics can be used to infer information on origin and properties of DOC and thus to characterize source zones of DOC in riparian zones (Hood et al., 2006; Hutchins et al., 2017; Sanderman et al., 2009).

Together with DOC, potential controlling variables of stream DOC dynamics (water level, discharge, precipitation, evapotranspiration and air and water temperature) were monitored and processed with respect to their frequency spectrum on the event- and seasonal scale. A hydrograph separation after Gustard and Demuth (2009) into high-frequency event flow (Q_{hb}) and low-frequency baseflow (Q_b) components was applied to the measured total discharge (Q_{tot}) time series. The antecedent aridity index (AI_t) after Barrow (1992) gives an estimate of the water balance in the last t days. Accordingly, AI_{60} was derived for the measurement period by dividing the cumulative sum of precipitation over the last 60 d (P_{60}) by the cumulative sum of potential evapotranspiration of the last 60 d (ET_{P60}). The discharge-normalized temperature of the preceding 30 d (DNT_{30}) was calculated by dividing the mean air temperature of the preceding 30 d by the mean discharge of the preceding 30 d. DNT_{30} gives an estimate of the ratio between temperature (which controls soil DOC production; e.g. Christ and David (1996)) and discharge (which controls DOC export; e.g. Hope et al. (1994)) in the last 30 d and therefore can potentially be related to the state of DOC storage in top soils.

In a next step, descriptive statistical tools were used to identify key controlling variables and related processes which lead to the monitored DOC dynamics. Therefore potential controlling variables were evaluated with regard to their impact on short-term (event-scale) and long-term (seasonal-scale) DOC concentration and quality fluctuations of the Rappbode stream. Concentration–discharge (C–Q) relationships during 38 single events were characterized and modelled by combinations of potential event-scale controlling hydrometeorological variables. Subsequently, the 38 parameter sets (intercepts and regression coefficients) of the single event models of the best variable combination (based on mean R^2 of all 38 models) were extracted for further analysis. To explain seasonal variations in the event-scale analysis, the 38 parameter sets were correlated with various seasonal-scale temporal aggregations of AI , DNT , Q_b , P and air temperature. Variables that showed strong correlations were then added in different combinations to the existing event model as potential predictors for seasonal variations in addition to the event-scale variance. Here, models of the dependent variables (C_{DOC} and DOC quality) always used the same predictor variables. Independent interactions between two predictor variables were generally allowed, implying that the measured hydroclimatic variables influence each other and thus cause a non-additive effect on the dependent variable. The predictive power of the most valid C_{DOC} and DOC quality models were then tested and evaluated.

3.3 Delineating functional zones of DOC export (Study 2)

Study 2 chemically and hydrologically connects explicit riparian DOC source zones with the Rappbode stream, and identifies and quantifies their dominant DOC export mechanism.

A multi-dimensional dataset was compiled from a study site that was established to intensively monitor spatial, chemical and hydrometeorological variables in the RZ and in the stream at high spatio-temporal resolution. The intensive monitoring campaign lasted from 12 April 2017 until 19 December 2018, the overall monitoring period lasted until 23 July 2019. Focus of the monitoring set up was to elucidate riparian DOC export from different angles and independent measures for high credibility.

A drone-generated digital elevation map (DEM, 1m resolution) revealed the floodplain's slope and surficial small-scale heterogeneities. Overall, 25 partly screened piezometers (2.54 cm diameter, HDPE, 10 cm screen) were installed in a rectangular grid pattern covering 50 m x 50 m (Fig. 1b) and equipped with pressure transducers (Levellogger, Solinst, Canada and Diver, van Essen, Netherlands), measuring at a 15-minute interval. The depth of the centers of the piezometer screens was variable ranging between 20 cm and 107 cm below ground (average = 75.2 cm). This was a tradeoff between having continuous water level measurements from the pressure transducers and covering the anticipated large variety of different DOC types in different soil layers and depths (Shen et al., 2015). In-stream samples to determine stream DOC composition were either taken as grab samples during maintenance every two weeks, or were sampled automatically (ISCO Autosampler triggered by flow rate) during event situations. Ambient weather data was captured by a weather station (WS-GP1, Delta-T, United Kingdom), placed about 250 m northwest of the study site.

In a first step (1), riparian DOC point samples were chemically classified and divided into two groups of distinct DOC properties. These DOC properties were then chemically compared and thus connected to DOC properties in stream runoff under differing hydrometeorological conditions.

In a second step (2), a drone derived high resolution DEM was used to identify small-scale topographical similarities of the under (1) grouped DOC point sources. Subsequently, the riparian DOC point sources were extrapolated to zones of similar topographical properties thus creating spatial explicit riparian DOC source zones.

(3) The hydrological contribution to stream flow generation of the under (2) delineated DOC source zones was then quantified using a numerical surface-subsurface water flow model. The modeled water flow and DOC properties from the chemical classification were then used to estimate DOC solute export from the delineated source zones. Ultimately, this allowed to develop a robust proxy to explicitly identify DOC source areas in riparian zones.

In more detail, the following methodological elaborations were used to develop the source zone delineation and quantification depicted above:

(1) *Chemical Classification of riparian DOC sources (FT-ICR-MS)*

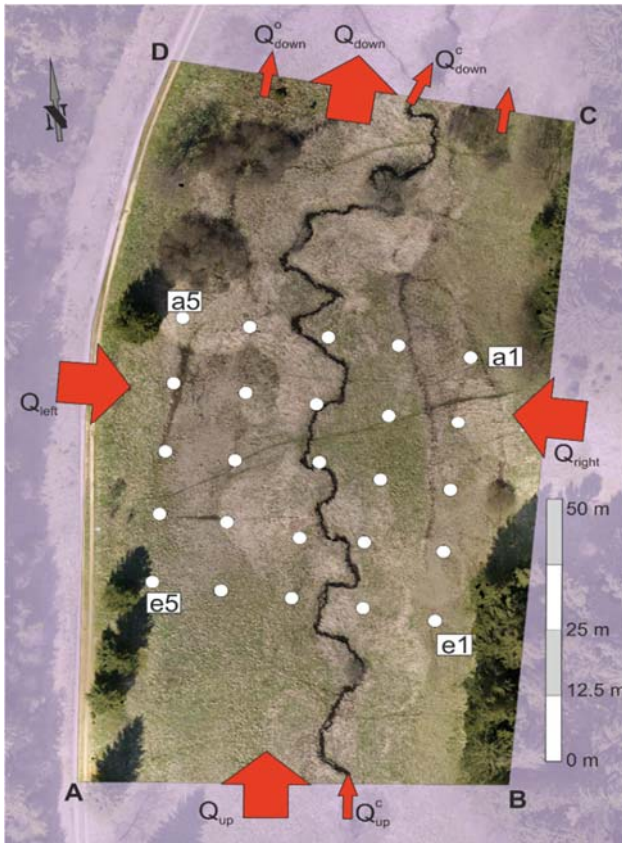
Chemical bulk composition of riparian DOC samples was measured via FT-ICR-MS. A principal component analysis with consecutive k-means cluster analysis was then applied to all riparian samples in order to group existing riparian DOC properties into two classes. These classes were then statistically compared (Wilcoxon rank-sum, Kolmogorov Smirnov, to test differences in mean and distribution of the two groups) to each other and to stream water samples during events and baseflow with the purpose to find differences in the riparian DOC classes as well as to chemically connect riparian DOC to DOC in the stream.

(2) *Map the DOC source areas identified in (1) in space*

A high resolution DEM (1m) was used to create a detailed map of TWI_{HR} values of the study site. Following, TWI_{HR} values referring to the respective DOC sample locations were statistically compared (KS, WC) according to the DOC groups created in (1). A threshold value was then derived from the statistics, separating the riparian zone into explicit source zones of high and low TWI_{HR} values referring to the respective DOC groups.

(3) *a) Quantify the hydrological contribution of the delineated DOC source zones to stream flow generation*

A numerical surface-subsurface water flow model (HGS) was used to quantify water fluxes in the riparian zone (Fig. 2). The compiled data set of the monitoring program was used for a rigorous calibration of the model. Exchange flux – describing the water flux between surface and subsurface was calculated for both explicit source zones of the RZ and compared to the overall water flux balance of the study site.



b) Estimate DOC solute export from the delineated source zones

Ultimately, surficial DOC solute export from the delineated source zones was estimated by multiplying the modeled water exchange flux data from high and low TWI_{HR} zones with the first, second and third quartile of the DOC concentration distribution of the associated DOC groups.

Figure 2. The boundary conditions of the study site (indicated by polygon A-D). Q_{up} : groundwater influx (const.), Q_{up}^c : channel influx (dynamic), Q_{down} : groundwater leaving the model site (dynamic), Q_{down}^c and Q_{down}^o : surface water leaving the model site through channel outlet and through CD (dynamic), Q_{left} and Q_{right} : groundwater discharge rate from side boundaries (const.). Red arrows indicate flow direction of the water. The 25 white points indicate wells which were used for model calibration. Labels of the piezometer run from a to e (lines) and 1 to 5 (columns), respectively.

3.4 Combining understanding of integrated processes and functional zones to derive a complexity reduced, mechanistic model of DOC export (Study 3)

To simulate daily stream flows and DOC concentrations in the Rappbode catchment, we utilized the coupled hydrological-biogeochemical model, developed by Birkel et al. (2014) as a starting point: The hydrological module comprises three linked bucket type hydrological reservoirs with soil moisture related runoff and recharge generation: a riparian saturation zone (S_{RZ} , unsaturated), upper hillslopes (S_{HS} , unsaturated) and a permanently saturated groundwater storage unit S_{GW} . The S_{HS} recharges S_{GW} (percolation) and S_{RZ} (surface and shallow saturation flow) at linear rates, but does not contribute to stream runoff. S_{GW} feeds the stream at linear rates, whereas S_{RZ} feeds the stream by a nonlinear function. Stream runoff is then determined by mixing two fluxes from parallel reservoirs (S_{RZ} and S_{GW}). DOC processing in the S_{HS} and S_{RZ} are calculated by an Arrhenius-type soil moisture and temperature dependent function. The S_{GW} does not allow DOC production (but mineralization represented by a linear loss parameter) and only receives DOC from the S_{HS} . DOC concentrations in the stream are consequently flux weighted average values of the contributing saturation area and groundwater runoff to the total streamflow.

The semi-distributed model from Birkel et al. (2014) was refined by adjusting its hydrological and biogeochemical module to the newly gained riparian conceptualization, developed from Study 1 and

2. In the following this model will be referred to as Tracer-Aided Coupled Hydrology-Biogeochemistry model (TACHyB, Fig. 3). A central feature of the TACHyB model is that the saturation area in the S_{RZ} is parameterized to generate an explicit threshold based, nonlinear runoff in response to precipitation inputs thus mimicking saturation overland flow that was shown to dominate overall runoff generation and DOC export in low relief RZs with hydromorphic soils (Study 2). Overall, the model was adjusted with the following mechanistic refinements and conceptual adaptations:

1. Dynamic, threshold induced riparian surface runoff with DOC export to the stream (Study 2) based on the antecedent aridity index of the preceding 60 days (AI_{60} ; Study 1)
2. Threshold induced hillslope hydrological contribution (McGuire and McDonnell, 2010)
3. Constraining maximum groundwater efflux (Hrachowitz et al., 2014) by adding a threshold based exchange flux between the groundwater reservoir and the riparian reservoir
4. Use of a soil temperature model to get more accurate DOC production values

In comparison to the original model (Birkel et al., 2014), the hydrological module needs to calibrate six more parameters (eleven in total). With seven calibrated biogeochemical parameters (needed to calculate DOC concentrations in the storage units), the TACHyB model did not differ to the initial model.

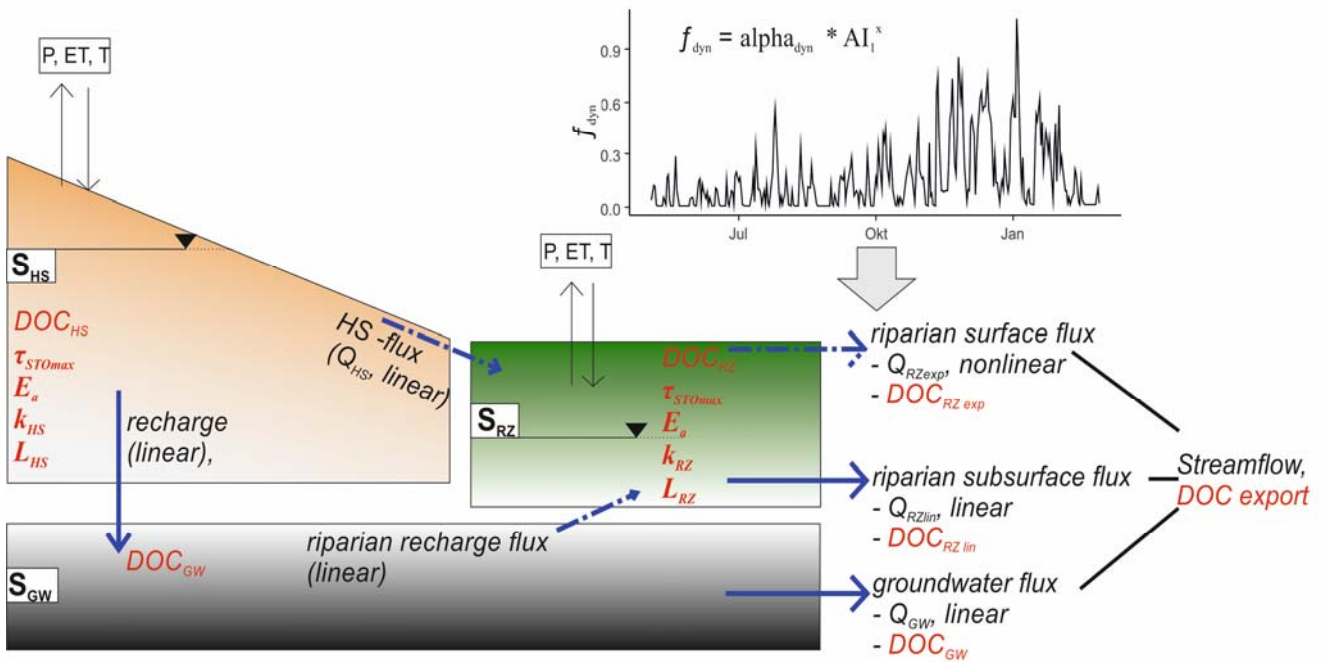


Figure 3. Diagram of the tracer aided coupled hydrological biogeochemical (TACHyB) model set up. The three storage units are groundwater (S_{GW}), hillslope (S_{HS}) and riparian zone (S_{RZ}). Blue arrows represent hydrological processes and respective DOC transfer between storages or to the stream. Dashed blue arrows indicate threshold controlled hydrological processes that occur timewise discontinuous. DOC is calculated based on an Arrhenius type DOC production and loss term that is based on soil moisture and soil temperature. The biogeochemistry processing parameters of each storage unit are shown in red: τ_{STOmax} is the maximum soil moisture deficit defining up to which deficit [mm] DOC processing is still possible; k_{HS} and k_{RZ} are the DOC production rate parameters for the HS and the RZ; L_{HS} , and L_{RZ} are DOC loss

parameters; E_a is the thermal activation energy defining the impact of temperature on the processing rates. Streamflow is generated by nonlinear riparian surface flux (Q_{RZexp}), linear riparian subsurface flux (Q_{RZlin}) and linear groundwater flux (Q_{GW}). Inlet shows the riparian nonlinear dynamic function (f_{dyn}) that is based on a nonlinear function by the linear coefficient $alpha_{dyn}$ and the aridity index of the preceding day (AI_i) with the nonlinearity exponent x . The f_{dyn} therefore regulates the intensity of Q_{RZexp} contributions to the streamflow.

Model calibration

In order to achieve a balanced rainfall-runoff and biogeochemical model calibration, we used the Kling-Gupta Efficiency criterion (KGE) that equally represents peak and low flow compartments of the runoff (Kling et al., 2012; Pool et al., 2018). The KGE focuses on three components of model errors (Eq. 1)

$$KGE = 1 - \sqrt{(r - 1)^2 + (\gamma - 1)^2 + (\beta - 1)^2} \quad (1)$$

Where r is the (spearman rank correlation coefficient r), γ is the variability and, and β the bias. Generally, if $KGE = 1$, the model perfectly represents the dataset. KGE values smaller than -0.41 indicate that the model is worse than the mean flow benchmark (e.g. Nash Sutcliffe Efficiency = 0; Nash and Sutcliffe (1970)). Rogelis et al. (2016) consider model performance to be ‘poor’ for $KGE < 0.5$.

To reduce critical overestimation of large flows in hydrological simulations (Criss and Winston, 2008), the volumetric efficiency (VE; Eq. 2) was calculated

$$VE = 1 - \frac{|\sum_{i=1}^n \chi_{sim,i} - \sum_{i=1}^n \chi_{obs,i}|}{\sum_{i=1}^n \chi_{obs,i}} \quad (2)$$

Where $\chi_{sim,i}$ and $\chi_{obs,i}$ are the observed and simulated values at time step i and n is the total number of time steps. VE ranges from 0 to 1 and represents the fraction of water delivered at the proper time.

Similar to Birkel et al. (2017), a combined objective function (OF) was then calculated from the KGE and the VE to calibrate the hydrological module according to Eq. 3

$$OF = 1 - \sqrt{(1 - KGE)^2 + (1 - VE)^2} \quad (3)$$

Since exported DOC loads are directly dependent on discharge, the KGE only was figured to be sufficient for the additional calibration of the DOC concentration in the biogeochemical module.

The NSGA_{II} algorithm (Deb et al., 2002) was used for calibration (Blank and Deb, 2020) of the hydrological and biogeochemical module parameters, which simultaneously optimized the modified Kling-Gupta efficiency (KGE + VE) of discharge and KGE only of stream DOC concentrations, respectively.

The NSGA_{II} follows the general outline of a genetic algorithm with a modified mating and survival selection. The best performing parameter sets of a random parent population ($N = 500$) are transferred to the random next generation ($N = 500$). Then, non-dominated sorting for the 500 best parameter sets is applied to the merged populations ($2N = 1000$) thus creating a new parent

population. Overall, 2,000 generations/iterations were calculated which of the 500 best parameter sets were chosen for further processing. Robustness of the parameter sets were controlled via a convergence criteria of the hypervolume.

In order to estimate the information content of DOC as a tracer in the multiobjective calibration (MOC) described above, we further applied a consecutive single objective calibration (CSOC): As a first step, only the hydrology module was calibrated (1). Consecutively to it the biogeochemical module calibration (2) used the hydrological parameter set produced in step (1) as fixed set of hydrological parameters. Again we ran 2,000 generations of 500 parameter populations, but the applied minimization yields only one “best” parameter set. The combination of the partial parameter sets from (1) and (2) were used to compare MOC and CSOC model performance in terms of Q and DOC as well as their internal fluxes.

Chapter IV – Results and Discussion

4.1 Dynamics of dissolved organic carbon quantity and quality in a headwater catchment (Study 1)

DOC concentration (C_{DOC}) together with DOC quality parameters specific UV absorption at 254 nm ($SUVA_{254}$) and the slope of the absorption between 275 nm and 295 nm ($S_{275-295}$) systematically changed with high-frequency components of discharge (Q_{hf}) – representative of quick flow – and seasonal-scale antecedent hydroclimatic conditions, represented by the aridity index of the preceding 60 d (AI_{60}) and the quotient of mean temperature and mean discharge of the preceding 30 d ($\frac{T_{30}}{Q_{30}}$), which we refer to as discharge-normalized temperature (DNT_{30}). Initial C_{DOC} in the stream was low during summer baseflow. Events led to partially distinct changes in C_{DOC} and DOC quality with Q_{hf} and lower frequency baseflow components (Q_{b}). The shift in DOC concentration and quality with increasing discharge was most pronounced in summer, followed by spring and autumn. DOC concentration and quality shifts in winter were least pronounced.

Several authors identified seasonality as an important driver for DOC dynamics (Ågren et al., 2007; Broder et al., 2017; Tunaley et al., 2016). However, the term “seasonality” is rather vague and often not clearly defined in terms of its impact on DOC export (Broder et al., 2017; Tunaley et al., 2016), which in turn impedes a quantitative comparison between catchments and different climates. The here presented hydroclimatic drivers AI_{60} and DNT_{30} are measurable and thus reflect the general seasonal dynamics in a quantifiable manner. We argue that analyzing the relationship between AI_{60} and DNT_{30} in combination with differences in DOC concentration and quality allows for a better assessment of the dominant processes for DOC concentration and quality variations than simple data classifications into the classes summer, autumn, winter and spring. AI_{60} is directly related to soil moisture and thus describes the potential for mobilizing DOC in riparian soils, whereas DNT_{30} describes the changes in DOC storage by relating the temperature dependent DOC production to prior mean hydrological export from riparian soils. Hence, the relationship between AI_{60} and DNT_{30} describes the export potential of DOC from riparian soils, which allows to conceptualize DOC exports under different hydroclimatic conditions.

To estimate how event-scale and seasonal controls interact to produce the observed nonlinear responses of DOC concentrations and quality in our study catchment, we compared three distinct, typical hydroclimatic states: (1) high DNT_{30} and low AI_{60} , representing warm and dry conditions mainly found in summer; (2) moderate DNT_{30} and AI_{60} , representing intermediate warm and wet conditions, mainly found in spring and autumn; and (3) low DNT_{30} and high AI_{60} , representing cold and wet conditions mainly found in winter.

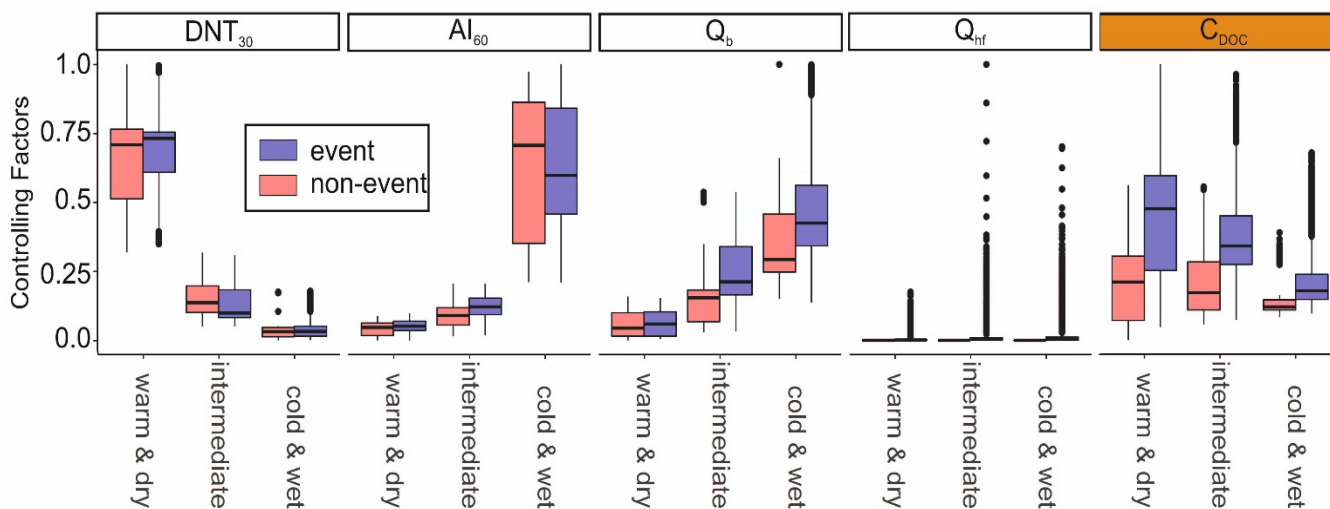


Figure 4. Box plots of hydroclimatic variables (controlling factors) and DOC concentration (response; orange box) classified into three hydroclimatic states: (1) warm and dry, (2) intermediate, (3) cold and wet. Red indicates non-event situations, and purple indicates event situations during the according states. Variables were rescaled for better illustration. Particular median C_{DOC} values during non-event situations were 4.13, 3.72 and 3.16 mg L^{-1} for the warm and dry, intermediate, and cold and wet states, respectively. Both warm and dry and intermediate states differ highly significantly (Kruskal–Wallis test, $p < 0.001$) from the cold and wet state.

4.1.1 Warm and dry conditions

Warm and dry conditions are hydroclimatically defined by high temperatures and low mean discharge (high DNT_{30}), relatively dry soil conditions (low AI_{60}), and low baseflow levels, as typically found in summer when the Rappbode is fed mainly by deeper riparian groundwater. During baseflow conditions highly processed DOC enters the stream via the deeper groundwater flow paths (Broder et al., 2017). DOC composition in deeper groundwater has been altered by sorption and biogeochemical processes (Inamdar et al., 2011; Kaiser and Kalbitz, 2012; Shen et al., 2015). Precipitation events can get partially buffered and retained in the soils (low Q_{hf} , state warm and dry in Fig. 4). Together with an increase of C_{DOC} , DOC quality during events changed markedly towards higher $SUVA_{254}$ values typical for higher aromaticity of the organic matter and associated with processed DOC (Hansen et al., 2016; Helms et al., 2008) and higher $S_{275-295}$ (but not as high as

in cold and wet situation) indicating a *relative* increase in low-molecular-weight components in comparison to the low flow signal.

The lack of moving water and high temperatures in the topsoil allow microbially driven DOC production to be higher than mineralization in the unsaturated riparian zone environment (Kalbitz et al., 2000; Luke et al., 2007), which we refer to as *net production* of DOC in the following. Since C_{DOC} during non-event situations was very low (Fig. 4), higher DOC export from the topsoil with different quality was able to override the low-flow DOC signal towards a riparian zone signal during events. Accordingly, summer events showed the steepest slope of C_{DOC} - Q_{hf} and quality- Q_{hf} relations (cf. 3.3) in summer. The steepness of the C-Q relationship of this additional DOC source contribution is ultimately determined by antecedent hydroclimatical conditions, which favor DOC net production and thus indicate a sensitivity to biogeochemistry-driven DOC export as found by Winterdahl et al. (2016) on top of a general-transport-limited system (Zarnetske et al., 2018). However, we expect summer events to generally have the lowest R^2 values since the retention of water in the RZ and the transition into different DOC pool signatures likely cause strong dispersion in the signal.

4.1.2 Intermediate conditions

Intermediate DNT_{30} and AI_{60} conditions, typically for spring and autumn periods, are defined by moderate temperatures and discharge (medium DNT_{30}), precipitation, and evapotranspiration (medium AI_{60}), which results in higher baseflow levels compared to warm and dry conditions. Strong precipitation events translate into a distinct discharge signal (high Q_{hf}) (intermediate state, Fig. 4). Conditions for the accumulation of DOC during non-event periods are less favorable than warm and dry periods due to colder temperatures that reduce the riparian DOC net production. During non-event conditions some of the shallow riparian DOC pools are already activated due to a generally higher groundwater table. Consequently, the mixing of riparian and deeper groundwater DOC pools translates into intermediate values of concentration and quality parameters.

Similar to the warm and dry conditions, the DOC signal changes both concentration and quality with increasing discharge during events. This process happens faster than during the warm and dry situation since antecedent wet conditions facilitate DOC mobilization from riparian soils instead of retaining the water. Hence the temporal shift between DOC and event induced discharge peak diminishes, resulting in higher R^2 values of C-Q and quality-Q relationships. Despite less DOC production and more efficient export mechanisms, we observed no exhaustion of exportable DOC during consecutive events, highlighting the large store of DOC in the comparably small riparian zone (Ledesma et al., 2015). The DOC quality barely changed during intermediate-state export events, indicating that the hydrology with still high groundwater levels that intercept the surface-

near DOC pool controls export. Intermediate conditions represent transition states, generally found in autumn and spring, which do not have the character and clarity of end-members. Yet, similar quality signals indicate the same process and location of source zone activation in autumn 2013 and 2014. However, observed concentration peaks developed differently, suggesting that the conditions for antecedent DOC storage and export during respective preceding warm and dry phases were different.

4.1.3 Cold and wet conditions

Cold and wet conditions, mainly found in winter, are defined by low temperatures and high mean discharge (low DNT_{30}), humid conditions (high AI_{60}), and high baseflow levels (cold and wet state, Fig. 4). Dilution due to the impermeability of the frozen soil surface (Laudon et al., 2007) is likely to occur under prolonged periods of temperatures below zero. In contrast to warm and dry conditions, high baseflow levels lead to a good hydrological connectivity of DOC sources to the stream also during non-event situations. However, the low temperature impairs riparian DOC production, especially in the topsoil thus leading to generally low C_{DOC} values indicative of a small ratio of DOC mass available for export to generated runoff in the riparian zone. Low $SUVA_{254}$ and high $S_{275-295}$ values were observed during that period, displaying a dominance of low-molecular-weight compounds in the stream. Precipitation events result in small slopes of the C_{DOC} and quality- Q_{hf} relationships. Since all riparian DOC pools are already connected to the stream, we attribute the small shift in DOC quality and C_{DOC} during events to a growing contribution (hydrological connection) of DOC source areas with similar DOC quality, rather than to the activation of new, differing DOC pools. In contrast to the relationship of C_{DOC} and $SUVA_{254}$ with discharge, R^2 of the $S_{275-295}$ - Q relationship drops during the cold and wet situation, indicating a decoupling from hydrological forcing.

4.2 Small-scale topography explains patterns and dynamics of dissolved organic carbon exports from the riparian zone of a temperate, forested catchment (Study 2)

While Study 1 investigated the temporal dynamics of riparian DOC export processes from an integrated in-stream perspective, Study 2 changes the perspective to the riparian zone itself in order to understand the spatial distribution of different DOC source zones and their temporal mobilization dynamics. The goal was to delineate functional zones of DOC export as well as their distinct export mechanisms at high spatiotemporal resolution in order to derive proxies of small-scale heterogeneity and its impact on DOC export, respectively. Such scale-bridging proxies can be utilized to represent small-scale processes in larger-scale catchment models.

4.2.1 Small-scale topographical heterogeneity delineates DOC source zones in terms of molecular composition and hydrological properties

Separating 66 samples from riparian surface- and groundwater according to their molecular DOC characteristics and high-resolution (local) topographical wetness index (TWI_{HR}) values from the respective sampling locations suggests the existence of two chemically differentiable DOC pools (DOC_I and DOC_{II} ; Fig. 5a) with distinct hydrology (Fig. 5b) and source zones (Fig. 5c) in the riparian study site. The molecular composition of DOC_I indicates processed plant-derived organic matter, similar to typical wetland sites with overall low organic matter turnover (Tfaily et al., 2018). In contrast, DOC_{II} represents more microbially derived, secondary metabolites indicative of increased microbial processing of organic matter from organic rich top-soil layers and DOC which is not adsorbed to mineral phases. High TWI_{HR} values – associated with DOC_I source zones – make up roughly 15% of the study site and represent zones with increased water and DOC inputs from adjacent areas, leading to hydrological upwelling and higher mean groundwater levels with concomitant waterlogging (Luke et al., 2007). Micro-topography and hydrological upwelling (here both represented by TWI_{HR}) can induce gradients in redox conditions (Frei et al., 2012) that restrict and shape DOC processing. High- TWI_{HR} zones thus reflect a general conserving environment for DOC due to anaerobic conditions even in the topmost soil layers (LaCroix et al., 2019) potentially leading to DOC accumulation. In contrast, zones with low TWI_{HR} values are generally characterized by lower mean groundwater levels and thus more oxygenated top soils, allowing for more biogeochemical processing and thus potentially less DOC accumulation. Overall we conclude that small-scale topographic heterogeneity (here represented by TWI_{HR}) can be linked to distinct DOC compositions and hydrological properties in RZs.

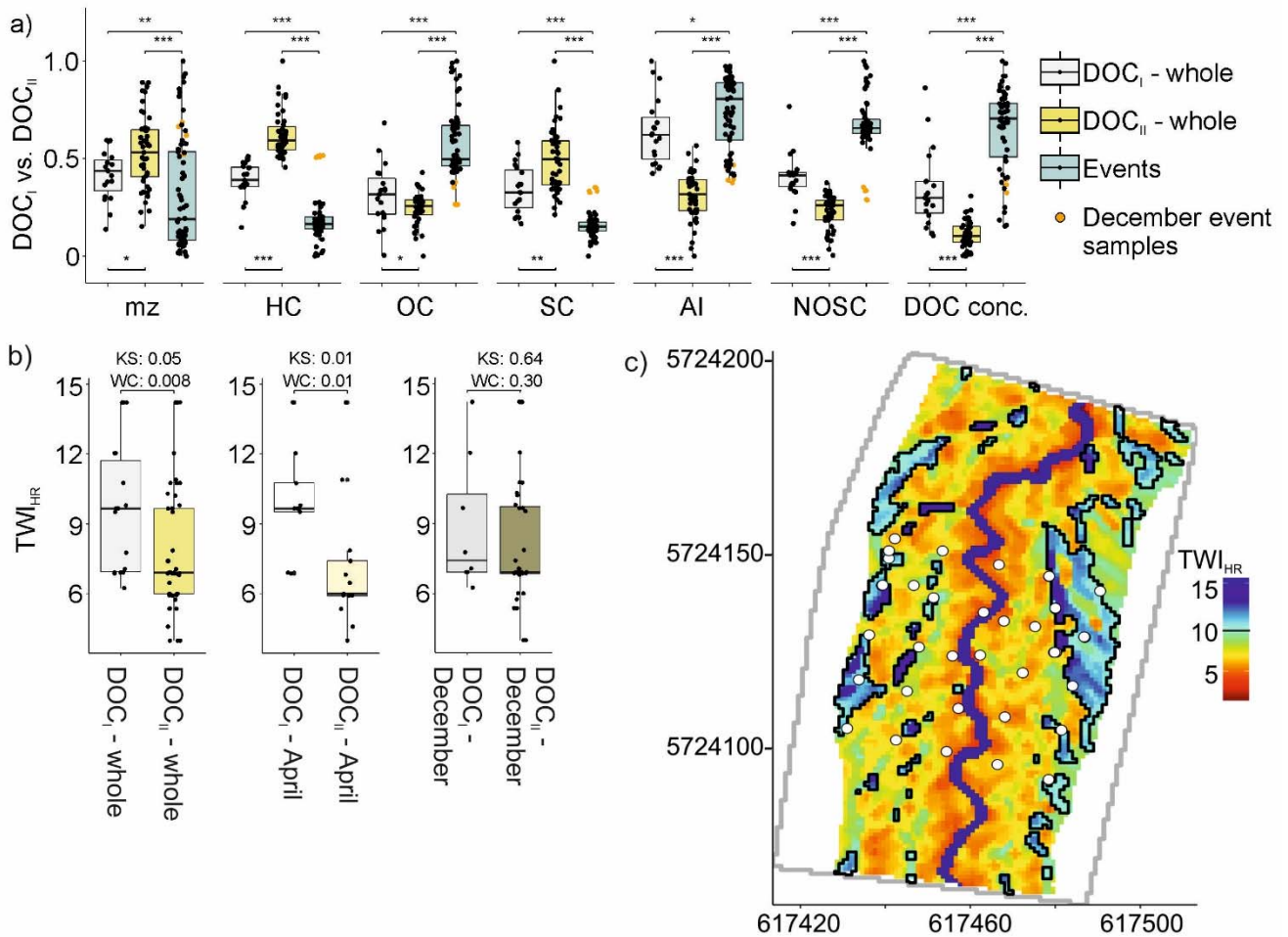


Figure 5. Biogeochemical, hydrological and topographical comparison of DOC_I and DOC_{II} pools. a) Boxplots from FT-ICR-MS derived weighted average (wa) molecular parameters wa_{mz} (mass to charge ratio), wa_{HC} (hydrogen to carbon ratio), wa_{OC} (oxygen to carbon ratio), wa_{SC} (sulfur to carbon ratio), wa_{AI} (aromaticity index) and wa_{NOSC} (nominal oxidation state of carbon) as well as DOC concentration (DOC conc.). Orange points indicate samples of one December event. Data was min-max normalized to values between 0 and 1 for better illustration. Asterisks indicate p-values of the Kolmogorov Smirnov test (***: < 0.001; **: < 0.01; *: < 0.05; NS: not significant). Test results between two boxplots are depicted above the respective connecting squared brackets. b) Boxplots of TWI_{HR} values as affiliated to the respective wells of DOC_I and DOC_{II} samples, partitioned into all samples ('whole'), the April sampling only ('April') and the December sampling event ('December'). Wilcoxon rank sum (WC) and Kolmogorov Smirnov (KS) test results are depicted above the squared brackets. c) High resolution TWI_{HR} map of the modeled site (excluding hillslopes). White points indicate sampling locations of riparian sampling; the Rappbode stream (flows from bottom to top) is indicated by the blue line. Black polygons are high TWI_{HR} zones (greater than 9.6; threshold displayed by black line in the legend), indicating DOC_I source areas.

4.2.2 Connecting riparian DOC sources to the stream

The physically-based model HydroGeoSphere showed that overland flow – especially in late autumn until spring – was the dominant runoff generation mechanism contributing 61% (± 12 % standard deviation) to the annual runoff of the stream. The model further confirmed that interconnected depressions in the microtopography (with high TWI_{HR} ; Fig. 5c) allow to channel potential precipitation inputs as well as upwelling of shallow subsurface flows towards the stream (Frei et al., 2012; Scheliga et al., 2019). Consequently, high TWI_{HR} zones react more directly and strongly to precipitation and in turn runoff generation than zones with low- TWI_{HR} values that can

retain water longer in case they are not fully saturated. Due to the significantly higher DOC concentrations in high TWI_{HR} zones (Fig. 5a), we expect overland flow from the respective DOC_I source zones to be the dominant DOC export pathway connecting riparian DOC sources to the stream at our study site.

Variations in stream DOC molecular composition that appeared on event-scale (Fig. 5a) and seasonal scale (not shown), further indicate a link between DOC export and groundwater level dynamics which ultimately drive hydrological connectivity. For December, hydrological modeling revealed fully saturated riparian conditions (Fig. 5b) activating the entire RZ for stream runoff generation. Since DOC_I and DOC_{II} then contributed to the stream DOC signal, this led to a stream DOC composition in-between that of the two riparian DOC clusters (Fig. 5a orange points). However, DOC_I and stream water DOC molecular compositions are converging during events with lower antecedent groundwater levels and partially unsaturated soils, suggesting that DOC_I becomes the predominant source when DOC_{II} is (still) depleted e.g. from snowmelt in April. Observed deviations of instream DOC from the riparian source DOC composition (Fig. 5a) might be a result of near- and instream processing (Dawson et al., 2001; Battin et al., 2003), but also inter- and intra-annual variability of hydroclimatic drivers like seasonality or antecedent soil conditions (Köhler et al., 2009; Strohmeier et al., 2013; Futter and de Wit, 2008). Yet we presented direct links between six major DOC molecular properties and the DOC concentration of riparian and stream water samples. Overall, combining hydrological modeling with detailed topographical analysis (TWI_{HR}) and chemical analysis enable a spatially explicit identification of riparian DOC source zones and their water- and DOC-contributions to the stream water signal at high credibility.

4.2.2 Quantifying riparian DOC export to the stream

Quantifying DOC exports from riparian hot spots to the stream has rarely been done (Bernhardt et al., 2017), most probably because capturing explicit mechanistic and spatio-temporal dynamics of small-scale “hotspots” and “hot moments” of DOC export is challenging. Based on our spatio-chemical classification and numerical water flow modeling, we roughly estimated that high TWI_{HR} zones exported $7.1 \cdot 10^6$ g DOC during the study period, which amounts to a nearly 20 times higher area-normalized DOC export from high TWI_{HR} zones than from low TWI_{HR} zones. The presented numbers are in line with DOC export estimated from hotspots in a forested stream in a humid continental climate (Wilson et al., 2013) and generally in the range of the magnitude of effects reported for hot spots at other sites (Bernhardt et al., 2017). Further, these findings translate into an overall dominance of DOC_I export from high TWI_{HR} zones during events, despite making up only about 15 % of the total study site area. With that our findings suggest a clear link between DOC

quality and lateral topographic heterogeneity (represented by TWI_{HR}) and support the modeling results from Frei et al. (2012). As with Ledesma et al. (2018b) our work therefore recommends to focus riparian DOC research on overall smaller scales. In addition we could show that surface flow from localized source areas is an important transport pathway for DOC towards the stream. Results of our study partly disagree with studies that have postulated one distinct “dominant source layer” (DSL) and predominantly horizontal flow in the subsurface (Ledesma et al., 2018b; Seibert et al., 2009) as the main transport mechanism for DOC. Instead, the shallow depth to bedrock, hydromorphic soils of low hydraulic conductivity and the humid climate at our site lead to generally high groundwater levels facilitating saturation-excess overland flow that in turn acts as the dominant DOC export mechanism to the stream. Within this setting, microtopography determines the location (lateral variability) of the dominant DOC source areas, but the dynamic mobilization of DOC during events is controlled by the hydrological drivers rainfall and snowmelt and their immediate effect on riparian groundwater levels (temporal heterogeneity).

4.3 Modelling dissolved organic carbon export from a catchment using a complexity-reduced, mechanistic approach (Study 3)

An expert-knowledge-driven strategy of constraining models can significantly increase predictive performance of a model and its skill to reproduce hydrological signatures (Hrachowitz et al., 2014). Such expert knowledge can be derived from the preliminary Studies 1 and 2. Study 2 generates a detailed link between functional DOC source zones in the riparian zone and the stream DOC signal, whereas Study 1 examines the hydroclimatical controls of the integrated response signal in the stream from the catchment perspective. Hence, combining the findings from Study 1 and 2 opens up the possibility to improve model conceptualizations by refining their internal mechanistic functioning while keeping the impact of small-scale mechanisms on the catchment scale in mind. Especially model validation by the application of external tracers and the additional costs/effort involved to check internal functioning are nowadays severely limiting our ability to transfer models between catchments. We argue that the DOC that enters the stream from the RZ by a replicable mechanism already carries integral information on its origin and fate. Calibrating hydrology and DOC concentrations simultaneously in a mechanistic state-of-the-art model (Hrachowitz et al., 2014) that distinctly differentiates between export mechanisms and respective DOC signals thus could help to constrain internal model functioning in such a way that both the hydrological and the biogeochemical constrained mechanisms may render the additional application of external tracer data for model calibration and validation redundant.

4.3.1 Finding the right model structure

Since surface flux in the Rappbode catchment was found to be a dominant transport mechanism for DOC export into the stream (Study 2), we implemented an explicit surface flux mechanism to the TACHyB model (Fig. 3). This surface flux is represented in the model by a dynamic and nonlinear function, which – in combination with its threshold activation – aims to represent the microtopography induced variable source zone activation (Study 2). If there was less than ≈ 1.7 times the amount of precipitation than evapotranspiration, each for the preceding 60 days ($AI_{60} < \tau_{dyn} \approx 1.7$; where τ_{dyn} represents the threshold value for surface runoff generation), subsurface flow paths can sufficiently drain the RZ, resulting in a linear runoff generation response from the riparian zone. In case of more than ≈ 1.7 times the amount of precipitation than evapotranspiration within the past 60 day period ($AI_{60} > \tau_{dyn}$), surface flux can occur in the RZ due to precipitation. With that, surface runoff generation is explicitly represented, therefore differing from a coefficient-based (thus not mechanistical) partitioning of excess water into fast and slow reacting reservoirs (e.g. in the FLEX model group; Fenicia et al. (2007)), or the continuously modeled – and thus undistinguishable – combined subsurface and surface flux calculations in e.g. Birkel et al. (2014; 2017; 2020).

Like postulated in McGuire and McDonnell (2010), a threshold-based (near) surface flux mechanism was further observed for the hillslope and consequently was likewise implemented into the model via AI_{60} . Such an aridity index based threshold value is physically interpretable since it gives a measure to determine the amount of excess precipitation/evapotranspiration until surface flux occurs/disappears. Moreover, we argue that groundwater discharge and its respective effective runoff generation cannot increase infinitely, if a riparian storage unit is conceptualized on top of the groundwater storage. Therefore we implemented a limit for maximum effective groundwater discharge beyond which exceeding groundwater feeds the riparian storage unit instead of draining into the stream. The provision and processing of DOC within the single storage units can sufficiently be parameterized by effects of soil moisture, temperature and DOC processing rate (Smith et al., 2007; Birkel et al., 2014; Lessels et al., 2015). However, when estimating DOC concentration in the riparian surface runoff in our model we did not account for processes that lower DOC concentration (like adsorption or mineralization), since we assumed that such processes occur primarily in the subsurface where e.g. exposure times (Oldham et al., 2013) are large compared to the shortly exposed surface runoff.

In summary, the biogeochemical module integrates the impact of key processes, which sufficiently describes the DOC provision in the catchment. We adapted the hydrological module by the addition of six additional parameters in order to optimally represent the timing and magnitude of impactful

hydrological mechanisms. Two additional parameters were used to explicitly simulate nonlinear and dynamic surface runoff generation in the RZ, one to parameterize linear transfer of excessive groundwater into the riparian storage. Three additional parameters are physically derivable and verifiable threshold values, meant to proxy the on-/offset and magnitude of the runoff generation while taking hydrological connectivity into account. These threshold values could be widely constraint in their initial calibration range by our observations and thus likely do not substantially change the model's parsimony. This approach assumably increases transferability, since DOC export limitation due to mobilization limitation was found to be of general significance (Wen et al., 2020). We therefore argue that the conceptually constraining aspect of the model structure outweighs the loss in parsimony that comes with the additional parameters.

4.3.2 Model performance

The simultaneous multi-objective calibration (MOC) of the TACHyB-model suggests a 'good' model calibration (Rogelis et al., 2016) for the hydrological and biogeochemical modules (0.79 and 0.73 for KGE_Q and KGE_{DOC} , respectively). The overall hydrological dynamics were well captured by the 500 best parameter sets, but snowmelt and rewetting periods were overestimated whereas small events that followed snowmelt were underestimated. High and low flow periods are dominated by outflows from single storages, allowing for a mechanistically more definite replication than periods with more equal or transitioning storage contributions (Birkel et al., 2017). The dampened shape of simulated riparian storage (proxying riparian groundwater level) as well as its high correlation with observed riparian depth to water table (DTW) suggest a correct hydrological representation of internal states and fluxes at event and seasonal scale (Beven, 2012; Broder and Biester, 2015). Modeled DOC concentrations of the storage unit did not show unrealistic values (1.9 – 21.8 mg L⁻¹) within the entire modeling period. Simulated DOC concentration in both the RZ and groundwater were in concentration range from respective water samples taken at five occasions (cf. Study 2 for more information on these occasions), despite neither hydrological nor biogeochemical internal fluxes/states were calibrated in our model.

With approximately 35% of the total DOC export happening in 10% of the time, the DOC export was dominated by the riparian fluxes, which is widely acknowledged (Birkel et al., 2017; Broder and Biester, 2015; Ledesma et al., 2018b). Although being the major contributor to stream runoff, the linear riparian flow exhibited lower DOC concentrations than the threshold controlled, nonlinear riparian flow that in turn contributed disproportionately strong (47% of total generated DOC load) to the stream DOC load. During low-flow periods only groundwater that typically contains small amounts of DOC consistently contributes to the stream. When precipitation occurs,

a distinct high DOC concentration signal from the RZ is able to overprint the low DOC concentration signal in the groundwater during low-flow periods (Broder and Biester, 2015). Since organic matter rich source zones in the top soil layers can only get activated if the groundwater level is close to the surface, we conclude that the event size and antecedent groundwater levels determine whether DOC is dominantly exported by riparian subsurface or surface flow.

To summarize, the TACHyB-model integrates findings from Study 2 that fast runoff generation in the form of surface flux is an important component of the system, which resulted in a satisfying and credible model performance. The depicted internal fluxes evaluation suggests that the model mechanistically works well, which is further supported by the independent validation of (non-calibrated) internal states. This strengthens the assumption that distinct DOC pools are activated under different hydro-climatic conditions, such that export dominantly happens within a short amount of time in order to create the observed chemodynamic DOC concentration enrichment patterns in streams.

4.3.3 On the value of DOC concentration to constrain the model

The DOC signal in streams is generated from the interaction of biogeochemical DOC processing and hydrological mobilization within the different storage units of a catchment. DOC that enters the stream already carries information about state of processing and hydrological connectivity in the riparian zone (Study 1). For example, DOC that comes from locations of high local topographical wetness has a distinctly different signature and export mechanism (surface export) than that from dryer locations (subsurface export; Study 2). Especially higher frequency data is able to disentangle such variable source zone contributions, because it resolves transitions between contributions of storage units that are induced by different hydroclimatic forcing (Study 1). With routinely measured in-stream DOC concentration data becoming more and more available at increasingly higher resolutions, this allows to better distinguish between the functioning of transition states (that are typically difficult to model (Birkel et al., 2017)) and endmember states (warm and dry, cold and wet; Study 1), which in turn enhances verifications of hydrological and biogeochemical modelling approaches. In the TaCHyB-model approach, we tried to make use of this mechanistical coupling to simultaneously calibrate DOC concentration and runoff in the Rappbode stream. To analyze the inherent information content of stream DOC variability, we compared the simultaneous multi-objective calibration (MOC) that was applied in the TACHyB-model with a calibration, where first, only the hydrological module is calibrated, and consecutively to it the biogeochemical module using the parameter set of the initial hydrological calibration. This consecutive single objective calibration (CSOC) exhibited positive KGE_Q values for the calibration and validation period, as well as a high

correlation of the riparian storage with the observed groundwater levels in the RZ, indicating a good mechanistic model representation of the hydrological functioning. However, the respective KGE_{DOC} of the CSOC expressed negative values for calibration and validation. Consequently, resulting DOC concentrations and water fluxes in the riparian storage are unrealistic, indicating that the model is prone to parameter equifinality. In comparison, storage validation of the MOC was correct for hydrology and DOC suggesting correct model functioning, although internal fluxes and states were not calibrated. This highlights the demand for robust and reliable model calibration and validation tools for internal and external fluxes and indicates that predictive hydrological models that happen to be calibrated without any further validation of internal model fluxes (Euser et al., 2013) have to be treated with care.

Overall, the parameterization from models that use a MOC approach with in-stream DOC at high frequency to calibrate hydrological fluxes should be (1) more robust in parameterization than e.g. for monthly or weekly time series and (2) also more finite than from CSOC models.

Chapter V – Summary, Conclusions and Outlook

5.1 Summary

To better understand, predict and ultimately control DOC fluxes from catchments not only is a scientific challenge, but also an important concern in water quality and environmental management. However, transferable mechanistic models of DOC export that are needed to predict future trends in solute export at various catchments have so far been limited by the fact that interactions of DOC with water are complex and appear pretty much ubiquitously in temperate catchments, which demands an understanding of relevant export processes at various scales and locations. Moreover, a generic modeling approach is then required that integrates physically-based, local model mechanisms and scale-independent processes that are valid for the whole catchment, while not being computationally challenging or having heavy input requirements, in order to keep the transferability high. The main objectives of this PhD project therefore were to investigate the hydrological and biogeochemical processes and controls of DOC export from riparian soils to the streams from catchment- and plot-scale (Studies 1 and 2, resp.), and subsequently merge the gained knowledge with the recent understanding of DOC export functioning to create and refine scale-independent mechanistical processes representations for a semi-distributed DOC export model (Study 3).

5.1.1 Investigation of the hydrological and biogeochemical processes and controls of DOC mobilization and export from riparian soils to the streams

The combination of hydrometeorological, in-stream DOC and discharge data analysis with explorative modeling (Study 1) revealed that seasonal-scale, antecedent hydrometeorological parameters aridity index of the preceding 60 days (AI_{60}) and discharge normalized temperature of the preceding 30 days (DNT_{30}) and their interaction are important predictors of in-stream DOC dynamics at the catchment outlet. The conducted top-down analysis (integrated catchment-scale processes) suites to describe endmember behavior during “warm and dry” (dry in terms of non-event) situations when the DOC export is mobilization limited due to a lack of hydrological connectivity, and cold and wet situations when DOC export is limited due to low DOC production rates with concurrent high hydrological mobilization, which keeps DOC concentrations in the generated runoff low. However, AI_{60} and DNT_{30} also suite to explicitly describe the riparian

functioning (like the establishment of hydrological connectivity) at hydrometeorological transition states (“intermediate state”) that typically are conceptualized with higher ambiguity in models, because of the roughly equipotent impact of hydrology and biogeochemistry on DOC export dynamics during such states.

The mobilization and transport of riparian DOC to the stream from the bottom-up perspective (plot-scale riparian mechanisms) has been evaluated with a fully distributed model in Study 2. Results indicate that surface runoff generation from the riparian zone plays a major role for DOC export dynamics of the Rappbode stream, furthermore confirming the hypothesis that riparian DOC export has a dominant impact on total DOC export in the catchment. Here, soil moisture content in the RZ directly controls the timing and magnitude of surface runoff generation, if a threshold value is surpassed (representative of groundwater level reaching to the surface), highlighting that groundwater dynamics constitute a first order control for DOC export dynamics in the Rappbode stream. Moreover, small-scale topography determines where DOC gets mobilized at or near the surface in the RZ. Locations of high local topographic wetness (TWI_{HR}) tend to generate surface runoff prior to locations of low TWI_{HR} . A comparison between DOC in riparian and stream water samples indicates that surface-near DOC from high TWI_{HR} zones gets transported to the stream predominantly during event situations, whereas deep soil layers contribute continuously to the stream DOC signal. Results thus allow to connect different functional zones of terrestrial DOC sources in the RZ with the temporal variability of the stream water DOC signal.

Together with the findings from Study 1 this suggests to accept the hypothesis that (threshold-controlled) small-scale variability in riparian DOC export is reflected in the stream during events that mobilize these variable DOC sources, suggesting that DOC dynamics in the stream have an inherent information content, reflective of the location of its particular riparian source zone as well as the timing of mobilization and state of processing during transport to the catchment outlet. Proxies that explicitly represent the timing and location of variable runoff contributions as a function of soil moisture content within the RZ – like the presented TWI_{HR} or the AI_{60} – thus can potentially be integrated in hydrological models in order to increase their mechanistic process representation.

5.1.2 Adapting a catchment-scale, semi distributed mechanistic model to the recent understanding of DOC export

In Study 3, a tracer-aided coupled hydrological-biogeochemical DOC export model (TACHyB-model) was adjusted based on observations and expert knowledge, i.a. derived from Studies 1 and 2. The main point was to implement justifiable, threshold-controlled, static hillslope- and dynamic riparian

surface flux mechanisms, as well as an exchange flux between groundwater and riparian storage. Since we demonstrated that the in-stream DOC signal already carries information from mobilization, timing and source location in it, we presumed that the strong coupling between hydrology and biogeochemistry in the RZ with respect to generated DOC export is sufficient to perform a multi-objective calibration approach, where in-stream DOC concentration and discharge data are used to simultaneously calibrate the hydrological and biogeochemical modules of the TACHyB-model. Calibration and validation results of Study 3 attest the applied multi-objective calibration (MOC) approach to be valid in terms of internal and external flux realization, suggesting that there is a direct relationship between riparian groundwater dynamics and DOC export, which can be used to reproduce and predict DOC flux variability at the catchment outlet. In contrast, a consecutive single objective calibration (CSOC), where the biogeochemical module is calibrated following the hydrological calibration (thus not utilizing the inherent information content of in-stream DOC to calibrate), produced unrealistic internal water and DOC model fluxes, highlighting that a model does not necessarily produce meaningful results when only the hydrological performance is regarded. We therefore consider the ubiquitously present DOC sources in catchments promising to substitute or complement the application of external tracers in the described semi-distributed model group, if the model correctly conceptualizes the dominant landscape structures and respective export mechanisms.

Since riparian surface runoff contributions make up nearly half of the total DOC export, the RZ as a main source zone for DOC export in headwater catchments could be confirmed. Here, the description of antecedent wetness turned out to be a reliable proxy to estimate soil-moisture related thresholds for surface runoff generation that allowed a robust and mechanistically justifiable parameterization of key DOC export mechanisms in the TACHyB-model. Explicit surface runoff generation mechanisms consequently should be considered in models to adequately capture solute flux dynamics in temperate headwater catchments with overall low riparian tilt. With that adding threshold-based model mechanisms to DOC export models is a promising approach to produce the right answers (DOC export) for the right reasons (plausible internal and external fluxes) as formulated by Kirchner (2006).

5.2 Conclusions and Outlook

This thesis highlights the inherent strong coupling between hydrological and biogeochemical functioning in the riparian zone and catchments in general. The highly multidimensional dataset, compiled at high resolution from a combination of in-situ hydrogeological, hydrological, chemical, topographical, meteorological, and soil physical field measurements, enabled us to analyze riparian

functioning from both top-down and bottom-up perspectives, which ultimately lead to a more holistic understanding of riparian functioning in terms of terrestrial DOC export to streams.

In turn, the presented data-driven approach allowed to derive physically meaningful proxies like the topographical wetness index (TWI) and the antecedent wetness index (AI) that can be used to represent spatiotemporal patterns and thresholds of runoff and DOC export generation in models, while requiring little additional computational cost for calibration. Multidimensionality as well as spatiotemporal resolution of measured geodata will generally increase in the time to come. Therefore it will more and more become our task to disentangle the information content of those datasets from multiple perspectives in order to create a more holistic and integrated picture of the processes in nature. The generated knowledge will allow us to explicitly answer increasingly complex questions with scientific based, “smart” solutions – like the general valid, scalable proxies (TWI_{HR} , AI_{60}) in this study that express timing and location of hydrological and biogeochemical information.

For future studies, validating the presented simultaneous calibration against a conservative, external tracer-based calibration could give additional information on the functioning of the internal, DOC-based calibration approach. Also, implementing additional integral data (e.g. from DOC quality, other solutes, major ions, pH, or heavy metals) should – given they provide complementary mechanistical/process information – further increase the model performance and credibility. To test the applicability and transferability of the TACHyB-model, we propose to evaluate the MOC approach with respect to different catchment types and sizes, as well as climate scenarios. This will in turn allow to directly derive possible management options, e.g. for mitigating climate change induced effects on DOC export behavior.

Analyzing use of already available, multidimensional geodata by an approach as presented in this thesis provides a template on how to improve mechanistical integrity in models. Resulting modeling approaches hence could be superior in answering environmental related model questions that concern multiple catchments.

References

- Ågren, A., Jansson, M., Ivarsson, H., Bishop, K., and Seibert, J.: Seasonal and runoff-related changes in total organic carbon concentrations in the River Öre, Northern Sweden, *Aquatic Sciences*, 70, 21-29, 10.1007/s00027-007-0943-9, 2007.
- Barrow, C. J.: World atlas of desertification (United nations environment programme), edited by N. Middleton and D. S. G. Thomas. Edward Arnold, London, 1992., *Land Degradation and Development*, 4, 249-249 pp., 1992.
- Battin, T. J., Kaplan, L. A., Denis Newbold, J., and Hansen, C. M.: Contributions of microbial biofilms to ecosystem processes in stream mesocosms, *Nature*, 426, 439-442, 10.1038/nature02152, 2003.
- Battin, T. J., Kaplan, L. A., Findlay, S., Hopkinson, C. S., Marti, E., Packman, A. I., Newbold, J. D., and Sabater, F.: Biophysical controls on organic carbon fluxes in fluvial networks, *Nature Geoscience*, 1, 95-100, 10.1038/ngeo101, 2008.
- Berggren, M., and del Giorgio, P. A.: Distinct patterns of microbial metabolism associated to riverine dissolved organic carbon of different source and quality, *Journal of Geophysical Research-Biogeosciences*, 120, 989-999, 10.1002/2015jg002963, 2015.
- Bernhardt, E. S., Blaszczyk, J. R., Ficken, C. D., Fork, M. L., Kaiser, K. E., and Seybold, E. C.: Control Points in Ecosystems: Moving Beyond the Hot Spot Hot Moment Concept, *Ecosystems*, 20, 665-682, 10.1007/s10021-016-0103-y, 2017.
- Beven, K.: Causal models as multiple working hypotheses about environmental processes, *Comptes Rendus Geoscience*, 344, 77-88, 10.1016/j.crte.2012.01.005, 2012.
- Birkel, C., Soulsby, C., and Tetzlaff, D.: Modelling catchment-scale water storage dynamics: reconciling dynamic storage with tracer-inferred passive storage, *Hydrological Processes*, 25, 3924-3936, 10.1002/hyp.8201, 2011.
- Birkel, C., Soulsby, C., and Tetzlaff, D.: Integrating parsimonious models of hydrological connectivity and soil biogeochemistry to simulate stream DOC dynamics, *Journal of Geophysical Research-Biogeosciences*, 119, 1030-1047, 10.1002/2013jg002551, 2014.
- Birkel, C., Broder, T., and Biester, H.: Nonlinear and threshold-dominated runoff generation controls DOC export in a small peat catchment, *Journal of Geophysical Research-Biogeosciences*, 122, 498-513, 10.1002/2016jg003621, 2017.
- Birkel, C., Duvert, C., Correa, A., Munksgaard, N. C., Maher, D. T., and Hutley, L. B.: Tracer-Aided Modeling in the Low-Relief, Wet-Dry Tropics Suggests Water Ages and DOC Export Are Driven by Seasonal Wetlands and Deep Groundwater, *Water Resources Research*, 56, e2019WR026175, 10.1029/2019wr026175, 2020.
- Bishop, K., Seibert, J., Koher, S., and Laudon, H.: Resolving the Double Paradox of rapidly mobilized old water with highly variable responses in runoff chemistry, *Hydrological Processes*, 18, 185-189, 10.1002/hyp.5209, 2004.
- Blank, J., and Deb, K.: Pymoo: Multi-Objective Optimization in Python, *IEEE Access*, 8, 89497-89509, 10.1109/ACCESS.2020.2990567, 2020.
- Broder, T., and Biester, H.: Hydrologic controls on DOC, As and Pb export from a polluted peatland - the importance of heavy rain events, antecedent moisture conditions and hydrological connectivity, *Biogeosciences*, 12, 4651-4664, 10.5194/bg-12-4651-2015, 2015.
- Broder, T., Knorr, K. H., and Biester, H.: Changes in dissolved organic matter quality in a peatland and forest headwater stream as a function of seasonality and hydrologic conditions, *Hydrology and Earth System Sciences*, 21, 2035-2051, 10.5194/hess-21-2035-2017, 2017.

- Chantigny, M. H.: Dissolved and water-extractable organic matter in soils: a review on the influence of land use and management practices, *Geoderma*, 113, 357-380, 10.1016/S0016-7061(02)00370-1, 2003.
- Christ, M. J., and David, M. B.: Temperature and moisture effects on the production of dissolved organic carbon in a Spodosol, *Soil Biology & Biochemistry*, 28, 1191-1199, 10.1016/0038-0717(96)00120-4, 1996.
- Cole, J. J., Prairie, Y. T., Caraco, N. F., McDowell, W. H., Tranvik, L. J., Striegl, R. G., Duarte, C. M., Kortelainen, P., Downing, J. A., Middelburg, J. J., and Melack, J.: Plumbing the global carbon cycle: Integrating inland waters into the terrestrial carbon budget, *Ecosystems*, 10, 171-184, 10.1007/s10021-006-9013-8, 2007.
- Creed, I. F., McKnight, D. M., Pellerin, B. A., Green, M. B., Bergamaschi, B. A., Aiken, G. R., Burns, D. A., Findlay, S. E. G., Shanley, J. B., Striegl, R. G., Aulenbach, B. T., Clow, D. W., Laudon, H., McGlynn, B. L., McGuire, K. J., Smith, R. A., and Stackpoole, S. M.: The river as a chemostat: fresh perspectives on dissolved organic matter flowing down the river continuum, *Canadian Journal of Fisheries and Aquatic Sciences*, 72, 1272-1285, 10.1139/cjfas-2014-0400, 2015.
- Criss, R. E., and Winston, W. E.: Do Nash values have value? Discussion and alternate proposals, *Hydrological Processes*, 22, 2723-2725, 10.1002/hyp.7072, 2008.
- Dawson, J. J. C., Bakewell, C., and Billett, M. F.: Is in-stream processing an important control on spatial changes in carbon fluxes in headwater catchments?, *Science of The Total Environment*, 265, 153-167, 10.1016/s0048-9697(00)00656-2, 2001.
- Deb, K., Pratap, A., Agarwal, S., and Meyarivan, T.: A fast and elitist multiobjective genetic algorithm: NSGA-II, *Ieee Transactions on Evolutionary Computation*, 6, 182-197, 10.1109/4235.996017, 2002.
- Dick, J. J., Tetzlaff, D., Birkel, C., and Soulsby, C.: Modelling landscape controls on dissolved organic carbon sources and fluxes to streams, *Biogeochemistry*, 122, 361-374, 10.1007/s10533-014-0046-3, 2015.
- Euser, T., Winsemius, H. C., Hrachowitz, M., Fenicia, F., Uhlenbrook, S., and Savenije, H. H. G.: A framework to assess the realism of model structures using hydrological signatures, *Hydrology and Earth System Sciences*, 17, 1893-1912, 10.5194/hess-17-1893-2013, 2013.
- Fenicia, F., Savenije, H., Matgen, P., and Pfister, L.: Is the groundwater reservoir linear? Learning from data in hydrological modelling, *Hydrology and Earth System Sciences*, 10, 139-150, 10.5194/hess-10-139-2006, 2006.
- Fenicia, F., Savenije, H. H. G., Matgen, P., and Pfister, L.: A comparison of alternative multiobjective calibration strategies for hydrological modeling, *Water Resources Research*, 43, Artn W03434, 10.1029/2006wr005098, 2007.
- Frei, S., Lischeid, G., and Fleckenstein, J. H.: Effects of micro-topography on surface-subsurface exchange and runoff generation in a virtual riparian wetland - A modeling study, *Advances in Water Resources*, 33, 1388-1401, 10.1016/j.advwatres.2010.07.006, 2010.
- Frei, S., Knorr, K. H., Peiffer, S., and Fleckenstein, J. H.: Surface micro-topography causes hot spots of biogeochemical activity in wetland systems: A virtual modeling experiment, *Journal of Geophysical Research-Biogeosciences*, 117, n/a-n/a, 10.1029/2012jg002012, 2012.
- Futter, M. N., and de Wit, H. A.: Testing seasonal and long-term controls of streamwater DOC using empirical and process-based models, *Sci Total Environ*, 407, 698-707, 10.1016/j.scitotenv.2008.10.002, 2008.
- Gustard, A., and Demuth, S.: Manual on Low-flow Estimation and Prediction, Operational Hydrology Report No. 50, World Meteorological Organization (WMO), 2009.
- Hansen, A. M., Kraus, T. E. C., Pellerin, B. A., Fleck, J. A., Downing, B. D., and Bergamaschi, B. A.: Optical properties of dissolved organic matter (DOM): Effects of biological and photolytic degradation, *Limnology and Oceanography*, 61, 1015-1032, 10.1002/lno.10270, 2016.

- Helms, J. R., Stubbins, A., Ritchie, J. D., Minor, E. C., Kieber, D. J., and Mopper, K.: Absorption spectral slopes and slope ratios as indicators of molecular weight, source, and photobleaching of chromophoric dissolved organic matter, *Limnology and Oceanography*, 53, 955-969, 10.4319/lo.2008.53.3.0955, 2008.
- Hood, E., Gooseff, M. N., and Johnson, S. L.: Changes in the character of stream water dissolved organic carbon during flushing in three small watersheds, Oregon, *Journal of Geophysical Research-Biogeosciences*, 111, 10.1029/2005jg000082, 2006.
- Hope, D., Billett, M. F., and Cresser, M. S.: A review of the export of carbon in river water: fluxes and processes, *Environ Pollut*, 84, 301-324, 10.1016/0269-7491(94)90142-2, 1994.
- Hrachowitz, M., Fovet, O., Ruiz, L., Euser, T., Gharari, S., Nijzink, R., Freer, J., Savenije, H. H. G., and Gascuel-Oudou, C.: Process consistency in models: The importance of system signatures, expert knowledge, and process complexity, *Water Resources Research*, 50, 7445-7469, 10.1002/2014wr015484, 2014.
- Hutchins, R. H. S., Aukes, P., Schiff, S. L., Dittmar, T., Prairie, Y. T., and del Giorgio, P. A.: The Optical, Chemical, and Molecular Dissolved Organic Matter Succession Along a Boreal Soil-Stream-River Continuum, *Journal of Geophysical Research-Biogeosciences*, 122, 2892-2908, 10.1002/2017jg004094, 2017.
- Inamdar, S., Finger, N., Singh, S., Mitchell, M., Levia, D., Bais, H., Scott, D., and McHale, P.: Dissolved organic matter (DOM) concentration and quality in a forested mid-Atlantic watershed, USA, *Biogeochemistry*, 108, 55-76, 10.1007/s10533-011-9572-4, 2011.
- Kaiser, K., and Kalbitz, K.: Cycling downwards - dissolved organic matter in soils, *Soil Biology & Biochemistry*, 52, 29-32, 10.1016/j.soilbio.2012.04.002, 2012.
- Kalbitz, K., Solinger, S., Park, J. H., Michalzik, B., and Matzner, E.: Controls on the dynamics of dissolved organic matter in soils: A review, *Soil Science*, 165, 277-304, 10.1097/00010694-200004000-00001, 2000.
- Kirchner, J. W.: Getting the right answers for the right reasons: Linking measurements, analyses, and models to advance the science of hydrology, *Water Resources Research*, 42, 10.1029/2005wr004362, 2006.
- Kling, H., Fuchs, M., and Paulin, M.: Runoff conditions in the upper Danube basin under an ensemble of climate change scenarios, *Journal of Hydrology*, 424, 264-277, 10.1016/j.jhydrol.2012.01.011, 2012.
- Knoben, W. J. M., Freer, J. E., and Woods, R. A.: Technical note: Inherent benchmark or not? Comparing Nash-Sutcliffe and Kling-Gupta efficiency scores, *Hydrology and Earth System Sciences*, 23, 4323-4331, 10.5194/hess-23-4323-2019, 2019.
- Köhler, S. J., Buffam, I., Laudon, H., and Bishop, K. H.: Climate's control of intra-annual and interannual variability of total organic carbon concentration and flux in two contrasting boreal landscape elements, *Journal of Geophysical Research*, 113, 10.1029/2007jg000629, 2008.
- Köhler, S. J., Buffam, I., Seibert, J., Bishop, K. H., and Laudon, H.: Dynamics of stream water TOC concentrations in a boreal headwater catchment: Controlling factors and implications for climate scenarios, *Journal of Hydrology*, 373, 44-56, 10.1016/j.jhydrol.2009.04.012, 2009.
- Kottek, M., Grieser, J., Beck, C., Rudolf, B., and Rubel, F.: World map of the Koppen-Geiger climate classification updated, *Meteorologische Zeitschrift*, 15, 259-263, 10.1127/0941-2948/2006/0130, 2006.
- Krause, S., Freer, J., Hannah, D. M., Howden, N. J. K., Wagener, T., and Worrall, F.: Catchment similarity concepts for understanding dynamic biogeochemical behaviour of river basins, *Hydrological Processes*, 28, 1554-1560, 10.1002/hyp.10093, 2014.
- LaCroix, R. E., Tfaily, M. M., McCreight, M., Jones, M. E., Spokas, L., and Keiluweit, M.: Shifting mineral and redox controls on carbon cycling in seasonally flooded mineral soils, *Biogeosciences*, 16, 2573-2589, 10.5194/bg-16-2573-2019, 2019.

- Larsen, S., Andersen, T., and Hessen, D. O.: Climate change predicted to cause severe increase of organic carbon in lakes, *Global Change Biology*, 17, 1186-1192, 10.1111/j.1365-2486.2010.02257.x, 2011.
- Laudon, H., Sjöblom, V., Buffam, I., Seibert, J., and Morth, M.: The role of catchment scale and landscape characteristics for runoff generation of boreal streams, *Journal of Hydrology*, 344, 198-209, 10.1016/j.jhydrol.2007.07.010, 2007.
- Ledesma, J. L., Grabs, T., Bishop, K. H., Schiff, S. L., and Kohler, S. J.: Potential for long-term transfer of dissolved organic carbon from riparian zones to streams in boreal catchments, *Glob Chang Biol*, 21, 2963-2979, 10.1111/gcb.12872, 2015.
- Ledesma, J. L., Futter, M. N., Laudon, H., Evans, C. D., and Kohler, S. J.: Boreal forest riparian zones regulate stream sulfate and dissolved organic carbon, *Sci Total Environ*, 560-561, 110-122, 10.1016/j.scitotenv.2016.03.230, 2016.
- Ledesma, J. L. J., Futter, M. N., Blackburn, M., Lidman, F., Grabs, T., Sponseller, R. A., Laudon, H., Bishop, K. H., and Kohler, S. J.: Towards an Improved Conceptualization of Riparian Zones in Boreal Forest Headwaters, *Ecosystems*, 21, 297-315, 10.1007/s10021-017-0149-5, 2018a.
- Ledesma, J. L. J., Kothawala, D. N., Bastviken, P., Maehder, S., Grabs, T., and Futter, M. N.: Stream Dissolved Organic Matter Composition Reflects the Riparian Zone, Not Upslope Soils in Boreal Forest Headwaters, *Water Resources Research*, 54, 3896-3912, 10.1029/2017wr021793, 2018b.
- Ledesma, J. L. J., Ruiz-Perez, G., Lupon, A., Poblador, S., Futter, M. N., Sabater, F., and Bernal, S.: Future changes in the Dominant Source Layer of riparian lateral water fluxes in a subhumid Mediterranean catchment, *Journal of Hydrology*, 595, 126014, 10.1016/j.jhydrol.2021.126014, 2021.
- Lessels, J. S., Tetzlaff, D., Carey, S. K., Smith, P., and Soulsby, C.: A coupled hydrology-biogeochemistry model to simulate dissolved organic carbon exports from a permafrost-influenced catchment, *Hydrological Processes*, 29, 5383-5396, 10.1002/hyp.10566, 2015.
- Lindström, G., Johansson, B., Persson, M., Gardelin, M., and Bergström, S.: Development and test of the distributed HBV-96 hydrological model, *Journal of hydrology*, 201, 272-288, 10.1016/S0022-1694(97)00041-3, 1997.
- Luke, S. H., Luckai, N. J., Burke, J. M., and Prepas, E. E.: Riparian areas in the Canadian boreal forest and linkages with water quality in streams, *Environmental Reviews*, 15, 79-97, 10.1139/A07-001, 2007.
- Matilainen, A., Gjessing, E. T., Lahtinen, T., Hed, L., Bhatnagar, A., and Sillanpää, M.: An overview of the methods used in the characterisation of natural organic matter (NOM) in relation to drinking water treatment, *Chemosphere*, 83, 1431-1442, 10.1016/j.chemosphere.2011.01.018, 2011.
- McGuire, K. J., and McDonnell, J. J.: Hydrological connectivity of hillslopes and streams: Characteristic time scales and nonlinearities, *Water Resources Research*, 46, 10.1029/2010wr009341, 2010.
- Monteith, D. T., Stoddard, J. L., Evans, C. D., de Wit, H. A., Forsius, M., Hogasen, T., Wilander, A., Skjelkvale, B. L., Jeffries, D. S., Vuorenmaa, J., Keller, B., Kopacek, J., and Vesely, J.: Dissolved organic carbon trends resulting from changes in atmospheric deposition chemistry, *Nature*, 450, 537-540, 10.1038/nature06316, 2007.
- Musolff, A., Fleckenstein, J. H., Opitz, M., Buttner, O., Kumar, R., and Tittel, J.: Spatio-temporal controls of dissolved organic carbon stream water concentrations, *Journal of Hydrology*, 566, 205-215, 10.1016/j.jhydrol.2018.09.011, 2018.
- Nash, J. E., and Sutcliffe, J. V.: River flow forecasting through conceptual models part I—A discussion of principles, *Journal of hydrology*, 10, 282-290, 10.1016/0022-1694(70)90255-6, 1970.
- Ojima, D. S., Galvin, K. A., and Turner, B. L.: The Global Impact of Land-Use Change, *Bioscience*, 44, 300-304, 10.2307/1312379, 1994.

- Oldham, C. E., Farrow, D. E., and Peiffer, S.: A generalized Damkohler number for classifying material processing in hydrological systems, *Hydrology and Earth System Sciences*, 17, 1133-1148, 10.5194/hess-17-1133-2013, 2013.
- Pinay, G., Peiffer, S., De Dreuzy, J. R., Krause, S., Hannah, D. M., Fleckenstein, J. H., Sebilo, M., Bishop, K., and Hubert-Moy, L.: Upscaling Nitrogen Removal Capacity from Local Hotspots to Low Stream Orders' Drainage Basins, *Ecosystems*, 18, 1101-1120, 10.1007/s10021-015-9878-5, 2015.
- Pool, S., Vis, M., and Seibert, J.: Evaluating model performance: a non-parametric variant of the Kling-Gupta efficiency, *EGU General Assembly*, 2018, 12053,
- Prairie, Y. T.: Carbocentric limnology: looking back, looking forward, *Canadian Journal of Fisheries and Aquatic Sciences*, 65, 543-548, 10.1139/F08-011, 2008.
- Raeke, J., Lechtenfeld, O. J., Tittel, J., Oosterwoud, M. R., Bornmann, K., and Reemtsma, T.: Linking the mobilization of dissolved organic matter in catchments and its removal in drinking water treatment to its molecular characteristics, *Water Res*, 113, 149-159, 10.1016/j.watres.2017.01.066, 2017.
- Raymond, P. A., Hartmann, J., Lauerwald, R., Sobek, S., McDonald, C., Hoover, M., Butman, D., Striegl, R., Mayorga, E., Humborg, C., Kortelainen, P., Durr, H., Meybeck, M., Ciais, P., and Guth, P.: Global carbon dioxide emissions from inland waters, *Nature*, 503, 355-359, 10.1038/nature12760, 2013.
- Rode, M., Wade, A. J., Cohen, M. J., Hensley, R. T., Bowes, M. J., Kirchner, J. W., Arhonditsis, G. B., Jordan, P., Kronvang, B., Halliday, S. J., Skeffington, R. A., Rozemeijer, J. C., Aubert, A. H., Rinke, K., and Jomaa, S.: Sensors in the Stream: The High-Frequency Wave of the Present, *Environ Sci Technol*, 50, 10297-10307, 10.1021/acs.est.6b02155, 2016.
- Rogelis, M. C., Werner, M., Obregón, N., and Wright, N.: Hydrological model assessment for flood early warning in a tropical high mountain basin, *Hydrology and Earth System Sciences Discussions*, 1-36, 10.5194/hess-2016-30, 2016.
- Sanderman, J., Lohse, K. A., Baldock, J. A., and Amundson, R.: Linking soils and streams: Sources and chemistry of dissolved organic matter in a small coastal watershed, *Water Resources Research*, 45, 10.1029/2008wr006977, 2009.
- Scheliga, B., Tetzlaff, D., Nuetzmann, G., and Soulsby, C.: Assessing runoff generation in riparian wetlands: monitoring groundwater-surface water dynamics at the micro-catchment scale, *Environmental Monitoring and Assessment*, 191, 1-25, 10.1007/s10661-019-7237-2, 2019.
- Seibert, J., Grabs, T., Kohler, S., Laudon, H., Winterdahl, M., and Bishop, K.: Linking soil- and stream-water chemistry based on a Riparian Flow-Concentration Integration Model, *Hydrology and Earth System Sciences*, 13, 2287-2297, 10.5194/hess-13-2287-2009, 2009.
- Seifert, A. G., Roth, V. N., Dittmar, T., Gleixner, G., Breuer, L., Houska, T., and Marxsen, J.: Comparing molecular composition of dissolved organic matter in soil and stream water: Influence of land use and chemical characteristics, *Sci Total Environ*, 571, 142-152, 10.1016/j.scitotenv.2016.07.033, 2016.
- Shen, Y., Chapelle, F. H., Strom, E. W., and Benner, R.: Origins and bioavailability of dissolved organic matter in groundwater, *Biogeochemistry*, 122, 61-78, 10.1007/s10533-014-0029-4, 2015.
- Sherene, T.: Mobility and transport of heavy metals in polluted soil environment, *Biological forum— an international journal*, 2010, 112-121,
- Smith, P., Smith, J., Flynn, H., Killham, K., Rangel-Castro, I., Foereid, B., Aitkenhead, M., Chapman, S., Towers, W., and Bell, J.: ECOSSE: Estimating Carbon in Organic Soils- Sequestration and Emissions, 978075591498 2, 2007.
- Spencer, R. G. M., Butler, K. D., and Aiken, G. R.: Dissolved organic carbon and chromophoric dissolved organic matter properties of rivers in the USA, *Journal of Geophysical Research- Biogeosciences*, 117, n/a-n/a, 10.1029/2011jg001928, 2012.

- Stanley, E. H., Powers, S. M., Lottig, N. R., Buffam, I., and Crawford, J. T.: Contemporary changes in dissolved organic carbon (DOC) in human-dominated rivers: is there a role for DOC management?, *Freshwater Biology*, 57, 26-42, 10.1111/j.1365-2427.2011.02613.x, 2012.
- Strohmeier, S., Knorr, K. H., Reichert, M., Frei, S., Fleckenstein, J. H., Peiffer, S., and Matzner, E.: Concentrations and fluxes of dissolved organic carbon in runoff from a forested catchment: insights from high frequency measurements, *Biogeosciences*, 10, 905-916, 10.5194/bg-10-905-2013, 2013.
- Strohmenger, L., Fovet, O., Hrachowitz, M., Salmon-Monviola, J., and Gascuel-Oudou, C.: Is a simple model based on two mixing reservoirs able to reproduce the intra-annual dynamics of DOC and NO₃ stream concentrations in an agricultural headwater catchment?, *Science of the Total Environment*, 794, 148715, 10.1016/j.scitotenv.2021.148715, 2021.
- Tfaily, M. M., Wilson, R. M., Cooper, W. T., Kostka, J. E., Hanson, P., and Chanton, J. P.: Vertical Stratification of Peat Pore Water Dissolved Organic Matter Composition in a Peat Bog in Northern Minnesota, *Journal of Geophysical Research-Biogeosciences*, 123, 479-494, 10.1002/2017jg004007, 2018.
- Tong, S. T., and Chen, W.: Modeling the relationship between land use and surface water quality, *J Environ Manage*, 66, 377-393, 10.1006/jema.2002.0593, 2002.
- Tunaley, C., Tetzlaff, D., Lessels, J., and Soulsby, C.: Linking high-frequency DOC dynamics to the age of connected water sources, *Water Resources Research*, 52, 5232-5247, 10.1002/2015wr018419, 2016.
- Wagner, S., Fair, J. H., Matt, S., Hosen, J. D., Raymond, P., Saiers, J., Shanley, J. B., Dittmar, T., and Stubbins, A.: Molecular Hysteresis: Hydrologically Driven Changes in Riverine Dissolved Organic Matter Chemistry During a Storm Event, *Journal of Geophysical Research-Biogeosciences*, 124, 759-774, 10.1029/2018jg004817, 2019.
- Weishaar, J. L., Aiken, G. R., Bergamaschi, B. A., Fram, M. S., Fujii, R., and Mopper, K.: Evaluation of specific ultraviolet absorbance as an indicator of the chemical composition and reactivity of dissolved organic carbon, *Environ Sci Technol*, 37, 4702-4708, 10.1021/es030360x, 2003.
- Wen, H., Perdrial, J., Abbott, B. W., Bernal, S., Dupas, R., Godsey, S. E., Harpold, A., Rizzo, D., Underwood, K., Adler, T., Sterle, G., and Li, L.: Temperature controls production but hydrology regulates export of dissolved organic carbon at the catchment scale, *Hydrology and Earth System Sciences*, 24, 945-966, 10.5194/hess-24-945-2020, 2020.
- Whitehead, P. G., Wilby, R. L., Battarbee, R. W., Kernan, M., and Wade, A. J.: A review of the potential impacts of climate change on surface water quality, *Hydrological Sciences Journal-Journal Des Sciences Hydrologiques*, 54, 101-123, 10.1623/hysj.54.1.101, 2009.
- Wilson, H. F., and Xenopoulos, M. A.: Effects of agricultural land use on the composition of fluvial dissolved organic matter, *Nature Geoscience*, 2, 37-41, 10.1038/ngeo391, 2008.
- Wilson, H. F., Saiers, J. E., Raymond, P. A., and Sobczak, W. V.: Hydrologic Drivers and Seasonality of Dissolved Organic Carbon Concentration, Nitrogen Content, Bioavailability, and Export in a Forested New England Stream, *Ecosystems*, 16, 604-616, 10.1007/s10021-013-9635-6, 2013.
- Winterdahl, M., Laudon, H., Lyon, S. W., Pers, C., and Bishop, K.: Sensitivity of stream dissolved organic carbon to temperature and discharge: Implications of future climates, *Journal of Geophysical Research-Biogeosciences*, 121, 126-144, 10.1002/2015jg002922, 2016.
- Wollschläger, U., Attinger, S., Borchardt, D., Brauns, M., Cuntz, M., Dietrich, P., Fleckenstein, J. H., Friese, K., Friesen, J., Harpke, A., Hildebrandt, A., Jäckel, G., Kamjunke, N., Knöller, K., Kögler, S., Kolditz, O., Krieg, R., Kumar, R., Lausch, A., Liess, M., Marx, A., Merz, R., Mueller, C., Musolff, A., Norf, H., Oswald, S. E., Rebmann, C., Reinstorf, F., Rode, M., Rink, K., Rinke, K., Samaniego, L., Vieweg, M., Vogel, H.-J., Weitere, M., Werban, U., Zink, M., and Zacharias, S.: The Bode hydrological observatory: a platform for integrated, interdisciplinary hydro-ecological research within the TERENO Harz/Central German Lowland Observatory, *Environmental Earth Sciences*, 76, 29, 10.1007/s12665-016-6327-5, 2016.

Zarnetske, J. P., Bouda, M., Abbott, B. W., Saiers, J., and Raymond, P. A.: Generality of Hydrologic Transport Limitation of Watershed Organic Carbon Flux Across Ecoregions of the United States, *Geophysical Research Letters*, 45, 11702-11711, 10.1029/2018gl080005, 2018.

Study 1: High-frequency measurements explain quantity and quality of dissolved organic carbon mobilization in a headwater catchment

Status: Published in Biogeosciences (16), 2019, DOI: 10.5194/bg-16-4497-2019

Authors: Benedikt J. Werner, Andreas Musolff, Oliver J. Lechtenfeld, Gerrit H. de Rooij, Marieke R. Oosterwoud, and Jan H. Fleckenstein

BJW, JHF, OJL, AM and GHdR planned and designed the research. MRO carried out parts of the field work and conducted a first version of data processing and analysis. BJW performed the statistical analysis and wrote the paper with contributions from all co-authors.

Own contribution:

- Concept and study design: 70%
- Data acquisition: 50%
- Data analysis: 90%
- Interpretation of the results: 80%
- Preparation of the manuscript: 90%

Biogeosciences, 16, 4497–4516, 2019
<https://doi.org/10.5194/bg-16-4497-2019>
 © Author(s) 2019. This work is distributed under
 the Creative Commons Attribution 4.0 License.



High-frequency measurements explain quantity and quality of dissolved organic carbon mobilization in a headwater catchment

Benedikt J. Werner¹, Andreas Musolff¹, Oliver J. Lechtenfeld², Gerrit H. de Rooij³, Marieke R. Oosterwoud¹, and Jan H. Fleckenstein¹

¹Department of Hydrogeology, Helmholtz Centre for Environmental Research – UFZ, 04318 Leipzig, Germany

²Department of Analytical Chemistry, Research group BioGeoOmics, Helmholtz Centre for Environmental Research – UFZ, 04318 Leipzig, Germany

³Department of Soil System Sciences, Helmholtz Centre for Environmental Research – UFZ, 06120 Halle, Germany

Correspondence: Benedikt J. Werner (benedikt.werner@ufz.de)

Received: 14 May 2019 – Discussion started: 16 May 2019

Revised: 2 September 2019 – Accepted: 23 October 2019 – Published: 28 November 2019

Abstract. Increasing dissolved organic carbon (DOC) concentrations and exports from headwater catchments impact the quality of downstream waters and pose challenges to water supply. The importance of riparian zones for DOC export from catchments in humid, temperate climates has generally been acknowledged, but the hydrological controls and biogeochemical factors that govern mobilization of DOC from riparian zones remain elusive. A high-frequency dataset (15 min resolution for over 1 year) from a headwater catchment in the Harz Mountains (Germany) was analyzed for dominant patterns in DOC concentration (C_{DOC}) and optical DOC quality parameters $S_{\text{UVA}254}$ and $S_{275-295}$ (spectral slope between 275 and 295 nm) on event and seasonal scales. Quality parameters and C_{DOC} systematically changed with increasing fractions of high-frequency quick flow (Q_{hf}) and antecedent hydroclimatic conditions, defined by the following metrics: aridity index (AI_{60}) of the preceding 60 d and the quotient of mean temperature (T_{30}) and mean discharge (Q_{30}) of the preceding 30 d, which we refer to as discharge-normalized temperature (DNT_{30}). Selected statistical multiple linear regression models for the complete time series ($R^2 = 0.72, 0.64$ and 0.65 for C_{DOC} , $S_{\text{UVA}254}$ and $S_{275-295}$, resp.) captured DOC dynamics based on event (Q_{hf} and base-flow) and seasonal-scale predictors (AI_{60} , DNT_{30}). The relative importance of seasonal-scale predictors allowed for the separation of three hydroclimatic states (warm and dry, cold and wet, and intermediate). The specific DOC quality for each state indicates a shift in the activated source zones and highlights the importance of antecedent conditions and their

impact on DOC accumulation and mobilization in the riparian zone. The warm and dry state results in high DOC concentrations during events and low concentrations between events and thus can be seen as mobilization limited, whereas the cold and wet state results in low concentration between and during events due to limited DOC accumulation in the riparian zone. The study demonstrates the considerable value of continuous high-frequency measurements of DOC quality and quantity and its (hydroclimatic) key controlling variables in quantitatively unraveling DOC mobilization in the riparian zone. These variables can be linked to DOC source activation by discharge events and the more seasonal control of DOC production in riparian soils.

1 Introduction

Dissolved organic carbon (DOC) in streams is a significant part of the global carbon cycle (Battin et al., 2009) and plays a vital role as a nutrient for aquatic ecosystems. Riverine exports of DOC from catchments can impair downstream aquatic ecology and water quality (Hruška et al., 2009) with potential implications for the treatment of drinking water from surface water reservoirs (Alarcon-Herrera et al., 1994). The pivotal role of DOC for surface water quality and ecology is not only related to the concentration (C_{DOC}) in the water, but also to the specific chemical composition of DOC, referred to here as DOC quality. For example, DOC quality defines the thermodynamically available energy (Stew-

art and Wetzel, 1981), which in turn affects the growth of microorganisms (Ågren et al., 2008). Consequently, changes in DOC quality could change the patterns of aquatic microbial metabolism resulting in altered ecosystem functioning (Berggren and del Giorgio, 2015). For managing water quality and aquatic ecology in surface waters, it is therefore not only important to understand the drivers and controls of DOC concentration, but also of the associated DOC quality. This study takes a step in this direction.

DOC concentrations in streams were found to be highly variable in time with strong controls being discharge (Zarnetske et al., 2018), climatic conditions (Winterdahl et al., 2016), or at longer timescales the prevailing biogeochemical regime (Musolff et al., 2017). DOC concentration variability is also closely linked to distinct DOC source zones in catchments and their hydrologic connectivity to the stream network (Broder et al., 2015; Birkel et al., 2017). In temperate humid climates most of the riverine DOC export is typically derived from terrestrial sources at or near the terrestrial–aquatic interface (Laudon et al., 2012; Ledesma et al., 2018; Musolff et al., 2018; Zarnetske et al., 2018). More specifically, the riparian zone is seen as a dominant source zone for DOC, defining potential DOC export loads and their temporal patterns (Ledesma et al., 2015; Musolff et al., 2018). In this zone, DOC export is strongly controlled by lateral hydrologic transport through shallow organic-rich soil layers, thus connecting different patches of differently processed DOC pools to the stream. The capacity of the riparian zone to drain and produce discharge and thus export DOC generally increases with the rise of the groundwater table during events. This causes a nonlinear increase in the lateral transmissivity of the riparian soil profile and the resulting subsurface flux to the stream, which has been called the transmissivity feedback mechanism (Bishop et al., 2004; Rodhe, 1989). However, distinct preferential flow paths in the subsurface (Hrachowitz et al., 2016) and at the surface (Frei et al., 2010) can also play a considerable role. The associated DOC export to the streams was found to be mostly transport limited (Zarnetske et al., 2018) with storm events generally generating most of the overall loads exported from catchments (Buffam et al., 2001; Hope et al., 1994). Daily precipitation and amount of discharge were found to be event-scale drivers (Bishop et al., 1990) defining magnitude and timing of DOC export. Strohmeier et al. (2013) therefore pointed at the importance of temporally resolved concentration measurements for accurate load estimates.

In addition to discharge and transport capacity, the biogeochemical regime in the riparian soils, which controls the buildup, size and quality of the exportable DOC pool, was identified as an additional important control for DOC export from catchments (Winterdahl et al., 2016). This buildup of exportable DOC pools in turn is strongly related to the hydroclimatic conditions like temperature and soil moisture content prior to an event (Birkel et al., 2017; Broder et al., 2017; Christ and David, 1996; Garcia-Pausas et al., 2008; Preston

et al., 2011), which to some degree also define the potential for hydrological connectivity and transport during the event (Birkel et al., 2017; Köhler et al., 2009; Shang et al., 2018). On a seasonal scale (roughly 1–3 months) hydroclimatic variables control intra-annual variability of DOC concentration and quality (Ågren et al., 2007; Hope et al., 1994; Köhler et al., 2009) and are hence considered important drivers of seasonal DOC export dynamics (Ågren et al., 2007; Birkel et al., 2014; Köhler et al., 2009; Seibert et al., 2009). In summary, DOC concentration and quality are jointly controlled by the hydrologic conditions during events (defining the timing and magnitude of DOC export) and the antecedent hydroclimatic conditions (defining size and quality of exportable DOC pools in the soil), resulting in a highly dynamic system with processes interacting at timescales ranging from the event scale of hours to days to timescales of seasons. Characterizing and quantifying such a dynamic system requires measurements of DOC concentration and quality at a sufficient temporal resolution. Yet, most studies to date have only focused on temporally aggregated data (Köhler et al., 2008) and the seasonal to annual timescale with little or no consideration of the strong interaction with event-scale variability of DOC quantity and quality (Bishop et al., 1990; Strohmeier et al., 2013).

Recent years have seen significant advances in sensing technologies for high-frequency in situ concentration measurements (Rode et al., 2016; Strohmeier et al., 2013), facilitating the assessment of the highly dynamic DOC delivery to streams (Tunaley et al., 2016). Differences in DOC quality observed during varying runoff conditions have been used to characterize source zone activation in smaller watersheds (Hood et al., 2006; Sanderman et al., 2009). Hence, the combination of high-frequency C_{DOC} measurements with additional spectral and analytical methods to characterize DOC quality (Herzprung et al., 2012; Raeke et al., 2017; Roth et al., 2013) at temporal resolutions capable of capturing the dynamics within hydrologic events provides an opportunity to significantly improve our mechanistic understanding of DOC mobilization, transport, and ultimately export from catchments (Berggren and del Giorgio, 2015; Creed et al., 2015; Köhler et al., 2009; Strohmeier et al., 2013). Broder et al. (2017) jointly evaluated DOC concentration and quality dynamics, but they were limited to hourly event data and data once every 2 weeks between events. Here we see great potential in the systematic analysis of high-frequency data for improving our understanding of the delicate interplay between hydrologic (mobilization and transport) and biogeochemical controls (buildup of exportable DOC pools) from the event to seasonal scales that ultimately control DOC export from catchments. This could also stimulate improvements in the formulation of models for DOC export to streams, which are often constrained in terms of transferability across spatiotemporal scales because of a mismatch between the scales of observations and those of the underlying processes (Zarnetske et al., 2018).

We hypothesize that seasonal- and event-scale DOC quantity and quality dynamics in headwater streams are dominantly controlled by the dynamic interplay between event-scale hydrologic mobilization and transport (delivery to the stream) and inter-event and seasonal biogeochemical processing (exportable DOC pools) in the riparian zone. Furthermore we hypothesize that continuous high-frequency measurements of C_{DOC} and spectral properties can be utilized to identify and quantify the key controls of DOC quantity and quality dynamics. The objectives of this study are (1) to use high-frequency in-stream observations of DOC quantity and quality during different seasons to elucidate the effects of hydroclimatic factors (which include frequency and intensity of rainfall and snowmelt events) on mobilization and export of DOC and (2) to establish a set of key controlling variables that captures important hydrologic, hydroclimatic and biogeochemical characteristics of the system to allow a quantitative assessment of stream DOC quantity and quality during different times of the year.

To this end, a high-frequency dataset on C_{DOC} and DOC quality from a 1st-order stream in central Germany was evaluated in terms of key controlling variables such as discharge, temperature and antecedent wetness conditions. The dominant drivers of seasonal- and event-scale variability of C_{DOC} and quality were extracted and assessed (a) by a correlation analysis of intra-annual variations (seasonal scale ≥ 1 month) and (b) by an analysis of the individual discharge events throughout the year (event scale, hours – days). In a final step (c), these drivers were interpreted mechanistically based on a multiple linear regression analysis covering the entire study period. The identified parameters are discussed with respect to underlying processes and synthesized in a conceptual model of DOC export.

2 Materials and methods

2.1 Study site

Measurements were conducted in a headwater catchment of the Rappbode stream ($51^{\circ}39'22.61''$ N, $10^{\circ}41'53.98''$ E, Fig. 1) located in the Harz Mountains, central Germany. The Rappbode stream flows into a large drinking water reservoir. Downstream of the reservoir it flows into the river Bode and eventually discharges (via the rivers Saale and Elbe) into the North Sea. The investigated part of the catchment has an area of 2.58 km^2 and a drainage density of 2.91 km km^{-2} . The catchment is mainly forested with spruce and pine trees (77 %); the remaining area is covered with grass (11 %) and other vegetation (12 %). Elevation ranges from 540 to 620 m above sea level; the mean topographic slope is 3.9° . The 90th percentile of the topographic wetness index as a measure for the extent of riparian wetlands in the catchment (Musolff et al., 2018) is 8.53 (median 6.77). The geology at this site consists mainly of graywacke, clay schist and di-

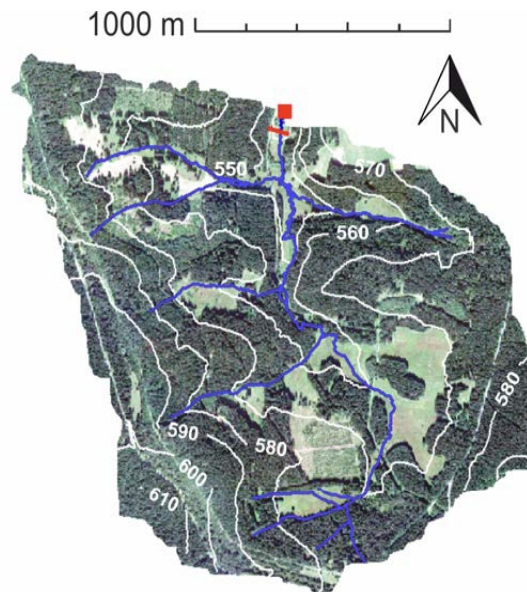


Figure 1. Topography of the Rappbode catchment with the UV-vis and discharge measurements at the outlet (red square). Transect for soil samples indicated by red line. Map data: ©Google, GeoBasis-DE-BKG.

abase (Wollschläger et al., 2016). Soils in the vicinity of the Rappbode spring are dominated by peat. Overall, one-quarter of the catchment is characterized by groundwater-influenced humic Gleysols and stagnic Gleysols, which are mainly found in the riparian zones. Riparian soils were mapped next to the Rappbode stream, 2 km downstream of the spring (Fig. 1). At this site, topsoil layer (A horizon) thickness in a transect was $17.7 \text{ cm} \pm 2.4 \text{ cm}$ on average ($n = 27$) up to 25 m off the stream. The study site has a temperate climate (Kottek et al., 2006), with a long-term mean temperature of 6.0°C and mean annual precipitation of 831 mm (Stiege weather station 12 km away from the study site, data provided by the German Weather Service, DWD).

2.2 Data basis

An overview of all variables utilized for site description and regression modeling as well as descriptive statistics of these variables are given in Table 1.

2.2.1 Monitoring of response variables: DOC concentration and quality

We used in situ absorption spectroscopy to estimate dissolved organic matter quantity and quality. For simplification and because carbon is the main focus of the paper, dissolved organic matter quality will be addressed as DOC quality in the following. DOC quality can be characterized by specific metrics based on the light-absorbing properties of dissolved

Table 1. Descriptive statistics of DOC and hydroclimatic variables; *N* refers to number of measurements; SD – standard deviation; Min – minimum of the measurements; Max – maximum of the measurements; CV – coefficient of variation. Class shows if the variable was utilized as response (*r*) or predictor (*p*) in statistical models.

Variable	Description	Class	<i>N</i>	Mean	SD	Min	Max	Median	CV
C_{DOC} ($mg\ L^{-1}$)	DOC concentration	<i>r</i>	42 427	4.60	1.94	1.49	13.05	4.24	0.42
$SUVA_{254}$ ($L\ m^{-1}\ mg\ C^{-1}$)	Specific UV absorbance at 254 nm	<i>r</i>	42 427	3.93	0.89	0.68	5.44	4.08	0.23
$S_{275-295}$ ($\times 10^{-3}\ nm^{-1}$)	Spectral slope between 275 and 295 nm	<i>r</i>	42 421	13.59	3.76	2.44	19.98	13.42	0.28
Q_{tot} ($m^3\ s^{-1}$)	Total discharge	–	42 427	0.03	0.07	0.002	1.98	0.01	2.81
Specific Q_{tot} (mm)	Specific total discharge	–	42 427	1.16	2.71	0.078	76.74	0.38	2.81
Q_{hr} ($m^3\ s^{-1}$)	High-frequency quick flow	<i>p</i>	39 371*	0.02	0.07	0.0001	1.97	0.002	4.51
Q_b ($m^3\ s^{-1}$)	Low-frequency baseflow	<i>p</i>	41 516*	0.01	0.01	0.002	0.06	0.007	0.91
P (mm d ⁻¹)	Precipitation	–	42 427	2.21	5.62	0.00	55.50	0.00	2.55
T (°C)	Air temperature	–	42 427	9.20	6.96	–11.75	31.77	9.15	0.76
ETP (mm d ⁻¹)	Potential evapotranspiration	–	20 344	3.01	4.99	0.00	25.98	0.35	1.66
$A/60$	Aridity index of the last 60 d	<i>p</i>	17 482	2.73	2.72	0.43	11.33	1.43	1.00
DWT_{30} (°C s m ⁻³)	Discharge normalized temperature of the last 30 d	<i>p</i>	42 427	921.37	919.56	–66.20	3095.86	501.27	1.00
DOC export ($g\ s^{-1}$)	DOC export	–	42 427	0.17	0.67	0.005	18.63	0.04	3.88

* *N* of Q_b and Q_{hr} differs from Q_{tot} due to the applied filtering method for baseflow separation.

organic compounds: $SUVA_{254}$ was calculated by normalizing the spectral absorption coefficient at 254 nm (SAC_{254}) for the corresponding C_{DOC} values. $SUVA_{254}$ correlates well with aromaticity of DOC and therefore can be used as an indicator of the general chemical composition and reactivity of organic carbon (Weishaar et al., 2003). To refine the understanding of DOC composition, the spectral slope between 275 and 295 nm, denoted $S_{275-295}$, was estimated from the adsorption spectra and calculated as described in Helms et al. (2008); a linear regression model was fitted for each time step to the logarithms of the absorption coefficients between 275 and 295 nm to derive the slope $S_{275-295}$. $S_{275-295}$ can help to distinguish between autochthonous and allochthonous DOC, molecular weights and processing (photobleaching and microbial degradation change aromaticity) (Helms et al., 2008). The general patterns of such DOC quality metrics can be used to infer information on origin and properties of DOC and thus to characterize source zones of DOC in riparian zones (Hood et al., 2006; Hutchins et al., 2017; Sanderman et al., 2009). An UV-vis probe (Spectrolyzer, scan Messtechnik GmbH, Austria) was installed in the stream (Fig. 1) from April 2013 to October 2014 to measure light absorption spectra from 220 to 720 nm in 2.5 nm steps every 15 min. There is a data gap from 11 December 2013 to 14 January 2014 due to general maintenance and recalibration of the UV-vis probe in the laboratory. Other gaps from 18 to 27 November 2013 and from 1 to 17 September 2014 were due to a probe failure; accordingly values were excluded a priori. Overall, the UV-vis dataset comprises 42 427 measurements. For a description of fouling correction, on-site probe maintenance and sampling procedure, refer to S1 in the Supplement.

After fouling correction, UV-vis measurements were used to derive C_{DOC} , $SUVA_{254}$ and $S_{275-295}$. For validation and calibration of C_{DOC} and $SUVA_{254}$, 28 grab samples were used that have been taken once every 2 weeks from the stream to measure the specific absorption coefficient at 254 nm (SAC_{254} (UVT P200, Real Tech Inc., Canada). Subsequently, C_{DOC} was measured in the laboratory by thermocatalytic oxidation at 900 °C with nondispersive infrared (NDIR) detection (DIMATOC® 2000, Dimatec Analysentechnik GmbH, Germany). A continuous time series of C_{DOC} from the UV-vis spectra was created using partial least-squares regression (PLSR) to the 28 concentration values via the R package pls (Mevik and Wehrens, 2007). The PLSR proved to robustly work with a large number of predicting variables and strong collinearities (Musolff et al., 2015; Vaughan et al., 2017). The procedure generally followed the method described in Etheridge et al. (2014) using all turbidity-compensated spectra within a single regression model, chosen by 10-fold cross validation of the training dataset. Through this method, C_{DOC} was defined by a local combination of several wavelengths that proved to yield better results than the predefined global settings provided by the probe (Vaughan et al., 2017).

$SUVA_{254}$ was calculated by dividing the spectral absorption coefficient at 254 nm (SAC_{254}) by the PLSR-derived C_{DOC} values. The resulting $SUVA_{254}$ values were then validated (but not calibrated) by the 28 $SUVA_{254}$ values derived from the manual SAC_{254} measurements in the field and the associated lab C_{DOC} measurements (see Sect. 3.1). As a second quality metric $S_{275-295}$ was estimated from the fouling-corrected adsorption spectra as described above and in Helms et al. (2008). There are no laboratory values available to verify $S_{275-295}$ calculations, so calculated values were verified by comparison to the literature.

2.2.2 Predictor variables: stream level and discharge, evapotranspiration, and antecedent wetness condition

Discharge Q_{tot} was calculated from a stage–discharge relationship, which was established based on the 15 min stage readings from a barometrically compensated pressure transducer (Solinst Levelogger, Canada) and manual discharge measurements once every 2 weeks using an electromagnetic flow meter ($n = 42$; MF pro, Ott, Germany).

Manually measured discharge maximum was $0.39 \text{ m}^3 \text{ s}^{-1}$ at a water level of 83.8 cm. Ungauged water levels above this value and the associated discharges were extrapolated from the stage–discharge relationship and found to be within a valid range when comparing to modeled discharge from the mesoscale hydrological model (mHM; Mueller et al., 2016; Samaniego et al., 2010). A hydrograph separation into event and baseflow components was applied following the method described by Gustard and Demuth (2009). Total discharge Q_{tot} was partitioned into a high-frequency quick flow (Q_{hf}) component, active during events, and a low-frequency component representing baseflow (Q_b). To derive the baseflow hydrograph, local flow minima of non-overlapping 5 d periods were selected and linearly connected to each other using the *lfstat* package (Koffler et al., 2016) in R (R-Core-Team, 2017). If the baseflow hydrograph exceeded the actual flow, it was constrained to equal the observed hydrograph of Q_{tot} . Consequently, subtracting the baseflow hydrograph (Q_b) from the total hydrograph of Q_{tot} yields the hydrograph of Q_{hf} , which has positive values during events ($Q_{tot} > Q_b$) and zero values during non-event periods (when $Q_{tot} = Q_b$). All consecutive positive values between two non-event periods (zero values) were considered one event and extracted from the complete dataset for further processing.

To characterize ambient weather conditions, a weather station (WS-GP1, Delta-T, UK) placed about 250 m northwest of the UV-vis probe provided data on air temperature (T), air humidity, wind direction and speed, solar radiation, and rainfall (P) at 30 min intervals. Measurements of the weather station started at 21 May 2013 until 26 November 2014. Measurements were at an hourly interval for the first 5 d, until 26 June 2013.

Potential evapotranspiration (ET_p) was calculated on an hourly basis from the weather data after the Penman–Monteith method (Allen et al., 1998). The antecedent aridity index (AI_t) gives an estimate of the water balance in the last t days and equals the aridity index for longer time periods given by Barrow (1992). Accordingly, AI_{60} was derived for the measurement period by dividing the cumulative sum of precipitation over the last 60 d (P_{60}) by the cumulative sum of ET_p of the last 60 d (ET_{P60}). As a consequence, time series of lumped variables start t days after the actual begin of the field observations.

The discharge-normalized temperature of the preceding 30 d (DNT_{30}) was calculated by dividing the mean air temperature of the preceding 30 d by the mean discharge of the preceding 30 d. DNT_{30} gives an estimate of the ratio between temperature (which controls soil DOC production; e.g., Christ and David, 1996) and discharge (which controls DOC export; e.g., Hope et al., 1994) in the last 30 d and therefore can potentially be related to the state of DOC storage in top soils. We chose AI_{60} and DNT_{30} as these variables turned out to work best in terms of variance inflation and interaction for the statistical modeling.

In order to obtain an analogous dataset, time series of all variables were constrained by excluding such observations that fell into the data gaps of the UV-vis probe (see Sect. 2.2.1).

2.3 Statistical analysis

Evaluation of the variable's predictive power was carried out for the entire dataset as well as for separated discharge events. Descriptive statistical tools were applied using the software R (R-Core-Team, 2017). Spearman's rank correlation was used to look for significant relations of C_{DOC} and DOC quality with potential controlling variables since concentration, discharge and solute loads in river systems usually have lognormal probability distributions while C – Q relationships can be described by power-law functions (Jawitz and Mitchell, 2011; Köhler et al., 2009; Rodríguez-Iturbe et al., 1992; Seibert et al., 2009).

2.3.1 Event-scale analysis

Consequently, concentration–discharge (C – Q) relationships were characterized and quantified in log-log space for the event analysis. Since metrics of DOC quality are typically normally distributed (Guarch-Ribot and Butturini, 2016; Sanderman et al., 2009), relationships between quality and Q_{tot} were analyzed in semi-log space. Corresponding C – Q and quality– Q relationships for each runoff event ($n = 38$, extracted with the method explained in Sect. 2.2.2) were represented by combinations of multiple linear regression models with Q_{tot} , Q_b and Q_{hf} and their log transformations as predictors. As recommended by Marquardt (1970) and Menard (2001), multicollinearity of predictors was taken into

account based on the variance inflation factor (VIF; R package car, Fox and Weisberg, 2011):

$$\text{VIF}_i = \frac{1}{1 - R_i^2} > 10, \quad (1)$$

where VIF_i is the variance inflation factor for every predictor variable i in the complete model, predicted by multiple linear regression from the remaining predictor variables of the complete model. R_i^2 is the corresponding coefficient of determination. Predictor variables were excluded from the model if Eq. (1) holds for predictor variable i .

The best overall combination of two variables for the prediction of events was chosen according to the best mean R^2 of all 38 single models. Hence, independent variable $\log(C_{\text{DOC}})$ is best predicted by a combination of both discharge components ($\log(Q_{\text{hf}})$ and Q_{b}) during single discharge events. Subsequently, the 38 triplets of intercepts and regression coefficients of these single models were extracted for further analysis. Note that the hysteresis loop size did not significantly bias regression coefficients obtained from this method (S2, Fig. S1 in the Supplement).

2.3.2 Seasonal-scale analysis

To explain seasonal variations in the event analysis, the 38 regression coefficient triplets were correlated with seasonal-scale antecedent key controlling variables. Variables which showed strong correlations were added in different combinations to the existing event model as potential predictors for seasonal variations in addition to the event-scale variance. Here, models of the dependent variables (C_{DOC} , $SUVA_{254}$ and $S_{275-295}$) always used the same predictor variables. The interaction between two predictor variables was generally used for modeling. This implies that the measured hydroclimatic variables influence each other and thus cause a non-additive effect on the dependent variable. Here, we write interaction terms as the product between the two interacting variables (variable1 \times variable2). Again, predictors (variables and interaction terms) were tested for multicollinearity and excluded from the complete model if Eq. (1) holds for variable i .

Akaike's information criterion (AIC) and R^2 were used for model selection and validation. The 5-fold cross validation was applied to estimate the prediction error. Once the most valid model was selected, the predictive power of the chosen predictors for the different models of C_{DOC} and DOC quality was tested. Partial models were built by stepwise dropping the least influencing predictors according to AIC and by comparing the subset of event-scale predictors with the subset of seasonal-scale predictors.

3 Results

3.1 Monitoring of DOC and hydroclimatic parameters

The basic statistics of UV-vis-derived C_{DOC} and DOC quality as well as hydroclimatic variables throughout the 1.5-year measurement period are given in Table 1.

The amount of precipitation during 2013 (665 mm) and 2014 (682 mm) was close to the long-term annual mean at the nearest weather station. Discharge shows event-type variability but in general followed the hydrological year, with the lowest values in late summer and highest values in spring (Fig. 2a). The highest discharge was $1.98 \text{ m}^3 \text{ s}^{-1}$ during snowmelt on 27 April 2014. With a coefficient of variation (CV) much higher than 1, the discharge regime can be described as erratic (Botter et al., 2013), indicating the importance of the quick flow component for discharge in the Rappbode catchment. Consequently, the variability of Q_{hf} mostly follows Q_{tot} , but without the seasonal baseflow trends. A total of 38 discharge events have been separated by discharge partitioning, yielding an average frequency of 0.086 d^{-1} (2.58 month^{-1}) at an average duration of 134 h per discharge event. A dry period occurred from 14 June to 23 July 2013, which resulted in a steady decline in discharge during that time (Fig. 2).

Air temperature exhibited strong seasonal patterns and was comparable to the seasonal mean at the nearest station. Daily sums of ET_P peaked in summer whereas ET_P in autumn and winter reached the minimum. The general pattern follows a typical seasonal sinusoidal shape (not shown).

The aridity index AI_{60} (median = 1.43) indicates a general wet climate with higher precipitation than potential evapotranspiration. AI_{60} peaked in winter whereas minimum values occurred in summer during the drought and in winter during the freezing period (Fig. 2b). Summer precipitation has only a small impact on AI_{60} . With a CV of 0.74, ET_{P60} generally has more influence on the variability of AI_{60} than P_{60} (CV = 0.53).

DNT_{30} peaked in summer whereas minimum values occurred in winter (Fig. 2b). Generally, Q_{30} (CV = 0.89) has more influence on the variability of DNT_{30} than T_{30} (CV = 0.53). Precipitation events in cold periods have only a small impact on DNT_{30} , and peaks due to precipitation are barely detectable.

C_{DOC} based on the PLS regression fits well to the DOC concentration measured in the lab ($R^2 = 0.97$, residual standard error: 0.68 mg L^{-1}) (Fig. 2c). The maximum deviation of PLS-based C_{DOC} from lab-measured C_{DOC} was 1.7 mg L^{-1} on 24 July 2013. We argue that the PLSR predicts the average characteristic composition of DOC rather well but hardly accounts for changes in DOC quality and thus spectral properties due to extreme situations like droughts and floods, which can strongly differ in DOC source area mobilization in comparison to average events (Vaughan et al., 2017). Accordingly, C_{DOC} and hence calculated $SUVA_{254}$

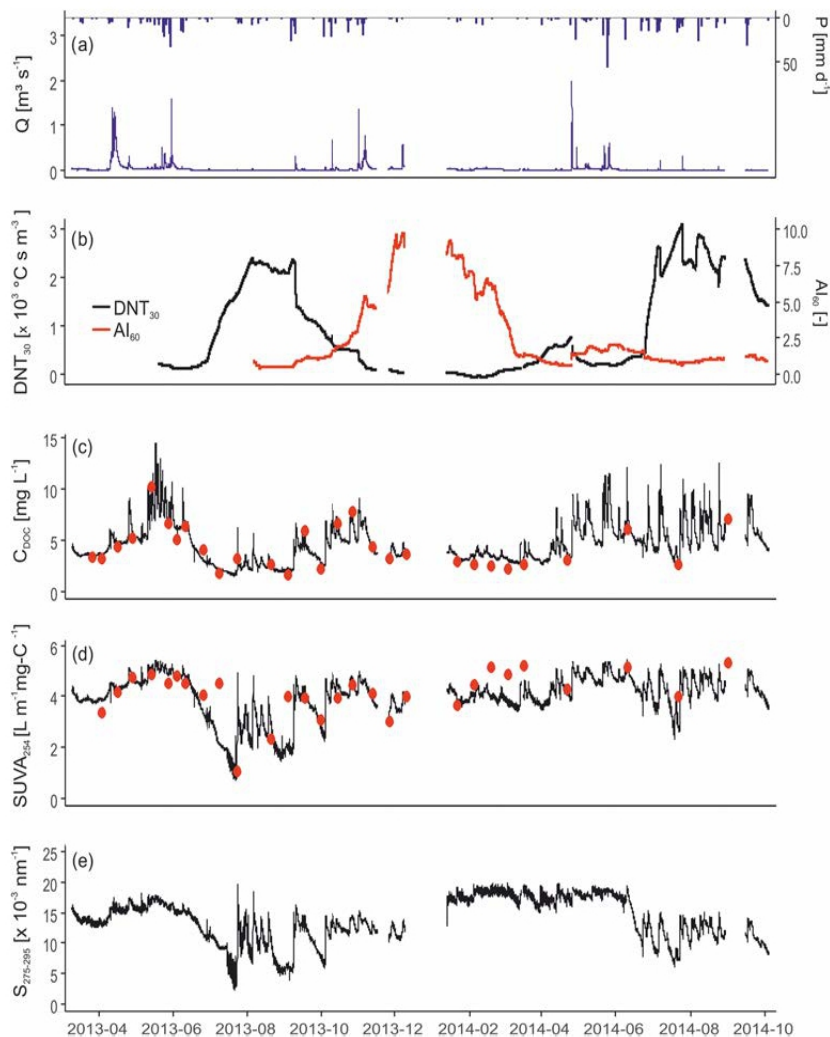


Figure 2. (a) Precipitation and discharge, (b) antecedent hydrometeorological conditions, (c) C_{DOC} , (d) $SUVA_{254}$ and (e) $S_{275-295}$ over the entire measurement period. C_{DOC} in (c) was fitted with PLSR to the measured grab samples (red dots). Grab samples (red dots) in the $SUVA_{254}$ values (d) were just used for validation.

values match the manual measurements to a lesser extent during such situations, leading to an overall R^2 of 0.5 for $SUVA_{254}$ values, but removing three measurements taken during longer dry periods (9 July, 4 September 2013, 23 July 2014) increases overall R^2 to 0.73.

There are no laboratory values available to verify $S_{275-295}$ calculations, but calculated values are of the same magnitude as reported in the literature (Helms et al., 2008; Spencer et al., 2012).

C_{DOC} , $SUVA_{254}$ and $S_{275-295}$ exhibit pronounced event-type variability over the entire year (Fig. 2c–e). In winter months, DOC was low in concentration, but had a distinct quality signature with high $S_{275-295}$ and $SUVA_{254}$ values (Fig. 2c–e). Furthermore, only small fluctuations of concen-

tration and quality were observed in winter. Summer months showed minimum C_{DOC} , $SUVA_{254}$ and $S_{275-295}$ values in both years during baseflow but also the most distinct C_{DOC} and quality variations during discharge events. Late summer and autumn C_{DOC} values were different between 2013 and 2014 with a pronounced temporal variability in 2014 compared to rather small fluctuations in 2013. DOC quality characteristics were similar in autumns of both years, exhibiting an average range compared to the entire measurement period. During events in spring and autumn, $S_{275-295}$ and $SUVA_{254}$ remained at a constant level, indicating the export of DOC of similar composition.

Exported DOC loads (Table 1) peaked during high-discharge events during spring and autumn and closely fol-

low the hydrograph (Fig. S2). Accordingly, the CV of the load is closer to that of the discharge than to the CV of DOC (Table 1). Maximum DOC export was found during the discharge event on 27 April 2014 with rates of up to 18.6 g s^{-1} . Although events in drier summer months show stronger concentration fluctuations, exported loads remain low.

3.2 Correlation analysis

Table 2 gives an overview regarding correlations in the entire dataset. We used Spearman’s rank correlation coefficient (r_s) correlation to determine the direction and strength of relationships between variables. C_{DOC} correlates strongest with $SUVA_{254}$, but r_s between C_{DOC} and $S_{275-295}$ and between $S_{275-295}$ and $SUVA_{254}$ is markedly smaller.

Correlations of Q_{tot} with $S_{275-295}$ are stronger than Q_{tot} with $SUVA_{254}$ and C_{DOC} . In comparison to Q_{tot} , correlations with Q_{hf} are markedly higher for C_{DOC} and $SUVA_{254}$, but lower for $S_{275-295}$. On the other hand, when relating C_{DOC} and metrics of quality to the baseflow fraction of discharge (Q_b), r_s is close to 0 for C_{DOC} and $SUVA_{254}$, but 0.61 for $S_{275-295}$. C_{DOC} and quality further correlate with antecedent discharge, temperature, discharge-normalized temperature (DNT_{30}) and aridity index ($AI_{6,14,60}$). C_{DOC} and $SUVA_{254}$ correlate best with AI_6 , whereas $S_{275-295}$ correlates with T_{30} , Q_{15} , Q_{30} , DNT_{30} and AI_{60} .

3.2.1 Event-scale analysis

High coefficients of determination (R^2) between C_{DOC} and DOC quality metrics with Q_{hf} and in the case of $S_{275-295}$ with Q_b underline the prominent role of discharge and its different timescales in DOC variability. Consequently, quantifying DOC mobilization for a range of individual events may provide information for better understanding direction, shape and strength of $C-Q$ relationships. The analysis of the response of C_{DOC} and DOC quality to discharge events covers 44 % of the entire time series. The relationship between C_{DOC} and Q_{tot} during events resembles a segmented slope in log-log space (Fig. S3a), similar to the $C-Q$ behavior described by Moatar et al. (2017), which inhibits a proper parameterization by the usually applied simple power-law regression. However, when detrending the discharge by baseflow subtraction, the resulting $C_{\text{DOC}}-Q_{\text{hf}}$ relationship is more linear in log-log space (Fig. S3b). This behavior occurs for the event-scale discharge variability of the entire dataset. For DOC quality metrics $SUVA_{254}$ and $S_{275-295}$, we applied a similar model to predict the non-transformed independent variables:

$$Y = a \log(Q_{\text{hf}}) + b Q_b + z, \quad (2)$$

where Y is $\log(C_{\text{DOC}})$, $SUVA_{254}$ or $S_{275-295}$, and a and b are regression coefficients and z is the intercept.

We applied Eq. (2) to 38 individual discharge events. The mean R^2 of all $\log(C_{\text{DOC}})$ models (one model for each dis-

Table 2. Spearman’s rank correlation coefficient (r_s) of possible controlling variables over the entire observation period. Only complete cases were used ($n = 17082$). All correlations are highly significant ($p < 0.001$) because of the large sample size. r_s with absolute values larger than 0.6 printed in bold for better readability. Numerical subscripts of T , Q , AI and DNT indicate how many preceding days were aggregated.

	$SUVA_{254}$	$S_{275-295}$	T	T_{15}	T_{30}	Q_{15}	Q_{30}	AI_6	AI_{14}	AI_{60}	DNT_{30}	Q_{tot}	Q_{hf}	Q_b
C_{DOC}	0.91	0.18	0.23	0.30	0.25	0.10	0.03	0.46	0.29	0.11	0.16	0.22	0.49	-0.08
$SUVA_{254}$		0.50	0.13	0.13	0.05	0.22	0.17	0.44	0.26	0.18	-0.05	0.37	0.59	0.08
$S_{275-295}$			-0.32	-0.53	-0.63	0.58	0.56	0.20	0.22	0.47	-0.66	0.67	0.57	0.61
T				0.70	0.68	-0.46	-0.51	-0.21	-0.35	-0.56	0.64	-0.48	-0.22	-0.61
T_{15}					0.96	-0.60	-0.64	-0.17	-0.39	-0.71	0.85	-0.63	-0.31	-0.79
T_{30}						-0.65	-0.68	-0.15	-0.35	-0.71	0.89	-0.66	-0.34	-0.81
Q_{15}							0.87	0.33	0.66	0.76	0.80	0.57	0.57	0.86
Q_{30}								0.19	0.45	0.81	0.89	0.71	0.49	0.79
AI_6									0.67	0.33	-0.18	0.53	0.60	0.37
AI_{14}										0.62	-0.43	0.64	0.56	0.60
AI_{60}											-0.86	0.47	0.47	0.73
DNT_{30}												-0.73	0.67	-0.86
Q_{tot}													-0.44	0.87
Q_{hf}														0.56

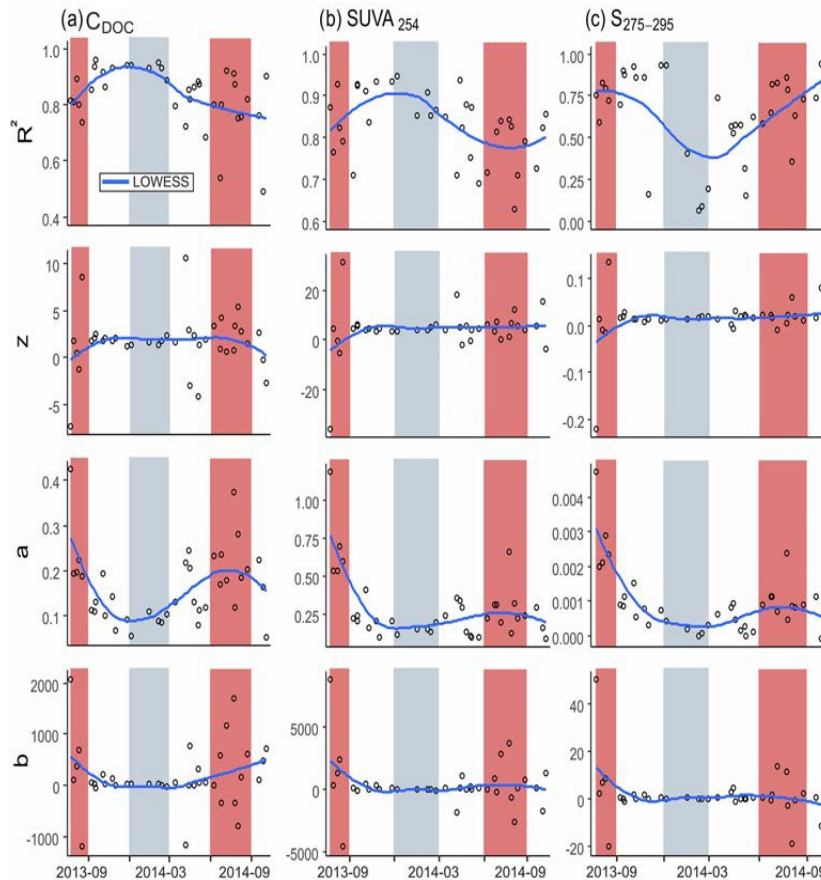


Figure 3. R^2 , intercept z , and regression coefficients a and b of the model predictors $\log(Q_{\text{hf}})$ and Q_b in Eq. (2) of all 38 events plotted against time. The headings in the top of the figure indicate which variable was represented by Y in Eq. (2). Blue lines indicate the locally weighted scatterplot smoothing (LOWESS), background colors indicate seasons (grey: winter; red: summer; white: autumn and spring). Note the different scales of the y axes.

charge event) is $0.84 (\pm 0.15)$. Respective mean R^2 values for $SUVA_{254}$ and $S_{275-295}$ were $0.83 (\pm 0.14)$ and $0.64 (\pm 0.26)$. Performance of the models is always better than a simple linear regression with $\log(Q_{\text{tot}})$ (mean R^2 for $\log(C_{\text{DOC}})$, $SUVA_{254}$ and $S_{275-295}$ is $0.76 (\pm 0.16)$, $0.70 (\pm 0.15)$ and $0.50 (\pm 0.26)$, respectively). R^2 of the models from Eq. (2) varies over time (Fig. 3). Dependent variables $\log(C_{\text{DOC}})$ and $SUVA_{254}$ show a similar behavior with maximum R^2 in autumn and winter and minimal R^2 values in spring and summer (Fig. 3a, b). R^2 values of the $S_{275-295}$ models show a different and less consistent pattern with higher variability between events than C_{DOC} and $SUVA_{254}$ models (Fig. 3c). In comparison to C_{DOC} and $SUVA_{254}$, $S_{275-295}$ values in winter and spring events have a systematically lower R^2 .

Coefficients of C_{DOC} and DOC quality models vary between the events (Fig. 3a–c). Coefficient a (regression coefficient of $\log(Q_{\text{hf}})$) shows low but more systematic variations over time, represented by a smaller CV in compari-

son to z and b (mean $CV_a = 0.76$, mean $CV_z = 2.58$, mean $CV_b = 5.30$ of the C_{DOC} , $SUVA_{254}$ and $S_{275-295}$ models). High a values indicate a stronger increase in C_{DOC} and change in quality of DOC with an increase in Q_{hf} , whereas small a values indicate only little change with increasing Q_{hf} . All three models show a distinct change in a from dry summer to autumn 2013. The summer months generally show the strongest variability in model coefficient, meaning that C_{DOC} and DOC quality reacted strongly and more variable to the comparable small discharge events. Winter months in contrast show the least variability in model coefficient a , indicating a more homogeneous reaction to discharge in this time of the year. Baseflow and intercept model coefficients b and z have a similar, less distinct pattern for all three models with higher parameter variability in summer compared to the other months.

3.2.2 Seasonal-scale analysis

A correlation analysis of the model coefficients a , b and intercept z was performed to identify the variables that explain their temporal dynamics (Table 3). More specifically, we aim to predict a , b and z by hydroclimatic conditions before and during the event represented by the medians of DNT_{30} and different temporal aggregations of AI , T and Q . Again, we rely on Spearman's rank correlation to characterize and quantify the relationships more independent of their shape. Intercept z as well as coefficient b (related to Q_b) do not show any correlation at $p < 0.001$. Regression coefficient a (related to Q_{hf}) shows good correlations ($p < 0.01$) with T_{15} , T_{30} , Q_{30} , AI_{60} and DNT_{30} for all models. But median values of DNT_{30} and AI_{60} are the only variables which show highly significant correlations ($p < 0.001$) with coefficient a for C_{DOC} as well as for the quality metrics models. The strongest increase in C_{DOC} within an event (high a) occurs when AI_{60} is low and DNT_{30} is high, which translates into events during warm and dry low flow situations. On the other hand, during cold and wet high-flow periods (AI_{60} and Q_b high, DNT_{30} low), large events (high Q_{hf}) produce a smaller increase in C_{DOC} . This situation typically occurs during winter.

Based on the highest r_s values in the correlation analysis for the event scale (Table 3), we selected DNT_{30} and AI_{60} as variables to explain seasonal variations in regression coefficient a . The results were used to build a regression model for all available data of C_{DOC} , $SUVA_{254}$ and $S_{275-295}$. We added to the model of Eq. (2) the seasonal-scale AI_{60} and DNT_{30} . In addition we added those interactions for which $VIF < 10$ (Eq. 1): $\log(Q_{hf}) \times Q_b$, $AI_{60} \times DNT_{30}$ and $DNT_{30} \times Q_b$. These two additions allow the model to account for temporal changes in the relationships of C_{DOC} and DOC quality with discharge. Note that we, again, rely on power-law behavior of C_{DOC} but logarithmic (semi-log) behavior for $SUVA_{254}$ and $S_{275-295}$ (above):

$$Y = z + a \log(Q_{hf}) + b Q_b + c AI_{60} + d DNT_{30} + i, \quad (3)$$

where Y represents one of the three dependent variables $\log(C_{DOC})$, $SUVA_{254}$ and $S_{275-295}$. a , b , c and d are regression coefficients, and z is the intercept. i indicates valid interaction terms ($VIF < 10$, Eq. 1) $\log(Q_{hf}) \times Q_b$, $AI_{60} \times DNT_{30}$ and $DNT_{30} \times Q_b$.

The results of the modeling are depicted in Table 4 and Fig. 4. A basic overview of all regression parameters and model statistics is given in Table S1. The C_{DOC} model performs best, explaining most of the overall variance ($R^2 = 0.72 \pm 0.04$ 5-fold cross-validation prediction error), compared to the mean R^2 of 0.84 for modeling single events only. $SUVA_{254}$ and $S_{275-295}$ models explain similar parts (0.64 ± 0.2 and 0.65 ± 0.0) of the overall variance compared to the mean R^2 for the events of 0.83 and 0.64, respectively. All models generally explain both seasonal- and event-scale variability (Fig. 4, R^2 ; see Table S2), but towards small values residuals of the DOC quality models tend to overestimate,

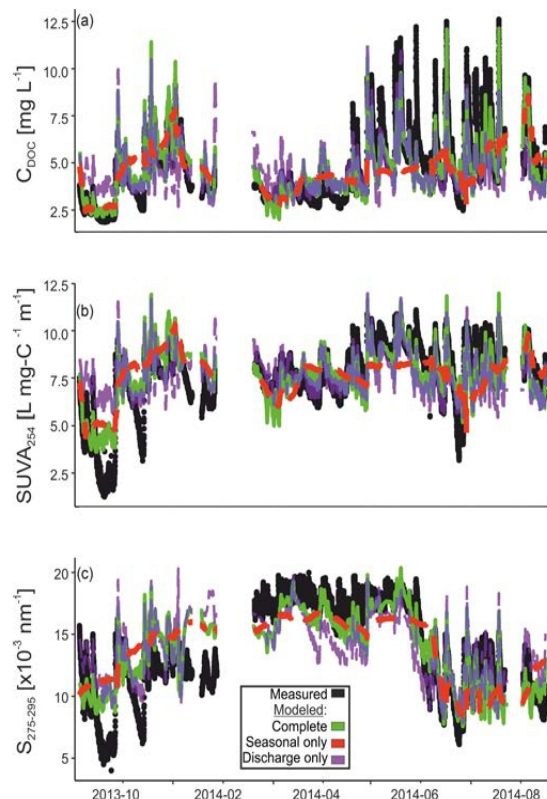


Figure 4. Comparison between measured (black) and multiple regression models of the complete predictors (green) as given by Eq. (3), only seasonal predictors AI_{60} and DNT_{30} plus their interaction (red) and only discharge predictors $\log(Q_{hf})$ and Q_b plus their interaction (purple) for (a) C_{DOC} , (b) $SUVA_{254}$ and (c) $S_{275-295}$ values. Complete and discharge only model were smoothed (5-hourly) for better visualization.

whereas residuals of the C_{DOC} model increase with increasing concentration (Fig. S4). Yet, 95 % of the residuals lie within a range of 1.08 to -0.90 mg L^{-1} , $\pm 0.44 \text{ L m}^{-1} \text{ mg-C}^{-1}$ and $\pm 2.2 \times 10^{-3} \text{ nm}^{-1}$ for the C_{DOC} , $SUVA_{254}$ and $S_{275-295}$ models, respectively.

Inspection of models taking only event-scale predictors ($\log(Q_{hf})$, Q_b and interaction) or only seasonal-scale predictors (AI_{60} , DNT_{30} plus their interaction) into account reveals that both sets of variables can explain a comparable part of the total variance (R^2 event scale: 0.40, 0.36 and 0.47; R^2 seasonal scale: 0.42, 0.36 and 0.48 for the C_{DOC} , $SUVA_{254}$ and $S_{275-295}$ models, respectively). Yet, when only using seasonal-scale drivers (AI_{60} and DNT_{30} plus their interaction), the general trend but no event-type variability is reproduced in the model (Fig. 4). On the other hand, the pure discharge model does not reproduce baseflow and peak height well during the seasons.

For the complete C_{DOC} and $SUVA_{254}$ model, seasonal-scale drivers AI_{60} and DNT_{30} plus their interaction

Table 3. Spearman's rank correlation coefficient (r_s) of the 38 C_{DOC} , $SUVA_{254}$ and $S_{275-295}$ model coefficients with hydroclimatic variables. Asterisks indicate p values (***: <0.001 ; **: <0.01 ; *: <0.05). r_s with absolute values larger than 0.6 are printed in bold.

Model parameters	T_{15}	T_{30}	Q_{15}	Q_{30}	AI_6	AI_{14}	AI_{60}	DNT_{30}	Q_{hf}	Q_b
$z(C_{\text{DOC}})$	0.05	0.05	0.02	-0.02	0.05	0.07	-0.09	0.03	0.15	-0.12
$a(C_{\text{DOC}})$	0.55***	0.52***	-0.48**	-0.43**	-0.52**	-0.65***	-0.66***	0.63***	-0.55***	-0.71***
$b(C_{\text{DOC}})$	0.25	0.25	-0.31	-0.31	-0.19	-0.33*	-0.15	0.32	-0.38*	-0.25
$z(SUVA_{254})$	0.07	0.06	0.04	-0.06	-0.10	0.04	-0.10	0.04	0.01	-0.09
$a(SUVA_{254})$	0.50**	0.51**	-0.50**	-0.40*	-0.42**	-0.56***	-0.64***	0.58***	-0.54***	-0.60***
$b(SUVA_{254})$	0.21	0.18	-0.32	-0.22	-0.10	-0.34*	-0.14	0.25	-0.29	-0.23
$z(S_{275-295})$	0.00	-0.02	0.21	0.11	-0.09	0.23	0.04	-0.10	-0.02	0.07
$a(S_{275-295})$	0.62***	0.63***	-0.54***	-0.41*	-0.28	-0.47**	-0.56***	0.62***	-0.47**	-0.64***
$b(S_{275-295})$	0.13	0.11	-0.31	-0.18	-0.12	-0.45**	-0.14	0.19	-0.20	-0.24

Table 4. Evaluation of the whole dataset model by dropping the least influencing variable according to AIC, starting from the complete models (Eq. 3).

C_{DOC} model	$R^2_{C_{\text{DOC}}}$	$SUVA_{254}$ model	$R^2_{SUVA_{254}}$	$S_{275-295}$ model	$R^2_{S_{275-295}}$
Complete	0.72	Complete	0.64	Complete	0.65
$-\log(Q_{\text{hf}}) \times Q_b$	0.71	$-DNT_{30} \times Q_b$	0.60	$-AI_{60} \times DNT_{30}$	0.65
$-DNT_{30} \times Q_b$	0.69	$-\log(Q_{\text{hf}}) \times Q_b$	0.56	$-\log(Q_{\text{hf}}) \times Q_b$	0.56
$-Q_b$	0.68	$-Q_b$	0.54	$-AI_{60}$	0.54
$-\log(Q_{\text{hf}})$	0.42	$-AI_{60} \times DNT_{30}$	0.35	$-DNT_{30} \times Q_b$	0.53
$-AI_{60} \times DNT_{30}$	0.02	$-DNT_{30}$	0.33	$-Q_b$	0.51
$-DNT_{30}$	0.02	$-AI_{60}$	0.31	$-DNT_{30}$	0.23
$-AI_{60}$	0	$-\log(Q_{\text{hf}})$	0	$-\log(Q_{\text{hf}})$	0

$DNT_{30} \times AI_{60}$ and event-scale driver $\log(Q_{\text{hf}})$ alone are the most important predictors, able to explain 68 % of the total variance for C_{DOC} and 54 % for $SUVA_{254}$ compared to 72 % and 64 % of the respective complete models (Table 4). In contrast to the C_{DOC} and $SUVA_{254}$ models, the interaction of seasonal-scale drivers ($DNT_{30} \times AI_{60}$) barely influences the R^2 of the $S_{275-295}$ model, but it is rather DNT_{30} plus the interaction of $DNT_{30} \times Q_b$ and event-scale hydrological drivers $\log(Q_{\text{hf}})$ and Q_b that alone can explain 54 % of the variance compared to 65 % of the complete model.

Interactions between AI_{60} and DNT_{30} play a crucial role in the C_{DOC} and $SUVA_{254}$ models. There is a small negative effect of increasing soil wetness during low DNT_{30} values and a small negative DNT_{30} effect for dry soils. However, if exposed to increasing AI_{60} values, the effect of medium and high DNT_{30} values changes towards a positive interaction. Hence, when AI_{60} is low and DNT_{30} is high, which typically occurs during the summer months (Fig. 2b) or vice versa in winter, interaction leads to the lowest mean C_{DOC} and $SUVA_{254}$ values during non-precipitation periods (Fig. S5a, b). With medium AI_{60} and DNT_{30} values around autumn and spring, the interaction (Fig. S5c) has a more positive influence on C_{DOC} and $SUVA_{254}$ values, resulting in higher baseflow C_{DOC} and $SUVA_{254}$ values. This interaction can thus

represent the change of regression coefficient a that was observed in the event analysis (Fig. 3). In comparison to the C_{DOC} and $SUVA_{254}$ models, for the $S_{275-295}$ model the interaction of $\log(Q_{\text{hf}})$ with Q_b has direct influence on the time-variant regression coefficient a and thus more influence on the R^2 (Table 4).

There is a positive effect of increasing Q_b at low and medium $\log(Q_{\text{hf}})$ values and a positive $\log(Q_{\text{hf}})$ effect during low Q_b . However, the effect of $\log(Q_{\text{hf}})$ changes towards a negative interaction if exposed to increasing Q_b so that $\log(Q_{\text{hf}})$ barely increases $S_{275-295}$ values during high Q_b situations.

4 Discussion

4.1 Performance of event-scale and complete models

Within 1 year, DOC concentration and quality dynamics fluctuate on event and seasonal scales. The regression models revealed that discharge had a different impact on observed DOC concentration than on observed DOC quality in the Rappbode stream at the seasonal scale (Fig. 3). We found that during summer initial C_{DOC} was low during baseflow while large amounts of DOC were available to be exported

from the riparian soils to the stream during events, leading to high model coefficient a (Fig. 3). Contrarily, the increase in concentration in winter is less pronounced (low model coefficient a , Fig. 3) because there is less DOC available to be washed out. Although the largest amounts of exportable DOC are to be expected at the end of the summer and in early autumn (Clark et al., 2005), C_{DOC} and DOC quality changed most distinctly with the discharge components Q_{hr} and Q_{b} in the summer (Fig. 3). Unfortunately, there were no DOC measurements of the riparian soil water available, which could further elucidate this discrepancy.

The regression models across the entire observed time series (Sect. 3.2.2) utilize event-scale drivers $\log(Q_{\text{hr}})$ and Q_{b} as well as more seasonally driven variables AI_{60} , DNT_{30} and their interactions to explain DOC concentrations and quality variations. We are aware that predictions based on statistical relationships between predictors and DOC responses, which are outside the range of the calibration data (e.g., during extreme droughts and flooding), have to be treated with care. Furthermore, validity and sensitivity of the statistical relationships to the predictors do not account for long-term changes in biogeochemical and hydroclimatic factors but can influence DOC export behavior on its own. Other influences not regarded in this model are the occurrence of chemical compounds like nitrogen (Garcia-Pausas et al., 2008), sulfate, chloride or acid deposition (Futter and de Wit, 2008), which all can impact the available forms, stability and mineralization of carbon in soils. Studying the interactions of DOC with other elements could therefore be useful to add understanding to the actual mobilization and processing mechanisms. But since we measured DOC in the stream, we view DOC as an integrated response signal, already carrying all the information from processing and transformation up to abiotic removal in the riparian zone. Thus, we argue that hydroclimatic and discharge dynamics as chosen here are a 1st-order controls of the DOC dynamics in the stream, represented by a high correlation coefficient (r_s) between hydroclimatic variables and DOC quantity and quality (Table 3) as well as an R^2 of 0.72 for the complete C_{DOC} model. Also, the complete C_{DOC} model represented the observed cumulative DOC export well with a Nash–Sutcliffe efficiency (NSE) of 0.998 throughout the year. Taken by themselves, seasonal-scale drivers ($DNT_{30} + AI_{60} + DNT_{30} \times AI_{60}$) were able to explain the same amount of C_{DOC} variability as hydrological event-scale drivers ($Q_{\text{hr}} + Q_{\text{b}} + Q_{\text{hr}} \times Q_{\text{b}}$). But with an NSE of 0.979 cumulative modeled DOC export from event-scale drivers resembled actual cumulative DOC export much better than seasonal-scale drivers alone (NSE = 0.783), indicating that predictors based on low-frequency measurements alone are not able to explain DOC export as accurately as those derived from higher-frequency measurements. The different export behavior obtained from DOC export modeling based on low- versus high-frequency measurements is most pronounced during events (Fig. S6), which again highlights the importance of high-frequency measurements.

We used an hourly resolution for modeling C_{DOC} and DOC quality ($\sim 17\,000$ values in ~ 1 year). In a low-frequency study, Köhler et al. (2009) took 470 stream water samples in 14 years (based on Köhler et al., 2008). Consequently the DOC concentration variance, which needed to be explained, shifted from a focus on seasonal-scale and inter-annual variations in Köhler et al. (2009) towards highly frequent fluctuations on top of the seasonal-scale shifts and thus a more holistic perspective in the present study. In addition, Köhler et al. (2009) did not analyze the processes which are responsible for the shifts between the models, which had been independently set up for snow-covered, melting and snow-free periods.

Other studies took higher observational frequency into account and added DOC source characterization to better understand the mobilization dynamics: e.g., Broder et al. (2017) and Tunaley et al. (2016) examined event-driven changes in DOC export in a headwater stream, based on highly resolved (15 min to 3 h frequency) events. Like in the present study, both found that antecedent wetness conditions and seasonality are related to DOC dynamics in streams. Both studies provided a qualitative and descriptive assessment only and concluded that a more specific understanding of how DOC gets exported from catchments (Tunaley et al., 2016) might become even more important with respect to future changes in the hydrologic regime due to climate change (Broder et al., 2017). We argue that we need a better quantitative understanding of hydrological and biogeochemical mechanisms and interactions based on time series of different key controlling variables covering all relevant process scales in terms of resolution and length.

Several authors identified seasonality as an important driver for DOC dynamics (Ågren et al., 2007; Broder et al., 2017; Tunaley et al., 2016). However, the term “seasonality” is rather vague and often not clearly defined in terms of its impact on DOC export. This makes its use for a quantitative comparison between catchments and different climates difficult. Therefore we used a set of more easily identifiable, quantitative hydroclimatic variables instead, which reflect the general seasonal dynamics (Table 3) and at the same time allow for a better assessment of the dominant processes for DOC concentration and quality variations.

In summary, we used high-frequency measurements of hydroclimatic variables and their interactions as a proxy representation for seasonality, which allows a more quantitative comparison to other catchments and a more in-depth evaluation of the system.

4.2 Hydroclimatic classification

To estimate how event-scale and seasonal controls interact to produce the observed nonlinear responses of DOC concentrations and quality in our study catchment, we can separate the observation period into three distinct hydroclimatic states. These three discrete system states were chosen to

highlight certain typical scenarios out of a continuum of hydroclimatical conditions, which are based on the seasonal-scale predictors of the complete regression models (Fig. 5): (1) high DNT_{30} and low AI_{60} , representing warm and dry situations mainly found in summer; (2) moderate DNT_{30} and AI_{60} , representing intermediate warm and wet situations, mainly found in spring and autumn; and (3) low DNT_{30} and high AI_{60} , representing cold and wet situations mainly found in winter. To synthesize our modeling results in terms of potential underlying mobilization processes, these three states were compared by looking at both event and non-event responses of DOC concentrations and quality during those states.

Daily mean C_{DOC} , $SUVA_{254}$ and $S_{275-295}$ values of 1.49 mg L^{-1} , $0.68 \text{ L m}^{-1} \text{ mg-C}^{-1}$ and $5.0 \times 10^{-3} \text{ nm}^{-1}$ were minimal at the end of the drought in August 2013, when baseflow levels were low, whereas values of 4.14 mg L^{-1} , $4.05 \text{ L m}^{-1} \text{ mg-C}^{-1}$ and $15.8 \times 10^{-3} \text{ nm}^{-1}$ were measured during phases with higher baseflow levels in the cold and wet state. C_{DOC} , $SUVA_{254}$ and $S_{275-295}$ values showed the strongest increase during warm and dry situations (Fig. 5) also indicated by the highest slopes of regression coefficient a (event-scale models, Fig. 3). Events during the intermediate state also showed elevated C_{DOC} , $SUVA_{254}$ and $S_{275-295}$ values, but in comparison to summer events at a decreased variance and range (Fig. 5). Changes due to events in cold and wet situations were small in range and variance. Variance and mean of $S_{275-295}$ were generally lower during warm and dry situations than during intermediate and cold and wet phases. Therefore we conclude that seasonal-scale hydroclimatical variance controls the overall variance of $S_{275-295}$, whereas C_{DOC} and $SUVA_{254}$ are driven through event-type variance.

4.3 Conceptual model of DOC mobilization from the riparian zone

The relationship between AI_{60} and DNT_{30} in combination with differences in DOC concentration and quality of the three states is of particular interest to support a mechanistic explanation for differing DOC export during events. Hence, these metrics can be utilized for conceptualizing DOC mobilization dynamics of seasonal-scale variations in C_{DOC} and the observed quality–discharge dependencies (Fig. 6).

4.3.1 Warm and dry situations

Warm and dry situations are hydroclimatically defined by high temperatures and low mean discharge (high DNT_{30}), relatively dry soil conditions (low AI_{60}), and low baseflow levels, as typically found in summer when the Rappbode is fed mainly by deeper riparian groundwater. During baseflow conditions highly processed DOC enters the stream via the deeper groundwater flow paths (Broder et al., 2017). DOC in deeper groundwater has usually passed through multiple

soil layers, and its amount and its composition has been altered by sorption and biogeochemical processes (Inamdar et al., 2011; Kaiser and Kalbitz, 2012; Shen et al., 2015). Low $S_{275-295}$ values indicate high molecular weight of DOC with a dominance of terrestrial waters (Helms et al., 2008; Spencer et al., 2012) entering the stream during that time. Precipitation events can get buffered and retarded in the soils (low Q_{hf}) (state warm and dry, Fig. 6). Due to the soil type and generally high groundwater tables in our catchment, soil moisture can remain high, even when there was no rainfall for some time. Yet, lower water contents can increase the mineralization rate compared to (oxygen-free) water-logged soils. However, Kalbitz et al. (2000) and citations therein report a positive correlation between mineralization rate and DOC concentration of the soil solutions. In consequence, DOC production can be higher than mineralization in the unsaturated riparian zone environment (Kalbitz et al., 2000; Luke et al., 2007) leading to a net production of DOC. Hence, favorable conditions for the accumulation of DOC during non-event periods exist in the subsurface due to the lack of moving water in the topsoil, where the high temperatures allow for (microbially driven) riparian DOC net production. To account for the positive balance between DOC removal mechanisms (mineralization, degradation) and DOC production in the riparian soil, we will use the term *net production* in the following.

We argue that the increase in C_{DOC} and change of DOC quality with discharge events is due to the addition of a new, distinct DOC source, located in the shallow riparian soils and connected via transmissivity feedback and preferential flow paths (Fig. S7). Since C_{DOC} during non-event situations was very low (Fig. 5), higher DOC concentrations exported from the topsoils with different quality were able to override the low-flow DOC signal towards a riparian zone signal. DOC quality during events changed markedly towards higher $SUVA_{254}$ values typical for higher aromaticity of the organic matter and associated with processed DOC (Hansen et al., 2016; Helms et al., 2008) and higher $S_{275-295}$ (but not as high as in cold and wet situation) indicating a *relative* increase in low-molecular-weight components in comparison to the low flow signal.

The (de)activation of an additional DOC source with changes in discharge could also explain the observed lower R^2 values in the event analysis during summer (Fig. 3) because in this situation C_{DOC} is not only driven by discharge but an addition of a differing DOC source that is not explained by the hydrological drivers of the event-scale models. The extent of this additional DOC source is determined by antecedent hydroclimatical conditions which favor DOC net production and thus indicate a sensitivity to biogeochemistry-driven DOC export as found by Winterdahl et al. (2016) on top of a general-transport-limited system (Zarnetske et al., 2018). Accordingly, event analysis showed the highest C_{DOC} and DOC quality peaks and revealed the steepest C_{DOC} – Q_{hf} and quality– Q_{hf} relations in summer. Af-

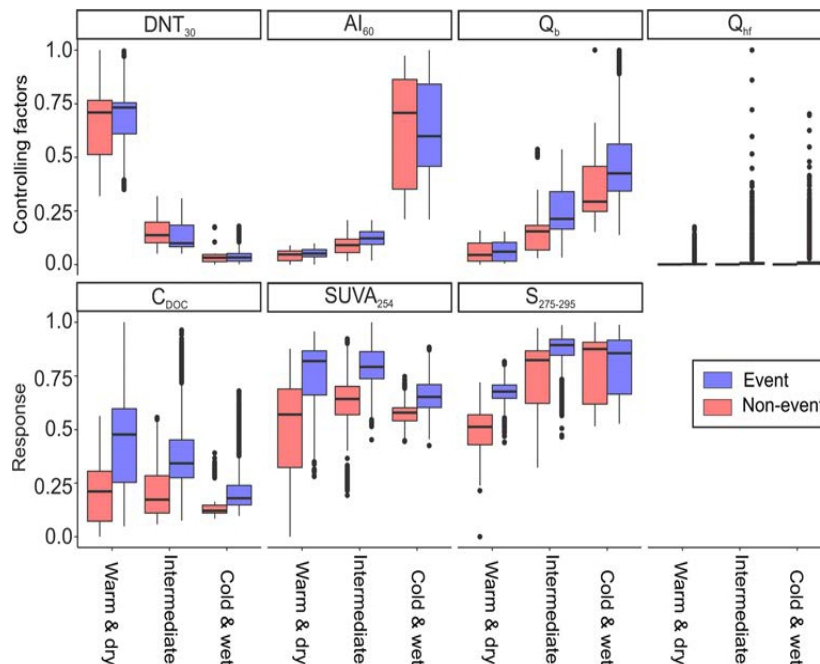


Figure 5. Box plots of hydroclimatic variables (controlling factors) and DOC quantity and quality metrics (response) classified into three hydroclimatic states: (1) warm and dry, (2) intermediate, (3) cold and wet. Red indicates non-event situations, and purple indicates event situations during the according states. Variables were rescaled for better illustration. Particular median C_{DOC} values during non-event situations were 4.13, 3.72 and 3.16 mg L^{-1} for the warm and dry, intermediate, and cold and wet states, respectively. Both warm and dry and intermediate states differ highly significantly (Kruskal–Wallis test, $p < 0.001$) from the cold and wet state.

ter the event, C_{DOC} and DOC quality metrics gradually drop back to the baseflow signal.

In contrast to our findings, Raeke et al. (2017) found higher-molecular-weight molecules at elevated discharge in three temperate catchments (including the one studied here). However, they used grab samples from different hydroclimatic situations and streams, thus potentially masking the event-scale dynamics of DOC mobilization as revealed in the current study. Also, the comparability between spectrophotometry and high-resolution mass spectrometry is questionable for DOC in general (Chen et al., 2016). But also the magnitude of in-stream processing and biodegradation could further influence DOC composition and hence $SUVA_{254}$ and $S_{275-295}$ measurements in stream water (Bernal et al., 2018; Hansen et al., 2016). However, Creed et al. (2015) and Nimick et al. (2011) stated that headwaters in general are dominated by allochthonous carbon with the role of in-stream processing increasing with stream order. Also, the role of in-stream processing at mean residence times below 1 d (which holds for our study site, 2 km downstream of the spring) was found to be minor (Kaplan et al., 2008; Köhler et al., 2002). Note that the wide riparian zone (several tens of meters) in our catchment consists of large parts of a flood plain, leaving only little possibility for leaf litter falling directly into the stream. Therefore, in-stream decomposition and leaf lit-

ter in the stream are likely to be of minor importance on our experimental site.

4.3.2 Intermediate state

Intermediate DNT_{30} and AI_{60} conditions are defined by moderate temperatures and discharge (medium DNT_{30}), precipitation, and evapotranspiration (medium AI_{60}), which results in higher baseflow levels compared to warm and dry conditions. Strong precipitation events translate into a distinct discharge signal (high Q_{hf}) (intermediate state, Fig. 6). Conditions for the accumulation of DOC during non-event periods are less favorable due to colder temperatures than warm and dry periods, decreasing the riparian DOC net production. During baseflow conditions some of the riparian DOC pools are already activated due to a higher groundwater table. This mixing of riparian and deeper groundwater DOC pools translates into intermediate values of concentration and quality parameters, even under non-event conditions.

In case precipitation increases discharge, the DOC signal changes both concentration and quality. This process happens faster than during the warm and dry situation since antecedent wet conditions facilitate DOC mobilization from riparian soils. Hence the temporal shift between DOC and discharge peak diminishes, resulting in higher R^2 values during

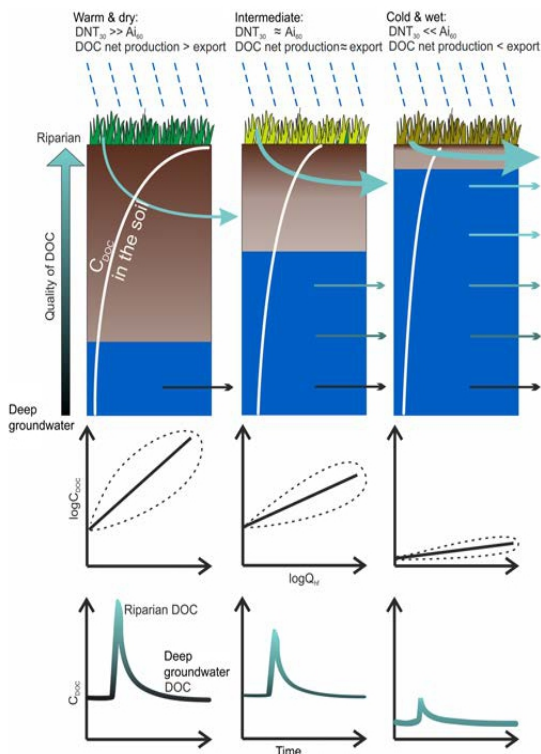


Figure 6. Conceptual model of riparian DOC export from precipitation during the three hydroclimatic states: warm and dry, intermediate, cold and wet. Depth of the soil column is around 0.5 m. Seasonal-scale variations in C_{DOC} in the soil solutions (summer vs. winter) were discussed in Kalbitz et al. (2000). Changing combinations between $SUVA_{254}$ and $S_{275-295}$ values are described as more groundwater-influenced (black) and more riparian-influenced (green) DOC quality. Arrows indicate the export of DOC; colors of the arrows refer to the respective DOC quality. Panels in the middle row show the relation between C_{DOC} and Q_{hr} during the three representative situations. Dashed lines indicate the “dispersion” of the point cloud (according R^2) during the events. Panels in the bottom line indicate the change of C_{DOC} during an event. Corresponding changes of colors indicate more groundwater-influenced (black) and more riparian-influenced (green) DOC quality. Baseflow levels under cold and wet conditions are usually higher than baseflow levels during the warm and dry phase (see Fig. 5). Thus, during the cold and wet situation, higher layers of soil, more enriched in DOC, are activated, but at the same time, there is also a tradeoff between amount of water and available DOC in the respective soil layers which can account for lower overall DOC concentrations.

events (Fig. 3). There was no exhaustion of the exportable DOC by consecutive events, although there is less DOC production paired with more effective export mechanisms, highlighting the large store of DOC in the comparably small riparian zone (Ledesma et al., 2015). The intermediate situation averages multiple situations (transition states in autumn and spring) and thus does not have the character and clarity of

the end-members. Similar quality signals indicate the same process and location of source zone activation in autumn 2013 and 2014. However, concentration peaks developed differently, suggesting that the conditions for antecedent DOC storage and export during preceding phases were different. For example, there were only small mobilization and storage limitations during intermediate DNT_{30} and AI_{60} levels in spring 2014, which translated into pronounced DOC loads exported during events. However, DOC quality, especially $S_{275-295}$, barely changed during these events. Elevated temperatures during this period cause a warming of riparian topsoil, which is rich in organic matter, and hence an increase in biological processing and DOC production. Declining, still high baseflow levels and soil moisture lead to increased DOC production and export during these events.

4.3.3 Cold and wet situations

Cold and wet situations, mainly found in winter, are defined by low temperatures and high mean discharge (low DNT_{30}), humid conditions (high AI_{60}), and high baseflow levels (cold and wet state, Fig. 6). Generally low C_{DOC} values indicate that less DOC mass is available in relation to the generated runoff in the riparian zone in comparison to the warm and dry situations. Unfavorable conditions for the net production of DOC during non-event periods exist in the topsoil, where the low temperature impairs riparian DOC production. Accordingly, low $SUVA_{254}$ and high $S_{275-295}$ values were observed during that period, indicating a relatively higher amount of low-molecular-weight compounds due to reduced DOC processing. Furthermore, high baseflow levels lead to a good hydrological connectivity of DOC sources to the stream during non-event situations.

Precipitation events result in small slopes of the C_{DOC} and quality– Q_{hr} relationships. Dilution due to the impermeability of the frozen soil surface (Laudon et al., 2007) is likely to occur under prolonged periods of temperatures below zero. Since riparian DOC pools are already connected to the stream, we attribute the small shift in DOC quality and C_{DOC} during events to a shift of the contribution (hydrological connection) of DOC source areas with similar DOC quality, rather than to the activation of new, differing DOC pools. The 1st-order hydrological forcing under largely saturated soil conditions could thus explain the high R^2 but low regression coefficient a of the event-scale models of C_{DOC} and $SUVA_{254}$ (Fig. 3) in the cold and wet state. On the other hand, a dominance of hydrological forcing also implies little influence of antecedent biogeochemical conditions during this state (Winterdahl et al., 2016). In contrast to C_{DOC} and $SUVA_{254}$, R^2 of $S_{275-295}$ drops during the cold and wet situation, indicating a decoupling from hydrologic forcing. The dominant hydrological state could be able to leach differing DOC from the riparian zone by shifts in physicochemical equilibria (Shen et al., 2015), thereby forming the corresponding quality. However, this finding needs further research.

The same observations of C_{DOC} and quality interaction during winter and spring (low DOC variance in winter, still low quality variance but strong C_{DOC} fluctuations in spring) were made in 2013. But due to the lack of weather data (the weather station was deployed 2 months after the sensor deployment, which inhibited derivation of AI and DNT for this period), no further statements can be made for this period (Fig. 2).

5 Conclusions

Seasonal- and event-scale DOC quantity and quality dynamics in headwater streams are dominantly controlled by the dynamic interplay between event-scale hydrological mobilization and transport (delivery to the stream) and inter-event and seasonal biogeochemical processing (exportable DOC pools) in the riparian zone. Observing DOC concentration and quality, together with hydroclimatic factors, at high frequency resolves dynamics at the temporal scale of the underlying hydrological and biogeochemical processes, which is unattainable with standard grab-sample monitoring. This allows for an improved, in-depth assessment of DOC export mechanisms as joint measurements of DOC quantity and quality give additional insights into source locations in the riparian zone, DOC processing and mobilization.

Observed DOC concentration, $SUVA_{254}$ and $S_{275-295}$ averaged at 4.06 , $3.93 \text{ L m}^{-1} \text{ mg-C}^{-1}$ and $13.59 \times 10^{-3} \text{ nm}^{-1}$, respectively, but were found to be highly variable in time. The analysis of event-scale variability revealed clear seasonal-scale shifts of the role of discharge in shaping DOC quantity and quality. Overall, the temporal dynamics of DOC concentration and quality can be explained by a few key controlling hydrological variables, which characterize instantaneous discharge, and hydroclimatic metrics, which define the conditions prior to the event.

The hydrological variables (Q_{hf} and Q_{b}) were able to explain 40 %, 36 % and 47 % of the overall variability of C_{DOC} , $SUVA_{254}$ and $S_{275-295}$ and play a crucial role in modeling DOC export. In comparison, seasonal-scale variables (AI_{60} and DNT_{30}) alone are able to explain similar percentages (42 %, 36 % and 48 % for C_{DOC} , $SUVA_{254}$ and $S_{275-295}$) of the overall variability of DOC quantity and quality but lack in adequately predicting exported DOC loads. Combining both sets of variables, as done in this study, significantly increases the predictive capacity of the overall models (72 %, 64 % and 65 % for C_{DOC} , $SUVA_{254}$ and $S_{275-295}$). Evaluation of the developed statistical models also highlights the importance of interactions between the seasonal-scale antecedent predictors AI_{60} and DNT_{30} for DOC concentration and quality dynamics. AI_{60} describes the potential for mobilizing DOC in riparian soils, whereas DNT_{30} describes the changes in DOC storage by looking at the relationship of DOC production and prior mean export from riparian soils. Hence, the relationship between AI_{60} and DNT_{30} describes the potential for export-

ing DOC from riparian soils and allows us to conceptualize DOC exports under differing hydroclimatic conditions. We found that cold and wet situations (AI_{60} high, DNT_{30} low) are not mobilization limited (high mobilization potential due to wet soils and high baseflow levels) but limited in production and processing (due to low temperatures). High hydrological connectivity leads to low C_{DOC} when the DOC net production is low compared to the DOC export. Here, events do not change the quality signature of the DOC in the stream since all riparian DOC sources had already been connected to the stream before. In contrast, we interpret warm and dry conditions (AI_{60} low, DNT_{30} high) as mainly mobilization-limited situations (drier soils, low baseflow levels). High DOC net production rates (high temperatures) and low hydrological connectivity lead to an accumulation of DOC in the upper soil layers of the riparian zone during non-event situations. Under those baseflow conditions low concentrations of highly processed DOC are exported from deeper soil layers to the stream. Overall, DOC quality varies the most during such warmer dry periods because events change the signature of DOC quality in the stream water by adding freshly processed DOC from upper riparian DOC sources to the older more intensely processed DOC from the underlying baseflow signature.

The findings reported and analyzed here provide a mechanistic explanation of the seasonally changing characteristics of DOC–discharge relationships and therefore can be utilized to infer the spatiotemporal dynamics of DOC origin in riparian zones from the DOC dynamics of headwater streams.

Our interpretation is based on the integrated signal of DOC concentration and quality measured in the stream. Accordingly, it remains partially unresolved, and the explicit processes in the riparian zone are responsible for the measured and conceptualized DOC dynamics in the Rappbode stream. Further research in the riparian zone with its shallow groundwater dynamics is necessary to fully mechanistically explain the explicit spatiotemporal mobilization patterns as well as to identify appropriate molecular markers that can be used to trace DOC from riparian source zones into the stream in order to better understand DOC mobilization processes.

The study demonstrates the considerable value of continuous high-frequency measurements of DOC quality and quantity and their key controlling variables in quantitatively unraveling DOC mobilization in the riparian zone. We believe our approach allows long-term DOC monitoring with a manageable allocation of time and resources as well as a better comparability between catchments of different seasonal characteristics. This study highlights the dependency of DOC export on hydroclimatic factors. Potential impacts of climate change on the amount and quality of exported DOC are therefore likely and should be further investigated.

Data availability. All datasets used in this synthesis are publicly available via the following link:

<https://doi.org/10.4211/hs.e0e6fbc0571149b79b1e75fa44d5c4ab>
(Werner, 2019)

Supplement. The supplement related to this article is available online at: <https://doi.org/10.5194/bg-16-4497-2019-supplement>.

Author contributions. JHF, OJL, AM and GHdR planned and designed the research. MRO carried out parts of the field work and conducted a first version of data processing and analysis. BJW performed the statistical analysis and wrote the paper with contributions from all co-authors.

Competing interests. The authors declare that they have no conflict of interest.

Acknowledgements. Special thanks to Toralf Keller for excellent and steady field work as well as to Wolf von Tümpling for the support in the laboratory.

Financial support. This research has been supported by the Federal Ministry of Education and Research Germany (grant no. BMBF, 02WT1290A).

The article processing charges for this open-access publication were covered by a Research Centre of the Helmholtz Association.

Review statement. This paper was edited by Tom J. Battin and reviewed by four anonymous referees.

References

- Ågren, A., Jansson, M., Ivarsson, H., Bishop, K., and Seibert, J.: Seasonal and runoff-related changes in total organic carbon concentrations in the River Öre, Northern Sweden, *Aquat. Sci.*, 70, 21–29, <https://doi.org/10.1007/s00027-007-0943-9>, 2007.
- Ågren, A., Berggren, M., Laudon, H., and Jansson, M.: Terrestrial export of highly bioavailable carbon from small boreal catchments in spring floods, *Freshwater Biol.*, 53, 964–972, <https://doi.org/10.1111/j.1365-2427.2008.01955.x>, 2008.
- Alarcon-Herrera, M. T., Bewtra, J. K., and Biswas, N.: Seasonal variations in humic substances and their reduction through water treatment processes, *Can. J. Civil Eng.*, 21, 173–179, <https://doi.org/10.1139/094-020>, 1994.
- Allen, R. G., Pereira, L. S., Raes, D., and Smith, M.: Crop evapotranspiration-Guidelines for computing crop water requirements-FAO Irrigation and drainage paper 56, FAO, Rome, Italy, 300 pp., 1998.
- Barrow, C. J.: World atlas of desertification (United nations environment programme), edited by: Middleton, N., Thomas, D. S. G., and Arnold, E., *Land Degrad. Dev.*, 3, 249–249, <https://doi.org/10.1002/ldr.3400030407>, 1992.
- Battin, T. J., Luyssaert, S., Kaplan, L. A., Aufdenkampe, A. K., Richter, A., and Tranvik, L. J.: The boundless carbon cycle, *Nat. Geosci.*, 2, 598–600, <https://doi.org/10.1038/ngeo618>, 2009.
- Berggren, M. and del Giorgio, P. A.: Distinct patterns of microbial metabolism associated to riverine dissolved organic carbon of different source and quality, *J. Geophys. Res.-Biogeo.*, 120, 989–999, <https://doi.org/10.1002/2015jg002963>, 2015.
- Bernal, S., Lupon, A., Catalán, N., Castelar, S., and Martí, E.: Decoupling of dissolved organic matter patterns between stream and riparian groundwater in a headwater forested catchment, *Hydrol. Earth Syst. Sci.*, 22, 1897–1910, <https://doi.org/10.5194/hess-22-1897-2018>, 2018.
- Birkel, C., Soulsby, C., and Tetzlaff, D.: Integrating parsimonious models of hydrological connectivity and soil biogeochemistry to simulate stream DOC dynamics, *J. Geophys. Res.-Biogeo.*, 119, 1030–1047, <https://doi.org/10.1002/2013jg002551>, 2014.
- Birkel, C., Broder, T., and Biester, H.: Nonlinear and threshold-dominated runoff generation controls DOC export in a small peat catchment, *J. Geophys. Res.-Biogeo.*, 122, 498–513, <https://doi.org/10.1002/2016jg003621>, 2017.
- Bishop, K., Seibert, J., Köhler, S., and Laudon, H.: Resolving the Double Paradox of rapidly mobilized old water with highly variable responses in runoff chemistry, *Hydrol. Process.*, 18, 185–189, <https://doi.org/10.1002/hyp.5209>, 2004.
- Bishop, K. H., Grip, H., and O'Neill, A.: The origins of acid runoff in a hillslope during storm events, *J. Hydrol.*, 116, 35–61, [https://doi.org/10.1016/0022-1694\(90\)90114-d](https://doi.org/10.1016/0022-1694(90)90114-d), 1990.
- Botter, G., Basso, S., Rodriguez-Iturbe, I., and Rinaldo, A.: Resilience of river flow regimes, *P. Natl. Acad. Sci.*, 110, 12925–12930, <https://doi.org/10.1073/pnas.1311920110>, 2013.
- Broder, T., Knorr, K. H., and Biester, H.: Changes in dissolved organic matter quality in a peatland and forest headwater stream as a function of seasonality and hydrologic conditions, *Hydrol. Earth Syst. Sci.*, 21, 2035–2051, <https://doi.org/10.5194/hess-21-2035-2017>, 2017.
- Buffam, I., Galloway, J. N., Blum, L. K., and McGlathery, K. J.: A stormflow/baseflow comparison of dissolved organic matter concentrations and bioavailability in an Appalachian stream, *Biogeochemistry*, 53, 269–306, <https://doi.org/10.1023/a:1010643432253>, 2001.
- Chen, M., Kim, S., Park, J. E., Jung, H. J., and Hur, J.: Structural and compositional changes of dissolved organic matter upon solid-phase extraction tracked by multiple analytical tools, *Anal. Bioanal. Chem.*, 408, 6249–6258, <https://doi.org/10.1007/s00216-016-9728-0>, 2016.
- Christ, M. J. and David, M. B.: Temperature and moisture effects on the production of dissolved organic carbon in a Spodosol, *Soil Biol. Biochem.*, 28, 1191–1199, [https://doi.org/10.1016/0038-0717\(96\)00120-4](https://doi.org/10.1016/0038-0717(96)00120-4), 1996.
- Clark, J. M., Chapman, P. J., Adamson, J. K., and Lane, S. N.: Influence of drought-induced acidification on the mobility of dissolved organic carbon in peat soils, *Glob. Change Biol.*, 11, 791–809, <https://doi.org/10.1111/j.1365-2486.2005.00937.x>, 2005.
- Creed, I. F., McKnight, D. M., Pellerin, B., Green, M. B., Bergamaschi, B., Aiken, G. R., Burns, D. A., Findlay, S. E. G., Shanley, J. B., Striegl, R. G., Aulenbach, B. T., Clow, D. W., Laudon, H., McGlynn, B. L., McGuire, K. J., Smith, R. A., and Stackpole, T. J.: Controls on the export of dissolved organic carbon from a large, forested catchment, *Hydrol. Earth Syst. Sci.*, 21, 2035–2051, <https://doi.org/10.5194/hess-21-2035-2017>, 2017.

- S. M.: The river as a chemostat: fresh perspectives on dissolved organic matter flowing down the river continuum, *Can. J. Fish. Aquat. Sci.*, 72, 1272–1285, <https://doi.org/10.1139/cjfas-2014-0400>, 2015.
- Etheridge, J. R., Birgand, F., Osborne, J. A., Osburn, C. L., Burchell, M. R., and Irving, J.: Using in situ ultraviolet-visual spectroscopy to measure nitrogen, carbon, phosphorus, and suspended solids concentrations at a high frequency in a brackish tidal marsh, *Limnol. Oceanogr.-Method.*, 12, 10–22, <https://doi.org/10.4319/lom.2014.12.10>, 2014.
- Fox, J. and Weisberg, S.: *An R Companion to Applied Regression*, Sage, 608 pp., 2011.
- Frei, S., Lischeid, G., and Fleckenstein, J. H.: Effects of micro-topography on surface–subsurface exchange and runoff generation in a virtual riparian wetland – A modeling study, *Adv. Water Resour.*, 33, 1388–1401, <https://doi.org/10.1016/j.advwatres.2010.07.006>, 2010.
- Futter, M. N. and de Wit, H. A.: Testing seasonal and long-term controls of streamwater DOC using empirical and process-based models, *Sci. Total Environ.*, 407, 698–707, <https://doi.org/10.1016/j.scitotenv.2008.10.002>, 2008.
- García-Pausas, J., Casals, P., Camarero, L., Hugué, C., Thompson, R., Sebastià, M.-T., and Romanya, J.: Factors regulating carbon mineralization in the surface and subsurface soils of Pyrenean mountain grasslands, *Soil Biol. Biochem.*, 40, 2803–2810, <https://doi.org/10.1016/j.soilbio.2008.08.001>, 2008.
- Guarch-Ribot, A. and Butturini, A.: Hydrological conditions regulate dissolved organic matter quality in an intermittent headwater stream. From drought to storm analysis, *Sci. Total Environ.*, 571, 1358–1369, <https://doi.org/10.1016/j.scitotenv.2016.07.060>, 2016.
- Gustard, A. and Demuth, S.: *Manual on Low-flow Estimation and Prediction*, World Meteorological Organization (WMO), 136 pp., 2009.
- Hansen, A. M., Kraus, T. E. C., Pellerin, B. A., Fleck, J. A., Downing, B. D., and Bergamaschi, B. A.: Optical properties of dissolved organic matter (DOM): Effects of biological and photolytic degradation, *Limnol. Oceanogr.*, 61, 1015–1032, <https://doi.org/10.1002/lno.10270>, 2016.
- Helms, J. R., Stubbins, A., Ritchie, J. D., Minor, E. C., Kieber, D. J., and Mopper, K.: Absorption spectral slopes and slope ratios as indicators of molecular weight, source, and photobleaching of chromophoric dissolved organic matter, *Limnol. Oceanogr.*, 53, 955–969, <https://doi.org/10.4319/lno.2008.53.3.0955>, 2008.
- Herzprung, P., von Tumpling, W., Hertkorn, N., Harir, M., Butner, O., Bravidor, J., Friese, K., and Schmitt-Kopplin, P.: Variations of DOM quality in inflows of a drinking water reservoir: linking of van Krevelen diagrams with EEMF spectra by rank correlation, *Environ. Sci. Technol.*, 46, 5511–5518, <https://doi.org/10.1021/es300345c>, 2012.
- Hood, E., Gooseff, M. N., and Johnson, S. L.: Changes in the character of stream water dissolved organic carbon during flushing in three small watersheds, Oregon, *J. Geophys. Res.-Biogeo.*, 111, G01007, <https://doi.org/10.1029/2005jg000082>, 2006.
- Hope, D., Billett, M. F., and Cresser, M. S.: A review of the export of carbon in river water: Fluxes and processes, *Environ. Pollut.*, 84, 301–324, [https://doi.org/10.1016/0269-7491\(94\)90142-2](https://doi.org/10.1016/0269-7491(94)90142-2), 1994.
- Hrachowitz, M., Benettin, P., van Breukelen, B. M., Fovet, O., Howden, N. J. K., Ruiz, L., van der Velde, Y., and Wade, A. J.: Transit times—the link between hydrology and water quality at the catchment scale, *Wiley Interdisciplinary Reviews: Water*, 3, 629–657, <https://doi.org/10.1002/wat2.1155>, 2016.
- Hruška, J., Krám, P., McDowell, W. H., and Oulehle, F.: Increased Dissolved Organic Carbon (DOC) in Central European Streams is Driven by Reductions in Ionic Strength Rather than Climate Change or Decreasing Acidity, *Environ. Sci. Technol.*, 43, 4320–4326, <https://doi.org/10.1021/es803645w>, 2009.
- Hutchins, R. H. S., Aukes, P., Schiff, S. L., Dittmar, T., Prairie, Y. T., and del Giorgio, P. A.: The Optical, Chemical, and Molecular Dissolved Organic Matter Succession Along a Boreal Soil-Stream-River Continuum, *J. Geophys. Res.-Biogeo.*, 122, 2892–2908, <https://doi.org/10.1002/2017jg004094>, 2017.
- Inamdar, S., Finger, N., Singh, S., Mitchell, M., Levia, D., Bais, H., Scott, D., and McHale, P.: Dissolved organic matter (DOM) concentration and quality in a forested mid-Atlantic watershed, USA, *Biogeochemistry*, 108, 55–76, <https://doi.org/10.1007/s10533-011-9572-4>, 2011.
- Jawitz, J. W. and Mitchell, J.: Temporal inequality in catchment discharge and solute export, *Water Resour. Res.*, 47, W00J14, <https://doi.org/10.1029/2010WR010197>, 2011.
- Kaiser, K. and Kalbitz, K.: Cycling downwards – dissolved organic matter in soils, *Soil Biol. Biochem.*, 52, 29–32, <https://doi.org/10.1016/j.soilbio.2012.04.002>, 2012.
- Kalbitz, K., Solinger, S., Park, J.-H., Michalzik, B., and Matzner, E.: Controls on the dynamics of dissolved organic matter in soils: a review, *Soil Sci.*, 165, 277–304, 2000.
- Kaplan, L. A., Wiegner, T. N., Newbold, J. D., Ostrom, P. H., and Gandhi, H.: Untangling the complex issue of dissolved organic carbon uptake: a stable isotope approach, *Freshwater Biol.*, 53, 855–864, <https://doi.org/10.1111/j.1365-2427.2007.01941.x>, 2008.
- Koffler, D., Gauster, T., and Laaha, G.: *lfstat: Calculation of Low Flow Statistics for Daily Stream Flow Data*, R package version 0.9.4, 2016.
- Köhler, S., Buffam, I., Jonsson, A., and Bishop, K.: Photochemical and microbial processing of stream and soil water dissolved organic matter in a boreal forested catchment in northern Sweden, *Aquat. Sci.*, 64, 269–281, <https://doi.org/10.1007/s00027-002-8071-z>, 2002.
- Köhler, S. J., Buffam, I., Laudon, H., and Bishop, K. H.: Climate’s control of intra-annual and interannual variability of total organic carbon concentration and flux in two contrasting boreal landscape elements, *J. Geophys. Res.*, 113, G03012, <https://doi.org/10.1029/2007jg000629>, 2008.
- Köhler, S. J., Buffam, I., Seibert, J., Bishop, K. H., and Laudon, H.: Dynamics of stream water TOC concentrations in a boreal headwater catchment: Controlling factors and implications for climate scenarios, *J. Hydrol.*, 373, 44–56, <https://doi.org/10.1016/j.jhydrol.2009.04.012>, 2009.
- Kotteck, M., Grieser, J., Beck, C., Rudolf, B., and Rubel, F.: World Map of the Köppen-Geiger climate classification updated, *Meteorol. Z.*, 15, 259–263, <https://doi.org/10.1127/0941-2948/2006/0130>, 2006.
- Laudon, H., Sjöblom, V., Buffam, I., Seibert, J., and Mörth, M.: The role of catchment scale and landscape characteristics for runoff generation of boreal streams, *J. Hydrol.*, 344, 198–209, <https://doi.org/10.1016/j.jhydrol.2007.07.010>, 2007.

- Laudon, H., Buttle, J., Carey, S. K., McDonnell, J., McGuire, K., Seibert, J., Shanley, J., Soulsby, C., and Tetzlaff, D.: Cross-regional prediction of long-term trajectory of stream water DOC response to climate change, *Geophys. Res. Lett.*, 39, L18404, <https://doi.org/10.1029/2012gl053033>, 2012.
- Ledesma, J. L., Grabs, T., Bishop, K. H., Schiff, S. L., and Kohler, S. J.: Potential for long-term transfer of dissolved organic carbon from riparian zones to streams in boreal catchments, *Glob. Change Biol.*, 21, 2963–2979, <https://doi.org/10.1111/gcb.12872>, 2015.
- Ledesma, J. L. J., Kothawala, D. N., Bastviken, P., Maehder, S., Grabs, T., and Futter, M. N.: Stream Dissolved Organic Matter Composition Reflects the Riparian Zone. Not Upslope Soils in Boreal Forest Headwaters, *Water Resour. Res.*, 54, 3896–3912, <https://doi.org/10.1029/2017WR021793>, 2018.
- Luke, S. H., Luckai, N. J., Burke, J. M., and Prepas, E. E.: Riparian areas in the Canadian boreal forest and linkages with water quality in streams, *Environ. Rev.*, 15, 79–97, <https://doi.org/10.1139/A07-001>, 2007.
- Marquardt, D. W.: Generalized Inverses, Ridge Regression, Biased Linear Estimation, and Nonlinear Estimation, *Technometrics*, 12, 591–612, <https://doi.org/10.2307/1267205>, 1970.
- Menard, S.: Applied logistic regression analysis, SAGE publications, 128 pp., 2001.
- Mevik, B.-H. and Wehrens, R.: The pls Package: Principal Component and Partial Least Squares Regression in R, *J. Stat. Softw.*, 18, 128 pp., <https://doi.org/10.18637/jss.v018.i02>, 2007.
- Moatar, F., Abbott, B. W., Minaudo, C., Curie, F., and Pinay, G.: Elemental properties, hydrology, and biology interact to shape concentration-discharge curves for carbon, nutrients, sediment, and major ions, *Water Resour. Res.*, 53, 1270–1287, <https://doi.org/10.1002/2016wr019635>, 2017.
- Mueller, C., Zink, M., Samaniego, L., Krieg, R., Merz, R., Rode, M., and Knöller, K.: Discharge Driven Nitrogen Dynamics in a Mesoscale River Basin As Constrained by Stable Isotope Patterns, *Environ. Sci. Technol.*, 50, 9187–9196, <https://doi.org/10.1021/acs.est.6b01057>, 2016.
- Musolff, A., Schmidt, C., Selle, B., and Fleckenstein, J. H.: Catchment controls on solute export, *Adv. Water Resour.*, 86, 133–146, <https://doi.org/10.1016/j.advwatres.2015.09.026>, 2015.
- Musolff, A., Selle, B., Büttner, O., Opitz, M., and Tittel, J.: Unexpected release of phosphate and organic carbon to streams linked to declining nitrogen depositions, *Glob. Change Biol.*, 23, 1891–1901, <https://doi.org/10.1111/gcb.13498>, 2017.
- Musolff, A., Fleckenstein, J. H., Opitz, M., Büttner, O., Kumar, R., and Tittel, J.: Spatio-temporal controls of dissolved organic carbon stream water concentrations, *J. Hydrol.*, 566, 205–215, <https://doi.org/10.1016/j.jhydrol.2018.09.011>, 2018.
- Nimick, D. A., Gammons, C. H., and Parker, S. R.: Diel biogeochemical processes and their effect on the aqueous chemistry of streams: A review, *Chem. Geol.*, 283, 3–17, <https://doi.org/10.1016/j.chemgeo.2010.08.017>, 2011.
- Preston, M. D., Eimers, M. C., and Watmough, S. A.: Effect of moisture and temperature variation on DOC release from a peatland: Conflicting results from laboratory, field and historical data analysis, *Sci. Total Environ.*, 409, 1235–1242, <https://doi.org/10.1016/j.scitotenv.2010.12.027>, 2011.
- Raeke, J., Lechtenfeld, O. J., Tittel, J., Oosterwoud, M. R., Bornmann, K., and Reemtsma, T.: Linking the mobilization of dissolved organic matter in catchments and its removal in drinking water treatment to its molecular characteristics, *Water Res.*, 113, 149–159, <https://doi.org/10.1016/j.watres.2017.01.066>, 2017.
- R-Core-Team: R: A Language and Environment for Statistical Computing, R Foundation for Statistical Computing, 2017.
- Rode, M., Wade, A. J., Cohen, M. J., Hensley, R. T., Bowes, M. J., Kirchner, J. W., Arhonditsis, G. B., Jordan, P., Kronvang, B., Halliday, S. J., Skeffington, R. A., Rozemeijer, J. C., Aubert, A. H., Rinke, K., and Jomaa, S.: Sensors in the Stream: The High-Frequency Wave of the Present, *Environ. Sci. Technol.*, 50, 10297–10307, <https://doi.org/10.1021/acs.est.6b02155>, 2016.
- Rodhe, A.: On the Generation of Stream Runoff in Till Soils: Paper presented at the Nordic Hydrological Conference (Rovaniemi, Finland, August – 1988), *Hydrol. Res.*, 20, 1–8, <https://doi.org/10.2166/nh.1989.0001>, 1989.
- Rodríguez-Iturbe, I., Ijász-Vásquez, E. J., Bras, R. L., and Tarboton, D. G.: Power law distributions of discharge mass and energy in river basins, *Water Resour. Res.*, 28, 1089–1093, <https://doi.org/10.1029/91WR03033>, 1992.
- Roth, V.-N., Dittmar, T., Gaupp, R., and Gleixner, G.: Latitude and pH driven trends in the molecular composition of DOM across a north south transect along the Yenisei River, *Geochim. Cosmochim. Ac.*, 123, 93–105, <https://doi.org/10.1016/j.gca.2013.09.002>, 2013.
- Samaniego, L., Kumar, R., and Attinger, S.: Multiscale parameter regionalization of a grid-based hydrologic model at the mesoscale, *Water Resour. Res.*, 46, W05523, <https://doi.org/10.1029/2008wr007327>, 2010.
- Sanderman, J., Lohse, K. A., Baldock, J. A., and Amundson, R.: Linking soils and streams: Sources and chemistry of dissolved organic matter in a small coastal watershed, *Water Resour. Res.*, 45, W03418, <https://doi.org/10.1029/2008wr006977>, 2009.
- Seibert, J., Grabs, T., Köhler, S., Laudon, H., Winterdahl, M., and Bishop, K.: Linking soil- and stream-water chemistry based on a Riparian Flow-Concentration Integration Model, *Hydrol. Earth Syst. Sci.*, 13, 2287–2297, <https://doi.org/10.5194/hess-13-2287-2009>, 2009.
- Shang, P., Lu, Y., Du, Y., Jaffé, R., Findlay, R. H., and Wynn, A.: Climatic and watershed controls of dissolved organic matter variation in streams across a gradient of agricultural land use, *Sci. Total Environ.*, 612, 1442–1453, <https://doi.org/10.1016/j.scitotenv.2017.08.322>, 2018.
- Shen, Y., Chapelle, F. H., Strom, E. W., and Benner, R.: Origins and bioavailability of dissolved organic matter in groundwater, *Biogeochemistry*, 122, 61–78, <https://doi.org/10.1007/s10533-014-0029-4>, 2015.
- Spencer, R. G. M., Butler, K. D., and Aiken, G. R.: Dissolved organic carbon and chromophoric dissolved organic matter properties of rivers in the USA, *J. Geophys. Res.-Biogeo.*, 117, G03001, <https://doi.org/10.1029/2011jg001928>, 2012.
- Stewart, A. and Wetzel, R.: Dissolved humic materials: Photodegradation, sediment effects, and reactivity with phosphate and calcium carbonate precipitation, *Arch. Hydrobiol.*, 92, 265–286, 1981.
- Strohmeier, S., Knorr, K. H., Reichert, M., Frei, S., Fleckenstein, J. H., Peiffer, S., and Matzner, E.: Concentrations and fluxes of dissolved organic carbon in runoff from a forested catchment: insights from high frequency measurements, *Biogeosciences*, 10, 905–916, <https://doi.org/10.5194/bg-10-905-2013>, 2013.

- Tunaley, C., Tetzlaff, D., Lessels, J., and Soulsby, C.: Linking high-frequency DOC dynamics to the age of connected water sources, *Water Resour. Res.*, 52, 5232–5247, <https://doi.org/10.1002/2015wr018419>, 2016.
- Vaughan, M. C. H., Bowden, W. B., Shanley, J. B., Vermilyea, A., Sleeper, R., Gold, A. J., Pradhanang, S. M., Inamdar, S. P., Levia, D. F., Andres, A. S., Birgand, F., and Schroth, A. W.: High-frequency dissolved organic carbon and nitrate measurements reveal differences in storm hysteresis and loading in relation to land cover and seasonality, *Water Resour. Res.*, 53, 5345–5363, <https://doi.org/10.1002/2017wr020491>, 2017.
- Weishaar, J. L., Aiken, G. R., Bergamaschi, B. A., Fram, M. S., Fujii, R., and Mopper, K.: Evaluation of Specific Ultraviolet Absorbance as an Indicator of the Chemical Composition and Reactivity of Dissolved Organic Carbon, *Environ. Sci. Technol.*, 37, 4702–4708, <https://doi.org/10.1021/es030360x>, 2003.
- Werner, B. J.: High frequency dataset of the upper Rappbode Catchment in the Harz Mountains, Germany, <https://doi.org/10.4211/hs.e0e6fbc0571149b79b1e75fa44d5c4ab>, last access: 14 May 2019.
- Winterdahl, M., Laudon, H., Lyon, S. W., Pers, C., and Bishop, K.: Sensitivity of stream dissolved organic carbon to temperature and discharge: Implications of future climates, *J. Geophys. Res.-Biogeo.*, 121, 126–144, <https://doi.org/10.1002/2015jg002922>, 2016.
- Wollschläger, U., Attinger, S., Borchardt, D., Brauns, M., Cuntz, M., Dietrich, P., Fleckenstein, J. H., Friese, K., Friesen, J., Harpke, A., Hildebrandt, A., Jäckel, G., Kamjunke, N., Knöller, K., Kögler, S., Kolditz, O., Krieg, R., Kumar, R., Lausch, A., Liess, M., Marx, A., Merz, R., Mueller, C., Musloff, A., Norf, H., Oswald, S. E., Rebmann, C., Reinstorf, F., Rode, M., Rink, K., Rinke, K., Samaniego, L., Vieweg, M., Vogel, H.-J., Weitere, M., Werban, U., Zink, M., and Zacharias, S.: The Bode hydrological observatory: a platform for integrated, interdisciplinary hydro-ecological research within the TERENO Harz/Central German Lowland Observatory, *Environ. Earth Sci.*, 76, 29 pp., <https://doi.org/10.1007/s12665-016-6327-5>, 2016.
- Zarnetske, J. P., Bouda, M., Abbott, B. W., Saiers, J., and Raymond, P. A.: Generality of Hydrologic Transport Limitation of Watershed Organic Carbon Flux Across Ecoregions of the United States, *Geophys. Res. Lett.*, 45, 11702–11711, <https://doi.org/10.1029/2018gl080005>, 2018.

Supplement of Biogeosciences, 16, 4497–4516, 2019
<https://doi.org/10.5194/bg-16-4497-2019-supplement>
© Author(s) 2019. This work is distributed under
the Creative Commons Attribution 4.0 License.



Supplement of

High-frequency measurements explain quantity and quality of dissolved organic carbon mobilization in a headwater catchment

Benedikt J. Werner et al.

Correspondence to: Benedikt J. Werner (benedikt.werner@ufz.de)

The copyright of individual parts of the supplement might differ from the CC BY 4.0 License.

S1 Description of fouling correction, onsite probe maintenance and water sampling

After every 12 measurements (3 h), the probe was automatically cleaned with compressed air to inhibit bio-fouling and the accumulation of sediments.

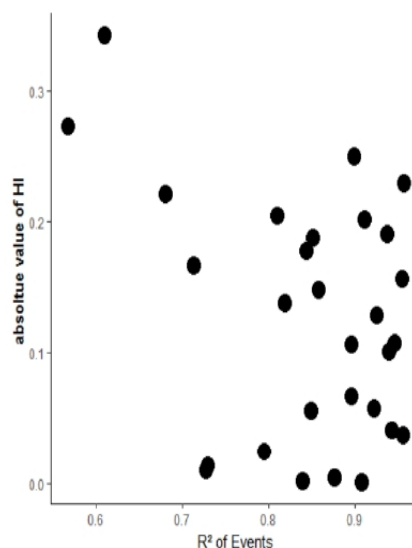
Onsite maintenance was conducted biweekly (cleaning manually with detergent and HCl, flushing with deionized water).

- 5 The first measurement after each cleaning was considered to represent the true absorption spectrum, with no bio-fouling or sediment influence. The difference between the last measurement before and the first one after maintenance showed how much the probe drifted within the two weeks since the last maintenance. Ahead of further (statistical) processing, each of the UV-Vis absorption spectra was corrected for this drift by subtracting an exponential function fitted to the raw data.

- For C_{DOC} measurements, sample water was filtered (0.45 μm cellulose acetate filter, Th.Geyer, Germany), acidified with 10 30% HCl to pH 2 and stored dark and cool in glass bottles until laboratory analysis was conducted.

S2 Impact of hysteresis loop size on regression slopes

- Although hysteresis of C-Q relationship potentially could explain some deviations of our hydrological event models we did not take hysteresis into account. However the high overall R^2 values of our event models (Figure 3) indicate that the influence of hysteresis on the R^2 should be minor. Evaluating hysteresis index (HI) after Lloyd et al. (2016) Lloyd et al. 15 (2016) against R^2 of events (Fig. S1) indicated a negative, but non-significant effect of magnitude of hysteresis (depicted as absolute value of HI) on R^2 (method of linear regression: $C_{DOC} \sim Q$, [$C_{DOC} \sim \log(Q)$ was used where appropriate]). Overall, Pearson correlation of HI- R^2 of Events was $r^2 = 0.12$ ($r_{\text{Pearson}} = -0.34$, $p = 0.07$), supporting the application of our method without explicit consideration of hysteresis effects.



20 Fig. S1: Absolute value of the hysteresis index (HI) plotted against R^2 of Events.

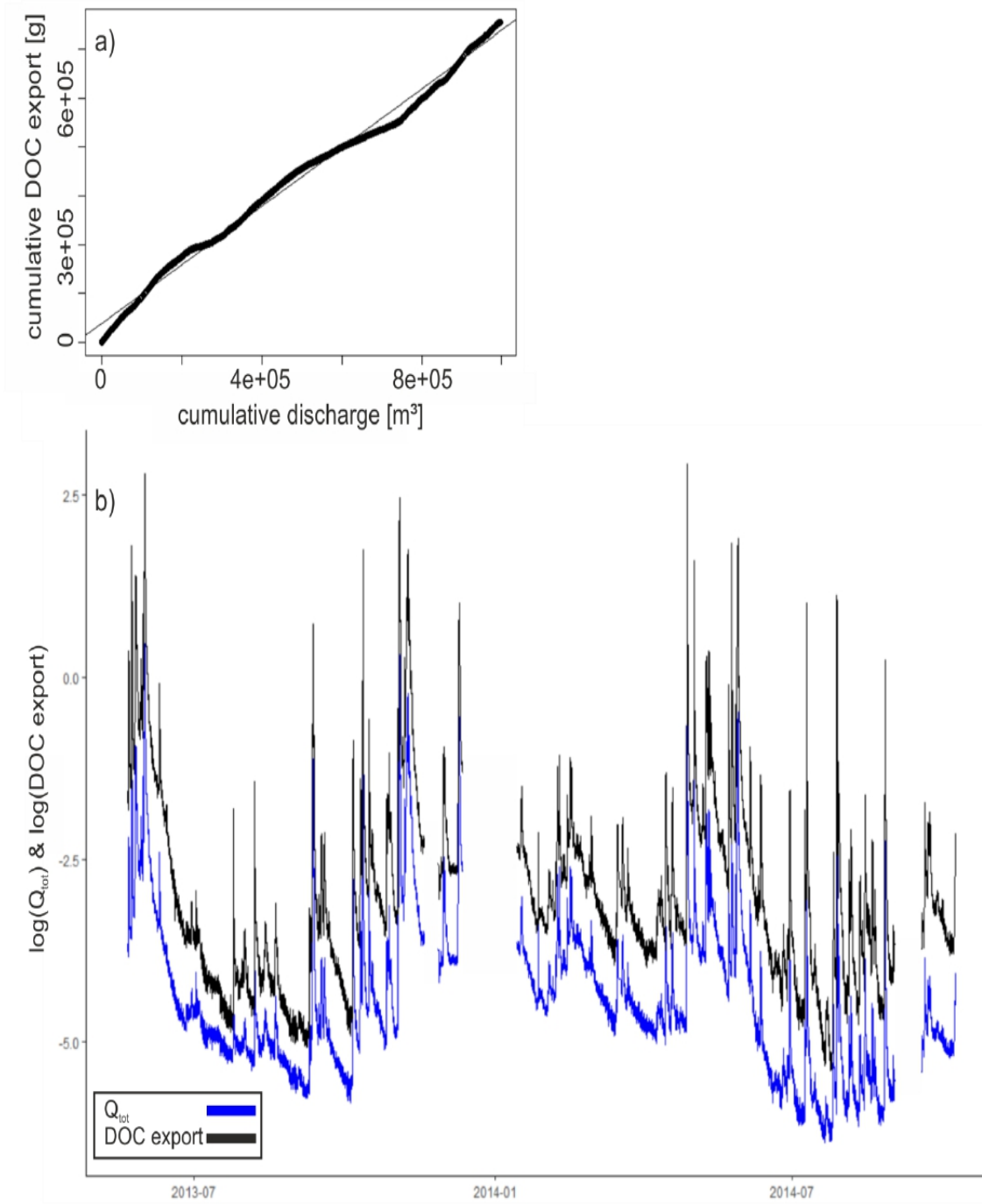


Fig. S2: a) cumulative discharge vs cumulative DOC export. Straight line indicates 1:1 line. b) Comparison of discharge and DOC export in log space over time.

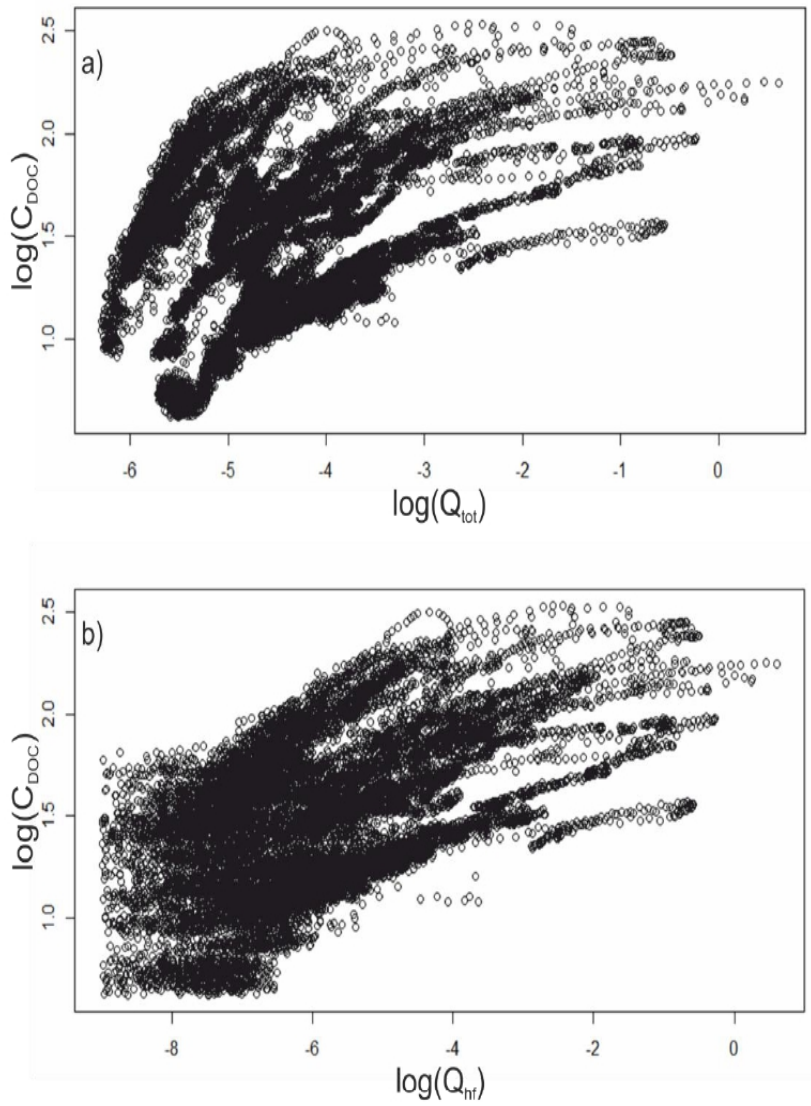


Fig. S3: Linearization of C_{DOC} by (a) Q_{tot} and (b) Q_{inf} in double log space.

5

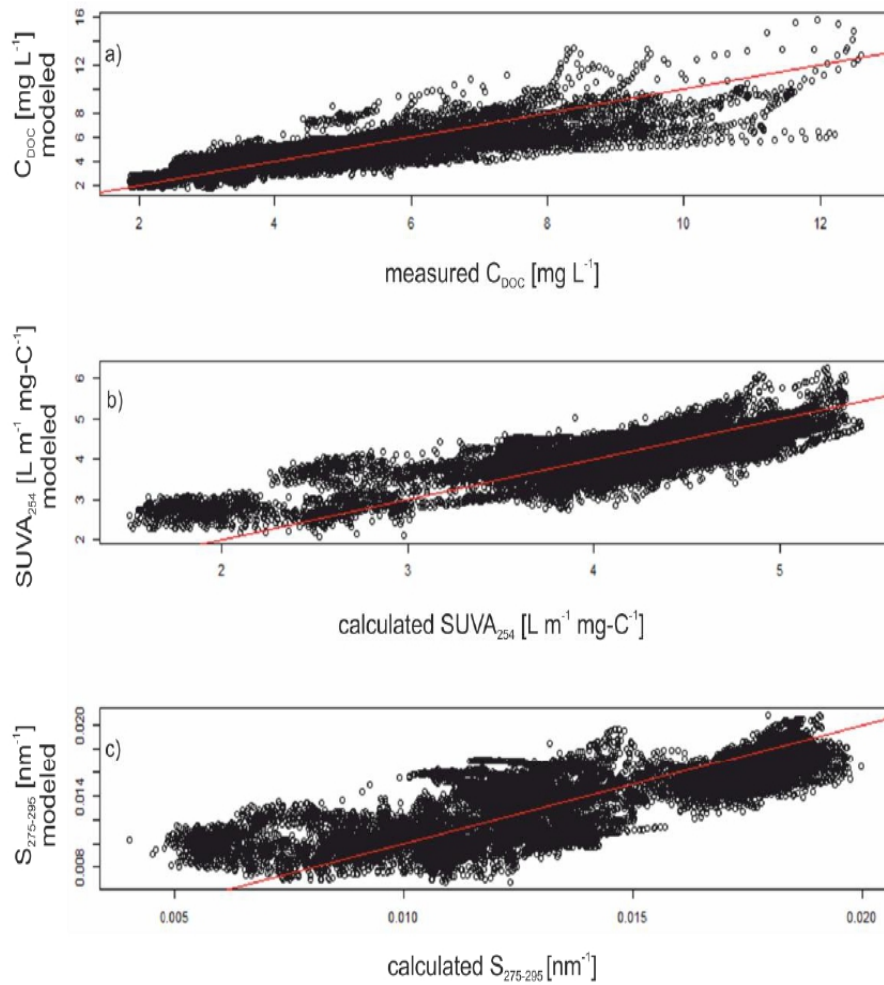


Fig. S4: Modelled vs. measured values of (a) C_{DOC} , (b) $SUVA_{254}$ and (c) $S_{275-295}$. Red line indicates 1:1 line. Maximum residuals are 6.03 mg L^{-1} , $-1.52 \text{ L m}^{-1} \text{ mg-C}^{-1}$ and $-6.5 \times 10^{-3} \text{ nm}^{-1}$ for the C_{DOC} , $SUVA_{254}$ and $S_{275-295}$ models, respectively.

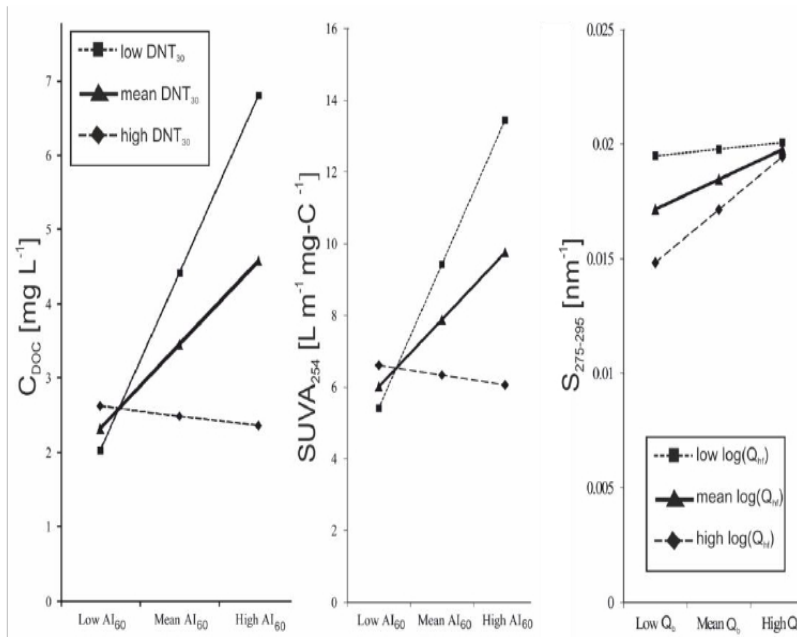
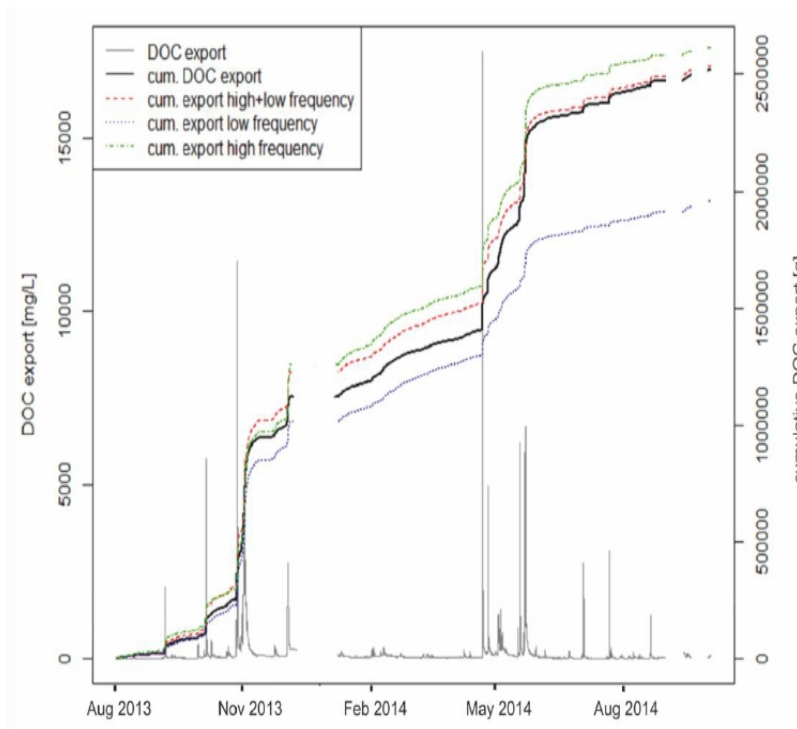


Fig. S5: Impact of the interaction $DNT_{30} \times AI_{60}$ on (a) C_{DOC} and (b) $SUVA_{254}$. Panel (c) shows the impact of the interaction $DNT_{30} \times Q_b$ on $S_{275-295}$



5

Fig. S 6: Cumulative modelled DOC export of high frequency ($Q_{hf} + Q_b + Q_{hf} \times Q_b$), low frequency ($DNT_{30} + AI_{60} + DNT_{30} \times AI_{60}$) and their combination (Eq. (3)), calculated cumulative DOC export (black) and DOC concentration (grey). Nash-Sutcliffe efficiency of DOC export was 0.998, 0.979 and 0.783.

5

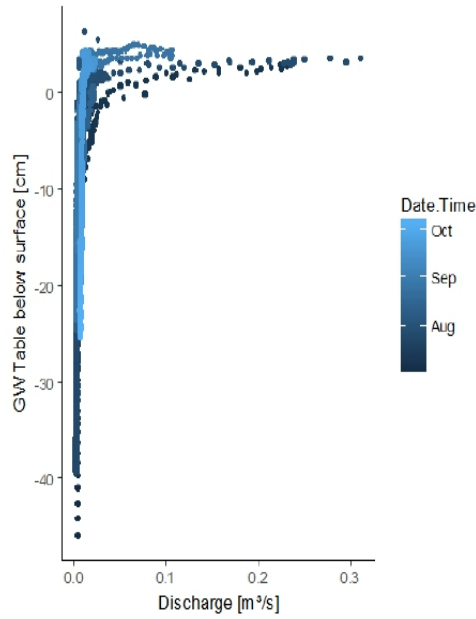


Fig. S 7: Relationship between stream discharge of the Rappbode stream and groundwater table of a nearby (30m) groundwater well. Colour coding indicates different time of the year.

5

Table S 1: Model evaluation of the C_{DOC} , $SUVA_{254}$ and $S_{275-295}$ models. All model parameters were highly significant ($p < 0.001$).

	C_{DOC} model			$SUVA_{254}$ model			$S_{275-295}$ model		
	Estimate	Std. Error	t value	Estimate	Std. Error	t value	Estimate	Std. Error	t value
Intercept	2.6E+00	1.1E-02	234.5	6.6E+00	2.5E-02	261.6	2.7E-02	1.3E-04	212.9
$\log(Q_{hd})$	1.9E-01	1.8E-03	109.0	4.0E-01	4.0E-03	99.4	1.7E-03	2.0E-05	86.7
AI_{60}	-5.2E-02	1.0E-03	-52.0	-1.1E-01	2.3E-03	-48.8	-5.1E-04	1.1E-05	-45.2
DNT_{30}	-3.1E-04	4.5E-06	-68.9	-6.3E-04	1.0E-05	-62.2	-6.8E-07	5.0E-08	-13.6
Q_b	-2.3E+01	6.8E-01	-34.4	-6.8E+01	1.5E+00	-44.1	-3.9E-01	7.7E-03	-50.8
$\log(Q_{hd}) \times Q_b$	-4.4E+00	1.4E-01	-31.4	-1.5E+01	3.2E-01	-45.7	-1.0E-01	1.6E-03	-63.2
$AI_{60} \times DNT_{30}$	5.6E-04	4.2E-06	133.0	9.5E-04	9.5E-06	100.4	-5.1E-07	4.8E-08	-10.8
$DNT_{30} \times Q_b$	-2.7E-02	8.1E-04	-33.8	-8.0E-02	1.8E-03	-43.8	-3.8E-04	9.2E-06	-41.9

Table S2: Overview of R^2 of the total dataset. Subsets of the modelled dataset were extracted and compared to the measured values.

	R^2 total	R^2 events only	R^2 non-events
		(subsetting from the whole dataset)	(subsetting from the whole dataset)
C_{DOC} model	0.72	0.61	0.67
$SUVA_{254}$ model	0.64	0.54	0.58
$S_{275-295}$ model	0.65	0.79	0.62

6

In the SI cited Literature

- 5 Lloyd, C. E. M., Freer, J. E., Johnes, P. J., and Collins, A. L.: Technical Note: Testing an improved index for analysing storm discharge-concentration hysteresis, *Hydrology and Earth System Sciences*, 20, 625-632, doi:10.5194/hess-20-625-2016, 2016.

Study 2: Small-scale topography explains patterns and dynamics of dissolved organic carbon exports from the riparian zone of a temperate, forested catchment

Status: Published in Hydrology and Earth System Sciences (25), 2021, DOI: 10.5194/hess-25-6067-2021

Authors: Benedikt J. Werner, Oliver J. Lechtenfeld, Andreas Musolff, Gerrit H. de Rooij, Jie Yang, Ralf Gründling, Ulrike Werban, and Jan H. Fleckenstein

BJW, JHF, OJL, AM and GHdR planned and designed the research. BJW performed the statistical analysis and wrote the paper with contributions from all co-authors. JY performed the hydrological modeling. BJW and OJL analyzed and interpreted the FT-ICR-MS data. UW implemented geophysical investigations. RG provided post-processed drone altimetry data.

Own contribution:

- Concept and study design: 80%
- Data acquisition: 80%
- Data analysis: 90%
- Interpretation of the results: 90%
- Preparation of the manuscript: 90%

Hydrol. Earth Syst. Sci., 25, 6067–6086, 2021
https://doi.org/10.5194/hess-25-6067-2021
© Author(s) 2021. This work is distributed under
the Creative Commons Attribution 4.0 License.



Small-scale topography explains patterns and dynamics of dissolved organic carbon exports from the riparian zone of a temperate, forested catchment

Benedikt J. Werner¹, Oliver J. Lechtenfeld², Andreas Musolff¹, Gerrit H. de Rooij³, Jie Yang¹, Ralf Gründling³, Ulrike Werban⁴, and Jan H. Fleckenstein^{1,5}

¹Department of Hydrogeology, Helmholtz Centre for Environmental Research – UFZ, 04318 Leipzig, Germany

²Research group BioGeoOmics, Department of Analytical Chemistry, Helmholtz Centre for Environmental Research – UFZ, 04318 Leipzig, Germany

³Department of Soil System Sciences, Helmholtz Centre for Environmental Research – UFZ, 06120 Halle, Germany

⁴Department of Monitoring and Exploration Technologies, Helmholtz Centre for Environmental Research – UFZ, 04318 Leipzig, Germany

⁵Hydrologic Modelling Unit, Bayreuth Center of Ecology and Environmental Research (BayCEER), University of Bayreuth, Bayreuth, Germany

Correspondence: Benedikt J. Werner (benedikt.werner@ufz.de)

Received: 5 February 2021 – Discussion started: 23 February 2021

Revised: 5 October 2021 – Accepted: 20 October 2021 – Published: 30 November 2021

Abstract. Export of dissolved organic carbon (DOC) from riparian zones (RZs) is an important component of temperate catchment carbon budgets, but export mechanisms are still poorly understood. Here we show that DOC export is predominantly controlled by the microtopography of the RZ (lateral variability) and by riparian groundwater level dynamics (temporal variability). From February 2017 until July 2019 we studied topography, DOC quality and water fluxes and pathways in the RZ of a small forested catchment and the receiving stream in central Germany. The chemical classification of the riparian groundwater and surface water samples ($n = 66$) by Fourier transform ion cyclotron resonance mass spectrometry revealed a cluster of plant-derived, aromatic and oxygen-rich DOC with high concentrations (DOC_I) and a cluster of microbially processed, saturated and heteroatom-enriched DOC with lower concentrations (DOC_{II}). The two DOC clusters were connected to locations with distinctly different values of the high-resolution topographic wetness index (TWI_{HR}; at 1 m resolution) within the study area. Numerical water flow modeling using the integrated surface–subsurface model HydroGeoSphere revealed that surface runoff from high-TWI_{HR} zones associated with the DOC_I cluster (DOC_I source zones) dominated overall discharge generation and therefore DOC export. Although correspond-

ing to only 15 % of the area in the studied RZ, the DOC_I source zones contributed 1.5 times the DOC export of the remaining 85 % of the area associated with DOC_{II} source zones. Accordingly, DOC quality in stream water sampled under five event flow conditions ($n = 73$) was closely reflecting the DOC_I quality. Our results suggest that DOC export by surface runoff along dynamically evolving surface flow networks can play a dominant role for DOC exports from RZs with overall low topographic relief and should consequently be considered in catchment-scale DOC export models. We propose that proxies of spatial heterogeneity such as the TWI_{HR} can help to delineate the most active source zones and provide a mechanistic basis for improved model conceptualization of DOC exports.

1 Introduction

Dissolved organic carbon (DOC) in streams and rivers is in itself of central ecological importance (Cole et al., 2007; Battin et al., 2008), but the amount and quality of DOC also shape water quality through interactions and co-export with other chemicals in terrestrial solute source areas (Ledezma

et al., 2016; Sherene, 2010), rivers and lakes (Prairie, 2008). Besides the ecological impacts, this alteration may also affect safety and costs of drinking water production (e.g. Wang et al., 2017). Changes in land use, climate and biogeochemical boundary conditions have increased DOC concentrations in surface waters and altered the quality of the exported DOC in the last decades (Larsen et al., 2011; Chantigny, 2003; Wilson and Xenopoulos, 2008). Routine management of DOC could therefore help to comply with water quality directives and lower the cost of drinking water purification (Mätiläinen et al., 2011), but understanding how DOC changes and moves within and across ecosystem interfaces, thus linking aquatic and terrestrial carbon cycles, is still limited by large knowledge gaps (Butman et al., 2018; Drake et al., 2018; Vachon et al., 2021) that so far impede proper DOC management (Stanley et al., 2012).

Lower-order streams make up a large fraction of the total river networks worldwide (Raymond et al., 2013), and their riparian zones (RZs) represent a main source for terrestrial DOC export (Ledesma et al., 2015; Musolff et al., 2018). Therefore, RZs of lower-order streams – as terrestrial–aquatic interfaces – constitute a general control unit, qualifying them as potential targets for DOC export management. However, describing and quantifying the effective DOC export from such RZs at the larger management scale still remains a challenge due to the high spatiotemporal variability of local mechanisms that control DOC accumulation, mobilization and transport in RZs (Pinay et al., 2015; Bernhardt et al., 2017; Krause et al., 2014). Large uphill contributing areas deliver a continuous supply of water to the RZ, leading to generally moist conditions with high groundwater levels, even during dry periods. Here, DOC accumulation rates are highest during anaerobic conditions at low temperatures due to low mineralization rates, whereas high mineralization rates can be realized in warmer, oxygenated zones in the soil (Luke et al., 2007). On the other hand, the amount of accumulated DOC and ultimately its export is also dependent on hydrological connection of DOC sources to the stream. Microtopography in RZs can induce hotspots of biogeochemical activity (Frei et al., 2012) that contribute disproportionately to nutrient turnover. Depressions in microtopography collect surficial water (Frei et al., 2010; Scheliga et al., 2019). If these puddles grow to connect with each other, continuous but possibly short-lived surface flow channels can develop that can connect hotspots of DOC production in the shallow soil layers of the RZ to the stream and carry DOC to the stream (during so-called hot moments). Therefore, microtopography in the RZ is considered a fundamental organizing structure for soil chemistry (Diamond et al., 2020) and hydrological connectivity (Frei et al., 2010; Scheliga et al., 2019) that can induce high spatiotemporal heterogeneity of DOC exports. Riparian topography and the dynamics of groundwater levels in the RZ thus can be key drivers of the spatiotemporal patterns of DOC export from RZs.

Several attempts have been made to characterize and quantify the dynamics of runoff generation in RZs and the associated variability of DOC transport to streams. However, to date model conceptualizations have mainly focused on the vertical distribution of DOC sources in the subsurface and to a lesser degree on horizontal heterogeneity induced by topography. For instance, the dominant source layer concept (Ledesma et al., 2015) focuses on depth-dependent differences in DOC pools in distinct soil layers of a boreal catchment. The dominant source layer concept is based on the transmissivity feedback mechanism (Bishop et al., 2004), which accounts for depth-dependent differences in hydraulic conductivities of soils and the resulting changes in the transmissivity of the soil profile under changing groundwater levels. This concept is taken up in the riparian profile flow-concentration integration model (RIM; Seibert et al., 2009) to model stream solute variability as a function of a nonlinear vertical distribution of pore water solute concentrations in riparian soils. Frei et al. (2010, 2012) were able to simulate the complex effects of riparian microtopography on runoff generation and the formation of biogeochemical hotspots in the subsurface, but their explorative model was computationally expensive and did not explicitly consider DOC transport. To date, variations in the lateral hydrological connectivity of a RZ to a stream have mainly been conceptualized in the context of spatially lumped catchment DOC export models by defining different source zones with variable activation (Dick et al., 2015), largely ignoring small-scale spatiotemporal variability in DOC export from individual, small landscape units (Ledesma et al., 2018a; Dick et al., 2015). Our study aims at bridging the gap between small-scale mechanistic understanding of DOC mobilization and export and its larger-scale, lumped description in most conceptual models.

Improved understanding of the dominant mechanisms of DOC generation and transport in small-scale landscape elements could help to find accessible proxies that can better describe the larger-scale effective DOC-export behavior of catchments (Grabs et al., 2012). Currently existing proxies are mainly based on landscape-scale characteristics like different land use types (Pisani et al., 2020), hydromapping based on convergence of topography (Laudon et al., 2016; Ploum et al., 2020), or general topographic wetness (Musolff et al., 2018; Fellman et al., 2017; Andersson and Nyberg, 2009) in boreal and temperate catchments, e.g. represented by the topographic wetness index TWI (Beven and Kirkby, 1979). However, these proxies are still relatively coarse and typically lump the entire RZ into larger spatial units (e.g. model cells). Accordingly, small-scale heterogeneity of topography and hydrological properties, which can significantly affect the hydrologic connectivity of local source zones to the stream (Frei et al., 2010) are not adequately represented.

We argue that refined proxies that explicitly capture the smaller-scale heterogeneity of riparian zones could generally improve our mechanistic understanding of DOC ex-

at 12 April 2017, where the multiparametric data set is most complete.

2.2.1 In-stream data sensors

Two PCM4 portable flow meters (Nivus, Germany) measured discharge in the Rappbode stream at a chosen inlet (PCM4_{in}, catchment area: 2.28 km² and outlet of the study site (PCM4_{out}, 2.54 km²), respectively. A pressure transducer (Solinst Levellogger, Canada) was installed at the center of the study site. All three probes measured water level every 15 min. Discharge at the center was then estimated via a stage–discharge relationship (stage was measured using a pressure transducer, $R^2 = 0.99$ (0.72 without the extreme value)), which was established based on biweekly manual discharge measurements using an electromagnetic flow meter ($n = 37$; MF pro, OTT, Germany). Maximum discharge measured manually was 0.22 m³ s⁻¹ on 28 February 2017 (the first measurement) at a water level of 37.9 cm. Manual measurements were recorded until 19 December 2018. The extrapolation of the stage–discharge relationship to a wider range of stages was found to be in a valid range (Werner et al., 2019). However, values larger than 0.22 m³ s⁻¹ are more uncertain than smaller values.

2.2.2 Weather station

A weather station (WS-GP1, Delta-T, UK) was placed about 250 m northwest of the study site in order to characterize ambient weather conditions. Air temperature, humidity, wind direction and speed, solar radiation, and rainfall were recorded at 30 min intervals. Potential evapotranspiration (ET_P) was calculated from the weather data after the Penman–Monteith method (Allen et al., 1998) also at a 30 min resolution.

2.2.3 Piezometer network

The DEM (Fig. 1b) revealed that the floodplain's slope in the direction of the stream (0.2 m/10 m) was steeper than the slope towards the stream (0.1 m/10 m). We expected that this would have ramifications for the direction of the slope of the groundwater level and its temporal dynamics. We installed a piezometer network aligned on a square grid, with one principal axis oriented in parallel to the stream and the other perpendicular to the stream, to capture the temporal dynamics of the groundwater levels in both principal directions of this slope. We positioned 25 partly screened piezometers (2.54 cm diameter, HDPE, 10 cm filter length) in a rectangular grid pattern adjacent to the Rappbode stream, comprising a piezometer network covering 50 m × 50 m (Fig. 1b). The A horizon in the piezometer holes was 17.7 ± 2.4 cm on average ($n = 27$) (Fig. 1). The well spacing was regularly 12.5 m in both principal directions of the grid, although installation depth was variable. The depth of the centers of the piezometer screens ranged between 20 and 107 cm below ground (average = 75.2 cm). This was a trade-off between having con-

tinuous water level measurements from the pressure transducers and covering the anticipated large variety of different DOC characteristics in different soil layers and depths (Shen et al., 2015). We equipped each piezometer with a pressure transducer (Levellogger, Solinst, Canada, and Diver, van Essen, the Netherlands), measuring at a 15 min interval. All pressure transducers were barometrically corrected and adjusted to manual measurements of the groundwater level at eight occasions during a 15-month measurement period (from 4 October 2017 to 19 December 2018). In addition we irregularly installed three wells with screens at 0.3 m depth (but no pressure transducers) inside the piezometer network for sampling near the surface. Figure S1 in the Supplement gives an overview of the installed screen depth and the soil horizon accessed by the screened section.

2.2.4 Sampling and maintenance

At the monitoring site along the Rappbode stream, we overall collected 68 stream event samples during five events, 66 riparian samples and five stream samples during five occasions (one stream sample per occasion), and 38 routine stream samples (every 2 weeks), which were analyzed for DOC concentration. The molecular composition of the DOC was determined via Fourier transform ion cyclotron resonance mass spectrometry (FT-ICR-MS; see Table S1 in the Supplement for detailed information). Autosamplers (6712 full-size portable sampler, Teledyne ISCO, USA) were triggered by the rate of water level increase to sample stream water during discharge-generating events at least once per hour. Autosampler bottles (PP) were soaked for 48 h in 0.1 N HCl prior to use. We prepared process blanks with deionized water to correct for eventual contamination during field work and sample processing. Due to the remoteness of the study site, we collected stream water autosampler samples within 4 d after the triggered event sampling. Samples were stored in the dark inside the sampler, and air temperature was always below 10 °C during that time. We are aware that the delayed sample retrieval constitutes a limitation of our study which may affect DOC concentration and composition, in particular with respect to labile DOC sources, e.g. leaf leachate (Catalán et al., 2021). Yet, Werner et al. (2019) concluded that in-stream processing and biodegradation are likely to be of minor importance at our experimental site. Further, DOC composition typically shifts towards more stable, allochthonous DOC quality during events (Werner et al., 2019). Hence, the major fraction of event DOC is expected to be unaffected within the first 4 measurement days (Mostovaya et al., 2016; Catalán et al., 2021). We collected riparian zone shallow groundwater samples from 3 to 18 out of the 28 installed piezometers depending on hydrological conditions during the five sampling dates. Generally groundwater sampling in summer turned out to be difficult due to low groundwater levels, which inhibited sampling of surface runoff and wells screened closer to the surface. To ensure a good comparability between sam-

ports from temperate catchments and potentially provide a means to infuse this understanding into DOC export models for larger scales. For example, Andersson and Nyberg (2009) proposed a skewed linear relationship between mean catchment-scale TWI and DOC concentration for various Swedish catchments, but it only performed well under wet conditions. We postulate that a riparian TWI, evaluated at a spatial resolution that resolves the small-scale topography within the RZ, could improve the mechanistic basis of the DOC–TWI relationship proposed by Anderson and Nyberg (2009), as it would be better able to resolve the actual contributing source zones of DOC during different wetness states. DOC production will be highest in the wet depressions of the microtopography within the RZ, which are defined by a high riparian TWI. Those depressions will also first be intercepted by a rising groundwater table during events, eventually leading to the development of surface flow networks (Frei et al., 2010) which episodically connect dominant DOC source zones with the stream. We therefore hypothesize that both DOC production and transport to the stream are significantly controlled by the microtopography of the RZ (lateral variability) and temporal dynamics of riparian groundwater level fluctuations (temporal variability). To test our hypothesis, we characterized the microtopography of a RZ using drone-based orthophotography to obtain a digital elevation model (DEM) at high spatial resolution (1 m). In addition, we monitored groundwater levels in a dense piezometer network, stream discharge, and DOC quantity and quality in stream water and groundwater. Stream flow generation and flow paths are modeled in detail with an integrated surface–subsurface numerical flow model, which explicitly accounts for microtopography of the RZ. Explicit subsurface and surface flow paths from the model and DOC fingerprinting based on high-resolution mass spectrometry were used to identify dominant DOC source zones in the RZ and quantify different flow paths to the stream, which cause the observed space and time patterns of in-stream DOC concentrations.

2 Materials and methods

2.1 Study site and site characterization

The study site is in a headwater catchment of the Rappbode stream (51°39′22.61″N, 10°41′53.98″E; Fig. 1) located in the Harz Mountains, central Germany. After draining into a drinking water reservoir, the Rappbode stream flows into the river Bode and discharges (through the rivers Saale and the Elbe) into the North Sea. The catchment has an area of 2.58 km² and a drainage density of 2.91 km km⁻¹. The study site has a temperate climate (Kottek et al., 2006), with a long-term mean air temperature of 6.0 °C and mean annual precipitation of 831 mm (Stiege weather station 12 km away from the study site; data were provided by the German Weather Service, DWD). The uncultivated and uninhabited catchment

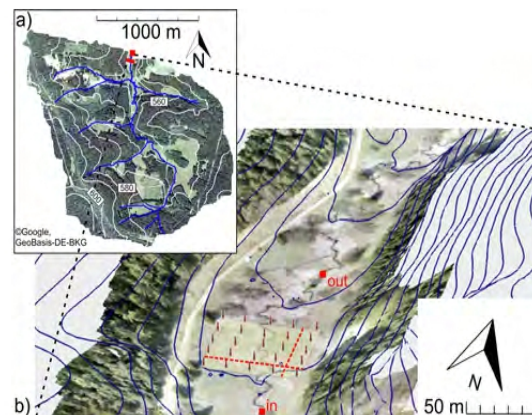


Figure 1. (a) Rappbode catchment and position of the study site (red square). (b) 3D view of the study site (red squares indicate inlet and outlet stream gauges). Red pins indicate the soil sampling transect and the piezometer network. Locations of electric resistivity tomography are indicated by dashed red lines. Note the 2.5-fold vertical exaggeration. Map data: © Google, GeoBasis-DE-BKG.

is predominantly forested with spruce and pine trees (77 %), 11 % is covered with grass, and 12 % is covered by other vegetation and a few unpaved roads. Elevation ranges from 540 to 620 m a.s.l.; the mean topographic slope is 3.9°. The geology at this site consists mainly of greywacke, clay schist and diabase (Wöllschläger et al., 2016). Soils in the spring area are dominated by peat and peat formation. Overall, 25 % of the catchment soils are humic and stagnic Gleysols that are distinctive of riparian zones.

We flew a drone over the study site to measure the topography and used the data to create a digital elevation model (DEM) of the area with a spatial resolution of 1 m. Electric resistivity tomography (Resecs DC resistivity meter system, Kiel, Germany) was applied at two transects (Fig. 1b) using a Wenner alpha configuration with an electrode distance of 0.5 m in order to explore structural consistencies of the subsurface. The 90th percentile of the topographic wetness index (TWI) as a measure for the extent of riparian wetlands in the catchment (Musolff et al., 2018) is 10.10 (median 7.58). The study site was chosen to be within this percentile of the Rappbode catchment TWI (derived from the DEM) and is thus regarded to be representative for riparian sites of the catchment.

2.2 The monitoring program

We carried out intensive field observations from 28 February 2017 until 19 December 2018, and we continued the data collection at a lower frequency until 23 July 2019. Note that within this campaign different probes cover partly different measurement periods due to a sequential deployment of the devices. Therefore, we decided to set the period of the monitoring campaign for the actual data analysis and modeling

pling dates, we decided to focus on April and December samples, when a complete set of groundwater and surface water data were available. Before riparian sample collection, we replaced water in the wells one to three times (based on the responsiveness of the wells) through pumping. We rinsed the flasks and the pump with sample water prior to sample collection and subsequently transferred 100 mL of sample into acid-rinsed (0.1 N HCl) and baked (500 °C, 4 h) glass bottles. Additionally, stream water was collected at each of the five riparian sampling occasions. Samples were stored dark and cool until further processing in the laboratory.

2.3 Chemical analysis

2.3.1 Sample processing and DOC determination

Samples were filtered (0.45 µm membrane cellulose acetate filters, rinsed with 20 mL of sample water to avoid bleeding; Th. Geyer, Germany) and acidified to pH 2 (HCl, 30 %, Merck, Germany) on site. Subsequently samples were stored cool (4 °C) and dark until timely DOC measurement and extraction in the laboratory.

DOC concentration was determined as non-purgeable organic carbon with a high-temperature catalytic oxidation system (multi N/C 3100, Analytik Jena, Jena, Germany) from acidified samples and extracts after solvent evaporation. Due to the small difference in DOC concentration between hourly and subhourly samples during events, we chose a lower time resolution for high-resolution mass spectrometry measurements. A volume of 15–200 mL ($n = 142$) was extracted via solid-phase extraction (SPE) using an automated system (FreeStyle, LC Tech, Obertaufkirchen, Germany) on 50 mg styrene-divinyl-polymer-type sorbent (Bond Elut PPL, Agilent Technologies, Santa Clara, CA, USA) to desalt the sample for subsequent direct infusion electrospray ionization mass spectrometry (DI-ESI-MS) according to Dittmar et al. (2008) and Raeker et al. (2017). The carbon-to-sorbent ratio (C : PPL) was 280 ± 130 (m/m , $n = 142$). The SPE-DOM (solid-phase extractable dissolved organic matter) was eluted with 1 mL methanol (Biosolve, Valkenswaard, the Netherlands), and stored at -20 °C until measurement. Carbon-based extraction efficiency was $56 \% \pm 15 \%$ (determined from $n = 133$ samples, Fig. S2 in the Supplement). This is in the range of typical extraction efficiencies obtained for freshwater samples (Raeker et al., 2017). Immediately prior to FT-ICR-MS analysis, extracts were diluted to 20 ppm and mixed 1 : 1 (v/v) with ultrapure water (Milli-Q Integral 5, Merck, Darmstadt, Germany).

2.3.2 FT-ICR-MS measurement

An FT-ICR mass spectrometer equipped with a dynamically harmonized analyzer cell (solariX XR, Bruker Daltonics Inc., Billerica, MA, USA) and a 12 T refrigerated actively shielded superconducting magnet (Bruker Biospin, Wissem-

bourg, France) instrument was used in ESI negative mode (capillary voltage: 4.2 kV) using an Apollo II source. Extracts were analyzed in random order with an autosampler (infusion rate: $10 \mu\text{L}\cdot\text{min}^{-1}$). For each spectrum, 256 scans were co-added in the mass range 150–1000 m/z with a 4 megaword time domain (resolution at 400 m/z was ca. 483 000). Mass spectra were internally recalibrated with a list of peaks (247–643 m/z , $n > 55$) commonly present in terrestrial DOM, and the mass accuracy after linear calibration was better than 0.13 ppm ($n = 142$). Peaks were considered if the signal-to-noise ratio (S/N) was greater than 4. Raw spectra were processed with Compass DataAnalysis 4.4 (Bruker Daltonics Inc., Billerica, MA, USA). Suwannee River Fulvic Acid (SRFA) reference sample and a pool sample (mix of randomly picked DOM extracts) were repeatedly measured to check instrument performance across multiple measurement days, and solvent and extraction blanks were measured with the samples.

2.3.3 FT-ICR-MS data processing

Molecular formulas were assigned to peaks in the range 0–750 m/z allowing for elemental compositions $\text{C}_{1-60}\text{H}_{0-122}\text{N}_{0-2}\text{O}_{0-40}\text{S}_{0-1}$ with an error range of ± 0.5 ppm according to Herzprung et al. (2020). Briefly, the following rules were applied: $0.3 \leq \text{H}/\text{C} \leq 2.5$, $0 \leq \text{O}/\text{C} \leq 1$, $0 \leq \text{N}/\text{C} \leq 1.5$, $0 \leq \text{DBE} \leq 25$ (double-bound equivalent, $\text{DBE} = 1 + 1/2 (2\text{C} - \text{H} + \text{N})$; Koch et al., 2014), $-10 \leq \text{DBE} - \text{O} \leq 10$ (Herzprung et al., 2014), and element probability rules proposed by Kind and Fiehn (2007). Isotopologue formulas (^{13}C , ^{34}S) were used for quality control but removed from the final data set as they represent duplicate chemical information. All peaks present in the instrument blank and in the SPE blanks were subtracted from the mass list. Relative peak intensities (RIs) were calculated based on the summed intensities of all assigned peaks in each sample. To ensure that the variance in DOC quality observed by FT-ICR-MS was not induced by systematic instrumental shifts at different times of the year, we quantified the variability of peak intensities based on 15 reference samples (SRFA) of the 4 measurement days. Subsequently, this variability was applied to every RI in measured samples to derive a mean error for the intensity (see Sect. S1 in the Supplement). We conclude that the analytical uncertainty from the FT-ICR-MS measurements between the different measurement dates has only a minor effect on the overall variance of the samples, which allows for the joint evaluation of all samples (see Sect. S1, Figs. S3 and S4 in the Supplement). Assigned molecular formula are termed compound throughout this article although they potentially represent multiple isomers.

2.4 Numerical water flow modeling

The numerical code HydroGeoSphere (HGS) was used to quantify water flow at the study site. HydroGeoSphere is a 3D numerical model describing fully coupled surface–subsurface variably saturated flow (Therrien et al., 2010). It solves Richards' equation for 3D variably saturated water flow in the subsurface domain, and it uses Manning's equation and the diffusive-wave approximation of the St. Venant equations to simulate surface flow in the 2D surface domain and 1D channel network (Yang et al., 2015). Using a dual-node coupling approach, HydroGeoSphere simulates the water exchange fluxes between the domains, providing the simulated infiltration/exfiltration fluxes. More details on the governing equations, coupling approach and general aspects of HydroGeoSphere can be found in Therrien et al. (2010).

Only the upper 2 m of the alluvial sediments were included in the flow simulation as an aquifer, because geological survey data showed that the electric resistivity dropped sharply below that depth, indicating the presence of bed rock (Fig. S5 in the Supplement). The subsurface was discretized into eight horizontal element layers, each composed of 6924 prisms. The layer thicknesses ranged from 0.05 m near the land surface to 0.5 m near the aquifer bottom. The horizontal cell sizes varied from 1 to 2 m. The 6924 uppermost 2D triangles of the 3D prismatic mesh were used to discretize the surface domain. The channel crossing the study site was discretized into 148 1D segments, which coincide with the segments of the 2D triangular mesh. The line element made up of the channel segments was treated as a Cauchy boundary with the stream stage being calculated based on the assumption of a rectangular cross-section with channel width and depth based on measurements.

2.4.1 Parameters

Horizontal variability of the saturated hydraulic conductivity K was calibrated using 38 pilot points (Tang et al., 2017; Moeck et al., 2015) distributed inside the study site. Each of these pilot points were associated with a K value, which was set to 0.1 m d^{-1} prior to calibration. For the vertical K heterogeneity, it was assumed that K was depth dependent and decreased exponentially when the aquifer was deeper than 0.2 m, as $K = K_0$ for $d < 0.2 \text{ m}$, and $K = K_0 e^{-\lambda d}$ for $d > 0.2 \text{ m}$, where K_0 is the hydraulic conductivity of the aquifer top determined from the horizontal K field; d is the depth below the land surface; and λ is a factor constraining the decreasing rate, which was set to 0 prior to calibration. These formulations captured the general decreasing trend of K with depth while also reflecting the fact that this decreasing trend was not significant in the upper 0.2 m of the soil, which contained most roots and mainly consisted of poorly decayed organic material.

The surface domain and channel domain were uniformly parameterized with Manning roughness coefficients (Man-

ning et al., 1891). Prior to calibration, the roughness coefficients were set to $6 \times 10^{-6} \text{ dm}^{-1/3}$, a typical value for floodplains/grassland. The parameters described above were selected as key parameters that could significantly influence the flow processes, and they were optimized during calibration (Table S2 in the Supplement). Other parameters were assigned for the model domain according to literature values from Yang et al. (2018) from a nearby (25 km) catchment with similar geological settings. Values were then adjusted during calibration (Table S2).

2.4.2 Boundary and initial conditions

Input data were defined at a 1 h time resolution for the simulation, and all higher-resolution data (15 min) were aggregated accordingly. For the aquifer top boundary, spatially uniform and temporally variable precipitation was applied to the surface domain. Spatially uniform and temporally variable potential ET, estimated using the climate data, was specified as model input with actual ET being simulated by the model (Therrien et al., 2010). For the upstream boundary AB (Fig. 2), a constant groundwater head gradient of 0.02 in the direction of the stream was assumed according to the measured groundwater levels, such that a groundwater flux (Q_{up}) entering the subsurface domain across AB could be determined using Darcy's law. A temporally variable flux Q_{up}^c was directly applied to the inlet of the channel domain, representing the measured channel discharge rate. The groundwater recharge rates via the two lateral boundaries of the model domain AD and BC (Q_{left} , Q_{right}) were estimated using $R \cdot A_{\text{con}}$, where R is the annual mean groundwater recharge rate in this area ($\sim 200 \text{ mm yr}^{-1}$), and A_{con} is the contributing surface area associated with each lateral boundary estimated from the DEM. The respective recharge fluxes Q_{left} and Q_{right} were calculated as $0.18 \text{ m}^3 \text{ s}^{-1}$ per unit length and $0.09 \text{ m}^3 \text{ s}^{-1}$ per unit length. They were also allowed to vary by 0.1 to 10 times their initial values during model calibration (Table S2). Water can exit the model domains through the downstream boundary CD, either via the subsurface calculated using a constant groundwater head gradient of 0.02 (Q_{down}) or via the surface domain (Q_{down}^o) and channel outlet (Q_{down}^c), calculated using a critical depth boundary condition (Therrien et al., 2010). All other model boundaries were assumed to be impermeable (no flow boundaries).

A steady-state model was obtained by running a preliminary simulation using time-invariant boundary conditions. The steady-state results were used as initial conditions for the actual transient simulations to reduce the influence from inappropriate initial conditions.

2.4.3 Calibration

Transient calibration was performed using the software package PEST, which uses the Marquardt method to minimize a target function (describing the error between modeled and

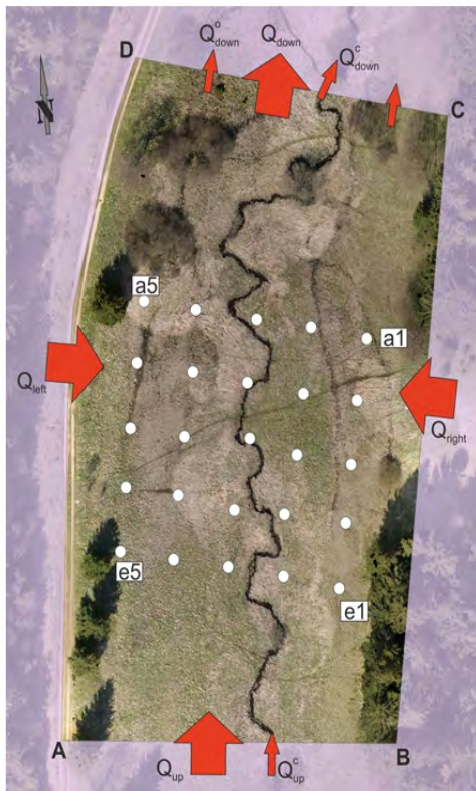


Figure 2. The boundary conditions of the study site (indicated by polygon A–D). Q_{up} : groundwater influx (const.), Q_{up}^c : channel influx (dynamic), Q_{down} : groundwater leaving the model site (dynamic), Q_{down}^c and Q_{down}^o : surface water leaving the model site through channel outlet and through CD (dynamic), Q_{left} and Q_{right} : groundwater recharge rate from side boundaries (const.). Red arrows indicate flow direction of the water. The 25 white points indicate wells which were used for model calibration. Labels of the piezometer run from a to e (lines) and 1 to 5 (columns).

measured variables; see Sect. S2 in the Supplement for the objective function) by varying the values of a given set of parameters until the optimization criterion is reached (Doherty and Hunt, 2010). The calibrated model parameters (Table S2) were set to be adjustable within the selected ranges around their initial values. The measured groundwater level time series at 25 observation wells and channel flux time series at the outlet (similar location to Q_{down}^o) were used to compare with the simulated ones (Fig. S6 in the Supplement), such that the target function could be calculated. Because two different data sets (groundwater level and channel flux) were used, a weighting scheme was selected to let the defined multi-objective function be dominated by the data set of groundwater levels. This was done because (i) we focused more on the groundwater flow and the associated surface–subsurface exchange fluxes and because (ii) the channel flux was relatively easy to reproduce by the model as measured

channel fluxes were directly assigned to the channel inlet. A 21 d period (15 November 2017 to 6 December 2017) was selected for the model calibration in view of the high CPU time demand for transient model runs, data availability constraints and data variability requirements. Wet and intermediate conditions generate almost all of the runoff of the riparian zone. The selected calibration period thus incorporates fluctuations during intermediate and high groundwater situations and therefore covers both system states (from subsurface-flux dominated to surface-flux dominated).

The time-variable groundwater levels were well replicated by the model for the wells near the channel (Fig. S6a). The wells close to the channel had better fits than those near the side boundaries (Fig. S6b), because the latter were more strongly constrained by the constant groundwater fluxes through the side boundaries. The calibrated flow model was used to quantify internal water flux data from specific regions in the riparian zone. Additionally, advective-dispersive particle-tracking was used on the flow field from the calibrated model to visualize surface and subsurface flow paths through the model domain. The surface flow paths are used to identify key runoff generation zones in the riparian zone.

2.5 Statistical methods

Statistical analysis was performed using R (R Core Team, 2014). Evaluation of geospatial properties was conducted via R in combination with ArcMap (ESRI, USA).

2.5.1 Chemical classification of potential DOC source zones

The peak-intensity-weighted average (wa) of the FT-ICR-MS-derived molecular parameters (mass to charge ratio (m/z), elemental ratios (H/C, O/C, N/C, S/C), nominal oxidation state of carbon (NOSC) and aromaticity index (AI)) was calculated for each sample by Eq. (1):

$$wa_p(x) = \frac{\sum p_i(x) \cdot \text{int}_i(x)}{\sum \text{int}_i(x)}, \quad (1)$$

where $wa_p(x)$ is the weighted average value for the molecular parameter p in sample x ; $p_i(x)$ is the derived value for the parameter p of each molecular formula i in sample x . Accordingly, $\text{int}_i(x)$ is the peak intensity for molecular formula i in sample x .

A principal component analysis (PCA) was then performed with the riparian samples ($n = 66$) using the FT-ICR-MS-derived wa molecular parameters of all molecular formulas commonly detected in all investigated samples of the monitoring site (i.e. including the event samples, $n = 68$, and the base flow samples, $n = 5$; Table S1), covering on average 40 % of the assigned intensities in each sample. A consecutive k -means clustering on the first two principal components (R package FactoMineR; Lê et al., 2008) was used to partition the riparian samples into two (as suggested by

the silhouette index; Rousseeuw, 1987) chemically distinct clusters, representing different DOC quality in the riparian groundwater. The Wilcoxon rank sum and the Kolmogorov Smirnov (KS) test were applied to identify significant differences in the distributions and medians of DOC concentration and FT-ICR-MS-derived molecular parameters for the two groundwater DOC clusters and stream water samples.

2.5.2 Hydromorphological classification of potential DOC source zones

Every groundwater level time series was correlated (Pearson's r) with the stream water level time series. Geomorphological analysis was conducted via the TWI, according to Eq. (2):

$$\text{TWI} = \log\left(\frac{f}{\tan(s)}\right), \quad (2)$$

where TWI is the topographic wetness index for each cell, f is the flow accumulation (the accumulated number of all cells topographically draining into a downslope cell) at each cell and s is the slope in radians of the respective cell. We applied the DInf algorithm to calculate a realistic hydrological routing (Tarboton, 1997). The DInf algorithm determines flow direction as the steepest downward slope on eight triangular facets formed in a 3×3 cell window centered on the cell of interest. To account for mathematical infinity/indefinite terms, zero slopes were set to 0.001 rad, and cells with no flow accumulation ($f = 0$) were set to 1 cell instead.

A smoothed map of the local high-resolution TWI (TWI_{HR}) values was created by assigning the median TWI value of the central cell and its 8 surrounding cells to the central cell. According to KS and F-test statistics, the resulting map represented the non-smoothed TWI distribution of the study site ($p_{KS} = 0.33$; $p_F = 0.76$). We applied the Wilcoxon rank sum to test for differences in TWI_{HR} distributions and medians of the two DOC clusters. The median TWI_{HR} value of the DOC_I cluster was used as a manually chosen threshold to separate the RZ into two explicit zones of high- and low-TWI_{HR} values. The water balance for the entire model site and the two TWI_{HR}-generated zones was then estimated and compared to each other between 12 April 2017 and 19 December 2018 by modeling with HydroGeoSphere.

3 Results

3.1 Hydroclimatic conditions and DOC chemical characterization

A summary of the statistics of discharge, groundwater level and climatic variables throughout the 15-month measurement period is presented in Table 1. Discharge showed high variability at the event scale. At annual scale, discharge expressed a clear seasonal pattern, with lowest values in late

Table 1. Summary statistics of climatic, hydrological and chemical parameters of the study site and samples collected during the monitoring campaign between 12 April 2017 and 19 December 2018. ET₀: potential evapotranspiration, and DOC conc.: DOC concentration. The symbol “wa” indicates peak-intensity-weighted average values of the FT-ICR-MS-derived molecular parameters: wa_{mz} (mass to charge ratio), wa_{HC} (hydrogen to carbon ratio), wa_{OC} (oxygen to carbon ratio), wa_{SC} (sulfur to carbon ratio), wa_{AI} (aromaticity index), and wa_{NOSC} (nominal oxidation state of carbon).

	Mean	SD	min	max
Air temperature [°C]	8.6	8.18	−18.9	34
Rain [mm h ^{−1}]	0.11	0.62	0	31.8
ET ₀ [mm d ^{−1}]	1.65	1.24	0	4.6
Stream water level [cm]	14.64	8.48	3.54	69.94
Discharge [L s ^{−1}]	58.7	92.9	8.2	1116.0
DOC conc. [mg L ^{−1}]*	3.80	2.77	0.69	15.77
wa _{mz} *	436	8	420	453
wa _{HC} *	1.28	0.05	1.15	1.41
wa _{OC} *	0.40	0.01	0.36	0.45
wa _{SC} (× 10 ³)*	8.6	2.2	4.9	15.8
wa _{AI} *	0.09	0.02	0.05	0.15
wa _{NOSC} *	−0.41	0.06	−0.55	−0.16

* for groundwater and riparian surface water samples taken from April 2018 to July 2019 (single spots were sampled multiple times throughout year, $n = 66$). A breakdown of average molecular parameters into the DOC clusters and the corresponding stream and event data can be found in Table S3.

summer and highest values in spring (Fig. 3c). Stream water level was highest during a flood event from 1 to 3 January 2018 when the Rappbode stream went over its bank. We decided to not include this event in the statistics, because we could not estimate the discharge for water levels higher than the stream banks. Yet observing this flood event helped to verify and understand riparian surface runoff pathways at our study site. The amount of precipitation during 2018 (580 mm) was below the long-term annual mean (831 mm) at the nearest official weather station. Air temperature exhibited a seasonal pattern and was above the long-term annual mean at the nearest station (8.6 vs. 6.0 °C).

Stream water levels (Fig. 3c) were closely coupled with groundwater levels, with lower and more fluctuating water levels in summer and less variable higher water levels in winter (Fig. 3b). Water level fluctuations in wells closer to the stream followed stream stage variations more closely than in the wells more distant to the stream, which showed more damped dynamics (Fig. 3a). This results in Spearman correlations (r_s) of groundwater level time series with the stream between 0.43 and 0.86 (mean of all $r_s = 0.60$). The groundwater table was shallow throughout the measurement period with highest values in winter and after snowmelt in spring (cf. red bars in Fig. 3b).

An overview of hydroclimatic data for the dates of DOC sampling (Fig. 3b and c) in the stream or the RZ is given in Table S4 in the Supplement. DOC concentrations in the

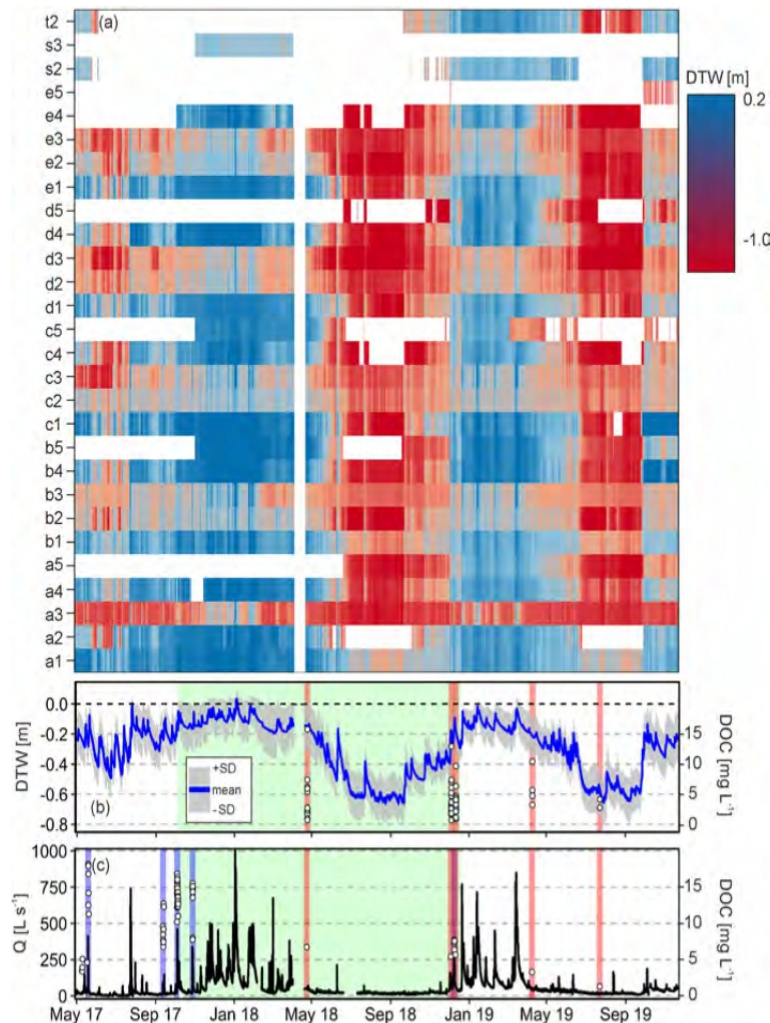


Figure 3. (a) Depth to water table (DTW) time series of all 28 riparian wells. White spaces indicate missing data in the time series: due to varying (de)installation times (if white in the beginning), sensor failure (white gaps in every time series) and dryness-induced disconnection of wells with the groundwater (white gaps in red areas). Locations of wells are depicted in Fig. 2. (b) Time series of mean DTW values (blue line) \pm the standard deviation (grey ribbon). A positive value of DTW indicates water ponding at the soil surface or that the piezometer measured a locally confined part of the aquifer. Red vertical bars indicate sampling dates of riparian groundwater. Points within the red bars show DOC concentration of respective riparian samples. Green area indicates the modeling period where ground water levels were used for calibration. (c) Discharge time series of the central pressure transducer. Blue vertical bars indicate stream water autosampler dates during events; red vertical bars indicate grab sampling dates of stream water. Points within blue and red bars show DOC concentrations according to stream water samples. Green area indicates the modeling period where ground water levels were used for calibration. Note that the flood event at the beginning of January 2018 is ungauged.

stream during events generally followed the hydrograph, with higher concentrations during higher water levels. DOC concentration and molecular properties across all riparian groundwater samples exhibited a distinct variability (Table 1). In general, DOC in riparian water samples was of an unsaturated and phenolic composition ($w_{\text{HC}} = 1.27 \pm 0.05$; $w_{\text{OC}} = 0.40 \pm 0.01$; $n = 66$), that is typically found in wetland surface soils (LaCroix et al., 2019). Stream event sam-

ples significantly differed ($p < 0.001$) from riparian samples and were more unsaturated ($w_{\text{HC}} = 1.17 \pm 0.05$; $n = 76$) and more oxygenated ($w_{\text{OC}} = 0.43 \pm 0.03$) as shown in Fig. S7 in the Supplement.

3.2 Classification and mapping of potential DOC sources

3.2.1 Chemical classification

A detailed overview of the FT-ICR-MS results of the distinct water samples can be found in Sect. S3, Tables S3 and S5, and Figs. S8–S10 in the Supplement. The PCA to classify riparian DOC quality was able to explain 66.3 % of the total variance of FT-ICR-MS peak intensities using two principal components (PCs). The *k*-means clustering based on the PCs then separated the riparian samples into two clusters of 19 and 47 samples (DOC_I and DOC_{II}, resp.; Fig. S11 in the Supplement), representing distinct DOC quality in the riparian zone. Weighted average molecular parameters were significantly different between the two clusters, allowing for a clear separation between DOC_I and DOC_{II} (Fig. 4a, Table S3). In contrast to the DOC_{II} cluster, samples belonging to the DOC_I cluster had higher DOC concentration, and their molecular composition was characterized by more oxidized (higher NOSC and wa_{OC}) and more aromatic molecules (higher wa_{AI}), with a lower fraction of heteroatoms (smaller wa_{SC}, wa_{NC} not shown) and a lower molecular weight (smaller wa_{mz}). Regarding the high-resolution event sampling, all samples were used, but inter-event variance of DOC properties was higher than intra-event variance. Therefore, we considered bulk sample properties of every event to be satisfactory for comparison with the riparian samples (Fig. 4a). Comparison of DOC_I and DOC_{II} molecular parameters and concentration with that of stream water sampled during rain events in spring, summer and autumn confirmed overall different DOC quality between riparian groundwater and stream water (based on median values and ranges; Fig. 4). However, median values of the DOC_I cluster were always closer to the median of stream water event samples than the respective DOC_{II} median. Moreover, the DOC molecular parameters of one event in December (Fig. 4a, orange dots) was in the range of the riparian samples but did not show much compositional variability within the event.

DOC_I samples from April ($n = 9$, Fig. 3) and December ($n = 9$) did not show significant differences in DOC molecular parameters (except wa_{HC}) and concentration (Fig. 4b). In addition, DOC concentration and quality in the stream samples (from the routine measurement program, non-event conditions) generally matched DOC_I concentration and quality in April and December (except wa_{HC} and wa_{AI}). In contrast, DOC_{II} samples from April ($n = 13$) and December ($n = 33$) differed significantly according to their wa_{mz}, wa_{HC}, wa_{AI}, wa_{NOSC} values and DOC concentration (Fig. 4c). While DOC concentration and quality of stream water samples from December were mostly within the range of the respective DOC_{II} samples, stream water samples from April were mostly outside the range of the DOC molecular parameters and concentrations of the respective DOC_{II} samples.

Both DOC clusters were associated with groundwater sampled at depth to water table (DTW) > -0.3 m in eight cases. Median high-resolution TWI (TWI_{HR}) values at the well position (see Sect. 2.5) were grouped according to their attribution to the DOC_I and DOC_{II} clusters based on the chemical characterization. Note that 7 (i.e. 6 wells and 1 surface pond sample) out of 15 locations occur in both DOC clusters as DOC quality varied over time. According to TWI_{HR} values also contribute to both clusters (Fig. 4d). In general, the median values of TWI_{HR} for wells attributed to samples of the DOC_I cluster were significantly higher (Wilcoxon rank sum $p < 0.008$) than respective values of the samples of DOC_{II} cluster (Fig. 4d). The distribution (median) of TWI_{HR} was different (higher) when comparing the TWI_{HR} values of DOC_I vs. DOC_{II} samples from April, whereas December samples did not show any statistically significant difference in their TWI_{HR} distribution or median.

3.2.2 Spatial mapping

The significant difference in median TWI_{HR} values of well locations contributing to the DOC_I and DOC_{II} clusters (Wilcoxon rank sum $p < 0.008$) was used to spatially separate potential source zones by using the median TWI_{HR} value of the well locations of the DOC_I cluster (9.66) as a threshold. Using this manually chosen threshold allowed us to allocate the samples of both DOC clusters to two distinct TWI_{HR}-based groups. In this way, more than 50 % of samples contributing to the DOC_I cluster constitutes one group while allowing less than 25 % (15 % in April) of the samples contributing to the DOC_{II} cluster in that group (again note that 7 out of overall 15 sampling locations appear in both TWI groups). Extending this TWI_{HR}-based grouping to the entire study site, the riparian zone was divided into zones of high-TWI_{HR} (DOC_I source zone in the following) and low-TWI_{HR} (DOC_{II} source zone) values (Fig. 5). The high-TWI_{HR} zones defined in this way represent 14.6 % of the area of the study site.

The HydroGeoSphere (HGS) model was then used to quantify the runoff generation from the delineated DOC_I source zones and to quantify their impact on total runoff generation and DOC export from the study site. According to our simulations, surface runoff, which we define here as all water running off at the surface eventually reaching the stream (originating from groundwater exfiltrating to the land surface or direct precipitation onto saturated areas), was the main source of total flow gain in the stream over the simulation period (Fig. 6). Surface inflows into the channel constituted 66 % of the total flow gain along the simulated stream segment over the simulation period. The median contribution of surficial runoff to total runoff generation during the model period was 61 % (± 12 % SD) but surface contributions increased up to 99 % during event situations. We selected the subsurface–surface exchange flux as a key descriptive variable for potential surface runoff con-

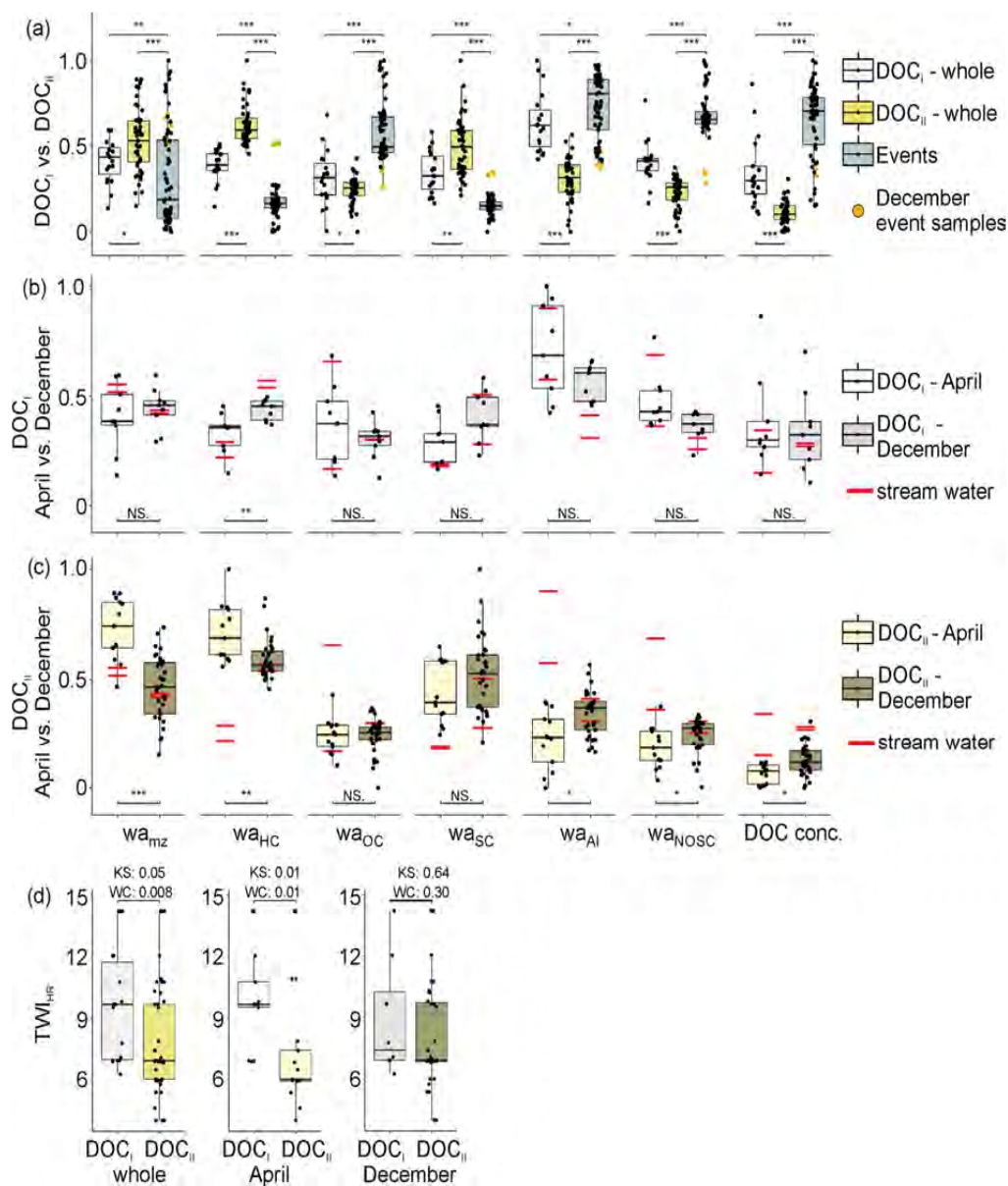


Figure 4. Comparison of FT-ICR-MS-derived weighted average (“wa”) molecular parameters w_{mz} (mass to charge ratio), w_{HC} (hydrogen to carbon ratio), w_{OC} (oxygen to carbon ratio), w_{SC} (sulfur to carbon ratio), w_{AI} (aromaticity index) and w_{NOSC} (nominal oxidation state of carbon) as well as DOC concentration (DOC conc.) and high-resolution TWI (TWI_{HR}) values of stream, DOC_I and DOC_{II} samples. (a) Boxplots of molecular parameters and DOC concentration of the DOC_I and DOC_{II} clusters. Orange dots indicate samples of one December event. (b) Boxplots of molecular parameters and DOC concentration of April and December DOC_I samples and all event samples. (c) Boxplots of molecular parameters and DOC concentration of April and December DOC_{II} samples and all event samples. Red horizontal lines in panels (b) and (c) indicate weighted averages of two April and two December stream water samples collected during the respective riparian groundwater sampling campaign. Data in panels (a–c) were min–max normalized to values between 0 and 1 for better illustration (see Table 1 for actual values). (d) Boxplots of TWI_{HR} values as affiliated to the respective wells of DOC_I and DOC_{II} samples. Wilcoxon rank sum (WC) and Kolmogorov–Smirnov (KS) test results are depicted above the squared brackets. Squared brackets above and below boxplots in (a–c) indicate the application of a KS test between two partitions. Asterisks indicate p values of the KS test (***: < 0.001; **: < 0.01; *: < 0.05; NS: not significant).

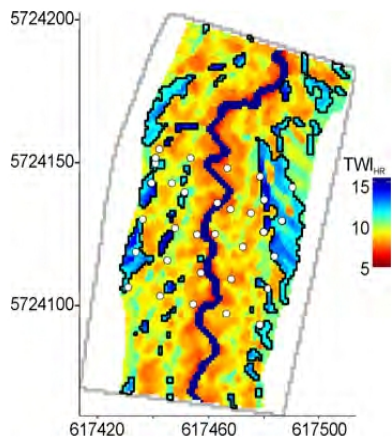


Figure 5. High-resolution TWI (TWI_{HR}) map of the modeled site (excluding hillslopes). White points indicate sampling locations; the Rappbode stream is indicated by the blue line. Black polygons are high- TWI_{HR} zones, indicating DOC_I source areas.

tributions, because it quantifies the availability of water at the surface for each cell of the model. Although there was a 1.5 times higher net surface water flux generation from low- TWI_{HR} zones throughout the modeling period (Fig. 6b), the median of the area-normalized water exchange flux for DOC_I source zone (high- TWI_{HR} zones; 0.026 m d^{-1}) was about 8.6 times higher than that for DOC_{II} source zones (low- TWI_{HR} zones; 0.003 m d^{-1}). This resulted in higher absolute exchange fluxes in high- TWI_{HR} zones in about 47 % of the modeling period. During (non-winter) runoff events, water exchange flux contribution of high- TWI_{HR} zones increased up to 100 % (negative or no exchange flux for DOC_{II} source zones in dry summer). Low- TWI_{HR} zones contributed more potential surface runoff at non-event winter conditions and flooding events when high overall exchange fluxes occurred under fully saturated soil conditions. Hydrological conditions were exemplary mapped for situations on 13 December 2017, immediately after an event under wet antecedent conditions, and on 29 August 2018, amidst a prolonged dry period in summer (Fig. S8; see Table S6 in the Supplement for corresponding water fluxes). High TWI_{HR} zones had the highest exchange fluxes and water depths in both wet and dry situations. Surface flow paths in winter intersect the high- TWI_{HR} zones establishing hydrologic connectivity between these zones and the stream, which is in line with our observations on DOC quality. The highest positive exchange flux values (GW exfiltration) occurred at the outer hillslope boundaries of the RZ, running parallel to the channel (values at the exact boundaries of the model have not been taken into account due to potential boundary effects). These exfiltration spots were located close to the strongest surface water infiltration spots. During the exemplary wet situation, the entire RZ was saturated with water besides the stream banks. Surficial runoff pathways then connect the DOC_I source ar-

reas (high- TWI_{HR} zones), running parallel to the stream and eventually entering it within the modeled domain.

3.3 Surface DOC export from high- TWI_{HR} and low- TWI_{HR} source zones

During the model period, wells in DOC_I source zones had a median DOC concentration of 5.8 mg L^{-1} (mean \pm SD: $6.2 \pm 2.7 \text{ mg L}^{-1}$), which was 2.3 times higher than the median for the DOC_{II} source wells ($2.7 \pm 1.2 \text{ mg L}^{-1}$). We assumed the DOC concentrations to stay in a range of mean \pm SD throughout the year (cf. Fig. 4b and c). DOC export was then roughly calculated by multiplying mean \pm SD of DOC_I and DOC_{II} concentrations with the absolute surface runoff volumes from the respective high- and low- TWI_{HR} zones. With that, mean overall export from high- TWI_{HR} zones exceeded that from low- TWI_{HR} zones in about 70 % of the time, although making up only 14.6 % of the total area. In absolute numbers, high- TWI_{HR} zones exported roughly 1.5 times the amount of DOC ($7.1 \times 10^6 \text{ g}$) to the stream than low- TWI_{HR} zones ($4.6 \times 10^6 \text{ g}$). This amounts to a nearly 20 times higher area-normalized DOC export from high- TWI_{HR} zones than from low- TWI_{HR} zones. Highest disparity between the export of the two source zones was during events in autumn and spring when surface water in the low- TWI_{HR} zone infiltrated instead of rapidly flowing into the stream (no DOC export from low- TWI_{HR} zones, Fig. 7) while high- TWI_{HR} zones exported DOC (positive spikes). Infiltrating conditions for the high- TWI_{HR} zone only occurred during summer events when DOC export was generally at the minimum (mean daily export rates of 3.1 and 17.3 g d^{-1} for low and high- TWI_{HR} zones, respectively), whereas equally high DOC export occurred in winter (234.2 and 267.2 g d^{-1} for low and high- TWI_{HR} zones, respectively). The median export from the high- TWI_{HR} zone was above that from low- TWI_{HR} zone in non-winter conditions, with the highest disparity between medians in spring and autumn (Fig. 7). Then high- TWI_{HR} zones exhibited exfiltrating conditions, whereas water in low- TWI_{HR} zones kept infiltrating.

4 Discussion

4.1 Small-scale topographical heterogeneity delineates DOC source zones in terms of molecular composition and hydrologic connectivity

RZs of lower-order streams constitute a manageable control unit for DOC export, but small-scale processes in the RZ are not well enough understood to properly predict DOC export. We hypothesized that DOC production and transport are predominantly controlled by the microtopography of the RZ (lateral variability) and by the location of the riparian groundwater level (temporal variability). Therefore, we identified DOC source areas within a riparian zone based on topographic and chemical analyses and evaluated the temporally

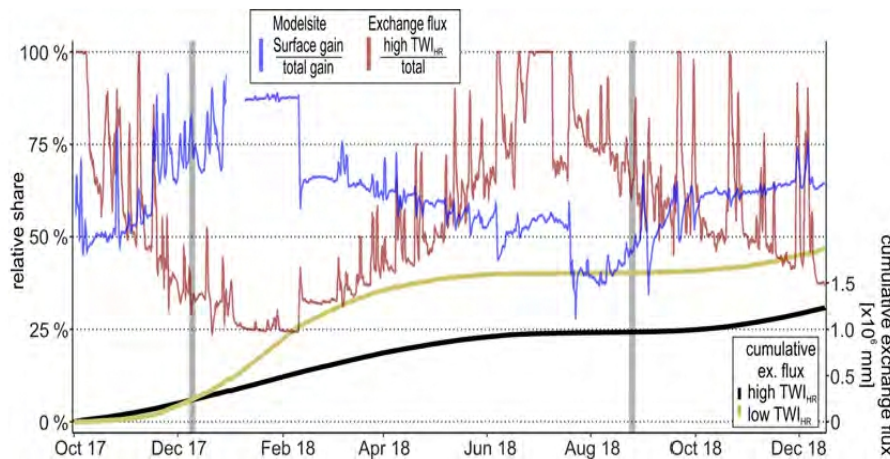


Figure 6. Share of surface runoff on total runoff generation (blue line) and of high-TWI_{HR} zone water exchange flux on total exchange flux in the model site (red). Data were smoothed to daily values for better visualization. The gap in the blue line in January 2018 is due to an ungauged flood event. Cumulative positive water exchange flux of high-TWI_{HR} (black) and low-TWI_{HR} (yellow) source zones are shown on the second vertical axis. Grey bars indicate modeling dates for a wet situation on 13 December 2017, right after an event and at dry conditions, and on 29 August 2018, amidst a longer dry period in summer (Fig. S8, Table S6).

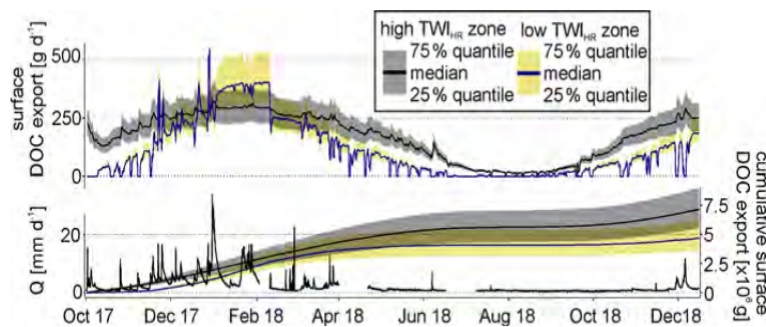


Figure 7. Absolute DOC surface export (25th, 50th and 75th percentiles) from high-TWI_{HR} (DOC_I quality) and low-TWI_{HR} (DOC_{II} quality) source zones. Underlying DOC concentration percentiles based on all riparian groundwater samples of each source zone. Cumulative positive DOC export (25th, 50th and 75th percentiles) from high- and low-TWI_{HR} zones are shown on the second y axis. Discharge rate (Q) (lower black line) is shown on the lower left vertical axis.

variable export of DOC from these source areas to the stream using numerical flow modeling.

In general, our chemical observations are in line with UV-Vis-derived DOC properties presented in Werner et al. (2019) for the same study site. Other RZs in temperate (Strohmeier et al., 2013; Raeke et al., 2017), boreal (Ledesma et al., 2018b) and mediterranean (Guarch-Ribot and Butturini, 2016) climates show a comparable DOC property spectrum. Separating the riparian DOC samples according to their chemical characteristics revealed two chemically distinct DOC clusters in the RZ (DOC_I and DOC_{II}). The molecular composition of DOC_I indicates processed plant-derived organic matter, similar to typical wetland sites (Tfaily et al., 2018). The high DOC concentrations and oxygen-rich and aromatic character point to overall low organic matter

turnover within the DOC_I source zones. With that, DOC_I is less available for microbial degradation (Mostovaya et al., 2017) but can readily be photodegraded (Wilske et al., 2020) and removed through sedimentation (Dadi et al., 2017) or in drinking water treatment (Raeke et al., 2017). In contrast, DOC_{II} (more saturated, oxygen-depleted and heteroatom-enriched) more represents microbial, secondary metabolites indicative of increased microbial processing of organic matter from organic rich top-soil layers and DOC which is not adsorbed to mineral phases. DOC of this chemical characteristic is typically found in deeper soil layers (Shen et al., 2015; Kaiser and Kalbitz, 2012; LaCroix et al., 2019). Yet, the DOC clusters were independent of sampling depth (note that a given sample location or depth (Fig. S1) can experience low or high groundwater levels at different times). Rather,

both DOC clusters were dividable by the TWI_{HR} value of the well locations from which the respective samples were collected, suggesting the existence of two DOC pools with distinct source zones in the study site. Although the chosen threshold value is arbitrary, and a small number of the wells switched from one DOC cluster to the other over time, separating DOC source zones based on TWI_{HR} is plausible from a process-based perspective. High TWI_{HR} values – connected to DOC_I source zones – represent zones with increased water and solute (DOC) inputs from adjacent areas, leading to hydrological upwelling and DOC processing by microtopography-induced gradients in redox conditions (Frei et al., 2012). Zones with high- TWI_{HR} values are generally connected to higher mean groundwater levels due to increased flow convergence to these zones and concomitant waterlogging (Luke et al., 2007), which can create a conserving environment for DOC due to anaerobic conditions even in the topmost soil layers (LaCroix et al., 2019), potentially leading to DOC accumulation. In contrast, zones with low- TWI_{HR} values are generally characterized by lower mean groundwater levels and thus more oxygenated top soils, allowing for more biogeochemical processing. Overall we conclude that small-scale topographic heterogeneity (here represented by TWI_{HR}) can be linked to DOC properties in RZs if the fluctuations of the groundwater level, which dynamically intersects with the surface microtopography, are properly accounted for.

4.2 Connecting riparian DOC sources to the stream

The close agreement between molecular parameter of the DOC_I and corresponding stream water samples in April and December suggest a predominant connectivity of DOC_I source zones with the stream in times of high groundwater levels. In addition, the DOC_I quality was similar between April and December, indicating a DOC pool that is not strongly affected by seasonality and hydrologic conditions (i.e. steady export also during the wet and cold state; cf. Werner et al., 2019). Therefore, DOC_I can be regarded as a permanently available source of DOC to the stream water. In contrast, the DOC_{II} molecular composition was reflected in the DOC composition of stream water in December but not in April, suggesting a connectivity of this pool during high flow periods but a potential depletion over time. Less organic matter input and lower biogeochemical process rates in winter and at the same time increased DOC export (at higher groundwater levels) may specifically deplete the DOC_{II} pool (Werner et al., 2019). The molecular composition of DOC_{II} samples in April thus may represent a pool of remaining DOC with low sorption affinity that was not depleted during high groundwater levels in winter (saturated and with larger molecular weight and oxygenation).

Variations in stream DOC molecular composition also appeared during events, indicating a link between DOC export and groundwater level dynamics which ultimately drive hydrological connectivity.

Fully saturated riparian conditions connected the DOC_I and DOC_{II} source zones with the stream in December, leading to a stream DOC quality with molecular parameters that were between the two riparian DOC clusters as also suggested by Werner et al. (2019) for this study site. On the other hand, DOC_I and stream water DOC molecular compositions are converging during events with lower antecedent groundwater levels and unsaturated soils, suggesting that DOC_I becomes the predominant source when DOC_{II} is (still) depleted, e.g. from snowmelt in April. We argue that changing load contributions from both riparian DOC source zones are induced by the prevailing hydrological situation, which distinctly shapes DOC export in this RZ. Observed deviations of in-stream DOC from the riparian source DOC composition might be a result of near-stream and in-stream processing (Dawson et al., 2001; Battin et al., 2003) but also inter- and intra-annual variability of hydroclimatic drivers like seasonality or antecedent soil conditions (Werner et al., 2019; Köhler et al., 2009; Strohmeier et al., 2013; Futter and de Wit, 2008). Yet we showed direct links between six major DOC molecular properties and the DOC concentration of riparian and stream water samples. In comparison to other studies, which have used integrated or indirect signals to derive information on DOC characteristics, like (specific) UV absorption and spectrophotometric slope values (Ledesma et al., 2018b; Werner et al., 2019), or electric conductivity and pH (Ploum et al., 2020), this allows for a spatially explicit alignment of riparian DOC source zones to stream water samples at higher credibility.

Additionally, the physically based model HGS independently showed that the dominant runoff generating mechanism (and thus potential DOC export pathway) at the study site is surface runoff from DOC_I source zones. The high- TWI_{HR} zones are characterized by morphological and hydrological conditions that produce more runoff per unit area and in turn they react more directly to precipitation than DOC_{II} source zones (with low- TWI_{HR} values). The microtopography allows for reinfiltration of overland flow and exfiltration of shallow saturated flow. However, our model runs (and field observations) confirmed the importance of surface flow actually entering the stream as the dominant runoff generation mechanism. Even though surface flow was nearly absent during the summer, snowmelt in spring and abundant rainfall in the autumn both generated periods with overland flow that were the main contributors to the annual runoff of the stream. Further confirmation that overland flow is the main delivery pathway of DOC to the stream can be found in the chemical fingerprints of individual source areas we sampled. Seven chemical characteristics of these sources (some of which are far from the stream) can be seen in the stream water as well, indicating that the hydrochemistry was not strongly affected when the water was carried from the source to the stream. This is consistent with a rapid delivery via overland flow but not with a slower flow rate through the chemically active subsurface. The volumetric range of event water in our catch-

ment is in line with studies mentioned in Klaus and McDonnell (2013), but our results deviate from their general conclusion that stream water predominantly comes from pre-event water from the subsurface. Most of the runoff generation in our study site occurs during events under saturated conditions with significant fractions of fresh event water from direct precipitation onto saturated surface areas. In that sense, the generated surface runoff is a mix of pre-event water that exfiltrates from the subsurface (as indicated in our study and suggested by Frei et al., 2012) with event water from precipitation. Surface contributions are linked to the landscape organization and topographic catchment characteristics (James and Roulet, 2009; Suecker et al., 2000). Our riparian study site has an overall low topographic relief (but steep hillslopes) and consists of hydromorphic soils of typically low hydraulic conductivity. Given the nature of this study site, overland flow is to be expected as a significant export pathway connecting riparian DOC sources to the stream.

4.3 Quantifying riparian DOC export to stream

Quantifying DOC exports from riparian hotspots to the stream has rarely been done (Bernhardt et al., 2017), most probably because capturing mechanistic and spatiotemporal dynamics of small-scale hotspots and hot moments is challenging. Further, the impact of vertical versus horizontal heterogeneity on solute export is still under debate, although mostly at the large scale (Herndon et al., 2015; Zhi et al., 2019). We found no statistically significant relation between sampling depth and well DOC classification in our samples, but the possibility of a bias exists since samples were predominantly taken in deeper soil layers – also due to the fact that there often was no near-surface water available when groundwater samples were taken. Yet, near-surface samples as well as deep samples appear in both clusters in more or less equal parts. The presence of microtopography-induced hotspots in RZs has been theoretically shown in a modeling study by Frei et al. (2012), who described a small-scale hydraulic and biogeochemical impact on nutrient processing in a generic wetland. In this study, we showed an overall dominance of DOC₁ export from high-TWI_{HR} zones during events, despite making up only about 15 % of the total study site area. Zones with a high-TWI_{HR} export 8.7 times more DOC than low-TWI_{HR} zones, which is in line with DOC export from hotspots in a forested stream in a humid continental climate (Wilson et al., 2013) and generally in range of different hotspot effect sizes (Bernhardt et al., 2017). Based on our spatiochemical classification and numerical water flow modeling, our findings suggest a clear link between DOC quality and lateral topographic heterogeneity (represented by TWI_{HR}) supporting the findings from Frei et al. (2012). As with Ledesma et al. (2018b), our work recommends to focus riparian DOC research on overall smaller scales, but in addition we showed that surface flow from localized source areas is an important carrier of DOC towards the stream. The re-

sults obtained from our study site therefore provide no direct evidence for the existence of a distinct dominant source layer in the subsurface (Ledesma et al., 2018b) and put a spatially lumped application of a riparian integration model as proposed by Seibert et al. (2009) into question. Both of these other approaches assume predominantly horizontal subsurface flow as the main transport mechanism for DOC. At our site, in contrast, the shallow depth to bedrock and the humid climate facilitated the creation of generally wet conditions, where saturation-excess overland flow can become the main mode of DOC export to the stream. Microtopography determines the location (lateral variability) of the dominant DOC source areas, but the dynamic mobilization of DOC during events is controlled by the hydrological drivers rainfall and snowmelt and their immediate effect on riparian groundwater levels (temporal heterogeneity).

4.4 Potential for future work and implications

Recent studies have concluded that lateral DOC fluxes from terrestrial to aquatic ecosystems are not well researched but contribute an important share of the global DOC budget (Zarnetske et al., 2018; Wen et al., 2020). In this regard, we found that surficial DOC export dominated overall DOC export to the stream at our study site. Yet surface DOC export is underrepresented in current model conceptualizations of lateral DOC export (Dick et al., 2015; Ledesma et al., 2018a; Bracken et al., 2013). Reasons for the exclusion might be due to the high complexity of representing the spatiotemporal heterogeneity of surface export in modeling concepts or just because it may play a minor role in other catchments. Considering highly resolved heterogeneity in large-scale models is not tractable, but understanding the export mechanisms of riparian zones at high spatial resolution allows us to better estimate overall DOC export potential of catchments as a function of climatic variability and general topographic structure (Jencso et al., 2009). Further investigating TWI_{HR} dynamics could lead to new approaches and concepts for better DOC export modeling: a general, coarse-scale relationship between soil moisture and potential surface runoff generation has already been proposed based on a catchment-scale, topography-driven runoff proxy (Gao et al., 2019; Birkel et al., 2020). The mechanistic connection between TWI_{HR} and surface DOC export in our study represents a similar general mechanism. This mechanism is potentially applicable to the entire riparian zone in small catchments (similar TWI_{HR} values should result in similar runoff generation), where stream runoff generation and DOC mobilization are inherently coupled. Respective model fluxes could be validated by each other thereby ensuring correct internal model functioning. Implementing the described DOC surface export mechanism to coupled hydrological-biogeochemical DOC export models (Dick et al., 2015; Lessels et al., 2015) could greatly improve the mechanistic basis of threshold-based and nonlinear model fluxes (Birkel et al., 2017). Combining a good mecha-

nistical biogeochemical and hydrological model representation with knowledge of DOC properties in respective DOC source zones could further reduce the need for tracer experiments in the field. The simultaneous simulation of fluxes of water and DOC of such a model combination facilitates internal model calibration and reduces equifinality (Abbott et al., 2016; Birkel et al., 2020), potentially leading to a more accurate upscaling of DOC export from RZs, especially for those with mild slopes and high groundwater levels.

5 Summary and conclusions

To elucidate spatial and temporal variability of DOC exports from riparian zones, this study combined a hydro-morphological classification of a humid temperate riparian zone with a chemical characterization of DOC in source zones and the stream and detailed modeling of water fluxes and flow paths. The chemical classification of riparian water samples via ultrahigh-resolution FT-ICR-MS revealed two distinct DOC clusters (DOC_I and DOC_{II}) in the riparian zone. Degrading plant material presumably contributes most to an aromatic, oxygen-rich DOC with high concentrations (DOC_I cluster), located in regions of high wetness in local topographic depressions. DOC_I is available for photo-degradation and can be relatively easily removed through sedimentation or later during drinking water treatment. The second cluster (DOC_{II}) reflects microbially processed, nonpolar (yet mobile) DOC with lower concentration and larger compositional variability across seasons that may be more persistent in the surface water. The source zones of DOC_I and DOC_{II} within the riparian zone can be separated and mapped by setting a threshold value for the high-resolution TWI (TWI_{HR}), suggesting the existence of two distinct DOC pools. The identification of source zones was achieved via independent measures (unsupervised chemical classification and TWI-based physical flux modeling), leading to higher credibility. The hydrological modeling revealed that the dominant runoff generation mechanism at the study site was surface runoff. We were able to quantify the contribution of each source zone to DOC export and noticed significant variations in those depending on the groundwater level and seasonal variations in the degree of depletion of the DOC_{II} pool. Mostly during events, DOC_I source zones, which make up only 15 % of the riparian area, exported 1.5 times more DOC than the remaining 85 % of the area associated with the DOC_{II} source zones. Highest discrepancy between the loads exported from the DOC_I and DOC_{II} zones was evident for events at intermediate antecedent wetness states (neither completely saturated nor very dry conditions). Overall we can confirm our initial hypothesis that DOC production and export are controlled by the lateral variability of topography within the RZ, interplaying with the temporal variability of groundwater levels. Understanding the export mechanisms of riparian zones at high spatial resolution al-

lows us to better estimate overall DOC export potential of catchments as a function of climatic variability and general topographic structure. In contrast to other studies in boreal catchments, this study highlights that DOC export from the riparian zone by surface runoff is important for DOC export from hydromorphic soils with overall low topographic riparian relief. Surface export should therefore not be neglected in DOC export models. Delineating activated source zones for DOC export by suitable proxies of the microtopography (here represented by TWI_{HR}) can help to identify source zones in existing DOC models as well as surface flow pathways from these sources to the stream. The combined biogeochemical and hydrological understanding of riparian DOC export generated here can be implemented in models. By doing so, fewer field tracer experiments may be needed while model calibration improves. This makes it easier to apply such models to a variety of RZs (especially those with mild slopes and high groundwater levels), possibly leading to catchment-scale model-based estimates of DOC export. This work showed that microtopography and the groundwater level are important determinants for DOC production and transport in a RZ. The microtopography varies only slowly with time and can be captured in a DEM (e.g. determined by a suitably equipped drone). Such a DEM enables researchers to identify probable source areas of DOC as well as potential flow paths that connect the source areas to the stream. Disrupting either the source areas or the flow paths (or both) can potentially reduce the DOC loading of the stream at low cost and with relatively little disturbance of the local ecosystem. Such measures might have to be repeated every few years, but even then, they may provide an attractive low-cost method to manage DOC in streams.

Data availability. All data sets used in this synthesis are publicly available via the following link: <https://doi.org/10.4211/hs.b32ba184414e475ba36a0bb193866ef1> (Werner, 2021).

Supplement. The supplement related to this article is available online at: <https://doi.org/10.5194/hess-25-6067-2021-supplement>.

Author contributions. BJW, JHF, OJL, AM and GHdR planned and designed the research. BJW performed the statistical analysis and wrote the paper with contributions from all co-authors. JY performed the hydrological modeling. BJW and OJL analyzed and interpreted the FT-ICR-MS data. UW implemented geophysical investigations. RG provided post-processed drone altimetry data.

Competing interests. Gerrit H. de Rooij is a member of the editorial board of the journal.

Disclaimer. Publisher's note: Copernicus Publications remains neutral with regard to jurisdictional claims in published maps and institutional affiliations.

Acknowledgements. Jan M. Kaesler is gratefully acknowledged for the FT-ICR-MS analysis at the Centre for Chemical Microscopy (ProVIS). We thank Toralf Keller for excellent and steady field work, Marco Pohle for geophysical field work, Kai Franze for software development, and Heidrun Paschke and Michaela Wunderlich for help with the DOC and nutrient analysis.

Financial support. This research was funded by the Helmholtz Research Program POF-III, Integrated Project "Water and Matter Flux Dynamics in Catchments". Additional funding was provided by the European Regional Development Funds (EFRE-Europe funds Saxony).

The article processing charges for this open-access publication were covered by the Helmholtz Centre for Environmental Research – UFZ.

Review statement. This paper was edited by Christian Stamm and reviewed by four anonymous referees.

References

- Abbott, B. W., Baranov, V., Mendoza-Lera, C., Nikolakopoulou, M., Harjung, A., Kolbe, T., Balasubramanian, M. N., Vaessen, T. N., Ciocca, F., Campeau, A., Wallin, M. B., Romeijn, P., Antonelli, M., Goncalves, J., Datry, T., Laverman, A. M., de Dreuzy, J. R., Hannah, D. M., Krause, S., Oldham, C., and Pinay, G.: Using multi-tracer inference to move beyond single-catchment ecohydrology, *Earth-Sci. Rev.*, 160, 19–42, <https://doi.org/10.1016/j.earscirev.2016.06.014>, 2016.
- Allen, R. G., Pereira, L. S., Raes, D., and Smith, M.: Crop evapotranspiration. Guidelines for computing crop water requirements, in: *Irrigation and Drainage*, edited by: FAO, FAO, Rome, 1998.
- Andersson, J.-O. and Nyberg, L.: Using official map data on topography, wetlands and vegetation cover for prediction of stream water chemistry in boreal headwater catchments, *Hydrol. Earth Syst. Sci.*, 13, 537–549, <https://doi.org/10.5194/hess-13-537-2009>, 2009.
- Battin, T. J., Kaplan, L. A., Newbold, J. D., and Hendricks, S. P.: A mixing model analysis of stream solute dynamics and the contribution of a hyporheic zone to ecosystem function, *Freshwater Biol.*, 48, 995–1014, <https://doi.org/10.1046/j.1365-2427.2003.01062.x>, 2003.
- Battin, T. J., Kaplan, L. A., Findlay, S., Hopkinson, C. S., Marti, E., Packman, A. I., Newbold, J. D., and Sabater, F.: Biophysical controls on organic carbon fluxes in fluvial networks, *Nat. Geosci.*, 1, 95–100, <https://doi.org/10.1038/ngeo101>, 2008.
- Bernhardt, E. S., Blaszcak, J. R., Ficken, C. D., Fork, M. L., Kaiser, K. E., and Seybold, E. C.: Control Points in Ecosystems: Moving Beyond the Hot Spot Hot Moment Concept, *Ecosystems*, 20, 665–682, <https://doi.org/10.1007/s10021-016-0103-y>, 2017.
- Beven, K. J. and Kirkby, M. J.: A physically based, variable contributing area model of basin hydrology, *Hydrolog. Sci. J.*, 24, 43–69, <https://doi.org/10.1080/02626667909491834>, 1979.
- Birkel, C., Broder, T., and Biester, H.: Nonlinear and threshold-dominated runoff generation controls DOC export in a small peat catchment, *J. Geophys. Res.-Biogeo.*, 122, 498–513, <https://doi.org/10.1002/2016jg003621>, 2017.
- Birkel, C., Duvert, C., Correa, A., Munksgaard, N. C., Maher, D. T., and Hutley, L. B.: Tracer-Aided Modeling in the Low-Relief, Wet-Dry Tropics Suggests Water Ages and DOC Export Are Driven by Seasonal Wetlands and Deep Groundwater, *Water Resour. Res.*, 56, e2019WR026175, <https://doi.org/10.1029/2019WR026175>, 2020.
- Bishop, K., Seibert, J., Koher, S., and Laudon, H.: Resolving the Double Paradox of rapidly mobilized old water with highly variable responses in runoff chemistry, *Hydrol. Process.*, 18, 185–189, <https://doi.org/10.1002/hyp.5209>, 2004.
- Bracken, L. J., Wainwright, J., Ali, G. A., Tetzlaff, D., Smith, M. W., Reaney, S. M., and Roy, A. G.: Concepts of hydrological connectivity: Research approaches, pathways and future agendas, *Earth-Sci. Rev.*, 119, 17–34, <https://doi.org/10.1016/j.earscirev.2013.02.001>, 2013.
- Butman, D. E., Striegl, R. G., Stackpoole, S. M., Del Giorgio, P., Prairie, Y., Pilcher, D., Raymond, P., Pellet, F. P., and Alcocer, J.: Inland waters, 568–595, <https://doi.org/10.7930/SOCCR2.2018.Ch14>, 2018.
- Catalán, N., Pastor, A., Borrego, C. M., Casas-Ruiz, J. P., Hawkes, J. A., Gutiérrez, C., von Schiller, D., and Marcé, R.: The relevance of environment vs. composition on dissolved organic matter degradation in freshwaters, *Limnol. Oceanogr.*, 66, 306–320, <https://doi.org/10.1002/lno.11606>, 2021.
- Chantigny, M. H.: Dissolved and water-extractable organic matter in soils: a review on the influence of land use and management practices, *Geoderma*, 113, 357–380, [https://doi.org/10.1016/S0016-7061\(02\)00370-1](https://doi.org/10.1016/S0016-7061(02)00370-1), 2003.
- Cole, J. J., Prairie, Y. T., Caraco, N. F., McDowell, W. H., Tranvik, L. J., Striegl, R. G., Duarte, C. M., Kortelainen, P., Downing, J. A., Middelburg, J. J., and Melack, J.: Plumbing the global carbon cycle: Integrating inland waters into the terrestrial carbon budget, *Ecosystems*, 10, 171–184, <https://doi.org/10.1007/s10021-006-9013-8>, 2007.
- Dadi, T., Harir, M., Hertkorn, N., Koschorreck, M., Schmitt-Kopplin, P., and Herzsprung, P.: Redox Conditions Affect Dissolved Organic Carbon Quality in Stratified Freshwaters, *Environ. Sci. Technol.*, 51, 13705–13713, <https://doi.org/10.1021/acs.est.7b04194>, 2017.
- Dawson, J. J. C., Bakewell, C., and Billett, M. F.: Is in-stream processing an important control on spatial changes in carbon fluxes in headwater catchments?, *Sci. Total Environ.*, 265, 153–167, [https://doi.org/10.1016/s0048-9697\(00\)00656-2](https://doi.org/10.1016/s0048-9697(00)00656-2), 2001.
- Diamond, J. S., McLaughlin, D. L., Slesak, R. A., and Stovall, A.: Microtopography is a fundamental organizing structure of vegetation and soil chemistry in black ash wetlands, *Biogeosciences*, 17, 901–915, <https://doi.org/10.5194/bg-17-901-2020>, 2020.
- Dick, J. J., Tetzlaff, D., Birkel, C., and Soulsby, C.: Modelling landscape controls on dissolved organic carbon sources and fluxes to streams, *Biogeochemistry*, 122, 361–374, <https://doi.org/10.1007/s10533-014-0046-3>, 2015.

- Dittmar, T., Koch, B., Hertkorn, N., and Kattner, G.: A simple and efficient method for the solid-phase extraction of dissolved organic matter (SPE-DOM) from seawater, *Limnol. Oceanogr.-Meth.*, 6, 230–235, <https://doi.org/10.4319/lom.2008.6.230>, 2008.
- Doherty, J. E. and Hunt, R. J.: Approaches to highly parameterized inversion: a guide to using PEST for groundwater-model calibration, US Department of the Interior, US Geological Survey, Virginia, 2010.
- Drake, T. W., Raymond, P. A., and Spencer, R. G. M.: Terrestrial carbon inputs to inland waters: A current synthesis of estimates and uncertainty, *Limnol. Oceanogr. Lett.*, 3, 132–142, <https://doi.org/10.1002/lo12.10055>, 2018.
- Fellman, J. B., Buma, B., Hood, E., Edwards, R. T., and D'Amore, D. V.: Linking LiDAR with streamwater biogeochemistry in coastal temperate rainforest watersheds, *Can. J. Fish. Aquat. Sci.*, 74, 801–811, <https://doi.org/10.1139/cjfas-2016-0130>, 2017.
- Frei, S., Lischeid, G., and Fleckenstein, J. H.: Effects of micro-topography on surface-subsurface exchange and runoff generation in a virtual riparian wetland – A modeling study, *Adv. Water Resour.*, 33, 1388–1401, <https://doi.org/10.1016/j.advwatres.2010.07.006>, 2010.
- Frei, S., Knorr, K. H., Peiffer, S., and Fleckenstein, J. H.: Surface micro-topography causes hot spots of biogeochemical activity in wetland systems: A virtual modeling experiment, *J. Geophys. Res.-Biogeo.*, 117, G00N12, <https://doi.org/10.1029/2012jg002012>, 2012.
- Futter, M. N. and de Wit, H. A.: Testing seasonal and long-term controls of streamwater DOC using empirical and process-based models, *Sci. Total Environ.*, 407, 698–707, <https://doi.org/10.1016/j.scitotenv.2008.10.002>, 2008.
- Gao, H., Birkel, C., Hrachowitz, M., Tetzlaff, D., Soulsby, C., and Savenije, H. H. G.: A simple topography-driven and calibration-free runoff generation module, *Hydrol. Earth Syst. Sci.*, 23, 787–809, <https://doi.org/10.5194/hess-23-787-2019>, 2019.
- Grabs, T., Bishop, K., Laudon, H., Lyon, S. W., and Seibert, J.: Riparian zone hydrology and soil water total organic carbon (TOC): implications for spatial variability and upscaling of lateral riparian TOC exports, *Biogeosciences*, 9, 3901–3916, <https://doi.org/10.5194/bg-9-3901-2012>, 2012.
- Guarch-Ribot, A. and Butturini, A.: Hydrological conditions regulate dissolved organic matter quality in an intermittent headwater stream. From drought to storm analysis, *Sci. Total Environ.*, 571, 1358–1369, <https://doi.org/10.1016/j.scitotenv.2016.07.060>, 2016.
- Herndon, E. M., Dere, A. L., Sullivan, P. L., Norris, D., Reynolds, B., and Brantley, S. L.: Landscape heterogeneity drives contrasting concentration–discharge relationships in shale headwater catchments, *Hydrol. Earth Syst. Sci.*, 19, 3333–3347, <https://doi.org/10.5194/hess-19-3333-2015>, 2015.
- Herzprung, P., Hertkorn, N., von Tümpling, W., Harir, M., Friese, K., and Schmitt-Kopplin, P.: Understanding molecular formula assignment of Fourier transform ion cyclotron resonance mass spectrometry data of natural organic matter from a chemical point of view, *Anal. Bioanal. Chem.*, 406, 7977–7987, <https://doi.org/10.1007/s00216-014-8249-y>, 2014.
- Herzprung, P., Wentzky, V., Kamjunke, N., von Tümpling, W., Wilske, C., Friese, K., Boehrer, B., Reemtsma, T., Rinke, K., and Lechtenfeld, O. J.: Improved Understanding of Dissolved Organic Matter Processing in Freshwater Using Complementary Experimental and Machine Learning Approaches, *Environ. Sci. Technol.*, 54, 13556–13565, <https://doi.org/10.1021/acs.est.0c02383>, 2020.
- James, A. L. and Roulet, N. T.: Antecedent moisture conditions and catchment morphology as controls on spatial patterns of runoff generation in small forest catchments, *J. Hydrol.*, 377, 351–366, <https://doi.org/10.1016/j.jhydrol.2009.08.039>, 2009.
- Jencso, K. G., McGlynn, B. L., Gooseff, M. N., Wondzell, S. M., Bencala, K. E., and Marshall, L. A.: Hydrologic connectivity between landscapes and streams: Transferring reach- and plot-scale understanding to the catchment scale, *Water Resour. Res.*, 45, W04428, <https://doi.org/10.1029/2008wr007225>, 2009.
- Kaiser, K. and Kalbitz, K.: Cycling downwards – dissolved organic matter in soils, *Soil Biol. Biochem.*, 52, 29–32, <https://doi.org/10.1016/j.soilbio.2012.04.002>, 2012.
- Kind, T. and Fiehn, O.: Seven Golden Rules for heuristic filtering of molecular formulas obtained by accurate mass spectrometry, *BMC Bioinformatics*, 8, 105, <https://doi.org/10.1186/1471-2105-8-105>, 2007.
- Klaus, J. and McDonnell, J. J.: Hydrograph separation using stable isotopes: Review and evaluation, *J. Hydrol.*, 505, 47–64, <https://doi.org/10.1016/j.jhydrol.2013.09.006>, 2013.
- Koch, B. P., Kattner, G., Witt, M., and Passow, U.: Molecular insights into the microbial formation of marine dissolved organic matter: recalcitrant or labile?, *Biogeosciences*, 11, 4173–4190, <https://doi.org/10.5194/bg-11-4173-2014>, 2014.
- Köhler, S. J., Buffam, I., Seibert, J., Bishop, K. H., and Laudon, H.: Dynamics of stream water TOC concentrations in a boreal headwater catchment: Controlling factors and implications for climate scenarios, *J. Hydrol.*, 373, 44–56, <https://doi.org/10.1016/j.jhydrol.2009.04.012>, 2009.
- Kotteck, M., Grieser, J., Beck, C., Rudolf, B., and Rubel, F.: World Map of the Köppen-Geiger climate classification updated, *Meteorol. Z.*, 15, 259–263, <https://doi.org/10.1127/0941-2948/2006/0130>, 2006.
- Krause, S., Freer, J., Hannah, D. M., Howden, N. J. K., Wagener, T., and Worrall, F.: Catchment similarity concepts for understanding dynamic biogeochemical behaviour of river basins, *Hydrol. Process.*, 28, 1554–1560, <https://doi.org/10.1002/hyp.10093>, 2014.
- LaCroix, R. E., Tfaily, M. M., McCreight, M., Jones, M. E., Spokas, L., and Keiluweit, M.: Shifting mineral and redox controls on carbon cycling in seasonally flooded mineral soils, *Biogeosciences*, 16, 2573–2589, <https://doi.org/10.5194/bg-16-2573-2019>, 2019.
- Larsen, S., Andersen, T., and Hessen, D. O.: Climate change predicted to cause severe increase of organic carbon in lakes, *Glob. Change Biol.*, 17, 1186–1192, <https://doi.org/10.1111/j.1365-2486.2010.02257.x>, 2011.
- Laudon, H., Kuglerova, L., Sponseller, R. A., Futter, M., Nordin, A., Bishop, K., Lundmark, T., Egnell, G., and Agren, A. M.: The role of biogeochemical hotspots, landscape heterogeneity, and hydrological connectivity for minimizing forestry effects on water quality, *Ambio*, 45, 152–162, <https://doi.org/10.1007/s13280-015-0751-8>, 2016.
- Lê, S., Josse, J., and Husson, F.: FactoMineR: An R Package for Multivariate Analysis, *J. Stat. Softw.*, 25, 1–18, <https://doi.org/10.18637/jss.v025.i01>, 2008.

- Ledesma, J. L., Grabs, T., Bishop, K. H., Schiff, S. L., and Kohler, S. J.: Potential for long-term transfer of dissolved organic carbon from riparian zones to streams in boreal catchments, *Glob. Change Biol.*, 21, 2963–2979, <https://doi.org/10.1111/gcb.12872>, 2015.
- Ledesma, J. L., Futter, M. N., Laudon, H., Evans, C. D., and Kohler, S. J.: Boreal forest riparian zones regulate stream sulfate and dissolved organic carbon, *Sci. Total Environ.*, 560–561, 110–122, <https://doi.org/10.1016/j.scitotenv.2016.03.230>, 2016.
- Ledesma, J. L. J., Futter, M. N., Blackburn, M., Lidman, F., Grabs, T., Sponseller, R. A., Laudon, H., Bishop, K. H., and Kohler, S. J.: Towards an Improved Conceptualization of Riparian Zones in Boreal Forest Headwaters, *Ecosystems*, 21, 297–315, <https://doi.org/10.1007/s10021-017-0149-5>, 2018a.
- Ledesma, J. L. J., Kothawala, D. N., Bastviken, P., Maehder, S., Grabs, T., and Futter, M. N.: Stream Dissolved Organic Matter Composition Reflects the Riparian Zone, Not Upslope Soils in Boreal Forest Headwaters, *Water Resour. Res.*, 54, 3896–3912, <https://doi.org/10.1029/2017wr021793>, 2018b.
- Lessels, J. S., Tetzlaff, D., Carey, S. K., Smith, P., and Soulsby, C.: A coupled hydrology–biogeochemistry model to simulate dissolved organic carbon exports from a permafrost-influenced catchment, *Hydrol. Process.*, 29, 5383–5396, <https://doi.org/10.1002/hyp.10566>, 2015.
- Luke, S. H., Luckai, N. J., Burke, J. M., and Prepas, E. E.: Riparian areas in the Canadian boreal forest and linkages with water quality in streams, *Environ. Rev.*, 15, 79–97, <https://doi.org/10.1139/A07-001>, 2007.
- Manning, R., Griffith, J. P., Pigot, T., and Vernon-Harcourt, L. F.: On the flow of water in open channels and pipes, *Transactions, Institution of Civ. Eng., Dublin, Ireland*, 1891.
- Matilainen, A., Gjessing, E. T., Lahtinen, T., Hed, L., Bhatnagar, A., and Sillanpää, M.: An overview of the methods used in the characterisation of natural organic matter (NOM) in relation to drinking water treatment, *Chemosphere*, 83, 1431–1442, <https://doi.org/10.1016/j.chemosphere.2011.01.018>, 2011.
- Moock, C., Hunkeler, D., and Brunner, P.: Tutorials as a flexible alternative to GUIs: An example for advanced model calibration using Pilot Points, *Environ. Modell. Softw.*, 66, 78–86, <https://doi.org/10.1016/j.envsoft.2014.12.018>, 2015.
- Mostovaya, A., Koehler, B., Guillemette, F., Brunberg, A.-K., and Tranvik, L. J.: Effects of compositional changes on reactivity continuum and decomposition kinetics of lake dissolved organic matter, *J. Geophys. Res.-Biogeo.*, 121, 1733–1746, <https://doi.org/10.1002/2016JG003359>, 2016.
- Mostovaya, A., Hawkes, J. A., Dittmar, T., and Tranvik, L. J.: Molecular Determinants of Dissolved Organic Matter Reactivity in Lake Water, *Front. Earth Sci.*, 5, 106, <https://doi.org/10.3389/feart.2017.00106>, 2017.
- Musolff, A., Fleckenstein, J. H., Opitz, M., Buttner, O., Kumar, R., and Tittel, J.: Spatio-temporal controls of dissolved organic carbon stream water concentrations, *J. Hydrol.*, 566, 205–215, <https://doi.org/10.1016/j.jhydrol.2018.09.011>, 2018.
- Pinay, G., Peiffer, S., De Dreuzy, J. R., Krause, S., Hannah, D. M., Fleckenstein, J. H., Sebilo, M., Bishop, K., and Hubert-Moy, L.: Upscaling Nitrogen Removal Capacity from Local Hotspots to Low Stream Orders' Drainage Basins, *Ecosystems*, 18, 1101–1120, <https://doi.org/10.1007/s10021-015-9878-5>, 2015.
- Pisani, O., Bosch, D. D., Coffin, A. W., Endale, D. M., Liebert, D., and Strickland, T. C.: Riparian land cover and hydrology influence stream dissolved organic matter composition in an agricultural watershed, *Sci. Total Environ.*, 717, 137165, <https://doi.org/10.1016/j.scitotenv.2020.137165>, 2020.
- Ploum, S. W., Laudon, H., Peralta-Tapia, A., and Kuglerová, L.: Are dissolved organic carbon concentrations in riparian groundwater linked to hydrological pathways in the boreal forest?, *Hydrol. Earth Syst. Sci.*, 24, 1709–1720, <https://doi.org/10.5194/hess-24-1709-2020>, 2020.
- Prairie, Y. T.: Carbocentric limnology: looking back, looking forward, *Can. J. Fish. Aquat. Sci.*, 65, 543–548, <https://doi.org/10.1139/f08-011>, 2008.
- R Core Team: R: A language and environment for statistical computing. R Foundation for Statistical Computing, Vienna, Austria, available at: <http://www.R-project.org/> (last access: 11 November 2020), 2014.
- Raeke, J., Lechtenfeld, O. J., Tittel, J., Oosterwoud, M. R., Bornmann, K., and Reemtsma, T.: Linking the mobilization of dissolved organic matter in catchments and its removal in drinking water treatment to its molecular characteristics, *Water Res.*, 113, 149–159, <https://doi.org/10.1016/j.watres.2017.01.066>, 2017.
- Raymond, P. A., Hartmann, J., Lauerwald, R., Sobek, S., McDonald, C., Hoover, M., Butman, D., Striegl, R., Mayorga, E., Humborg, C., Kortelainen, P., Dürr, H., Meybeck, M., Ciais, P., and Guth, P.: Global carbon dioxide emissions from inland waters, *Nature*, 503, 355–359, <https://doi.org/10.1038/nature12760>, 2013.
- Rousseuw, P. J.: Silhouettes – a Graphical Aid to the Interpretation and Validation of Cluster-Analysis, *J. Comput. Appl. Math.*, 20, 53–65, [https://doi.org/10.1016/0377-0427\(87\)90125-7](https://doi.org/10.1016/0377-0427(87)90125-7), 1987.
- Scheliga, B., Tetzlaff, D., Nuetzmann, G., and Soulsby, C.: Assessing runoff generation in riparian wetlands: monitoring groundwater–surface water dynamics at the micro-catchment scale, *Environ. Monit. Assess.*, 191, 116, <https://doi.org/10.1007/s10661-019-7237-2>, 2019.
- Seibert, J., Grabs, T., Köhler, S., Laudon, H., Winterdahl, M., and Bishop, K.: Linking soil- and stream-water chemistry based on a Riparian Flow-Concentration Integration Model, *Hydrol. Earth Syst. Sci.*, 13, 2287–2297, <https://doi.org/10.5194/hess-13-2287-2009>, 2009.
- Shen, Y., Chapelle, F. H., Strom, E. W., and Benner, R.: Origins and bioavailability of dissolved organic matter in groundwater, *Biogeochemistry*, 122, 61–78, <https://doi.org/10.1007/s10533-014-0029-4>, 2015.
- Sherene, T.: Mobility and transport of heavy metals in polluted soil environment, *Biological Forum – An International Journal*, 2, 112–121, 2010.
- Stanley, E. H., Powers, S. M., Lottig, N. R., Buffam, I., and Crawford, J. T.: Contemporary changes in dissolved organic carbon (DOC) in human-dominated rivers: is there a role for DOC management?, *Freshwater Biol.*, 57, 26–42, <https://doi.org/10.1111/j.1365-2427.2011.02613.x>, 2012.
- Strohmeier, S., Knorr, K.-H., Reichert, M., Frei, S., Fleckenstein, J. H., Peiffer, S., and Matzner, E.: Concentrations and fluxes of dissolved organic carbon in runoff from a forested catchment: insights from high frequency measurements, *Biogeosciences*, 10, 905–916, <https://doi.org/10.5194/bg-10-905-2013>, 2013.

- Suecker, J. K., Ryan, J. N., Kendall, C., and Jarrett, R. D.: Determination of hydrologic pathways during snowmelt for alpine/subalpine basins, Rocky Mountain National Park, Colorado, *Water Resour. Res.*, 36, 63–75, 2000.
- Tang, Q., Kurtz, W., Schilling, O. S., Brunner, P., Vereecken, H., and Franssen, H. J. H.: The influence of riverbed heterogeneity patterns on river-aquifer exchange fluxes under different connection regimes, *J. Hydrol.*, 554, 383–396, <https://doi.org/10.1016/j.jhydrol.2017.09.031>, 2017.
- Tarboton, D. G.: A new method for the determination of flow directions and upslope areas in grid digital elevation models, *Water Resour. Res.*, 33, 309–319, <https://doi.org/10.1029/96wr03137>, 1997.
- Tfaily, M. M., Wilson, R. M., Cooper, W. T., Kostka, J. E., Hanson, P., and Chanton, J. P.: Vertical Stratification of Peat Pore Water Dissolved Organic Matter Composition in a Peat Bog in Northern Minnesota, *J. Geophys. Res.-Biogeo.*, 123, 479–494, <https://doi.org/10.1002/2017jg004007>, 2018.
- Therrien, R., McLaren, R., Sudicky, E., and Panday, S.: HydroGeoSphere: A three-dimensional numerical model describing fully-integrated subsurface and surface flow and solute transport, Groundwater Simulations Group, University of Waterloo, Waterloo, ON, 2010.
- Vachon, D., Sponseller, R. A., and Karlsson, J.: Integrating carbon emission, accumulation and transport in inland waters to understand their role in the global carbon cycle, *Glob. Change Biol.*, 27, 719–727, <https://doi.org/10.1111/gcb.15448>, 2021.
- Wang, X., Zhang, H., Zhang, Y., Shi, Q., Wang, J., Yu, J., and Yang, M.: New Insights into Trihalomethane and Haloacetic Acid Formation Potentials: Correlation with the Molecular Composition of Natural Organic Matter in Source Water, *Environ. Sci. Technol.*, 51, 2015–2021, <https://doi.org/10.1021/acs.est.6b04817>, 2017.
- Wen, H., Perdrial, J., Abbott, B. W., Bernal, S., Dupas, R., Godsey, S. E., Harpold, A., Rizzo, D., Underwood, K., Adler, T., Sterle, G., and Li, L.: Temperature controls production but hydrology regulates export of dissolved organic carbon at the catchment scale, *Hydrol. Earth Syst. Sci.*, 24, 945–966, <https://doi.org/10.5194/hess-24-945-2020>, 2020.
- Werner, B. J.: High resolution spatial, chemical (dissolved organic carbon) and hydrological dataset of the upper Rappbode Catchment in the temperate Harz Mountains, Germany, HydroShare [data set], <https://doi.org/10.4211/hs.b32ba184414e475ba36a0bb193866ef1>, 2021.
- Werner, B. J., Musolff, A., Lechtenfeld, O. J., de Rooij, G. H., Oosterveld, M. R., and Fleckenstein, J. H.: High-frequency measurements explain quantity and quality of dissolved organic carbon mobilization in a headwater catchment, *Biogeosciences*, 16, 4497–4516, <https://doi.org/10.5194/bg-16-4497-2019>, 2019.
- Wilske, C., Herzsprung, P., Lechtenfeld, O. J., Kamjunke, N., and von Tümpling, W.: Photochemically Induced Changes of Dissolved Organic Matter in a Humic-Rich and Forested Stream, *Water*, 12, 331, <https://doi.org/10.3390/w12020331>, 2020.
- Wilson, H. F. and Xenopoulos, M. A.: Effects of agricultural land use on the composition of fluvial dissolved organic matter, *Nat. Geosci.*, 2, 37–41, <https://doi.org/10.1038/ngeo391>, 2008.
- Wilson, H. F., Saiers, J. E., Raymond, P. A., and Sobczak, W. V.: Hydrologic Drivers and Seasonality of Dissolved Organic Carbon Concentration, Nitrogen Content, Bioavailability, and Export in a Forested New England Stream, *Ecosystems*, 16, 604–616, <https://doi.org/10.1007/s10021-013-9635-6>, 2013.
- Wollschläger, U., Attinger, S., Borchardt, D., Brauns, M., Cuntz, M., Dietrich, P., Fleckenstein, J. H., Friese, K., Friesen, J., Harpke, A., Hildebrandt, A., Jäckel, G., Kamjunke, N., Knöller, K., Kögler, S., Kolditz, O., Krieg, R., Kumar, R., Lausch, A., Liess, M., Marx, A., Merz, R., Mueller, C., Musolff, A., Norf, H., Oswald, S. E., Rebmann, C., Reinstorf, F., Rode, M., Rink, K., Rinke, K., Samaniego, L., Vieweg, M., Vogel, H.-J., Weitere, M., Werban, U., Zink, M., and Zacharias, S.: The Bode hydrological observatory: a platform for integrated, interdisciplinary hydro-ecological research within the TERENO Harz/Central German Lowland Observatory, *Environ. Earth Sci.*, 76, 1–25, <https://doi.org/10.1007/s12665-016-6327-5>, 2016.
- Yang, J., Graf, T., and Ptak, T.: Impact of climate change on freshwater resources in a heterogeneous coastal aquifer of Bremerhaven, Germany: A three-dimensional modeling study, *J. Contam. Hydrol.*, 177–178, 107–121, <https://doi.org/10.1016/j.jconhyd.2015.03.014>, 2015.
- Yang, J., Heidbuchel, I., Musolff, A., Reinstorf, F., and Fleckenstein, J. H.: Exploring the Dynamics of Transit Times and Subsurface Mixing in a Small Agricultural Catchment, *Water Resour. Res.*, 54, 2317–2335, <https://doi.org/10.1002/2017wr021896>, 2018.
- Zarnetske, J. P., Bouda, M., Abbott, B. W., Saiers, J., and Raymond, P. A.: Generality of Hydrologic Transport Limitation of Watershed Organic Carbon Flux Across Ecoregions of the United States, *Geophys. Res. Lett.*, 45, 11702–11711, <https://doi.org/10.1029/2018gl080005>, 2018.
- Zhi, W., Li, L., Dong, W., Brown, W., Kaye, J., Steefel, C., and Williams, K. H.: Distinct Source Water Chemistry Shapes Contrasting Concentration-Discharge Patterns, *Water Resour. Res.*, 55, 4233–4251, <https://doi.org/10.1029/2018WR024257>, 2019.

Supplement of Hydrol. Earth Syst. Sci., 25, 6067–6086, 2021
<https://doi.org/10.5194/hess-25-6067-2021-supplement>
© Author(s) 2021. CC BY 4.0 License.



Hydrology and
Earth System
Sciences

Open Access

The EGU logo features the letters 'EGU' in a bold, sans-serif font, enclosed within a circular graphic element that resembles a stylized globe or a circular arrow.

Supplement of

Small-scale topography explains patterns and dynamics of dissolved organic carbon exports from the riparian zone of a temperate, forested catchment

Benedikt J. Werner et al.

Correspondence to: Benedikt J. Werner (benedikt.werner@ufz.de)

The copyright of individual parts of the supplement might differ from the article licence.

S1: Estimating variability of FT-ICR-MS samples across measurement days

To ensure that the molecular composition variance between riparian and stream water samples ($n = 142$, including three extra samples from further upstream, which were sample together with the samples from the study site) from different dates was not artificially induced due to systematic instrumental shifts in FT-ICR-MS measurements, a simulation of errors for molecular formulas (MF) peak intensities was conducted based on 15 SRFA (Suwannee River Fulvic Acid, an aquatic DOM reference) samples measured at the four measurement days. From this, a general error was derived for every MF intensity in the data matrix.

In this approach, we first calculated the mean coefficient of variance for the normalized peak intensities of every common MF detected in the 15 SRFA reference samples ($n = 422$) according to Eq. (A1):

$$10 \quad CV_{ref,j} = \frac{SD_{ref,j}}{mean_{ref,j}}, \quad (A1)$$

Where $CV_{ref,j}$ is the coefficient of variance of every common MF j in the references, $SD_{ref,j}$ is the according standard deviation and $mean_{ref,j}$ is the according mean peak intensity of these MFs. These $CV_{ref,j}$ were found to scale with the normalized peak intensity I ($r^2 = 0.43$, $p < 0.0001$) within the reference sample set (Fig. S3) and thus were considered transferable to the actual water samples to determine the according standard deviation of every measured MF intensity. We subsequently assigned each common MF intensity j (1 to 471) of each sample i (1 to 142) its own standard deviation based on the scaling of $CV_{ref,j}$ by setting the actual measured sample intensities as new mean. Equation (A1) then transposes into Eq. (A2):

$$SD_{i,j} = CV_{mean,ref} \cdot I_{i,j}, \quad (A2)$$

Where $SD_{i,j}$ is the standard deviation of common MF j in sample i , $CV_{mean,ref}$ the mean coefficient of variation of all common MFs in the references and $I_{i,j}$ the actual measured intensity of common MF j in sample i . This resulted in the common MF sample intensity-matrix m ($i:j$) and a SD-matrix k of a SD for every value in the intensity-matrix m also with the dimension ($i:j$).

In a next step we randomly picked a value out of every normal distribution around the intensities $I_{i,j}$, where the mean was defined by the values in the sample intensity-matrix m and the SD by corresponding value in the SD-matrix k . Accordingly we get a modified common MF sample matrix accounting for analytical uncertainty. To check the robustness of clustering with bootstrapping, this step was repeated 300 times. The 300 matrices were then combined into one matrix with still 471 variables (MF) but $142 \cdot 300 = 42900$ samples (so every sample in the matrix now is present 300 times with slightly different intensities). For this dataset we performed k-means clustering (for two clusters) and analyzed in which cluster the 300 different versions of each sample occurred. The probability of a sample to be assigned to one cluster was then calculated for every sample (for all 300 variations), thus quantifying the stability of the cluster affinity. Our bootstrapping approach revealed that 12 out of 142 samples changed cluster affiliation (Fig. S4) in 1 to 141 times out of 300 cases, with 6 samples (4 % of the samples) having a probability of $p > 0.05$ to switch between clusters. These 6 samples did not seem to have systematic similarities.

We thus conclude that the analytical uncertainty from the FT-ICR-MS measurements between the different
 35 measurement dates does only little affect the overall variance (here clustering) of the samples, which allows a
 comparison of all samples against each other.

S2: Objective function of the HydroGeoSphere model calibration (Eq. (A3))

$$\text{Multi - Objective function} = \sum_{i=1}^{i=nq} w_q (O_q^i - S_q^i)^2 + \sum_{i=1}^{i=nl} w_l (O_l^i - S_l^i)^2 \quad (\text{A3})$$

Where O_q^i and S_q^i are the observed and simulated discharge. nq is the number of number of the discharge
 40 observations (611). O_l^i and S_l^i are the observed and simulated groundwater level. nl is the number of groundwater
 level observations (110140). w_q and w_l are the weights for the two observation groups, both being assigned with
 the value of 1 in the calibration. Because the observation number of groundwater level was significantly larger
 than that of the discharge, this multi-objective function highlight the importance of the groundwater levels, such
 that the 94% of the multi-objective function for the calibrated best-fit was attributed to groundwater levels.

45 S3: Overview of FT-ICR MS results from stream and riparian samples

The formula assignment and blank filtering resulted in 3693 ± 960 MF (range: 1292 – 5625, $n = 142$) assigned to
 16797 \pm 2835 peaks (range: 9251 – 21511) in the mass range 150 – 1000 m/z. The assigned MF represented on
 average (24 ± 5) % of the total intensity in the mass spectra. In 93 spectra, multiple assignments (for 1 – 13 peaks,
 with $m/z > 650$) were present and these peaks represented < 0.12 % of the total intensity of all assigned MF.

50 Overall, 18910 unique MF were detected in all samples ($n = 142$), 6650 (3164) of them were present in at least 10
 % (50 %) of the samples (Fig. S9). Shared among all 142 samples were 471 MF representing on average (40 ± 4)
 % of the summed intensity of all assigned MF in each sample. The 471 MF were distributed to 315 CHO, 150
 CHNO and 6 CHOS formulas.

The riparian and stream samples were considerably different in terms of their average molecular composition
 55 (Table S5, Fig. S10). Note that in contrast to the PCA, here all 142 samples were considered (i.e. also the extra
 upstream samples, cf. Table S1). The PCA was run with all common MF found in 139 samples (i.e. 66 riparian,
 68 event and 5 base flow samples), resulting in 482 common MF.

Table S1: Overview on sampling in the Rappbode stream and its adjacent riparian zone. GW: groundwater, SW: surface water. DOC concentration and DOC properties (see section 2.3 – FTICRMS measurements) was determined for all samples except the routine stream samples, where only DOC concentration was determined.

	Time of the Year	Interval [h]	All Samples <i>n</i> = 253	Samples FT-ICR MS <i>n</i> = 142	
Event 1	20 May 2017	1	24	11	
Event 2	13 Sep 2017	1.5	24	8	
Event 3	05 Oct 2017	1	48	35	68 event samples
Event 4	29 Oct 2017	2	24	9	
Event 5	09 Dec 2018	0.75	24	5	
Routine stream sampling	Oct 2017 - Oct 2018	Every second week with gaps in winter	38	-	
Riparian zone					
GW and SW routine sampling	24 Apr 2018 04 Dec 2018 11 Dec 2018		71 (3-24 per date)	19 24 20	66 riparian +
+1 Stream water sample per date (RB_dn)	09 Apr 2019 23 Jul 2019	-		5 3	5 base flow samples
Grab sampling at the Rappbode source (RB_up)	24 Apr 2018 04 Dec 2018 23 Jul 2019	-	3	3	3 upstream samples

Table S2: The main parameters and their values used in this study. Asterisked parameters were subject to model calibration.

Parameter	Process	Spatial distribution	Value of best fit
Hydraulic conductivity*	Subsurface	Distributed	Elemental values from K field
Porosity	Subsurface	Uniform	0.56 [-]
Residual saturation	Subsurface	Uniform	0.08 [-]
Manning roughness coefficient*	Surface	Uniform	$6.34 \cdot 10^{-6} \text{ day m}^{-1/3}$
Manning roughness coefficient*	Channel	Uniform	$1.69 \cdot 10^{-6} \text{ day m}^{-1/3}$
Evaporation/root depth	ET	Uniform	0.5 m
<i>van Genuchten functions (Therrien et al., 2010):</i>			
α	Subsurface	Uniform	3.6 m^{-1}
β	Subsurface	Uniform	2.0 [-]
Residual saturation	Subsurface	Uniform	0.08 [-]
Fluxes from side boundaries:			
Q_{left}^*	Subsurface	Uniform	$0.88 \text{ m}^3 \text{ s}^{-1} \text{ per unit length}$
Q_{right}^*	Subsurface	Uniform	$0.35 \text{ m}^3 \text{ s}^{-1} \text{ per unit length}$

Table S3: Mean FT-ICR-MS derived molecular formula properties of the samples of the two DOC classes and the event samples.

Sample Group	n	w_{amz}		w_{ahc}		w_{aoc}		$w_{avc} (x10^3)$		$w_{asc} (x10^3)$		w_{aai}		w_{avosc}	
		mean	sd	mean	sd	mean	sd	mean	sd	mean	sd	mean	sd	mean	sd
DOC _I	19	432	5	1.223	0.029	0.404	0.020	18.8	2.4	7.2	1.6	0.115	0.018	-0.345	0.062
DOC _{II}	47	437	8	1.296	0.036	0.395	0.010	17.9	2.7	9.2	2.2	0.082	0.012	-0.434	0.043
Events	76	429	12	1.170	0.048	0.433	0.025	20.7	2.2	5.0	1.2	0.122	0.021	-0.231	0.092

70

75 **Table S4: Hydro climatic overview (average (minimum/maximum)) of the preceding 5 days of sampling in the stream and the riparian zone. Bold dates mark event sampling in the stream. Others are riparian zone sampling dates. Note that sampling on 24.04.2018 happened right after a data gap. Thus the statistic values only represent rough estimations of the prevailing conditions. NA means no data available.**

Sampling	Temp [°C]	Rain [mm 30min ⁻¹]	ET [mm h ⁻¹]	Q [L s ⁻¹]
20.05.2017	15.12 (6.1/25.8)	0.15 (0/8.2)	0.06 (0/0.253)	58.87 (18.39/411.52)
13.09.2017	11.09 (7.1/15.5)	0.12 (0/3.8)	0.025 (0/0.163)	11.36 (5.67/60.40)
05.10.2017	9.85 (5.5/16.6)	0.15 (0/2)	0.02 (0/0.166)	29.7 (13.31/94.37)
29.10.2017	9.03 (4.6/13.7)	0.12 (0/2.8)	0.01 (0/0.08)	40.49 (16.61/338.30)
09.12.2018	-0.29 (-4.6/3.7)	0.08 (0/2)	0.005 (0/0.073)	166.7 (107.0/453.1)
24.04.2018*	10.26*	NA*	0.02	49.54
04.12.2018	4.74 (0.6/9.8)	0.20 (0/4)	0.005 (0/0.037)	65.36 (32.24/160.19)
11.12.2018	3.84 (0.3/8.7)	0.27 (0/3.6)	0.003 (0/0.029)	132.09 (48.50/349.22)
09.04.2019	7.49 (-1.2/18.4)	0 (0/0)	0.042(0/0.21)	57.76(43.03/83.77)
23.07.2019	17.24 (9.6/27.1)	0.037 (0/3.8)	0.060 (0/0.23)	16.02 (8.87/23.84)

*There was a data gap for the preceding 20 days. The depicted values thus depict only mean values of 1 day before the data gap (04.04.2018), measurement date and one day after the sampling in order to get a rough approximation of the prevalent hydro climatic situation.

80

Table S5: Sample details, FT-ICR-MS derived molecular formula class distribution, and mean values of molecular formula descriptors for all 142 samples. Bold sample names denoted “BW_” are event samplings and “RB_” denote routine samplings in the stream. Cluster affiliation only refers to riparian water samples. MF: molecular formulas; wa: weighted average of w_{am} (mass to charge ratio), w_{HC} (hydrogen to carbon ratio), w_{OC} (oxygen to carbon ratio), w_{SC} (sulfur to carbon ratio), w_{AI} (aromaticity index), w_{NOSC} (nominal oxidation state of carbon).

Sample Name	Cluster affiliation	Sample Type	Date and Time of Sampling	DOC [mg/L]	Water Level / Depth to GW [cm]	Total MF	CHO	CHNO	CHNOS	CHOS	other	w _{am}	w _{HC}	w _{OC}	w _{SC}	w _{AI}	w _{NOSC}	
BW_05		Stream event sample	10.05.2017 19:30	3.47	6	4565	2102	1611	311	540	1	457	1.142	0.487	0.019	0.005	0.1	-0.1
BW_10		Stream event sample	11.05.2017 00:30	3.38	5	4496	2058	1609	322	504	3	454	1.15	0.482	0.02	0.005	0.1	-0.12
BW_15		Stream event sample	11.05.2017 05:30	3.92	5	4498	2063	1580	306	546	3	454	1.142	0.484	0.02	0.006	0.1	-0.1
BW_20		Stream event sample	11.05.2017 10:30	5.07	6	4615	2132	1662	284	536	1	449	1.144	0.48	0.021	0.006	0.1	-0.11
BW_49		Stream event sample	18.05.2017 15:00	4.61	6	4190	2011	1485	211	483	0	450	1.108	0.49	0.02	0.004	0.11	-0.06
BW_26		Stream event sample	20.05.2017 08:00	18.16	21	4166	2121	1426	151	467	1	451	1.104	0.485	0.02	0.004	0.12	-0.06
BW_28		Stream event sample	20.05.2017 10:00	17.96	17	4005	2033	1356	178	434	4	453	1.102	0.491	0.021	0.005	0.11	-0.05
BW_40		Stream event sample	20.05.2017 12:00	12.51	9	3838	1947	1311	149	429	2	446	1.11	0.473	0.021	0.004	0.12	-0.09
BW_31		Stream event sample	20.05.2017 13:00	16.82	13	3991	1966	1388	194	438	5	442	1.117	0.463	0.021	0.004	0.13	-0.12
BW_35		Stream event sample	20.05.2017 17:00	14.2	11	3930	1977	1362	162	426	3	437	1.106	0.472	0.022	0.005	0.13	-0.09
BW_48		Stream event sample	21.05.2017 06:00	11.28	9	3801	1858	1335	156	452	0	439	1.145	0.448	0.022	0.005	0.12	-0.17
BW_50		Stream event sample	13.09.2017 10:15	9.59	14	3400	1760	1154	65	416	5	438	1.185	0.452	0.02	0.005	0.09	-0.21
BW_52		Stream event sample	13.09.2017 13:15	8.48	14	3164	1655	1087	50	385	7	440	1.185	0.453	0.02	0.005	0.09	-0.21
BW_55		Stream event sample	13.09.2017 17:45	7.69	8	3861	1932	1352	91	482	4	443	1.187	0.452	0.02	0.005	0.09	-0.21
BW_60		Stream event sample	14.09.2017 01:15	6.77	6	3276	1699	1117	51	404	5	439	1.188	0.452	0.02	0.005	0.09	-0.21
BW_62		Stream event sample	14.09.2017 04:15	7.43	5	3437	1730	1207	75	421	4	437	1.18	0.448	0.021	0.005	0.1	-0.21
BW_65		Stream event sample	14.09.2017 08:45	9.2	4	3169	1637	1083	53	393	3	436	1.184	0.449	0.021	0.005	0.1	-0.21
BW_68		Stream event sample	14.09.2017 13:15	12.73	4	3157	1657	1083	57	359	1	432	1.186	0.447	0.021	0.005	0.1	-0.22
BW_73		Stream event sample	14.09.2017 20:45	12.29	6	2762	1483	919	52	302	6	435	1.183	0.451	0.02	0.005	0.1	-0.21

Sample Name	Cluster affiliation	Sample Type	Date and Time of Sampling	DOC [mg/L]	Water Level / Depth to GW [cm]	Total MF	CHO	CHNO	CHNOS	CHOS	other	w _{am}	w _{HC}	w _{OC}	w _{SC}	w _{AI}	w _{NOSC}	
BW_76		Stream event sample	05.10.2017 10:30	10.23	11	3094	1595	1065	53	376	5	415	1.149	0.419	0.024	0.005	0.15	-0.23
BW_77		Stream event sample	05.10.2017 11:30	12.21	16	3011	1562	1031	51	361	6	414	1.146	0.426	0.024	0.005	0.15	-0.21
BW_78		Stream event sample	05.10.2017 12:30	14.07	19	2853	1499	961	48	340	5	415	1.144	0.422	0.023	0.005	0.15	-0.22
BW_88		Stream event sample	05.10.2017 12:30	16.82	26	2622	1434	845	39	296	8	415	1.136	0.427	0.024	0.005	0.15	-0.2
BW_79		Stream event sample	05.10.2017 13:30	14.37	22	3013	1558	1038	63	351	3	417	1.159	0.421	0.023	0.005	0.14	-0.24
BW_80		Stream event sample	05.10.2017 14:30	14.1	26	3090	1631	1018	73	366	2	417	1.155	0.419	0.022	0.004	0.14	-0.24
BW_81		Stream event sample	05.10.2017 15:30	14.8	31	2829	1525	934	47	319	4	418	1.161	0.419	0.022	0.004	0.14	-0.25
BW_82		Stream event sample	05.10.2017 16:30	15.41	36	2734	1495	908	39	287	5	427	1.129	0.449	0.022	0.004	0.13	-0.16
BW_83		Stream event sample	05.10.2017 17:30	14.76	41	3171	1734	1067	64	302	4	422	1.164	0.424	0.021	0.004	0.13	-0.24
BW_84		Stream event sample	05.10.2017 18:30	15.77	40	2674	1471	874	51	275	3	419	1.154	0.422	0.021	0.004	0.14	-0.24
BW_85		Stream event sample	05.10.2017 19:30	15.2	37	2788	1529	898	53	302	6	415	1.156	0.42	0.022	0.005	0.14	-0.24
BW_86		Stream event sample	05.10.2017 20:30	16.37	34	2709	1457	891	45	309	7	420	1.149	0.424	0.021	0.005	0.14	-0.23
BW_87		Stream event sample	05.10.2017 21:30	15.84	30	2814	1518	922	44	328	2	419	1.153	0.423	0.021	0.005	0.14	-0.23
BW_89		Stream event sample	05.10.2017 23:30	16.05	23	2643	1415	869	53	302	4	418	1.15	0.423	0.021	0.005	0.14	-0.23
BW_90		Stream event sample	06.10.2017 00:30	14.84	21	2764	1474	911	47	329	3	420	1.156	0.424	0.021	0.005	0.14	-0.23
BW_91		Stream event sample	06.10.2017 01:30	14.09	18	2731	1433	905	52	334	7	418	1.142	0.426	0.022	0.005	0.14	-0.21
BW_92		Stream event sample	06.10.2017 02:30	13.69	17	2647	1400	866	49	329	3	417	1.166	0.424	0.022	0.005	0.14	-0.24
BW_93		Stream event sample	06.10.2017 03:30	12.98	15	2830	1483	948	42	357	0	419	1.157	0.426	0.022	0.005	0.14	-0.23
BW_94		Stream event sample	06.10.2017 04:30	12.23	14	2632	1386	887	31	321	7	417	1.154	0.422	0.022	0.005	0.14	-0.23
BW_96		Stream event sample	06.10.2017 06:30	12.66	13	2541	1347	839	48	301	6	416	1.147	0.425	0.023	0.005	0.14	-0.22
BW_97		Stream event sample	06.10.2017 07:30	12.65	13	2719	1459	907	54	296	3	417	1.137	0.433	0.023	0.005	0.14	-0.19
BW_98		Stream event sample	06.10.2017 08:30	12.98	13	2871	1536	968	56	309	2	419	1.151	0.427	0.022	0.004	0.14	-0.22
BW_99		Stream event sample	06.10.2017 09:30	13.03	14	2979	1542	1032	61	338	6	418	1.151	0.421	0.023	0.005	0.14	-0.23
BW_100		Stream event sample	06.10.2017 10:30	13.74	14	2973	1585	1004	46	332	6	419	1.161	0.423	0.022	0.005	0.14	-0.24
BW_101		Stream event sample	06.10.2017 11:30	14.27	15	2927	1560	990	41	333	3	420	1.147	0.426	0.023	0.004	0.14	-0.22

Sample Name	Cluster affiliation	Sample Type	Date and Time of Sampling	DOC [mg/L]	Water Level / Depth to GW [cm]	Total MF	CHO	CHNO	CHNOS	CHOS	other	W _{het}	W _{hc}	W _{bc}	W _{oc}	W _{lc}	W _{at}	W _{hosc}
BW_102		Stream event sample	06.10.2017 12:30	12.74	16	2966	1561	995	52	354	4	420	1.152	0.425	0.022	0.005	0.14	-0.23
BW_103		Stream event sample	06.10.2017 13:30	13.71	17	2786	1476	919	58	325	8	417	1.157	0.42	0.023	0.005	0.14	-0.24
BW_104		Stream event sample	06.10.2017 14:30	12.86	18	2771	1468	917	58	322	6	417	1.159	0.412	0.023	0.005	0.15	-0.26
BW_105		Stream event sample	06.10.2017 15:30	13.55	19	3078	1645	1031	63	333	6	420	1.154	0.426	0.022	0.004	0.14	-0.23
BW_106		Stream event sample	06.10.2017 16:30	13.52	20	2715	1446	921	54	291	3	418	1.156	0.428	0.022	0.004	0.14	-0.23
BW_107		Stream event sample	06.10.2017 17:30	13.6	20	2683	1419	916	35	310	3	417	1.144	0.43	0.023	0.005	0.14	-0.21
BW_108		Stream event sample	06.10.2017 18:30	13.05	21	2876	1509	991	35	336	5	420	1.152	0.43	0.022	0.005	0.14	-0.22
BW_110		Stream event sample	06.10.2017 20:30	12.32	22	2701	1402	946	41	309	3	417	1.149	0.426	0.023	0.005	0.14	-0.22
BW_111		Stream event sample	06.10.2017 21:30	12.69	21	2738	1446	915	52	320	5	419	1.148	0.424	0.022	0.005	0.14	-0.22
BW_113		Stream event sample	06.10.2017 23:30	10.99	18	2873	1473	981	41	375	3	419	1.15	0.427	0.022	0.005	0.14	-0.22
BW_115		Stream event sample	29.10.2017	13.63	NA	2528	1409	839	34	239	7	423	1.158	0.44	0.021	0.004	0.12	-0.21
BW_116		Stream event sample	29.10.2017	14.77	NA	2593	1407	901	46	237	2	425	1.157	0.444	0.022	0.004	0.12	-0.2
BW_117		Stream event sample	29.10.2017	15.06	NA	2326	1315	749	52	207	3	426	1.149	0.447	0.021	0.004	0.12	-0.18
BW_118		Stream event sample	29.10.2017	15.52	NA	2693	1481	912	44	250	6	427	1.143	0.446	0.021	0.004	0.12	-0.18
BW_119		Stream event sample	29.10.2017	15.1	NA	2184	1225	717	38	200	4	425	1.146	0.442	0.02	0.004	0.13	-0.19
BW_120		Stream event sample	29.10.2017	14.36	NA	2242	1268	732	25	213	4	422	1.137	0.454	0.021	0.004	0.12	-0.16
BW_121		Stream event sample	29.10.2017	13.55	NA	2236	1294	708	32	195	7	428	1.159	0.443	0.019	0.003	0.12	-0.21
BW_122		Stream event sample	29.10.2017	7.98	NA	2319	1277	761	34	243	4	429	1.171	0.439	0.019	0.004	0.11	-0.23
BW_123		Stream event sample	29.10.2017	7.76	NA	2573	1393	858	41	271	10	431	1.17	0.439	0.02	0.004	0.11	-0.23
BW_125		Stream event sample	09.12.2018 10:15	7.11	34	5092	2266	1700	280	840	6	441	1.262	0.409	0.016	0.007	0.09	-0.38
BW_128		Stream event sample	09.12.2018 12:30	7.73	35	4940	2206	1682	249	798	5	437	1.262	0.398	0.016	0.007	0.1	-0.4
BW_136		Stream event sample	09.12.2018 18:30	7.38	29	4911	2205	1636	266	800	4	437	1.261	0.398	0.016	0.007	0.1	-0.4
BW_141		Stream event sample	09.12.2018 22:15	6.38	25	5323	2363	1791	305	862	2	443	1.26	0.409	0.016	0.007	0.09	-0.38
BW_146		Stream event sample	10.12.2018 02:00	7.58	21	5334	2343	1804	298	886	3	444	1.259	0.412	0.016	0.007	0.09	-0.37

8

Sample Name	Cluster affiliation	Sample Type	Date and Time of Sampling	DOC [mg/L]	Water Level / Depth to GW [cm]	Total MF	CHO	CHNO	CHNOS	CHOS	other	W _{het}	W _{hc}	W _{bc}	W _{oc}	W _{lc}	W _{at}	W _{hosc}
A5-1	II	Low groundwater sample	24.04.2018	2.05	NA	3419	1165	1305	309	634	6	434	1.413	0.39	0.027	0.011	0.05	-0.53
B1-1	I	Low groundwater sample	24.04.2018	5.37	-3	3036	1366	1112	107	447	4	423	1.233	0.433	0.024	0.008	0.1	-0.28
B2-1	II	Low groundwater sample	24.04.2018	2.5	-26	4006	1752	1581	175	497	1	440	1.287	0.397	0.021	0.006	0.09	-0.42
B3-1	II	Low groundwater sample	24.04.2018	0.85	-34	3316	1276	1269	237	530	4	450	1.316	0.401	0.02	0.008	0.06	-0.44
B4-1	I	Low groundwater sample	24.04.2018	7.4	0	3290	1518	1149	103	511	9	433	1.212	0.425	0.021	0.007	0.1	-0.29
B5-1	II	Low groundwater sample	24.04.2018	2.74	2	3263	1251	1215	242	549	6	453	1.355	0.396	0.021	0.008	0.05	-0.49
C1-1	I	Low groundwater sample	24.04.2018	6.18	1	3386	1609	1239	149	388	1	440	1.215	0.412	0.019	0.005	0.11	-0.33
C2-1	II	Low groundwater sample	24.04.2018	0.86	-23	3427	1403	1380	230	405	9	452	1.292	0.401	0.022	0.007	0.07	-0.41
C3-1	II	Low groundwater sample	24.04.2018	2.14	-28	3525	1553	1190	218	557	7	439	1.343	0.377	0.02	0.01	0.09	-0.51
C4-1	II	Low groundwater sample	24.04.2018	2.61	-5	3939	1736	1392	216	592	3	446	1.292	0.388	0.016	0.006	0.08	-0.46
C5-1	II	Low groundwater sample	24.04.2018	1.69	-2	3503	1382	1246	263	609	3	453	1.36	0.402	0.021	0.01	0.06	-0.47
D1-1	I	Low groundwater sample	24.04.2018	5.91	-3	3850	1810	1317	170	548	5	440	1.243	0.418	0.02	0.007	0.09	-0.33
D2-1	II	Low groundwater sample	24.04.2018	2.36	-33	3702	1667	1291	185	557	2	442	1.284	0.392	0.019	0.008	0.09	-0.43
D3-1	II	Low groundwater sample	24.04.2018	2.69	-34	3841	1548	1372	271	646	4	448	1.334	0.384	0.021	0.01	0.08	-0.48
D4-1	II	Low groundwater sample	24.04.2018	1	-4	3243	1234	1186	253	564	6	442	1.358	0.384	0.023	0.01	0.07	-0.5
D5-1	II	Low groundwater sample	24.04.2018	0.73	NA	3341	1354	1326	214	443	4	451	1.292	0.401	0.022	0.007	0.07	-0.41
A50-1	II	Surface pond sample	24.04.2018	1.88	0	3673	1640	1423	169	433	8	443	1.275	0.419	0.022	0.006	0.07	-0.36

9

Sample Name	Cluster affiliation	Sample Type	Date and Time of Sampling	DOC [mg/L]	Water Level / Depth to GW [cm]	Total MF	CHO	CHNO	CHNOS	CHOS	other	W _{am}	W _{bc}	W _{oc}	W _{bc}	W _{bc}	W _{bc}	W _{bc}
S3O-1	I	Surface pond sample	24.04.2018	15.77	0	3108	1491	1126	103	381	7	431	1.148	0.451	0.024	0.005	0.12	-0.16
RB_up-1		Rappbode streamwater sample	24.04.2018 14:15	6.83	22	3223	1556	1170	86	409	2	439	1.183	0.445	0.02	0.005	0.1	-0.22
RB_da-1		Rappbode streamwater sample	24.04.2018 15:45	6.72	11	3065	1497	1071	83	411	3	437	1.171	0.448	0.02	0.005	0.11	-0.2
C1-2	II	High groundwater sample	04.12.2018	3.43	-8	5012	2105	1697	308	898	4	436	1.271	0.397	0.015	0.009	0.09	-0.41
D2-2	II	High groundwater sample	04.12.2018	1.97	-31	5143	2262	1778	295	806	2	440	1.243	0.39	0.017	0.007	0.11	-0.4
E2-2	II	High groundwater sample	04.12.2018	2.4	-25	4911	1965	1941	368	634	3	446	1.274	0.4	0.017	0.007	0.08	-0.41
C3b-2	II	High groundwater sample	04.12.2018	2.4	NA	5625	2258	2050	444	870	3	440	1.277	0.396	0.018	0.009	0.09	-0.41
RB_up-2		Rappbode streamwater sample	04.12.2018	5.47	22	1906	916	583	51	355	1	426	1.28	0.404	0.016	0.008	0.08	-0.41
RB_da-2		Rappbode streamwater sample	04.12.2018	5.42	22	5231	2168	1724	369	966	4	433	1.269	0.403	0.017	0.009	0.09	-0.39
A2-2	II	High groundwater sample	04.12.2018	2.76	-11	3924	1603	1315	208	793	5	436	1.271	0.41	0.017	0.01	0.08	-0.38
A4-2	II	High groundwater sample	04.12.2018	2.51	-11	1474	830	340	34	263	7	428	1.265	0.381	0.011	0.007	0.1	-0.46
B1-2	II	High groundwater sample	04.12.2018	3.45	-13	4222	1602	1418	325	873	4	428	1.311	0.411	0.016	0.016	0.07	-0.41
B3-2	II	High groundwater sample	04.12.2018	3.01	-20	5204	1931	2087	421	760	5	442	1.273	0.409	0.018	0.01	0.07	-0.38
B4-2	II	High groundwater sample	04.12.2018	3.25	-6	5072	1844	1791	466	969	2	436	1.285	0.403	0.016	0.012	0.08	-0.41
C4-2	II	High groundwater sample	04.12.2018	2.08	-16	4965	1846	1718	489	910	2	438	1.305	0.401	0.014	0.012	0.07	-0.44
D1-2	II	High groundwater sample	04.12.2018	6.08	-17	4427	1782	1505	254	880	6	435	1.269	0.408	0.015	0.01	0.08	-0.39
D4-2	II	High groundwater sample	04.12.2018	1.55	-32	5074	1846	1828	504	892	4	439	1.301	0.393	0.016	0.01	0.07	-0.45

10

Sample Name	Cluster affiliation	Sample Type	Date and Time of Sampling	DOC [mg/L]	Water Level / Depth to GW [cm]	Total MF	CHO	CHNO	CHNOS	CHOS	other	W _{am}	W _{bc}	W _{oc}	W _{bc}	W _{bc}	W _{bc}	W _{bc}
E1-2	I	High groundwater sample	04.12.2018	7	-14	5027	2066	1790	310	854	7	440	1.251	0.401	0.017	0.008	0.1	-0.38
E4-2	II	High groundwater sample	04.12.2018	0.69	-13	5165	2313	1763	312	765	12	434	1.293	0.364	0.014	0.007	0.1	-0.51
E5-2	II	High groundwater sample	04.12.2018	3.68	-38	4059	1512	1401	322	820	4	441	1.361	0.393	0.018	0.014	0.07	-0.49
B2b-2	II	High groundwater sample	04.12.2018	1.72	NA	4921	1965	1960	343	650	3	442	1.257	0.4	0.019	0.007	0.09	-0.38
S2-2	II	High groundwater sample	04.12.2018	2.61	-16	4511	1735	1500	349	923	4	432	1.292	0.399	0.016	0.011	0.08	-0.42
T2-2	II	High groundwater sample	04.12.2018	1.81	-8	5361	2003	1872	434	1048	4	424	1.328	0.397	0.018	0.013	0.08	-0.46
MO-2	I	Surface pond sample	04.12.2018	7.37	0	4244	1876	1293	181	891	3	435	1.243	0.418	0.016	0.01	0.1	-0.34
B4O-2	I	Surface pond sample	04.12.2018	12.94	0	4217	1857	1415	171	770	4	427	1.223	0.404	0.019	0.009	0.12	-0.34
B5O-2	II	Surface pond sample	04.12.2018	4.69	0	1292	670	423	33	158	8	428	1.297	0.4	0.019	0.006	0.07	-0.43
T2O-2	I	Surface pond sample	04.12.2018	5.22	0	5117	2102	1702	354	956	3	435	1.25	0.408	0.018	0.009	0.1	-0.36
A2O-2	II	Surface pond sample	04.12.2018	4.81		4069	1671	1332	232	829	5	428	1.28	0.4	0.017	0.011	0.09	-0.41
B2-3	II	High groundwater sample	11.12.2018	2.11	-25	4548	1835	1691	343	674	5	430	1.28	0.379	0.019	0.007	0.1	-0.45
T2-3	II	High groundwater sample	11.12.2018	2.14	-9	4892	1924	1652	408	906	2	429	1.292	0.386	0.017	0.01	0.09	-0.45
S1-3	I	High groundwater sample	11.12.2018	6.33	NA	4331	1970	1482	200	676	3	437	1.217	0.407	0.018	0.006	0.11	-0.33
S3-3	II	High groundwater sample	11.12.2018	4.08	NA	4857	2020	1585	338	910	4	439	1.259	0.398	0.015	0.008	0.09	-0.4
C1-3	I	High groundwater sample	11.12.2018	4.36	-9	4332	1955	1427	233	714	3	432	1.256	0.38	0.016	0.008	0.11	-0.43
T2O-3	I	Surface pond sample	11.12.2018	9.68	0	4391	1931	1518	193	746	3	433	1.22	0.407	0.019	0.007	0.11	-0.33
B2O-3	II	Surface pond sample	11.12.2018	4.65	0	4724	2036	1611	269	801	7	439	1.258	0.4	0.016	0.008	0.09	-0.4
RB_da-3		Rappbode streamwater sample	11.12.2018	5.67	13	1919	989	578	37	311	4	432	1.279	0.402	0.014	0.006	0.08	-0.42

11

Sample Name	Cluster affiliation	Sample Type	Date and Time of Sampling	DOC [mg/L]	Water Level / Depth to GW [cm]	Total MF	CHO	CHNO	CHNOS	CHOS	other	W _{het}	W _{hlc}	W _{hlc}	W _{hlc}	W _{hlc}	W _{hlc}	W _{hlc}
A1-3	II	High groundwater sample	11.12.2018	2.25	-12	4385	1802	1416	272	883	12	421	1.317	0.379	0.015	0.011	0.09	-0.49
A2-3	II	High groundwater sample	11.12.2018	3.65	-10	4813	1881	1642	367	920	3	434	1.272	0.397	0.017	0.01	0.09	-0.41
A3-3	II	High groundwater sample	11.12.2018	0.88	-48	4293	1799	1546	303	640	5	434	1.301	0.392	0.017	0.008	0.08	-0.45
A4-3	I	High groundwater sample	11.12.2018	3.65	-11	4220	1859	1240	204	916	1	427	1.232	0.392	0.015	0.01	0.12	-0.38
B1-3	II	High groundwater sample	11.12.2018	2.85	-15	4692	1791	1645	345	909	2	426	1.275	0.402	0.018	0.012	0.09	-0.39
B3-3	II	High groundwater sample	11.12.2018	3.27	-27	5102	1951	1763	390	995	3	432	1.279	0.395	0.017	0.01	0.09	-0.42
B4-3	II	High groundwater sample	11.12.2018	4.07	-5	4197	1641	1624	281	649	2	432	1.27	0.397	0.019	0.009	0.09	-0.4
B5-3	II	High groundwater sample	11.12.2018	1.1	-7	4288	1816	1449	310	700	13	424	1.371	0.375	0.017	0.011	0.07	-0.55
B2b-3	II	High groundwater sample	11.12.2018	2.67	NA	4034	1637	1564	263	566	4	431	1.26	0.393	0.02	0.008	0.09	-0.4
S2-3	II	High groundwater sample	11.12.2018	3.29	-16	4941	1963	1670	377	929	2	437	1.267	0.403	0.017	0.009	0.09	-0.39
A2O-3	II	Surface pond sample	11.12.2018	3.78	0	4842	2061	1629	285	866	1	445	1.266	0.398	0.015	0.008	0.09	-0.41
B5O-3	I	Surface pond sample	11.12.2018	2.53	0	4521	2046	1643	193	633	6	434	1.245	0.399	0.02	0.006	0.1	-0.37
S2O-4	I	Surface pond sample	09.04.2019	5.66	0	4754	2270	1614	164	703	3	436	1.18	0.391	0.018	0.005	0.15	-0.33
RB_dn-4		Rappbode streamwater sample	09.04.2019	3.29	10	4532	2219	1476	132	702	3	438	1.192	0.385	0.015	0.005	0.14	-0.37
A2-4	I	High groundwater sample	09.04.2019	4.74	-11	3820	1939	1338	85	453	5	430	1.187	0.381	0.018	0.005	0.15	-0.36
B4-4	I	High groundwater sample	09.04.2019	10.44	-3	3964	1969	1308	115	566	6	420	1.214	0.392	0.02	0.009	0.14	-0.35
B5-4	I	High groundwater sample	09.04.2019	3.21	-3	4948	2246	1666	254	777	5	431	1.212	0.389	0.018	0.007	0.13	-0.37

12

Sample Name	Cluster affiliation	Sample Type	Date and Time of Sampling	DOC [mg/L]	Water Level / Depth to GW [cm]	Total MF	CHO	CHNO	CHNOS	CHOS	other	W _{het}	W _{hlc}	W _{hlc}	W _{hlc}	W _{hlc}	W _{hlc}	W _{hlc}
RB_dn-5		Rappbode streamwater sample	23.07.2019	1.3	5	3862	1549	1544	251	507	11	441	1.363	0.374	0.018	0.006	0.07	-0.55
RB_up-5		Rappbode streamwater sample	23.07.2019	9.54	10	4228	1821	1459	249	687	12	416	1.292	0.365	0.02	0.011	0.12	-0.48
B5-5	I	High groundwater sample	23.07.2019	2.76	-53	4463	2145	1554	199	555	10	427	1.261	0.365	0.018	0.006	0.12	-0.46
B_C1-5	II	High groundwater sample	23.07.2019	4.13	-48	3741	1676	1225	137	700	3	433	1.296	0.394	0.016	0.008	0.08	-0.44

90

13

Table S6: Overview of model results. Absolute values and comparison of the water fluxes in the study site for a dry (29 Aug 2018) and wet (13 Dec 2017) situation. Negative fluxes indicate exit out of the system.

	Dry [mm d ⁻¹]	Wet [mm d ⁻¹]	Absolute change [mm d ⁻¹]	Rel. change factor [-]
Channel in	45.04	1315.08	1270.04	29.2
Channel out	-45.71	-1321.10	1275.39	28.9
Channel gain total	0.67	6.06	5.39	9.1
Channel gain from subsurface	0.60	5.83	5.23	9.7
Channel gain from surface	0.07	0.23	0.17	3.4
Channel loss total	0.00	0.00	0.00	NA
Subsurface in	0.10	0.17	0.07	1.7
Subsurface out	-0.20	-0.29	0.10	1.5
Subsurface gain	0.10	0.13	0.03	1.3
Outflow exit through surface	-0.47	-14.75	14.28	31.4
Total runoff gain	1.23	20.94	19.71	17.0

95

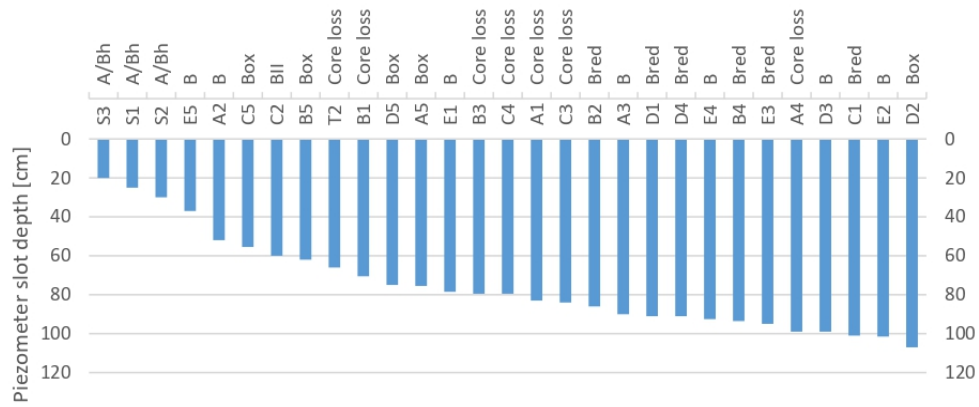


Figure S1: Overview of depth of slots and soil types of the piezometer network.

100

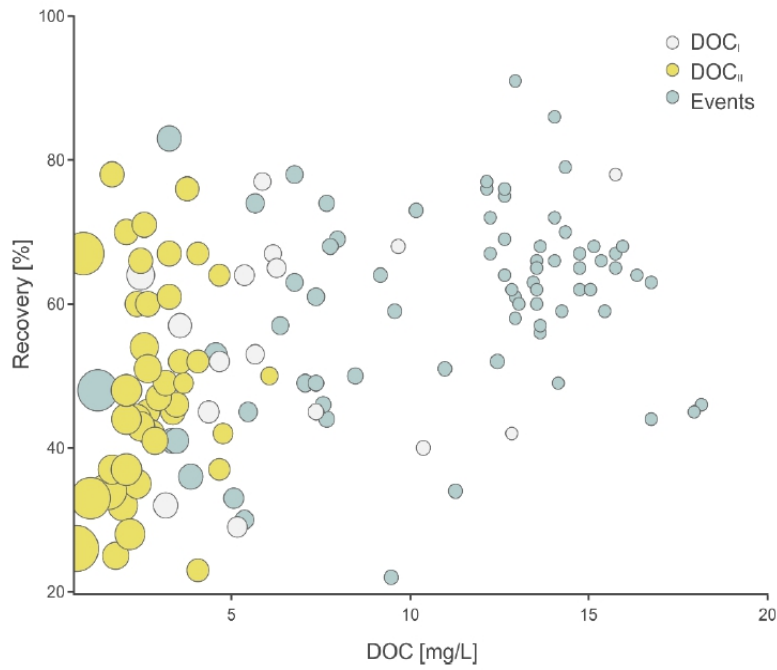
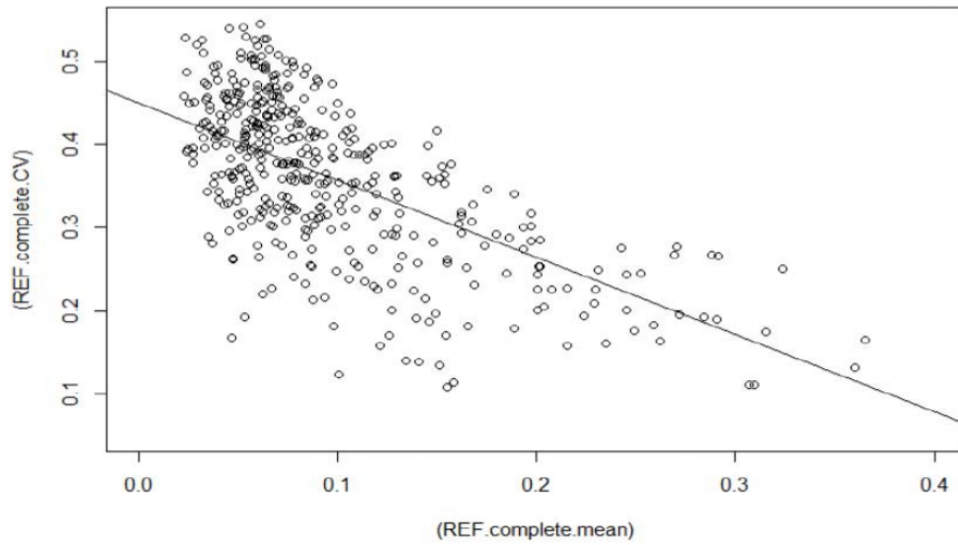
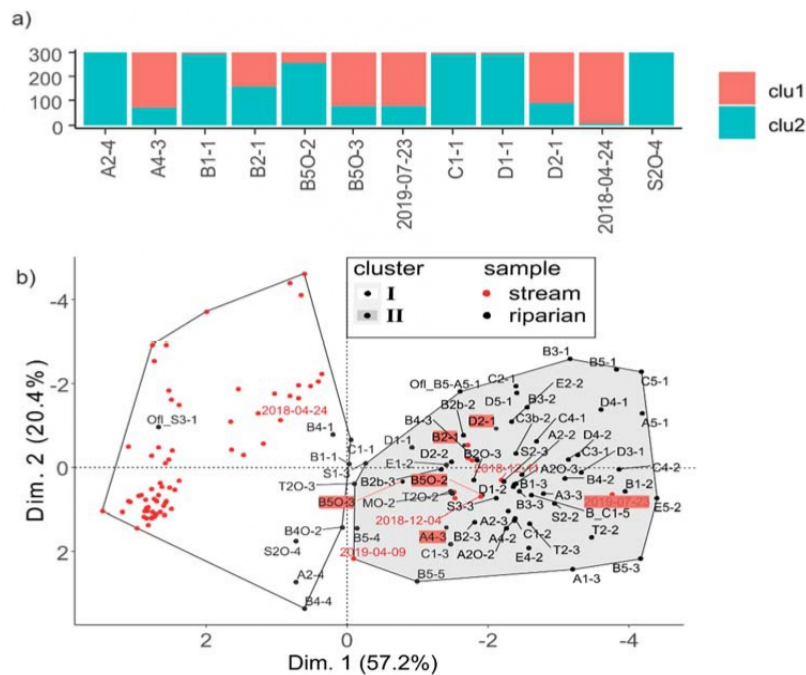


Figure S2: Quality control of solid phase extraction for DOC samples. SPE recovery vs sample DOC concentration for stream samples (blue) and riparian samples of type DOC_I (grey) and DOC_{II} (yellow) with dot size corresponding to the sample volume used for the extraction (range: 15-200 mL, $n = 133$).

105



110 **Figure S3: Coefficient of variation (*REF.complete.CV*) versus the mean normalized intensities (*REF.complete.mean*) of the common FT-ICR-MS reference samples compounds ($n = 422$). Black line indicates linear regression. Mean *REF.complete.CV* was 0.36.**



115 **Figure S4: a) Bootstrapping of cluster analysis. Only samples are depicted where the random deviation made samples switch between the two clusters. Overall there are 142 samples. b) Visualization of k-means clustering results of all samples. Highlighted samples in red indicate samples with a probability of $p > 0.05$ to switch between clusters (see (a)). Samples marked with red dates indicate stream water samples of riparian sampling dates.**

120

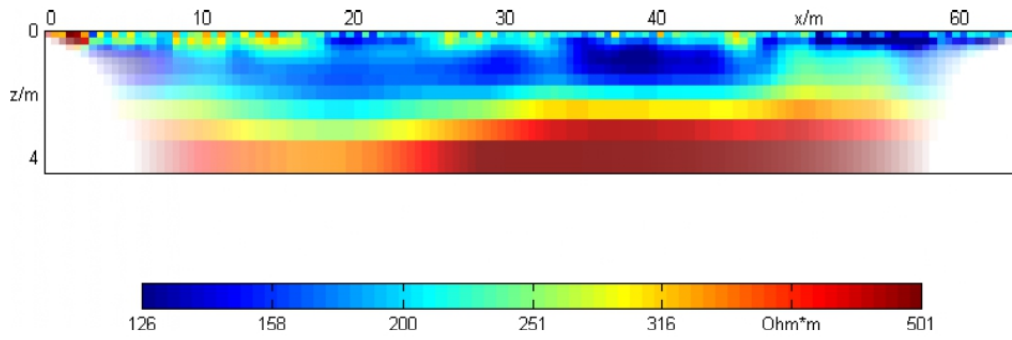


Figure S5: Electrical resistivity plot of the transect AB derived from geoelectrics.

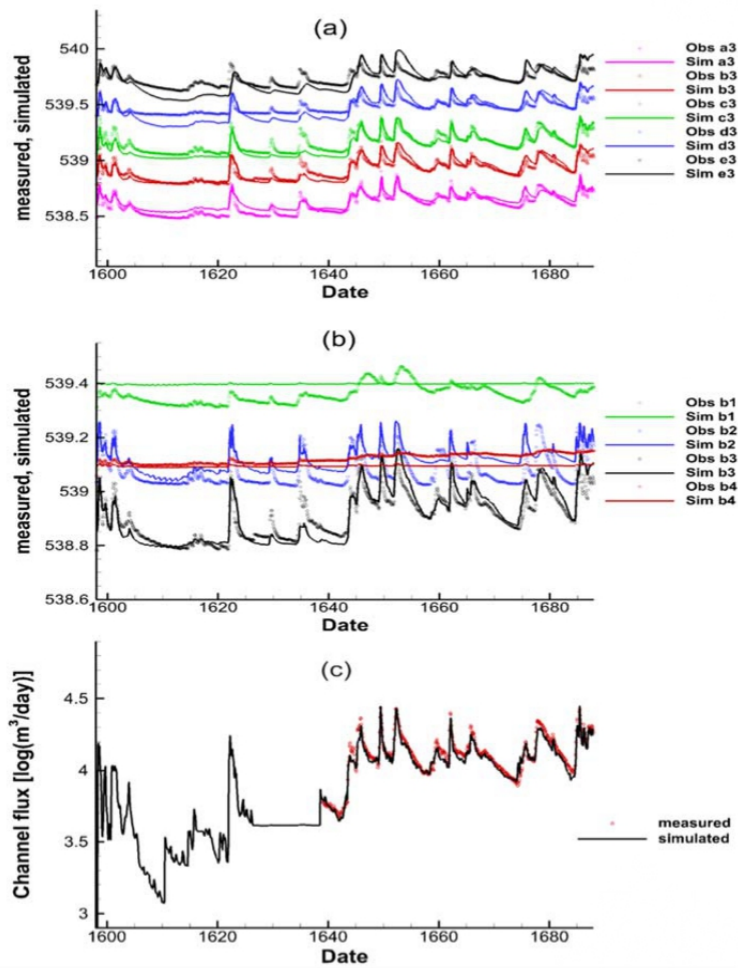
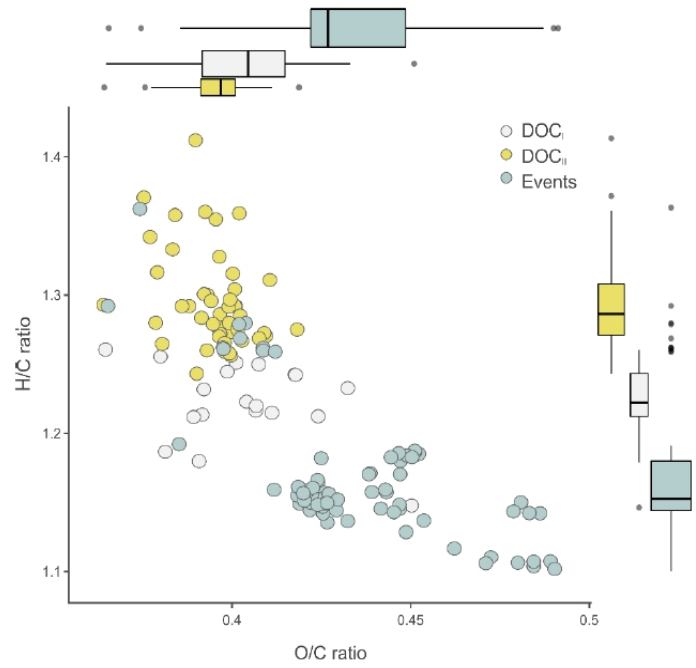


Figure S6: Comparison between the simulated groundwater levels and the measured ones for (a) five wells close to the channel, and for (b) wells along cross-section B, with the well b2 and b3 closer to channel, and b1 and b4 close to side boundaries. (c) Comparison between the simulated and the measured channel fluxes at the outlet.

125

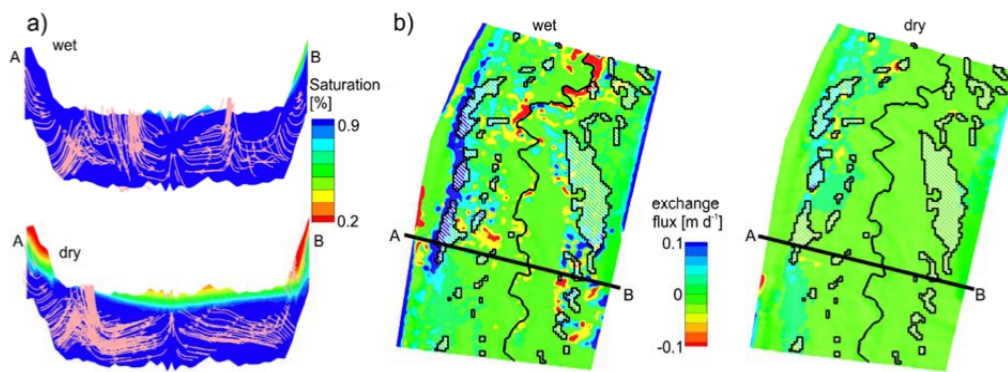


130

Figure S7: Aggregated van Krevelen plot of all FT-ICR-MS sample of stream (blue) and riparian origin with type DOC_I (grey) and DOC_{II} (yellow). Data represent the intensity weighted average (wa) of the molecular H/C and O/C ratios considering all valid MF in these samples ($n = 142$). See also Table S5 for individual values.

135

140



145

Figure S8: Panels a) & b) show the hydrological condition in the riparian zone for a wet situation on 13 Dec 2017, right after an event and at dry conditions and on 29 Aug 2018, amidst of a longer dry period in summer. a) Subsurface flow paths (pink arrows) along a vertical cross-section along a transect in the modeled riparian zone (indicated by black lines from A to B in (b)). b) Exchange flux (positive values = groundwater exfiltration).

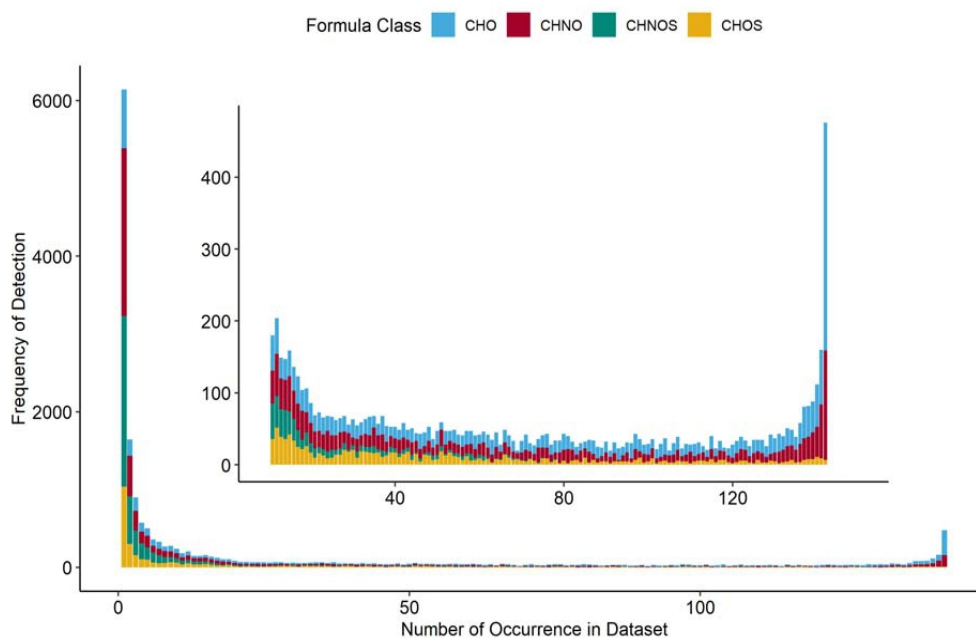
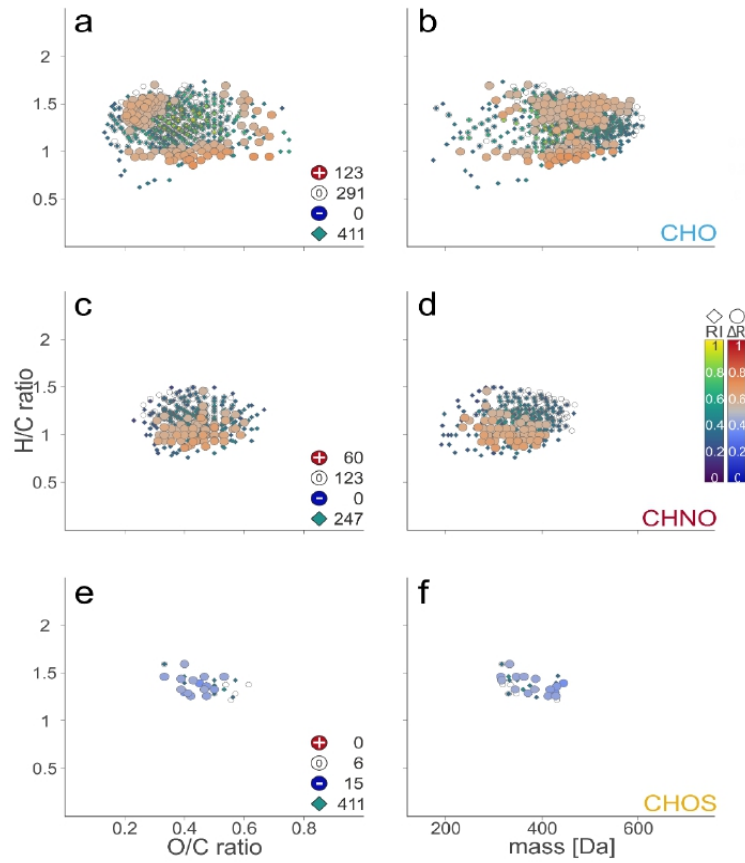


Figure S9: Frequency of detection of molecular formulas in the entire data set ($n = 142$). Formulas classes are represented as CHO (blue), CHNO (red), CHNOS (cyan), and CHOS (yellow) and the inset shows only MF occurring in at least 10 samples.

150



155 **Figure S10:** Molecular H/C vs O/C (a, c, e) and H/C vs mass (b, d, f) plot of averaged stream ($n = 76$), DOCI ($n = 19$) and DOClI ($n = 47$) sample groups. Group averages were calculated based on those molecular formulas (MF) which occur in all samples of the respective groups and the normalized peak intensities (reference to the base peak: RI) were used. The data are displayed based on the scaled normalized intensity difference between DOCI and DOClI (circles, $\Delta RI = RI(DOCI)/[RI(DOCI) + RI(DOClI)]$, red (+) indicates higher intensity in DOCI, blue (-) higher intensity in DOClI) and split according to formula classes (CHO: a, b; CHNO: c, d; CHOS: e, f). Only those MF are considered, which occur in both group averages ($n = 618$) and MF which were not significantly different between both group averages are displayed as open circles (0). Underlying is distribution of normalized intensity values (RI, diamonds) of the stream group average. See also Table S3 for aggregated values.

160

165

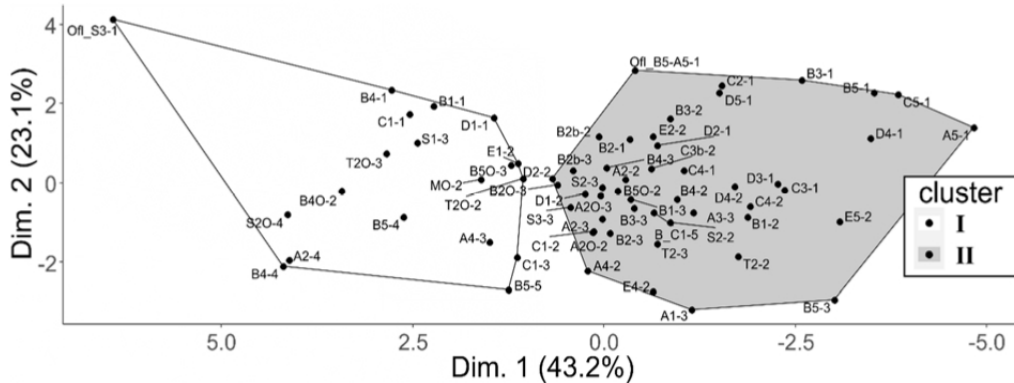


Figure S11: Visualization of the k-means cluster analysis on principal components for riparian samples only.

170

20

Additional Reference:

- 175 Therrien, R., McLaren, R., Sudicky, E., and Panday, S.: HydroGeoSphere: A three-dimensional numerical model describing fully-integrated subsurface and surface flow and solute transport, Groundwater Simulations Group, University of Waterloo, Waterloo, ON, 2010.

Study 3: Modelling dissolved organic carbon export from a temperate headwater catchment using a complexity-reduced, mechanistic approach

Status: Ready for submission to Journal of Geophysical Research.

Authors: Benedikt J. Werner, Linus S. Schauer, Andreas Musolff, Christian Birkel and Jan H. Fleckenstein

BJW, JHF and AM planned and designed the research. BJW performed the statistical model analysis and wrote the paper with contributions from all co-authors. CB provided the initial model. LS and BJW edited and scripted the initial model.

Own contribution:

- Concept and study design: 90%
- Data acquisition: 100%
- Data analysis: 90%
- Interpretation of the results: 90%
- Preparation of the manuscript: 90%

Modelling dissolved organic carbon export from a temperate headwater catchment using a complexity-reduced, mechanistic approach

Benedikt J. Werner¹, Linus S. Schauer², Andreas Musolff¹, Christian Birkel³, Jan H. Fleckenstein^{1,2}

¹Department of Hydrogeology, Helmholtz Centre for Environmental Research – UFZ, 04318 Leipzig, Germany

²Hydrologic Modelling Unit, Bayreuth Center of Ecology and Environmental Research (BayCEER), University of Bayreuth, Bayreuth, Germany

³Department of Geography, University of Costa Rica, San Pedro, Costa Rica

Correspondence to: Benedikt J. Werner (benedikt.werner@ufz.de)

Abstract. Dissolved organic carbon (DOC) concentrations in headwater streams have shown critical upward trends in the last decades with potentially harmful environmental consequences. The complexity of the processes controlling DOC export and timing have so far impeded a broader application of DOC export models to predict future trends. In this paper an existing semi-distributed coupled hydrology-biogeochemistry model for DOC export was mechanistically refined by the implementation of justifiable, threshold-controlled, (surface) flux mechanisms. Besides, we figured that the strong coupling between hydrology and biogeochemistry in the riparian zone with respect to generated DOC export is sufficient to simultaneously calibrate the model's hydrological and biogeochemical modules without calibrating on additional data. Calibration (Kling-Gupta efficiency of 0.79 and 0.73 for the hydrological and biogeochemical module, respectively) and validation revealed a robust and mechanistically justifiable parameterization of key internal and external water and DOC fluxes, suggesting a direct relationship between riparian groundwater dynamics and DOC export that can be used to reproduce and predict DOC flux variability at the catchment outlet. Since fast water flow components make up large fractions of the total DOC export in temperate headwater catchments with overall low riparian tilt, explicit surface runoff generation mechanisms should be considered in respective models to adequately capture solute flux dynamics. Here, the description of antecedent wetness was a reliable proxy to estimate soil-moisture related thresholds. Calibrating the biogeochemical module following the hydrological calibration produced unrealistic internal model fluxes, revealing that despite having a good hydrological performance models do not necessarily depict meaningful results. We conclude that in-stream DOC dynamics from the ubiquitously present DOC sources in catchments may complement the application of artificial tracers for model calibration. Together with the implemented, explicit mechanistic representation of surface flux, this in turn should increase the applicability of the model to a range of different catchments.

1. Introduction

Changes in land use and climate put pressure on water quantity, water quality and ecological state in freshwater ecosystems (Larsen et al., 2011; Chantigny, 2003; Wilson and Xenopoulos, 2008). For example, instream dissolved organic carbon (DOC) concentrations have been going up in headwater catchments in the last decades (Worrall et al., 2003), impacting the aquatic ecosystem, but also threatening the safety of drinking water from reservoirs by impairing raw water quality, increasing the costs for filtration and the potential for toxic byproducts during chlorination (Tong and Chen, 2002; Ojima et al., 1994; Whitehead et al., 2009). Yet, the complete dimension of this problem's controls as well as present and future impact are still poorly understood (Stanley et al., 2012; Evans et al., 2005). Therefore, predictive modelling is an indispensable tool to understand and explore potential DOC loads exported from catchments under future scenarios of climate and land use change (Stanley et al., 2012).

Application of such models, however, are rare. One reason is that the ubiquitous sources of organic material in catchments from which DOC can be derived, together with the complex hydrological flow paths that may temporal discontinuously deliver it to the streams are difficult to implement into tractable modelling approaches. Especially, export processes in riparian zones (RZs) – which are considered a major source for riverine DOC (Ledesma et al., 2015; Musolff et al., 2018) – need to be precisely represented in predictive DOC models at catchment scale. More specifically, riparian DOC is predominantly mobilized and exported from shallow organic soil horizons by fast lateral water flow, which in turn is a function of local groundwater level dynamics (Seibert et al., 2009). A growing body of literature additionally stresses that DOC production and export are not spatially uniform within RZs, but rather governed by nonlinear and threshold-type dynamics (Dick et al., 2015; Ledesma et al., 2018b; Wen et al., 2020; Werner et al., 2021). The timing of DOC export is dependent on the establishment of the mentioned groundwater-driven hydrological connections of DOC source zones to the stream, while the magnitude of DOC export is further shaped by the biogeochemical settings that control DOC processing (Wen et al., 2020). Both the hydrological connectivity and the biogeochemical DOC processing are a function of the interplay between small-scale geomorphological setting and groundwater dynamics, which are ultimately driven by the prevailing and antecedent hydroclimatic conditions (Ledesma et al., 2018a; Werner et al., 2019).

There are established conceptualizations for DOC export from RZs that break this complex system down into spatially lumped integrated functional relationships without explicitly acknowledging such small-scale spatio-temporal variability (Seibert et al., 2009; Ledesma et al., 2018a; Birkel et al., 2014). For instance the riparian profile flow-concentration integration model (RIM; Seibert et al. (2009)) models stream solute variability as a function of a nonlinear vertical distribution of pore water solute concentrations while accounting for depth-dependent differences in hydraulic conductivities of riparian soils. However, these type of models rely on a predefined distribution of pore water concentrations and a given discharge and are thus rather tools to explore concentration variability and their underlying controls within the RZ than to predict DOC fluxes under changing boundary conditions. In contrast, there are highly complex model concepts that capture the mechanisms of small-scale DOC mobilization in RZs. E.g., Frei et al. (2012) were able to simulate the complex effects of riparian microtopography

on runoff generation and the formation of biogeochemical hotspots in the subsurface. This more explorative model was computationally expensive and applicable to smaller-scale problems of a few meters only making it hard to be transferred to the catchment scale.

For robust projections of DOC export at the catchment-scale, models are needed that, on the one hand are sufficiently mechanistic to adequately capture the complex, dynamic riparian fluxes for “the right reasons” (Kirchner, 2006), and on the other hand reduced enough in overall model complexity to remain tractable and transferable to other catchments. In this regard, a balanced approach could be semi-distributed models, which represent dominant landscape units in the catchment and the fluxes between them, while at the same time account for the dominant processes and internal fluxes within the units. For example, Birkel et al. (2014) and Dick et al. (2015) conceptualized the catchment into the typical compartments hillslope, groundwater and riparian zone to model catchment DOC export. They represented (near) surface flux in the RZ unit by a power law function of riparian soil moisture content and used additional tracer data (stable water isotopes) to calibrate the model. Strohmenger et al. (2021) successfully modeled discharge, DOC and nitrate concentration in a small headwater catchment in northern France using the hydrological FLEX model (Fenicia et al., 2006) and constant solute concentration two reservoir mixing, but stated high uncertainty due to the lack of validation data and resulting parameter equifinality.

In fact, many of those semi-distributed models represent dominant processes in a somewhat mechanistic way and typically yield good overall performance metrics for the fluxes at the catchment outlet (Strohmenger et al., 2021; Lessels et al., 2015; Euser et al., 2013; Birkel et al., 2014; Dick et al., 2015; Birkel et al., 2020). However, internal fluxes and states are hardly ever validated (Hrachowitz et al., 2014), although an independent evaluation of the internal model functioning is key to constrain and test models (Birkel et al., 2017). Hrachowitz et al. (2014) suggested to determine suitable model conceptualizations based on their internal and external flux and state properties, because such constraints have higher mechanistic information content than simple parameter constraints in hydrological models. Hence, such prior process and model constraints – e.g. through the implementation of threshold values (Werner et al., 2021), expert knowledge or additional data (Hrachowitz et al., 2014) – can help to increase model performance and credibility.

Since hydrological dynamics are a key control of DOC export in RZs (Wen et al., 2020), flaws in the hydrological conceptualization directly interact with the parameterization of DOC mobilization and transport. In order to reduce model uncertainty in this regard, additional tracer data such as water isotopes are often used to validate hydrological fluxes and flowpaths. However, the additional effort of measuring tracer data at a sufficient frequency over years – see e.g. Birkel et al. (2014; 2017) or Dick et al. (2015) – is expensive and thus not always feasible. Consequently, a substitute is required if tracers are not at hand in order to improve model calibration and validation, and to enable better transferability of model concepts to other catchments.

We argue that the biogeochemical processes of DOC production and mineralization are inherently coupled to hydrological controls of mobilization and hydrological connectivity regulating DOC export from RZs. The DOC that enters the stream from the RZ thus already carries integral information on its origin and distinct flowpath to the stream. Werner et al. (2021) could show that microtopography-induced small sized hot spots of biogeochemical activity contribute disproportionately strong to

DOC export via dynamically evolving surface flow paths. However, despite their potential high impact on DOC export, the respective surface flow mechanisms are often not explicitly represented in models. We therefore postulate that calibrating hydrologic fluxes and DOC concentrations simultaneously in a mechanistically sound, state-of-the-art model, will improve overall model performance and validity for both, the hydrological and the biogeochemical fluxes. Such an approach has the potential to result in a complexity reduced DOC export model at the catchment scale with improved functionality and robustness for predictions that can be calibrated at relatively low additional cost.

Along those lines the main objectives of this study are:

- (1) finding the right model structure through adapting an existing semi-distributed model (Birkel et al., 2014) to better represent recent understanding of event-scale water flow and DOC export variability in a temperate catchment with low riparian relief
- (2) assess and evaluate the role and information content of coupled DOC concentration and discharge data obtained at the catchment outlet for the calibration of internal and external water and DOC model fluxes
- (3) apply the model and discuss its validity and implications for future model applications at catchment-scale

2. Study site

The Rappbode headwater catchment is located in the Harz Mountains in Saxony-Anhalt, central Germany (Fig. 1). The catchment comprises an area of 2.58 km² and drains into the Rappbode drinking water reservoir. Further downstream, below the reservoir the Rappbode stream flows into the river Bode and eventually via the Saale and Elbe into the North Sea. The climate of the Harz Mountains is temperate and generally colder and wetter than the surrounding landscape. The Rappbode catchment is located between the Braunlage (609 m NHN, mean annual precipitation: 910 mm (1990-2020), mean annual temperature: 7.5°C; 10 km to the northwest) and Stiege (494 m NHN, 760 mm (1990-2020), 8.1°C; 12 km to the east) weather stations and is assumed to have a mean annual precipitation and temperature comparable to the arithmetic mean of the values from those two weather stations. The elevation of the catchment ranges between 540 m and 620 m NHN. The catchment is predominantly forested with spruce and pine trees (77%) while 11% is covered by grass and other vegetation. The geology of the Harz Mountains is dominated by Paleozoic rocks such as graywacke, clay schist and diabase (Wollschläger et al., 2016). One quarter of the soils in the catchment are influenced by groundwater (humic Gleysols and stagnic Gleysols) that are typical for riparian zones. We therefore predefined the RZ area in this catchment to be 25% of the total catchment area.

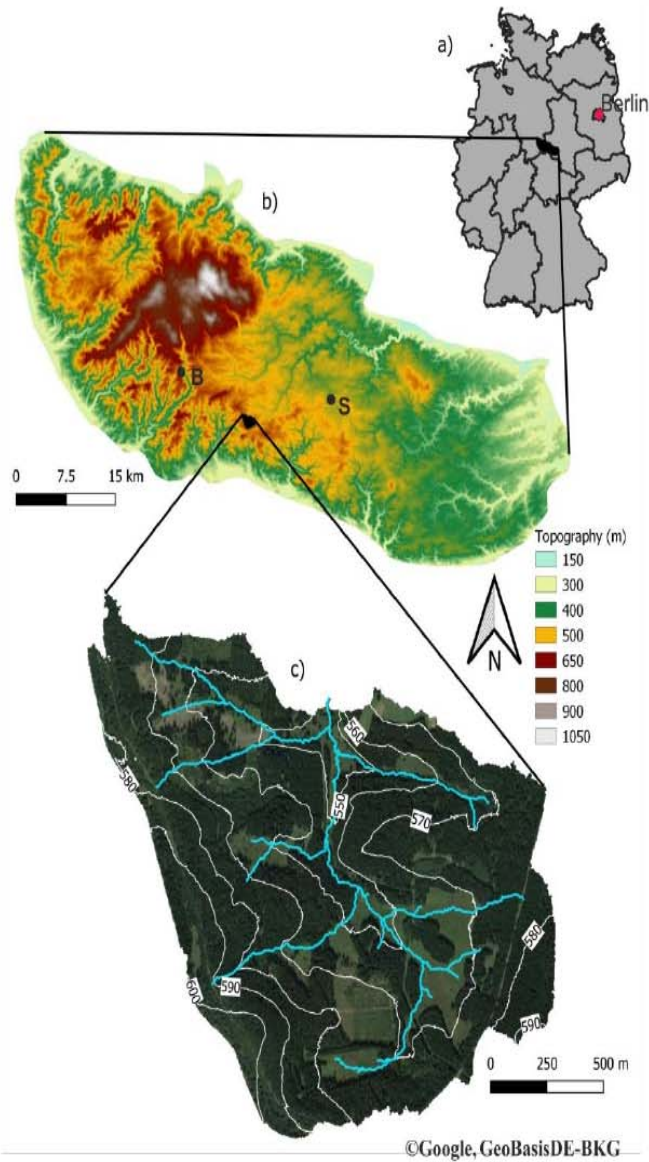


Figure 1. a) Overview map of Germany and the location of the Harz Mountains. b) Topography of the Harz Mountains and the location of the studied catchment. Black dots 'B' and 'S' indicate the location of the weather stations Braunlage and Stiege. c) Altitude and riverine system based on digital elevation data (1 meter resolution). Map data: ©Google, GeoBasisDE-BKG.

3. Data and Methods

3.1 Hydro-meteorological and DOC concentration data

For a detailed description of the data collection and treatment see Werner et al. (2019; 2021). The compiled data set describes overall 1549 days covering the period between 21 May 2013 to 30 Apr 2014 (Werner et al., 2019) and 16 Mar 2017 to 25 Jun 2020 (Werner et al., 2021). All time series were aggregated to daily values (see respective sections in the following) for model application.

Discharge was calculated from a stage–discharge relationship, which was established based on the 15 min stage readings from a barometrically compensated pressure transducer (Solinst Levellogger, Canada) and manual discharge measurements approximately once every 2 weeks using an electromagnetic flow meter ($n=42$; MF pro, Ott, Germany).

We installed a weather station 250 m downstream (north) of the catchment outlet to measure meteorological data. Potential evapotranspiration (ET_{pot}) was calculated from the meteorological data after Penman-Monteith (Allen et al., 1998). Since the riparian zone was wet most of the time during the study period, we figured ET_{pot} to be roughly equal to the actual evapotranspiration. However, replacing the used potential evapotranspiration value by actual evapotranspiration values that are adjusted to the respective storage units could be an interesting approach to further refine the model in future studies.

When comparing our meteorological data with the two closest official weather stations (DWD station Braunlage and Stiege, 10 km and 12 km distance to the Rappbode catchment; Fig. 1b) at a daily aggregation, it turned out that precipitation data was deviating especially in winter during snow fall, leading to shifts in hydrological mass balances. Consequently, days with inconsistent rainfall data were interpolated (weighted mean) between these two nearby official weather stations, which improved overall mass balance. Finally, short data gaps (< 4 h) due to instrument maintenance were linearly interpolated in the dataset to create a continuous input series for modeling.

Groundwater level data was obtained from a piezometer field located in the riparian zone in close vicinity upstream of the catchment outlet (Fig. 1b). Each of the 25 piezometers was equipped with a pressure transducer (Levellogger, Solinst, Canada and Diver, van Essen, Netherlands), measuring at a 15-minute interval. All pressure transducers were barometrically corrected and adjusted to manual measurements of the groundwater level at 8 occasions during the 15 months measurement period (from 04 October 2017 to 19 December 2018). Only the mean groundwater level of all available groundwater time series was used in this study.

A detailed description of DOC measurements and calibration procedures is provided by Werner et al. (2019 and 2021). An UV-Vis probe (spectro::lyser, s::can, Austria) measured DOC in-situ during the study period at 15 minutes time steps, but data gaps exist due to probe failure (up to two week gaps), on-site maintenance (up to 1h) or due to snow and ice in winter, when the study site was not accessible (2 – 4 months in winter). For calibration, routine DOC stream water samples were collected every two weeks (except inaccessible periods in winter), filtered and stored cool until further analysis in the laboratory (TOC Analyzer, Analytic Jena GmbH, Germany). Furthermore, five runoff events were auto-sampled ($n = 66$, 30 min or 60 min

interval; 6712 Full-Size Portable Sampler, Teledyne ISCO, United States) to increase the range of the DOC calibration. Samples were analyzed by thermo-catalytic oxidation at 900 °C with non-dispersive infrared detection (DIMATOC® 2000, Dimatec Analysentechnik GmbH, Germany). Drift in the data due to biofilm formation on the UV-vis probe was corrected where possible according to the method described in Werner et al. (2019). Stream water samples were taken next to the gauging station at the catchment outlet (Fig. 1c). For the 2013/2014 period, the DOC time series from Werner et al. (2019) was used. In-situ DOC measurements for the 2017-2020 period were pre-processed like the 2013/2014 dataset. Here, the DOC concentration was derived by fitting the manufacturer's estimated DOC concentration (derived from an internal algorithm based in the measured UV-vis spectra) to 106 DOC measurements from grab samples. DOC was further measured in groundwater samples from the piezometer field on 5 occasions between 2017 and 2020 (Werner et al., 2021). Table 1 summarizes the basic catchment descriptors and data used in this study, and Fig. 2 shows the time series used for the measurement period (corresponding to three full hydrological years).

Table 1. Basic statistics of hydro-meteorological and DOC data from the Rappbode study site based on observations from June 2013 to June 2014 and May 2017 to June 2020. ET_{pot} : potential evapotranspiration; sd: standard deviation.

	Elevation [m]	mean annual precipitation [mm]	mean annual ET_{pot} [mm]	mean annual runoff [mm]	mean annual DOC [mg L ⁻¹]
mean	572	968	282	686	2.83
range	538 - 617	827 - 1162	251 - 303	332 - 844	1.64 - 4.29
sd	13	140	24	238	1.34

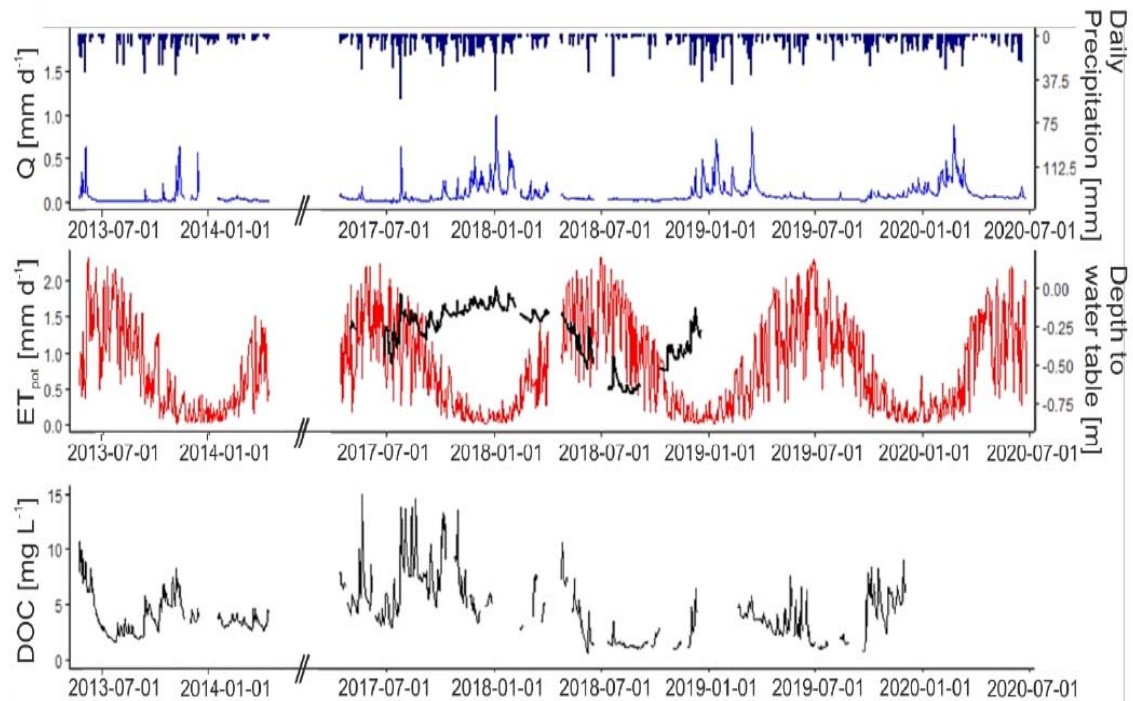


Figure 2. Overview of the time series that were used for modeling. a) Discharge (Q; blue lines) and precipitation (dark blue bars; second y axis), b) potential evapotranspiration (ET_{pot} ; red) and mean depth to water table (black line; second y axis) and c) DOC concentration data. Note the gap in time between 2014 and 2017 for all x axis. See (Werner et al., 2019; 2021) for a detailed description of the DOC calibration.

3.2 Model Development and Adaption

Birkel et al. (2014) proposed a semi-distributed model for water flow and DOC exports that was based on the general conceptual understanding of catchment and riparian zone functioning in a catchment in Scotland. Their area-normalized model consists of three interlinked functional units: the hillslope (HS), the riparian zone (RZ) and the groundwater (GW) storage. The dominant hydrological and biogeochemical catchment processes are represented within a rainfall-runoff (hydrological module) module and, coupled to it, a DOC processing module (biogeochemical module) that ultimately determines DOC concentration and export for each storage unit. The hydrological module reflects the spatial distinction of the RZ and HS as unsaturated storage units. Subsurface and surface runoff contributions from the RZ into the stream are represented by a soil moisture controlled linear and nonlinear runoff generation. Linear recharge processes on the HS, either recharge the GW through percolation or feed the RZ through interflow, but do not directly contribute to the stream. A permanently saturated groundwater storage unit (GW) – that is linearly recharged by the HS – steadily feeds the stream at low rates, defined by a linear function. Consequently, the runoff into the stream is calculated by adding up the parallel fluxes from the riparian storage (shallow riparian groundwater and surface flow) and groundwater storage (deeper groundwater) units.

The biogeochemical module conceptualizes the DOC production and mineralization dynamics in the three hydrological storages (HS, RZ and GW). DOC concentration in the RZ and HS storage are determined by an Arrhenius-type soil moisture

and temperature dependent function. In addition, the GW and RZ storages (both receiving DOC flux from the HS) are regulated by a DOC loss parameter that represents DOC mineralization. Respective DOC export loads from storages to the stream are calculated as the product of the calculated DOC concentration and the hydrological runoff generation flux. Final stream DOC concentration is then calculated as mixing from two reservoirs (GW and RZ) that export DOC to the stream.

The model was successfully applied in temperate (Birkel et al., 2014) and oceanic (Dick et al., 2015; Birkel et al., 2017) settings, showcasing its general ability to adequately represent DOC export mechanisms in different climates. Birkel et al. (2020) further illustrated the model's transferability to other catchments by successfully adapting the model to the wet-dry tropics. We therefore also considered the underlying general model setup as a good starting point for an adaption to a riparian zone functioning as described in Werner et al. (2021).

In the following, we will refer to this adapted model as Tracer-Aided Coupled Hydrology-Biogeochemistry model (TACHyB). Both modules (hydrologic and biogeochemical) of the TACHyB-model were adjusted and constrained according to "expert knowledge" (Hrachowitz et al., 2014), generated from previous work in the Rappbode catchment (Werner et al., 2019; Werner et al., 2021). The adapted model was set up in Python programming language (vanRossum, 1995) and incorporates the following hydrological and biogeochemical processes and refinements:

1. Dynamic, threshold induced riparian surface runoff with DOC export to the stream (Werner et al., 2021) based on the antecedent aridity index of the preceding 60 days (AI_{60} ; Werner et al. (2019)).
2. Threshold induced onset of surface near hillslope runoff to the riparian zone (Tromp-van Meerveld and McDonnell, 2006; McGuire and McDonnell, 2010)
3. Constraining maximum groundwater efflux by adding a threshold based exchange flux between the groundwater reservoir and the riparian reservoir (Werner et al., 2021)
4. Use of a soil temperature model to more accurately determine soil temperature induced temporal dynamics of DOC processing (Köhler et al., 2008)

By incorporating these points, we believe to conceptually design the model such that it more explicitly represents the dominant mechanisms that are responsible for DOC export dynamics in very gently sloping riparian soils with low hydraulic conductivity, as they are common in temperate headwater catchments. The rainfall-runoff module uses eleven calibrated parameters (initially: five), which are briefly explained in Table 2. Three of the six additional parameters are physically based threshold values, two were used to create the dynamic function of surface runoff and the remaining one was used to implement the exchange flux between groundwater and riparian zone. Figure 3 gives an overview of the conceptual model structure. As described above the extent of the riparian wetland area was set to be 25% of total catchment area, while the HS made up the remaining 75% of the surface area.

The upper hillslope storage (S_{HS}) directly drains a fractional volume of water into the riparian wetland storage (S_{RZ}) via the flux Q_{HS} using the linear rate coefficient a . This flux Q_{HS} is threshold controlled via τ_{HS} , as suggested by McGuire and

McDonnell (2010). We found the 60 day antecedent wetness index (Werner et al., 2019) as a suitable indicator for soil moisture dependent saturation excess flow (Fig. S1) according to Eq. 1:

$$AI_i = \frac{\sum_0^i P_i}{\sum_0^i ET_i} \quad (1)$$

Where AI_i is the aridity index of the preceding day, P_i and ET_i are the accumulated precipitation [mm] and accumulated potential evapotranspiration [mm] of the preceding i days, respectively. i was set to 60.

The S_{HS} also recharges the groundwater storage (S_{GW}) using the linear rate coefficient r . S_{GW} then contributes linearly to stream water up to a maximum value τ_{GW} using the linear rate coefficient b . If τ_{GW} is reached, all additional flux generated from S_{GW} recharges the riparian zone storage (S_{RZ}) emulating that the groundwater can only rise up to the level where the riparian storage unit that is conceptualized on top of S_{GW} begins. In S_{RZ} , stream water can be generated via the flux Q_{RZlm} using the linear rate coefficient c , representing subsurface flow towards the stream, and a nonlinear dynamic function ($f_{\dot{q}_n}$) that is representative of the observed surface runoff (Q_{RZexp}) in this study site – if a threshold value ($\tau_{\dot{q}_n}$) in 60 day antecedent aridity index (representative of soil moisture; Fig. S1) is exceeded (Eq. 2).

if $AI_{60} > \tau_{\dot{q}_n}$:

$$Q_{RZexp,i} = f_{\dot{q}_n} * S_{RZ,i}^{(1+\alpha)} \quad (2a)$$

$$f_{\dot{q}_n} = \alpha_{\dot{q}_n} * AI_1^x \quad (2b)$$

where AI_{60} represents the 60 day antecedent aridity index, $\tau_{\dot{q}_n}$ describes the threshold value in 60 day antecedent aridity index, $Q_{RZexp,i}$ is the simulated surface runoff in the RZ at time step i , $f_{\dot{q}_n}$ describes the dynamic parameter from the soil moisture dependent function, $S_{RZ,i}$ the water content of the riparian storage at time step i , α is the non-linearity parameter for the surface runoff, $\alpha_{\dot{q}_n}$ is the linear coefficient of the dynamic function, x the nonlinearity index.

The antecedent aridity index was set to one day (AI_1) as is typically used for antecedent precipitation index calculations that are connected to runoff (Ali et al., 2010). With that $f_{\dot{q}_n}$ is depending on rainfall amounts and evapotranspiration. This formulation differs from Birkel et al. (2010) who used antecedent precipitation of (calibrated) i days instead.

Figure 3 provides a conceptual overview of the model set up, inlet in Fig. 3 shows the behavior of AI_1 controlled $f_{\dot{q}_n}$ over time. Such a temporally dynamic model structure reflects the basic hydrologic understanding of the dominant runoff generation processes (Werner et al., 2019; 2021). Similar threshold induced runoff mechanisms have recently been represented in a model for temporally active riparian runoff generation in the wet-dry tropics (Birkel et al., 2020).

The DOC module requires seven calibrated parameters. The DOC concentration depends on a mass balance of organic carbon production and losses due to mineralization (Birkel et al., 2014; Dick et al., 2015). DOC is produced according to an Arrhenius-type, nonlinear DOC production rate modulator (Eq. 3a) that is related to soil moisture (Eq. 3b) and soil temperature (Eq. 3c)

$$DOC_{stim,i} = k_x * f(SM) * f(T) \quad (3a)$$

$$f(SM) = \frac{\tau_{STOmax} - S_{RZ,i}}{\tau_{STOmax}} \quad (3b)$$

$$f(T) = E_a^{(T_i - \bar{T})} \quad (3c)$$

where $DOC_{sim,i}$ is the DOC concentration at time step i , k_x the DOC production rate coefficient in the RZ (k_{RZ}) or the Hillslope (k_{HS}); $f(SM)$ a soil moisture dependent modulator; $f(T)$ the temperature modulator of the rate coefficient k_x . τ_{STOmax} is the maximum soil moisture deficit ($\tau_{STOmax} < -1$) at which DOC processing (production or loss) is happening, $S_{RZ,i}$ the water content of the riparian storage at time step i (corresponding to soil moisture content). Temperature dependence of the processing kinetics in the RZ is expressed by the activation energy E_a ($E_{a,up}$ for the HS, resp.). T_i is the soil temperature at time step i , \bar{T} is the reference soil temperature (overall mean soil temperature of the 1.5 a lasting dataset in 30 cm depth). T_i was modeled from air temperature by an adapted version of multiple linear regression as applied in Köhler et al. (2008). Modulator functions $f(SM)$ and $f(T)$ are only defined for values greater than 0. The higher temperatures and the wetter soils are the more DOC is processed ($S_{RZ,i} > 0$; $T_i > \bar{T}$), or is lost ($S_{RZ,i} > \tau_{STOmax}$; $T_i < \bar{T}$). Dried out soils for $S_{RZ,i} = \tau_{STOmax}$ lead to $f(SM) = 0$ and thus do not process DOC anymore. Note that after $DOC_{sim,i}$ was calculated, the linear rate coefficients LQ_{HS} and LQ_{RZ} additionally reduce simulated DOC concentrations. This procedure was applied in order to be able to distinguish between DOC production in the riparian surface runoff (Q_{RZexp}) that was modeled without DOC reducing processes and riparian linear subsurface runoff (Q_{RZlin}) that was modeled as DOC with loss due to e.g. mineralization and sorption processes subsequent to hydrological mixing with HS and GW DOC contributions and ultimate DOC. The model was initiated for soil carbon concentrations set to average measured DOC concentrations of soil and groundwater (Table 1).

Table 2. Overview of all 18 calibrated parameters (11 hydrological and 7 biogeochemical parameters). Numbers in squared brackets show the initial range that was used as a starting point for calibration. Min, mean and max depict statistics of the 500 best parameter sets after model calibration. SHS: Hillslope storage, SRZ: riparian zone storage, SGW: groundwater storage.

Parameter & [initial range]	units	min	mean	max	description	
<u>Hydrological parameters</u>						
τ_{GW}	[0, 5]	mm	3.17	4.09	4.77	Threshold value for maximum SGW to stream- contribution
τ_{HS}	[0, 12]	-	9.04	9.59	10.48	Threshold value for direct SHS runoff into the SRZ
τ_{dyn}	[1.1, 2]	-	1.71	1.73	1.83	Threshold value for nonlinear riparian flux from SRZ to stream
a	[0, 1]	d ⁻¹	0.47	0.7	1	Recession coefficient from SHS to SRZ
b	[0, 1]	d ⁻¹	0	0.01	0.01	Recession coefficient from SGW to stream
b_2	[0, 0.25]	d ⁻¹	0.004	0.009	0.018	Recession coefficient from SGW to SRZ
r	[0, 1]	d ⁻¹	0.13	0.2	0.32	recession coefficient from SHS to SGW reservoir
c	[0, 1]	d ⁻¹	0.11	0.19	0.36	recession coefficient for linear runoff from SRZ to stream
α	[0, 1]	-	0.26	0.31	0.45	Nonlinearity parameter for runoff from SRZ to stream
x	[0, 1]	-	0	0.47	1	Exponent of the nonlinearity function
α_{dyn}	[0, 1]	-	0.01	0.07	0.1	Linear coefficient of the nonlinearity function
<u>Biogeochemical parameters</u>						
τ_{STOmax}	[-3000, -1]	mm	-1298.3	-206.29	-8.05	Threshold value for soil moisture dependent DOC production

k_{HS}	[0, 50]	mg L ⁻¹	3.29	4.87	5.29	Rate coefficient for DOC production in the S _{HS}
k_{RZ}	[0, 50]	mg L ⁻¹	11.79	12.18	12.52	Rate coefficient for DOC production in the S _{RZ}
E_{RZ}	[1, 2]	-	1.04	1.04	1.04	Activation energy for DOC production in the S _{RZ}
E_{HS}	[1, 2]	-	1.08	1.18	1.31	Activation energy for DOC production in the S _{HS}
LQ_{HS}	[0, 1]	-	0.45	0.49	0.59	DOC loss term during transport from S _{HS} to S _{GW}
LQ_{RZ}	[0, 1]	-	0.6	0.63	0.66	DOC loss term in the S _{RZ}

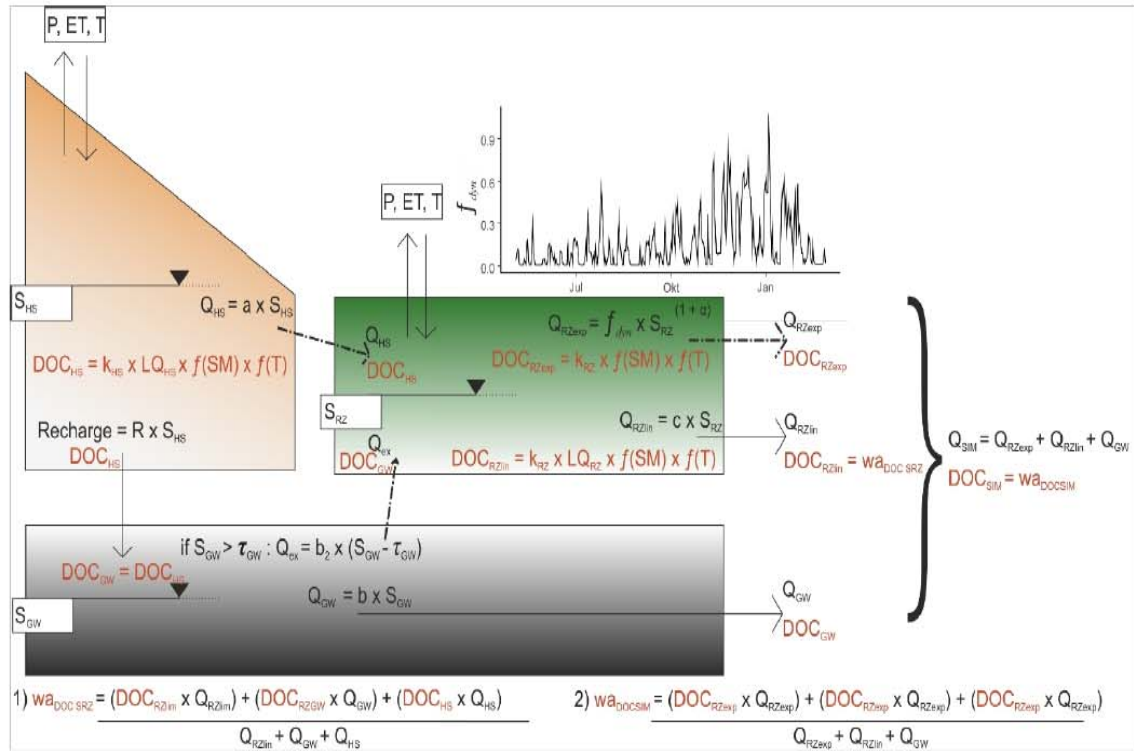


Figure 3. Conceptual diagram of the tracer aided coupled hydrological biogeochemical (TACHyB) model set up. The three storage units are groundwater (S_{GW}), hillslope (S_{HS}) and riparian zone (S_{RZ}). Blue arrows represent hydrological processes and respective DOC transfer between storages or to the stream. Dashed black arrows indicate threshold controlled hydrological processes that occur timewise discontinuous. DOC is calculated based on an Arrhenius type (Eq. 3a) DOC production (k_{HS} and k_{RZ} , resp.) and loss term (LQ_{HS} and LQ_{RZ} , resp.) that is based on soil moisture ($f(SM)$; Eq. 3b) and soil temperature ($f(T)$; Eq. 3c). The biogeochemistry processing parameters of each storage unit are shown in red: τ_{STOmax} is the maximum soil moisture deficit defining up to which deficit [mm] DOC processing is still possible; k_{HS} and k_{RZ} are the DOC production rate parameters for the HS and the RZ; LQ_{HS} , and LQ_{RZ} are DOC loss parameters for HS and RZ, resp.; E_a is the thermal activation energy defining the impact of temperature on the processing rates. Streamflow (Q_{SIM}) is generated by nonlinear riparian surface flux (Q_{RZexp}), linear riparian subsurface flux (Q_{RZin}) and linear groundwater flux (Q_{GW}). Inlet shows the riparian nonlinear dynamic function (f_{dyn}) over time (Eq. 2b) that regulates the intensity of Q_{RZexp} contributions to the streamflow. Simulated DOC concentration in the Q_{RZin} and streamflow (DOC_{SIM}), are calculated as flow weighted average (formulas 1) and 2) in the Figure) DOC concentration of the S_{RZ} and streamflow components, respectively.

3.3 Model Calibration and Evaluation

The model was calibrated using a multiobjective optimization procedure, utilizing the python package pymoo (Blank and Deb, 2020). The optimization used the NSGAII algorithm of Deb et al. (2002), with the goal to find the best performing parameter sets. The NSGAII is an iterative process where in a first step a random parent population P_0 within the initial parameter range and an offspring population O_0 each of size N are created. In the main loop a combined population R_t of size $2N$ is created by merging the parent and offspring populations. This ensures elitism, the operation of transferring the best performing parameter sets of the parent population to the next generation, thus enhancing the algorithm efficiency. Then, non-dominated sorting is applied to R_t . Achieving a balanced rainfall-runoff model requires simulation of peak as well as low-flows and thus an objective function that represents the runoff distribution to equal parts. We used the Kling-Gupta Efficiency (KGE), after Kling et al. (2012) and Pool et al. (2018), as the criterion which focuses on three components of model errors (Eq. 4)

$$KGE = 1 - \sqrt{(r - 1)^2 + (\gamma - 1)^2 + (\beta - 1)^2} \quad (4)$$

where r is the (pearson correlation coefficient), γ is the variance, and β the bias. Generally, if $KGE = 1$, the model perfectly represents the dataset. KGE values smaller than -0.41 indicate that the model is worse than the mean flow benchmark. However, note that the Nash Sutcliffe Efficiency and KGE cannot be directly compared due to their non-unique relationship (Knoben et al., 2019). Rogelis et al. (2016) consider model performance to be ‘poor’ for $KGE < 0.5$.

Since a correct hydrological mass balance is critical to avoid overestimation of large flows in hydrologic simulations (Cris and Winston, 2008), the volumetric efficiency (VE; Eq. 5) was calculated

$$VE = 1 - \frac{|\sum_{i=1}^n \chi_i - \sum_{i=1}^n \chi_{obs,i}|}{\sum_{i=1}^n \chi_{obs,i}} \quad (5)$$

where χ_i and $\chi_{obs,i}$ are the observed and simulated values at timestep i and n is the total number of time steps. VE ranges from 0 to 1 and represents the fraction of water delivered at the proper time.

Similar to Birkel et al. (2017), a weighted, combined objective function (OF) was then calculated from the KGE and the VE (Eq. 5) to calibrate the hydrological module:

$$OF = 1 - \sqrt{(1 - KGE)^2 * 0.75 + (1 - VE)^2 * 0.25} \quad (6)$$

On the other hand, the KGE (Eq. 4) – as a straightforward, balanced objective function – was figured to be sufficient for the calibration of the DOC concentration in the biogeochemical module.

Before running the model, the whole dataset was split into a calibration periods (from 21 April 2013 to 12 Apr 2014 and from 13 Apr 2017 to 21 April 2018) and a validation period (22 April 2018 to 21 June 2020). Calibration was undertaken by simultaneously minimizing the rainfall-runoff and the DOC model objective functions with overall 18 parameters. Therefore, we ran 500 parameter populations over 2,000 generations with a total of 1,000,000 iterations for reproducibility (Deb et al., 2002). After optimization, the overall best 500 sets of parameters were retained for simulation envelopes, as indicators of parameter uncertainty for water and DOC budgets. The parameter distributions from these calibration steps were analyzed to assess parameter sensitivity and collinearity using the software environment R (R Core Team; 2017). Validation (applying the OF (Eq. 5) and KGE (Eq. 4) on discharge and DOC concentration, resp. of the validation period) was carried out to estimate model robustness.

In order to estimate the information content of DOC concentrations as a tracer in the multiobjective calibration (MOC) approach, we further applied a consecutive single objective calibration (CSOC) (1) of the hydrology module with a consecutive DOC module calibration (2) that used the hydrological parameter set produced in step (1). Again we ran 2,000 generations of 500 parameter populations. We then took the one “best” parameter set of the hydrological calibration and applied the consecutive biogeochemical calibration. The combination of the 500 partial parameter sets from (1) and (2) were used to compare MOC and CSOC model performance in terms of Q and DOC as well as their internal fluxes.

4 Results

4.1 Hydro-meteorological and DOC dynamics

The 4-year lasting study period (from 21 May 2013 to 12 Apr 2014 and from 13 Apr 2017 to 25 Jun 2020) had a precipitation average of 968 mm per year which was above the long-term (1990-2020) average of 831 mm (Table 1). The study period in 2013-2014 was dryer (annual mean: 2.2 mm d⁻¹) than 2017-2020 (2.7 mm d⁻¹). Note that deviations to the long term average values from weather stations may exist due to the seasonal biased dataset. Potential evapotranspiration remained relatively constant at around 280 mm yr⁻¹ (standard deviation SD ± 24 mm yr⁻¹). The study site has a pronounced seasonality, with generally low groundwater levels, low runoff and higher temperatures and evapotranspiration (ET) in summer (July until September). In the summer precipitation events usually have little impact on runoff rate (Werner et al., 2019). When ET declines in autumn (October to December), runoff gets increasingly impacted by rainfall events up to peak runoff values in winter (January to March) with lowest ET values and groundwater levels close to the soil surface (Fig. 2b). The peak runoff events often correspond to snowmelt events as in the case of the maximum event registered during the study period on 01 to 03 January 2018 when the Rappbode stream went over-bank. We did not include this peak in the statistics, because we could not exactly estimate the discharge for water levels higher than the stream banks (> 1 mm h⁻¹).

Average stream DOC concentrations were 4.25 ± 2.5 mg L⁻¹ with high values during events in late spring and early autumn (maximum 14.8 mg L⁻¹ on 20 May 2017). Throughout the year, DOC concentrations exhibit a pronounced event-type

variability, with highest intra-event variability during summer months, whereas winter months expressed smallest event fluctuations. The DOC concentration generally follows the hydroclimatically induced seasonal variations with generally lowest concentrations during warm and dry situations (typically during non-event summer) followed by cold and wet situations (winter) and, transitioning between these two situations, highest values in intermediate situations (autumn and spring). For a detailed analysis of DOC and runoff variability in-stream and the RZ see Werner et al. (2019; 2021). The lowest DOC concentrations were measured during the late dry season at $>1 \text{ mg L}^{-1}$ in summer 2018, similar to the low concentrations obtained in deeper riparian groundwater as shown in Rogelis et al. (2016).

4.2 Model calibration

The TACHyB-model calibration (2013 – 2014 & May 2017 – May 2018) yielded a combined objective function (VE + KGE_Q) mean value of 0.81 for the simulated streamflow and a KGE_{DOC} of 0.73 for instream DOC concentrations (Table 3). The KGE values of both modules were comparable (Table 3) during calibration. Respective single terms that define the KGE_Q and KGE_{DOC} values were within a 0.05 range. The KGE_Q performance decreased for the validation period (May 2018 - June 2020; Table 3) by 0.08, whereas the combined objective function value dropped by 0.14 showing a recession in the VE between calibration and validation periods. The KGE_{DOC} dropped during the validation period in comparison to the calibration period by 0.21, mainly due to an increase (+ 0.34) in the bias term of the KGE function.

Table 3. Mean performance of the TACHyB-model performance for June 2013 - May 2014 & May 2017 - May 2018 calibration periods. Cross validation for May 2018 - June 2020 period. VE: Volumetric efficiency (Eq. 5), KGE: Kling-Gupta-Efficiency of the discharge/DOC model (Eq. 4); r_p (pearson correlation) γ (variance) and bias (β) are the single components of the KGE equation (Eq. 4).

	Q [mm d ⁻¹]	DOC [mg L ⁻¹]	Q [mm d ⁻¹]	DOC [mg L ⁻¹]
	Calibration period		Validation period	
VE+KGE	0.81	-	0.67	-
KGE	0.79	0.73	0.71	0.52
$(r_p - 1)^2$	0.18	0.23	0.20	0.30
$(\gamma - 1)^2$	0.10	0.14	0.18	0.10
$(\beta - 1)^2$	0.07	0.02	0.11	0.36

The model could reproduce seasonal and event-scale fluctuations of discharge and DOC concentrations. Envelopes defined by the 500 best sets of parameters (see 3.3) are mostly covering the measured variability of runoff and DOC concentration during the entire study period (Fig. 4). The observed deviations during the fast transition from the dry into the wet season (e.g. Sep 2013, Dec 2018; Fig. 4) and vice versa is typically difficult to simulate with rainfall-runoff models since several storages are active with proportions changing in time (Birkel et al., 2017; Strohmenger et al., 2021; Birkel et al., 2011). The observed seasonal variations in Q and DOC concentration were simulated well, with adequate magnitude of runoff events in winter and spring (e.g. from January 1, 2018 to January 13, 2018). The timing and magnitude of major events were captured well (e.g. on

June 1, 2018). Also the model differentiates between storage contributions during smaller events (e.g. between October 15, 2017 and November 15, 2017) overall proving its capability to reproduce small and large as well as slow and fast dynamics. On the other side, the model overestimated DOC concentrations during low-flow/drought periods (e.g. from May 1, 2018 to December 1, 2018). During low-flow periods, for example from July 1, 2019 to October 1, 2019, the DOC concentration is relatively stagnant around 2.5 mg L^{-1} , overall leading to an R^2 of 0.65 and 0.57 for measured vs. simulated runoff and DOC, respectively (Fig. S2).

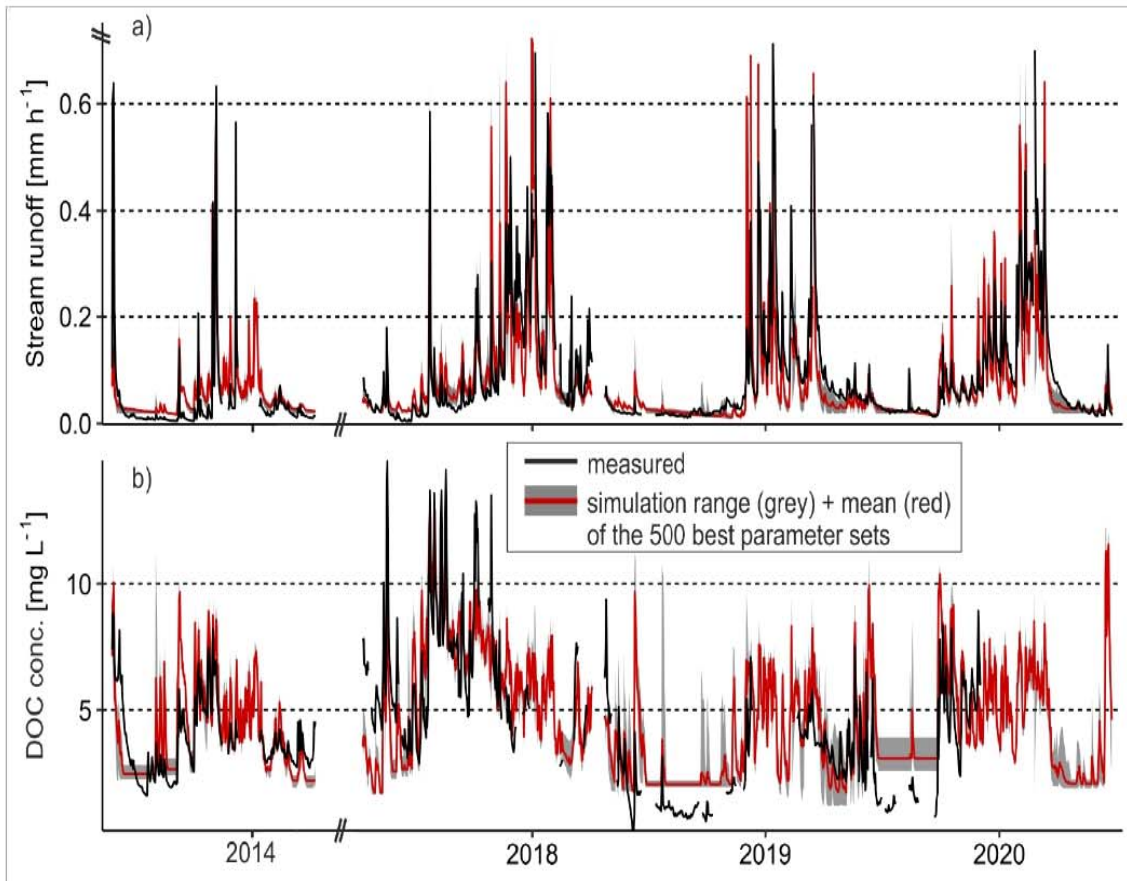


Figure 4. Simulation range of the 500 best parameter sets (grey ribbon) of the hydrological (a) and biogeochemical (b) module. Red line indicates the mean of the 500 best parameter sets. Black line depicts observed stream runoff and DOC concentrations, respectively. Note the time axis break between June 2014 and April 2017 in a) and b). Further note the y axis break a) for better illustration (maximum measured runoff was 0.99 mm on 04 Jan 2018; respective model range was between 1.04 mm and 1.54 mm , averaging 1.31 mm).

Modelled internal state variables

In a next step, the TACHyB-model behavior was checked against independently measured state variables such as riparian depth to water table (DTW) and respective riparian DOC concentrations in the RZ. The TACHyB-model simulates a quick storage response in the riparian wetland reservoir and a delayed deeper groundwater dynamic due to a slower recharge (Fig. 5a, b). The groundwater reservoir (S_{GW}) dynamics reflect the measured shallow groundwater water level dynamics in the RZ

(pearson correlation $r_p = 0.77$), but in a dampened matter. Compared to S_{GW} , the median of the best 500 simulations of the riparian reservoir storage values (S_{RZ}) was better correlated with the measured mean shallow groundwater level ($r_p = 0.89$) in the RZ close to the catchment outlet (Fig. 4a, Fig. 1).

The modelled riparian DOC concentrations ($1.9 - 21.8 \text{ mg L}^{-1}$) were in a range comparable to the measured concentrations in shallow riparian groundwater samples ($1.2 - 16.8 \text{ mg L}^{-1}$) during that time (Fig. 4c).

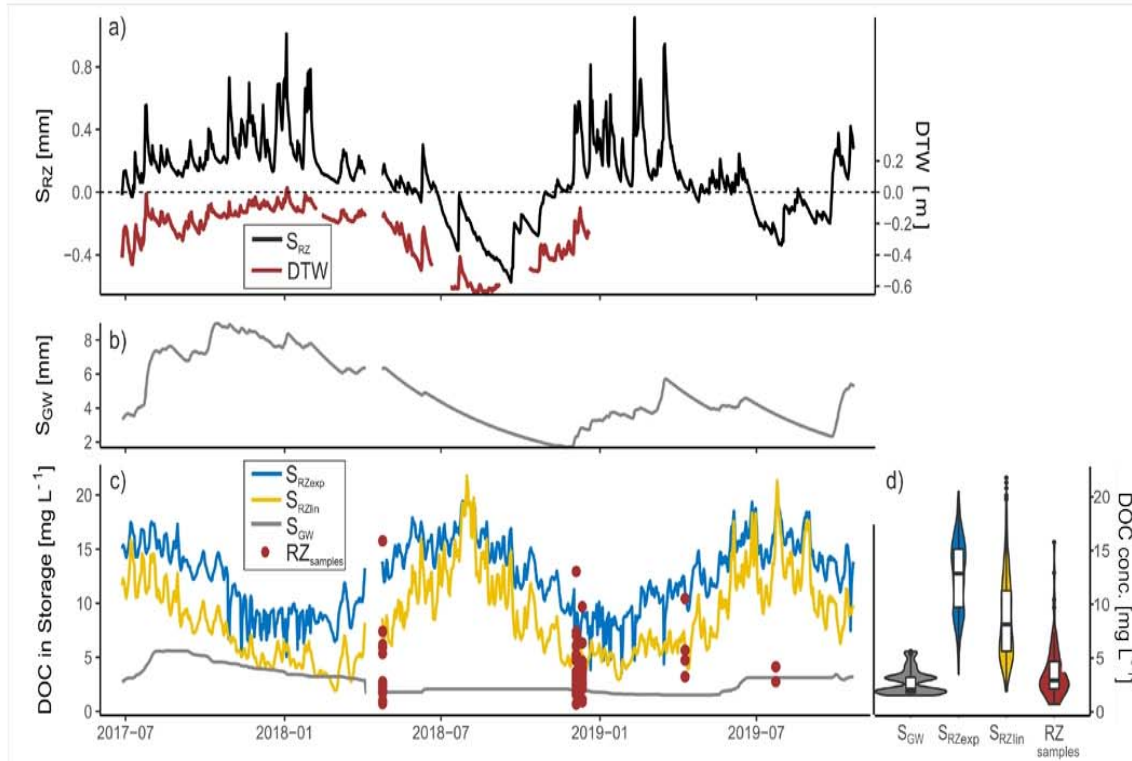


Figure 5. Comparison between storage dynamics of the TACHyB-model. a) Comparison between modelled riparian storage content (S_{RZ} , black) and mean depth to water level (DTW) (red, second y-axis) observed in the riparian groundwater, near the catchment outlet. If S_{RZ} is below 0 mm, the storage does not generate stream runoff. The amount of negativity in S_{RZ} describes how dry the storage falls and hence how much additional soil moisture is necessary to generate runoff again. b) Modelled groundwater storage (S_{GW} , grey). c) Comparison of modelled DOC concentrations in contributions from exponential riparian runoff (S_{RZexp} , blue), linear riparian runoff (S_{RZlin} , yellow) and groundwater (S_{GW} , grey). Manually measured riparian surface water and shallow groundwater DOC samples are displayed as red dots. d) Violin plots of the modelled DOC concentration distributions of S_{GW} , S_{RZexp} , S_{RZlin} and measured riparian zone (RZ) samples. Colors according to (c). Year 2013-2014 of the time series not shown. Note that the distribution of $RZ_{samples}$, representing 5 sampling events, does not reflect the distribution of the simulated DOC continuum in storage (c). Further a bias towards (lower) more groundwater influenced DOC concentrations has to be assumed for the $RZ_{samples}$ distribution since DOC in the soil surface runoff was only available during appropriate wet conditions.

Model parameters

The best 500 parameter sets are clearly constrained in their ranges in comparison to their initial values (Fig. S3) and clear maxima for many of the parameters, indicating parameter sensitivity. However, some of the constrained parameter distributions appear to be bi- and multimodal (e.g. for a , b , k_{HS}). The parameters a (mean 0.70 d^{-1}) and r (mean 0.20 d^{-1}), which control the flux from the hillslope storage to the riparian storage and the groundwater storage respectively, are higher than parameter b (mean 0.007 d^{-1}), responsible for linear groundwater contributions. Parameter c (mean 0.19 d^{-1}), controlling the riparian linear

flow is roughly 30 times bigger than parameter b . The production rate coefficient in the hillslope (k_{HS} , mean 4.9 mg L^{-1}) is smaller than in the riparian storage equivalent (k_{rip} , mean 12.2 mg L^{-1}). Also, the loss parameter in the riparian storage (LQ_{RZ} , mean 0.63) is bigger than in the hillslope contribution to groundwater (LQ_{HS} , mean 0.49). The activation energy parameter for the DOC production term in the RZ (Ea) is closely constrained to a mean of 1.04 whereas the equivalent in the HS (Ea_{ip}) averages at 1.18.

Water and DOC export

Overall, the DOC export from the GW and riparian storages modeled by TACHyB is $447.4 \text{ kg DOC} \cdot \text{km}^{-2} \cdot \text{a}^{-1}$ during the study period. In more detail, Q_{GW} contributed 31% (36.7 mm) of the total stream runoff (118.1 mm) and delivered 16% (99.0 mg m^{-2}) of the total DOC load (705.5 mg m^{-2} , Fig. 6) within the study period. Respectively, Q_{RZim} was active 66% of the time and accounted for 36% (41.9 mm) of the total stream runoff and 39% (274.8 mg m^{-2}) of the total DOC load (Fig. S4). The Q_{RZexp} was active during 43% of the observation time, contributing 33.4% (39.5 mm) of runoff and 47% (331.3 mg m^{-2}) of the total DOC load. With that, the TACHyB-model generates around 86% of the total stream DOC load from the riparian zone.

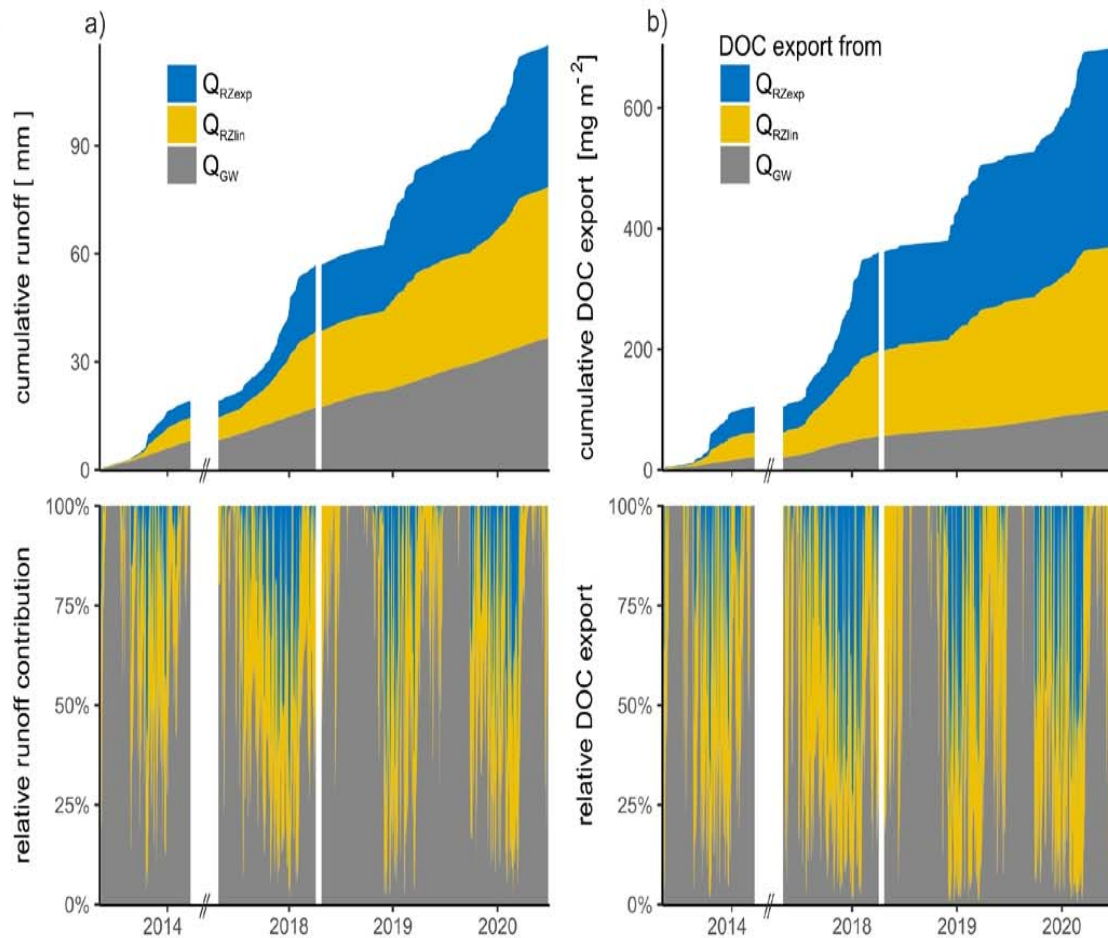


Figure 6. a) Absolute cumulative sum (top) and relative (bottom) partitioning of nonlinear riparian runoff (blue), linear riparian runoff (yellow) and groundwater contributions (grey). b) Absolute cumulative sum (top) and relative (bottom) partitioning of DOC export from nonlinear riparian runoff (blue), linear riparian runoff (yellow) and groundwater (grey). Note the time axis break between June 2014 and April 2017. White space in 2018 due to a data gap.

4.3 Comparison to consecutive single objective calibration (CSOC)

In order to estimate the information content of stream DOC concentration as a tracer to calibrate our model, we compared two different calibration approaches: 1) the multiobjective calibration (MOC), where the DOC module and the hydrological module are calibrated simultaneously as described in chapter 3.3. and 2) a consecutive single objective calibration (CSOC), where first the hydrological module is calibrated and subsequently the DOC module is calibrated.

The performance of the CSOC was similar in KGE_Q model performance but clearly differed from the MOC in KGE_{DOC} with strongly negative values. This negative CSOC performance of the DOC module is attributable to all three components of the KGE equation (Eq. 4) but in particular to major differences in variance.

All CSOC derived model parameters deviate significantly (Kolmogorov-Smirnov test; $p < 0.001$) from the MOC parameters (e.g. τ_{GW} , b , c , k_{DOC} , LQ_{RZ} , Fig. S5) and therefore as a whole are not represented in the best 500 parameter sets from the MOC.

Most pronounced difference in storage dynamics can be seen in mean S_{GW} (4.6 mm and 2.9 mm for CSOC and MOC) that represents the largest storage in both models. Respective Q_{GW} fluxes are comparable in magnitude and temporal dynamics. There are also strong differences in the size of the riparian storage S_{RZ} that averages 0.09 mm for the MOC, but -0.07 mm for the CSOC. Consequently, the CSOC model more often expresses negative values in the S_{RZ} (and thus no discharge generation and DOC export at all) than the MOC resulting in lower mean Q_{RZexp} flux (0.03 mm d⁻¹ and 0.01 mm d⁻¹ for the MOC and CSOC). Thus, both model approaches show clear differences in the nonlinear, riparian DOC export in total amount as well as the timing when riparian surface export actively contributes to the stream. On the other hand, the CSOC model exhibits higher Q_{RZim} , resulting in overall comparable Q_{RZtot} fluxes (80.1 mm d⁻¹ and 82.0 mm d⁻¹ for the CSOC and MOC model, resp.).

Comparison of the storage contributions to DOC export in both calibration approaches revealed that DOC export from the GW and riparian storages modeled by CSOC was markedly higher (2693.8 kg DOC·km⁻²·a⁻¹ vs. 705.5 kg DOC·km⁻²·a⁻¹). In the CSOC approach, the total stream DOC load was to a large extent generated by the GW (76% of total stream load generation), followed by contributions of the linear surface component (19% of total riparian DOC export) and the nonlinear riparian export components (5% of total).

The CSOC derived hydrological parameterization reached KGE_Q values, comparable to the MOC- KGE_Q , also for the validation period. However, the CSOC derived DOC parameterization was adjusted to the hydrological calibration in order to replicate the observed in-stream DOC dynamic. While the nonlinear riparian flux expressed DOC concentrations in a still reasonable range (2.0 mg L⁻¹ – 28.6 mg L⁻¹), concentration values of the linear riparian flux (274.0 mg L⁻¹) and groundwater flux (352.0 mg L⁻¹) were implausible. Consequently, the CSOC model does not adequately represent internal (Figures S6 and S7) or external (Table S1) model DOC fluxes.

5 Discussion

5.1 Finding the right model structure

As Hrachowitz et al. (2014) point out, an expert-knowledge-driven strategy of constraining models can significantly increase predictive performance of a model and its ability to reproduce hydrological signatures, but Dick et al. (2015) and Birkel et al. (2017) emphasize that the simple structure of lumped storage models so far prevents the analysis of small-scale processes and questions of spatial heterogeneity. We argue that a detailed understanding of the interplay between plot-scale RZ DOC export mechanisms and catchment-scale hydroclimatic controls of the integrated DOC response signal opens up the possibility to adjust and complement semi-distributed models through integrating scale-independent proxies into relevant DOC export mechanisms. The magnitude and dynamic of DOC export is largely (and scale-independently) controlled by the evolution of distinct flow paths during runoff generation that ultimately determine the timing and location of export from distinct source zones (Wen et al., 2020). Thus, a model representation of these distinct DOC fluxes is mandatory, to avoid the model to compensate for the wrong mechanistic reasons. Moreover, getting the hydrological module mechanistically right even at the

small scale consequently is key for the performance of DOC export models, since correct hydrological model fluxes are a fundamental prerequisite to minimize error propagation in biogeochemical processes for catchment scale solute export.

In Werner et al. (2021), 61% of the total DOC export were attributed to a DOC pool from locations within the RZ of generally low DTW and thus a high local topographical wetness index (TWI) that facilitates surface runoff (Rinderer et al., 2014). Hence, it could be assumed that the generated riparian surface runoff mainly mobilizes DOC from such source zones, while the riparian subsurface flow is associated with DOC from drier places with higher DTW (low local TWI). To reflect the lateral spatial heterogeneity of contributions to surface runoff generation in the RZ of the Rappbode catchment as found in Werner et al. (2021), we implemented an explicit surface flow mechanism that is threshold-controlled by an aridity index of the preceding 60 days (Werner et al., 2019). Such an aridity index based threshold value is physically interpretable since observations suggested that surface runoff occurs when precipitation within the preceding 60 days exceeds potential evapotranspiration during that time (Fig. S1) and hence (the already close to surface) riparian groundwater rises up to the surface and from there drains into the stream. As a result of this mechanism, occurrence of surface runoff can be calibrated explicitly and physically meaningful as compared to deriving it from over saturation of the calibrated (but not validated) riparian storage, as was done in e.g. the FLEX model group (Euser et al., 2013), or to a combined nonlinear function (Birkel et al., 2014; 2017; Strohmenger et al., 2021) that does not clearly distinguish between subsurface and surface flux mechanism. Note that although we consider the proposed DOC export mechanisms in Werner et al. (2021) valid, a quantitative comparison between their modeled surface DOC export loads and this study has to be treated with care since their research was done at plot scale while we look at the catchment scale. However, the analysis of the onset of surface runoff in their study already gave a good indication on how to constrain the initial calibration range of this threshold value.

In the original model from Birkel et al. (2014), the upper hillslope storage fractionally drains into the riparian storage via surface (near) water movement. Tromp-van Meerveld and McDonnell (2006) suggest this mechanism to be potentially threshold controlled. Therefore, we controlled this flux in the TACHyB-model by implementing a threshold value that is based on the aridity index of the preceding 60 days (Werner et al., 2019). Again, this is supported by an observation-well in our catchment (not shown) that served as an indicator to constrain the initial calibration range. In terms of the groundwater storage unit, we argue that groundwater cannot feed the stream at endless rates, if a riparian zone storage unit is conceptualized on top of the groundwater storage unit. Therefore, the magnitude of this physically meaningful limit value was estimated by using low-flow segments of the discharge time-series at the catchment outlet, which further constrained the model structure.

The provision and processing of DOC within the single storage units can sufficiently be parameterized by effects of soil moisture, temperature and DOC processing rate (Smith et al., 2007; Birkel et al., 2014; Lessels et al., 2015). However, when estimating DOC concentration in the riparian surface runoff in our model we did not account for processes that lower DOC concentration (like adsorption or mineralization), since we assumed that such processes occur primarily in the subsurface where e.g. exposure times (Oldham et al., 2013) are large compared to the shortly exposed surface runoff. The groundwater-fed low-flow (Q_{GW} in the TACHyB-model) typically has limited contact to the organic matter rich soil layers, resulting in low mean DOC concentrations and consistently small contributions of DOC to the stream, which has also been observed by Dick

et al. (2015). Consistency of the groundwater DOC was evaluated and constraint by stream DOC concentration values during low flow events as well as deeper groundwater DOC concentrations. During precipitation events, the shallow groundwater and associated low DOC concentration gets overprinted by a distinct high DOC concentration signal from the top soil layers (Broder and Biester, 2015; Werner et al., 2019; 2021). During smaller events and lower groundwater levels the exported DOC load is dominated by the subsurface riparian flow ($Q_{RZ/m}$), since organic matter rich source zones near the surface do not get activated. This is in accordance with the variable source zone activation concept at various scales (Dick et al., 2015; Werner et al., 2021) and fits to the model output.

Overall, the implementation of a threshold-controlled, dynamic function for surface runoff generation, a threshold value for surface near runoff from the hillslope and a limited exchange flux between S_{GW} and S_{RZ} demand to implement six additional parameters into the hydrological module of our adapted model. Two additional parameters were used to explicitly simulate nonlinear and dynamic surface runoff generation in the RZ, one to parameterize linear transfer of excessive groundwater into the riparian storage. Three additional parameters are physically derivable and verifiable threshold values that could be widely constrained in their initial calibration range by preceding observations in the study site and thus do not substantially change the model's parsimony. We therefore assume that the conceptual and constraining aspect on the model structure outweighs the loss in parsimony that comes with the additional parameters.

5.2 Model performance

The TACHyB-model used a multi objective calibration (MOC; simultaneously calibrated hydrology and DOC concentrations) that yielded KGE values greater than 0.5 for hydrology and biogeochemistry (Table 3), which is considered a 'good' model performance (Rogelis et al., 2016). The general hydrological dynamics were well captured in the model and consistent with the processes reported in other studies on DOC export in the catchment (Werner et al., 2019; 2021). The independent validation of internal states (internal fluxes/storages were not calibrated) supports the credibility in the model set up. More specifically, high correlation between observed riparian depth to water table (DTW) and simulated riparian storage condition as well as the dampened variability of the groundwater storage unit suggest a correct hydrological representation of internal states and potentially internal fluxes at event and seasonal scale (Beven, 2012; Broder and Biester, 2015). Simulated DOC concentration in both the RZ and the groundwater were in a plausible range in comparison to respective water samples during five occasions (Fig. 5). In this sense, modeled DOC concentrations in the riparian and groundwater storage did express realistic values during the entire modeling period. Yet, the availability of additional (continuous) DOC concentration data in the RZ and GW could help to further constrain the model and better evaluate the temporal DOC concentration dynamics in the storages.

As a drawback, quantifying the catchment's response on extreme wet situations (< 1% of the study period) like floods remains unfeasible, because floods and respective DOC export are hard to gauge in our catchment. Also, the TACHyB-model overestimated DOC concentration in the stream during prolonged low-flow periods when only groundwater storage was active. The DOC concentration was generally low and likely more significantly affected by instream processing during such periods,

which might explain the deviations. In terms of total DOC export, such low-flow periods contribute only small amounts of DOC, which is why we did not put further emphasis into better representing low-flow dynamics. Additionally, DOC concentrations during rewetting after prolonged drought periods were partly overestimated, indicating that in particular these initial storage contributions might not be timed appropriately. Such transition periods have more variable storage contributions, which makes them mechanistically harder to model than high- and low-flow periods that are typically dominated by output of a single storage (Birkel et al., 2017). Due to their rare occurrence (once to twice per year), we consider the described shifts in transition periods with overestimated DOC concentrations relatively low impactful in terms of total DOC export.

Almost 35% of the total DOC export happened in 10% of the time, which is comparable to the relationship that Broder and Biester (2015) found in a similar catchment, where about 40% of the DOC load was exported in 10% of the time. The linear riparian flow (representative of subsurface riparian flow) accounted for the majority of stream runoff, but exhibited lower DOC concentrations than the nonlinear riparian flow (representative of surface runoff) which reflects findings from Werner et al. (2021) and Broder and Biester (2015). The nonlinear riparian flow contributed disproportionately strong (47% of total generated DOC load) to the stream DOC load. A comparison to findings from Birkel et al. (2017) who attributed 60% of the DOC load to the nonlinear runoff generation is non-valid, since they combined linear and nonlinear runoff in their nonlinear function.

In summary, the mechanistical adaptation of the TACHyB-model on the basis of previous studies allowed for a meaningful representation of the DOC export dynamic through plausible and consistent (in terms of internal and external fluxes) hydrologic and biogeochemical fluxes from the studied area. The implementation of threshold based model mechanisms to represent the onset of fast surface flow components in the RZ allowed to incorporate recent understanding of event-scale water flow and DOC export variability in the Rappbode catchment (Werner et al., 2021), which resulted in a satisfying and credible model performance. With that the TACHyB-model looks promising to produce the right answers (DOC export) for the right reasons (plausible internal and external fluxes) as postulated by Kirchner (2006).

5.3 On the value of DOC concentration observations to constrain the model

The application of external tracers and the additional costs and efforts involved are still severely limiting our ability to calibrate and validate small scale mechanisms like microtopography induced surface DOC export (Werner et al., 2021) as well as to transfer applicable models to other catchments (Birkel et al., 2014). Hrachowitz et al. (2016) showed that the utilization of water age can shed light on the mixing processes in different parts of the catchment and thereby improve process understanding. Birkel et al. (2020) successfully applied this approach in a tropical catchment, but determining water age is expensive.

By utilizing the strong coupling between hydrology and biogeochemistry through a multi-objective calibration (MOC) approach that simultaneously calibrates the hydrological and biogeochemical module, we obtained a good model performance in terms of simulated discharge and DOC concentration at the catchment outlet, but also in terms of internal fluxes and process consistency in the TACHyB-model. We argue that the DOC that enters the stream from the Rappbode RZ already carries integral information of its origin and fate. For example, Werner et al. (2021) found that riparian DOC that comes from spots

of high local topographical wetness has a distinctly different concentration and export mechanism (surface export) than that of dryer spots (subsurface export). Especially higher resolution data is able to disentangle such variable source zone contributions, because it resolves differences between storage unit contributions that are induced by different hydroclimatical forcing (Werner et al., 2019). In general, this means that DOC concentration time-series contain important information about dominant flow paths in catchments that are majorly controlled by riparian runoff generation. In-stream DOC dynamics of such catchments therefore can substitute or complement the application of tracers (e.g. water isotopes or solutes) for calibration of hydrology and biogeochemistry, when there is detailed information on different mobilization and transport mechanisms of DOC available.

In order to test the value high-resolution DOC concentration observations to constrain the model calibration we compared the MOC performance with a consecutive single objective calibration (CSOC) approach, where DOC concentration at the catchment outlet is calibrated following the discharge calibration. Like in the MOC approach, the CSOC approach exhibited positive KGE values for the hydrological calibration and validation period (Table S1). Without being further constraint, the temporal dynamics of the riparian storage in the CSOC setup indicate a good mechanical translation of hydroclimatical drivers into hydrological output generation. Thus, all model mechanisms are represented in both MOC and CSOC approaches. In comparison to the CSOC approach however, MOC modifies the magnitude and impact of these mechanisms on runoff generation by altering the threshold value and timing, as well as the partitioning between surface runoff and subsurface runoff. Moreover, the KGE_{DOC} from the CSOC expressed negative values for calibration and validation with resulting simulated DOC concentrations in the riparian storage being largely overestimated. The biogeochemical fluxes, which are coupled to the hydrological fluxes, consequently proved the single objective calibration of the hydrological module to be wrong despite its good external water flux performance. Additionally, Kolmogorov-Smirnov test statistics suggest that parameter sets, compiled by MOC and CSOC are not from the same distribution ($p < 0.001$ for every parameter, Fig. S5). We conclude that it is not enough to just calibrate a model on the integral hydrograph at the catchment outlet alone. Rather model performance needs to be evaluated and validated by incorporating additional information. This is especially noteworthy, because numerous predictive hydrological models are calibrated without any further (external or internal) tracer data and lack a validation of internal model fluxes (Euser et al., 2013; Hrachowitz et al., 2014).

In summary, at first glance the hydrological module of CSOC and MOC both deliver reasonable results. However, a more detailed analysis of internal and external fluxes validation reveals that the CSOC leads to a misconception in storage DOC concentrations, indicating that the hydrological module is subject to equifinality. In comparison to the CSOC model, the independent storage validation of the MOC approach was correct for hydrology and DOC suggesting. Applying a MOC approach that integrates in-stream DOC concentration data therefore successfully constrained parameters and reduced equifinality. Thus, we see DOC data as a promising substitute, if a tracer such as stable water isotopes to calibrate and validate purely hydrological and coupled hydrological-biogeochemical models is not available.

6 Conclusions and Outlook

In this study, we constrained the model structure of a tracer-aided coupled hydrological-biogeochemical (TACHyB) DOC export model based on observations and expert knowledge. The main point of model adjustment was the implementation of justifiable, threshold-controlled, hillslope- and dynamic riparian surface flux mechanisms, as well as an exchange flux between groundwater and riparian storage. We view DOC concentration in the stream as an integrated response signal already carrying information from mobilization, timing and source location in it, thus exhibiting the strong coupling between hydrology and biogeochemistry. Calibration was therefore conducted by a multi-objective approach, where in-stream DOC concentration and discharge data were used to simultaneously calibrate the hydrological and biogeochemical modules of the model. Validation of internal model fluxes against depth to riparian groundwater levels and DOC concentrations in the respective groundwater as well as performance analysis of external model fluxes revealed that the joint calibration of hydrology and DOC concentration allows a robust and mechanistically justifiable parameterization of key DOC export mechanisms. A comparison of the applied multi-objective calibration (MOC) with a consecutive single objective calibration (CSOC), where the biogeochemical module is calibrated following the hydrological calibration, reveals that despite having a good hydrological performance ($KGE = 0.79$ and 0.82 for MOC and CSOC, resp.), such a model does not necessarily produce meaningful internal and external fluxes and states of DOC export (KGE for DOC concentration at the catchment outlet = 0.73 and <0 for MOC and CSOC, resp.). The differences between CSOC and MOC in model validity therefore implicate that a single objective calibration of a hydrological model has to be treated with care, if nothing is known about an internal flux validation to support the credibility of the model. We therefore conclude that the information content inherent to in-stream high-frequency DOC data can substitute the application of external tracers if the model correctly conceptualizes the dominant landscape structures and respective export mechanisms. Using these available DOC time series together with other routinely measurable stream variables like pH, EC or temperature could not only add valuable information on biogeochemical influences, but also enable a path to more closely examine mixing between storages. Implementing in-stream DOC quality measures that can be directly measured with DOC concentration into model validation is yet another promising section to get more confidence into explicitly distinguishing between different riparian DOC pools and respective export mechanisms.

Moreover, our study showed that antecedent wetness might decide whether certain hydrological thresholds are reached and thus whether subsurface or surface runoff generation dominate DOC export during events. In this regard, MOC model results confirm that threshold controlled fast water flow components, representative for riparian surface flow, make up important parts (47%) of the total DOC export. Surface runoff can deliver nutrients or contaminants directly and unbuffered to the stream, which may impact stream-water ecology. Therefore, surface runoff contributions should be explicitly taken into account in hydrological model conceptualizations. Moreover, climate change will likely affect groundwater in riparian zones. This could potentially have impacts on the solute export loads and dominant mechanisms of catchments with nowadays high groundwater levels, since the change in hydroclimatic preconditions also changes the frequency of when thresholds for the generation of

solute export are reached. Putting more effort into investigating thresholds of hydrological connectivity therefore should be considered in future studies to adequately capture solute flux dynamics in climate change scenarios.

Our model is an adaption of an already established model group that is partially comparable to each other and showcasing the flexibility of semi-distributed conceptual models to different catchments of different climatic regions. With routinely measured in-stream DOC concentration data becoming more and more available, this allows to enhance verifications of hydrological and biogeochemical modelling approaches, which in turn will ultimately allow to test the model over a broader range of scales of similar catchments (small, temperate headwater with low relief riparian zone), thereby elucidating its transferability. Calibrating hydrological models with internal tracer data (like DOC) thus is a promising approach for future models to reach the goal of mechanistical models with adequate parsimony and transferability to still be applicable for management.

Data availability. All datasets used in this synthesis are publicly available via the following links:

<https://doi.org/10.4211/hs.b32ba184414e475ba36a0bb193866ef1> (Werner, 2019) and

<https://doi.org/10.4211/hs.e0e6fbc0571149b79b1e75fa44d5c4ab> (Werner, 2021).

Supplement. The supplement related to this article is available online at:

Author contributions. BJW, JHF and AM planned and designed the research. BJW performed the statistical model analysis and wrote the paper with contributions from all co-authors. CB provided the initial model. LS and BJW edited and scripted the initial model.

Competing interests. The authors declare no competing interests

Acknowledgements. XXX.

Financial support. This research was funded by the Helmholtz Research Program POF-III, Integrated Project "Water and Matter Flux Dynamics in Catchments".

8 References

- Ali, S., Ghosh, N., and Singh, R.: Rainfall–runoff simulation using a normalized antecedent precipitation index, *Hydrological Sciences Journal–Journal des Sciences Hydrologiques*, 55, 266-274, 2010.
- Beven, K.: Causal models as multiple working hypotheses about environmental processes, *Comptes Rendus Geoscience*, 344, 77-88, 10.1016/j.crte.2012.01.005, 2012.
- Birkel, C., Tetzlaff, D., Dunn, S., and Soulsby, C.: Towards a simple dynamic process conceptualization in rainfall–runoff models using multi-criteria calibration and tracers in temperate, upland catchments, *Hydrological Processes: An International Journal*, 24, 260-275, 2010.
- Birkel, C., Soulsby, C., and Tetzlaff, D.: Modelling catchment-scale water storage dynamics: reconciling dynamic storage with tracer-inferred passive storage, *Hydrological Processes*, 25, 3924-3936, 10.1002/hyp.8201, 2011.
- Birkel, C., Soulsby, C., and Tetzlaff, D.: Integrating parsimonious models of hydrological connectivity and soil biogeochemistry to simulate stream DOC dynamics, *Journal of Geophysical Research-Biogeosciences*, 119, 1030-1047, 10.1002/2013jg002551, 2014.
- Birkel, C., Broder, T., and Biester, H.: Nonlinear and threshold-dominated runoff generation controls DOC export in a small peat catchment, *Journal of Geophysical Research-Biogeosciences*, 122, 498-513, 10.1002/2016jg003621, 2017.
- Birkel, C., Duvert, C., Correa, A., Munksgaard, N. C., Maher, D. T., and Hutley, L. B.: Tracer-Aided Modeling in the Low-Relief, Wet-Dry Tropics Suggests Water Ages and DOC Export Are Driven by Seasonal Wetlands and Deep Groundwater, *Water Resources Research*, 56, e2019WR026175, 10.1029/2019wr026175, 2020.
- Blank, J., and Deb, K.: Pymoo: Multi-Objective Optimization in Python, *IEEE Access*, 8, 89497-89509, 10.1109/ACCESS.2020.2990567, 2020.
- Broder, T., and Biester, H.: Hydrologic controls on DOC, As and Pb export from a polluted peatland - the importance of heavy rain events, antecedent moisture conditions and hydrological connectivity, *Biogeosciences*, 12, 4651-4664, 10.5194/bg-12-4651-2015, 2015.
- Chantigny, M. H.: Dissolved and water-extractable organic matter in soils: a review on the influence of land use and management practices, *Geoderma*, 113, 357-380, 10.1016/S0016-7061(02)00370-1, 2003.
- Criss, R. E., and Winston, W. E.: Do Nash values have value? Discussion and alternate proposals, *Hydrological Processes*, 22, 2723-2725, 10.1002/hyp.7072, 2008.
- Deb, K., Pratap, A., Agarwal, S., and Meyarivan, T.: A fast and elitist multiobjective genetic algorithm: NSGA-II, *Ieee Transactions on Evolutionary Computation*, 6, 182-197, 10.1109/4235.996017, 2002.
- Dick, J. J., Tetzlaff, D., Birkel, C., and Soulsby, C.: Modelling landscape controls on dissolved organic carbon sources and fluxes to streams, *Biogeochemistry*, 122, 361-374, 10.1007/s10533-014-0046-3, 2015.
- Euser, T., Winsemius, H. C., Hrachowitz, M., Fenicia, F., Uhlenbrook, S., and Savenije, H. H. G.: A framework to assess the realism of model structures using hydrological signatures, *Hydrology and Earth System Sciences*, 17, 1893-1912, 10.5194/hess-17-1893-2013, 2013.

- Evans, C. D., Monteith, D. T., and Cooper, D. M.: Long-term increases in surface water dissolved organic carbon: observations, possible causes and environmental impacts, *Environ Pollut*, 137, 55-71, 10.1016/j.envpol.2004.12.031, 2005.
- Fenicia, F., Savenije, H., Matgen, P., and Pfister, L.: Is the groundwater reservoir linear? Learning from data in hydrological modelling, *Hydrology and Earth System Sciences*, 10, 139-150, 10.5194/hess-10-139-2006, 2006.
- Frei, S., Knorr, K. H., Peiffer, S., and Fleckenstein, J. H.: Surface micro-topography causes hot spots of biogeochemical activity in wetland systems: A virtual modeling experiment, *Journal of Geophysical Research-Biogeosciences*, 117, n/a-n/a, 10.1029/2012jg002012, 2012.
- Hrachowitz, M., Fovet, O., Ruiz, L., Euser, T., Gharari, S., Nijzink, R., Freer, J., Savenije, H. H. G., and Gascuel-Oudou, C.: Process consistency in models: The importance of system signatures, expert knowledge, and process complexity, *Water Resources Research*, 50, 7445-7469, 10.1002/2014wr015484, 2014.
- Hrachowitz, M., Benettin, P., van Breukelen, B. M., Fovet, O., Howden, N. J. K., Ruiz, L., van der Velde, Y., and Wade, A. J.: Transit times-the link between hydrology and water quality at the catchment scale, *Wiley Interdisciplinary Reviews: Water*, 3, 629-657, 10.1002/wat2.1155, 2016.
- Kirchner, J. W.: Getting the right answers for the right reasons: Linking measurements, analyses, and models to advance the science of hydrology, *Water Resources Research*, 42, 10.1029/2005wr004362, 2006.
- Kling, H., Fuchs, M., and Paulin, M.: Runoff conditions in the upper Danube basin under an ensemble of climate change scenarios, *Journal of Hydrology*, 424, 264-277, 10.1016/j.jhydrol.2012.01.011, 2012.
- Knoben, W. J. M., Freer, J. E., and Woods, R. A.: Technical note: Inherent benchmark or not? Comparing Nash-Sutcliffe and Kling-Gupta efficiency scores, *Hydrology and Earth System Sciences*, 23, 4323-4331, 10.5194/hess-23-4323-2019, 2019.
- Köhler, S. J., Buffam, I., Laudon, H., and Bishop, K. H.: Climate's control of intra-annual and interannual variability of total organic carbon concentration and flux in two contrasting boreal landscape elements, *J. Geophys. Res.*, 113, G03012, 10.1029/2007JG000629, 2008.
- Krause, S., Freer, J., Hannah, D. M., Howden, N. J. K., Wagener, T., and Worrall, F.: Catchment similarity concepts for understanding dynamic biogeochemical behaviour of river basins, *Hydrological Processes*, 28, 1554-1560, 10.1002/hyp.10093, 2014.
- Larsen, S., Andersen, T., and Hessen, D. O.: Climate change predicted to cause severe increase of organic carbon in lakes, *Global Change Biology*, 17, 1186-1192, 10.1111/j.1365-2486.2010.02257.x, 2011.
- Ledesma, J. L., Grabs, T., Bishop, K. H., Schiff, S. L., and Kohler, S. J.: Potential for long-term transfer of dissolved organic carbon from riparian zones to streams in boreal catchments, *Glob Chang Biol*, 21, 2963-2979, 10.1111/gcb.12872, 2015.
- Ledesma, J. L. J., Futter, M. N., Blackburn, M., Lidman, F., Grabs, T., Sponseller, R. A., Laudon, H., Bishop, K. H., and Kohler, S. J.: Towards an Improved Conceptualization of Riparian Zones in Boreal Forest Headwaters, *Ecosystems*, 21, 297-315, 10.1007/s10021-017-0149-5, 2018a.
- Ledesma, J. L. J., Kothawala, D. N., Bastviken, P., Maehder, S., Grabs, T., and Futter, M. N.: Stream Dissolved Organic Matter Composition Reflects the Riparian Zone, Not Upslope Soils in Boreal Forest Headwaters, *Water Resources Research*, 54, 3896-3912, 10.1029/2017wr021793, 2018b.

- Lessels, J. S., Tetzlaff, D., Carey, S. K., Smith, P., and Soulsby, C.: A coupled hydrology-biogeochemistry model to simulate dissolved organic carbon exports from a permafrost-influenced catchment, *Hydrological Processes*, 29, 5383-5396, 10.1002/hyp.10566, 2015.
- McGuire, K. J., and McDonnell, J. J.: Hydrological connectivity of hillslopes and streams: Characteristic time scales and nonlinearities, *Water Resources Research*, 46, 10.1029/2010wr009341, 2010.
- Musolff, A., Fleckenstein, J. H., Opitz, M., Buttner, O., Kumar, R., and Tittel, J.: Spatio-temporal controls of dissolved organic carbon stream water concentrations, *Journal of Hydrology*, 566, 205-215, 10.1016/j.jhydrol.2018.09.011, 2018.
- Ojima, D. S., Galvin, K. A., and Turner, B. L.: The Global Impact of Land-Use Change, *Bioscience*, 44, 300-304, 10.2307/1312379, 1994.
- Oldham, C. E., Farrow, D. E., and Peiffer, S.: A generalized Damkohler number for classifying material processing in hydrological systems, *Hydrology and Earth System Sciences*, 17, 1133-1148, 10.5194/hess-17-1133-2013, 2013.
- Pool, S., Vis, M., and Seibert, J.: Evaluating model performance: a non-parametric variant of the Kling-Gupta efficiency, *EGU General Assembly*, 2018, 12053,
- Rinderer, M., Van Meerveld, H., and Seibert, J.: Topographic controls on shallow groundwater levels in a steep, prealpine catchment: When are the TWI assumptions valid?, *Water Resources Research*, 50, 6067-6080, 2014.
- Rogelis, M. C., Werner, M., Obregón, N., and Wright, N.: Hydrological model assessment for flood early warning in a tropical high mountain basin, *Hydrology and Earth System Sciences Discussions*, 1-36, 10.5194/hess-2016-30, 2016.
- Seibert, J., Grabs, T., Kohler, S., Laudon, H., Winterdahl, M., and Bishop, K.: Linking soil- and stream-water chemistry based on a Riparian Flow-Concentration Integration Model, *Hydrology and Earth System Sciences*, 13, 2287-2297, 10.5194/hess-13-2287-2009, 2009.
- Smith, P., Smith, J., Flynn, H., Killham, K., Rangel-Castro, I., Foereid, B., Aitkenhead, M., Chapman, S., Towers, W., and Bell, J.: ECOSSE: Estimating Carbon in Organic Soils-Sequestration and Emissions, 978075591498 2, 2007.
- Stanley, E. H., Powers, S. M., Lottig, N. R., Buffam, I., and Crawford, J. T.: Contemporary changes in dissolved organic carbon (DOC) in human-dominated rivers: is there a role for DOC management?, *Freshwater Biology*, 57, 26-42, 10.1111/j.1365-2427.2011.02613.x, 2012.
- Strohmeier, L., Fovet, O., Hrachowitz, M., Salmon-Monviola, J., and Gascuel-Oudou, C.: Is a simple model based on two mixing reservoirs able to reproduce the intra-annual dynamics of DOC and NO₃ stream concentrations in an agricultural headwater catchment?, *Science of the Total Environment*, 794, 148715, 10.1016/j.scitotenv.2021.148715, 2021.
- Team, R. C.: R: A language and environment for statistical computing, R Foundation for Statistical Computing, Vienna, Austria. <https://www.R-project.org>, 2019.
- Tong, S. T., and Chen, W.: Modeling the relationship between land use and surface water quality, *J Environ Manage*, 66, 377-393, 10.1006/jema.2002.0593, 2002.
- Tromp-van Meerveld, H., and McDonnell, J.: Threshold relations in subsurface stormflow: 2. The fill and spill hypothesis, *Water Resources Research*, 42, 2006.
- vanRossum, G.: Python reference manual, Department of Computer Science [CS], 1995.

- Wen, H., Perdrial, J., Abbott, B. W., Bernal, S., Dupas, R., Godsey, S. E., Harpold, A., Rizzo, D., Underwood, K., Adler, T., Sterle, G., and Li, L.: Temperature controls production but hydrology regulates export of dissolved organic carbon at the catchment scale, *Hydrology and Earth System Sciences*, 24, 945-966, 10.5194/hess-24-945-2020, 2020.
- Werner, B. J.: High frequency dataset of the upper Rappbode Catchment in the Harz Mountains, Germany, in, 2019.
- Werner, B. J., Musolff, A., Lechtenfeld, O. J., de Rooij, G. H., Oosterwoud, M. R., and Fleckenstein, J. H.: High-frequency measurements explain quantity and quality of dissolved organic carbon mobilization in a headwater catchment, *Biogeosciences*, 16, 4497-4516, 10.5194/bg-16-4497-2019, 2019.
- Werner, B. J.: High resolution spatial, chemical (dissolved organic carbon) and hydrological dataset of the upper Rappbode Catchment in the temperate Harz Mountains, Germany, in, 2021.
- Werner, B. J., Lechtenfeld, O. J., Musolff, A., de Rooij, G. H., Yang, J., Gründling, R., Werban, U., and Fleckenstein, J. H.: Small-scale topography explains patterns and dynamics of dissolved organic carbon exports from the riparian zone of a temperate, forested catchment, *Hydrology and Earth System Sciences*, 25, 6067-6086, 2021.
- Whitehead, P. G., Wilby, R. L., Battarbee, R. W., Kernan, M., and Wade, A. J.: A review of the potential impacts of climate change on surface water quality, *Hydrological Sciences Journal-Journal Des Sciences Hydrologiques*, 54, 101-123, 10.1623/hysj.54.1.101, 2009.
- Wilson, H. F., and Xenopoulos, M. A.: Effects of agricultural land use on the composition of fluvial dissolved organic matter, *Nature Geoscience*, 2, 37-41, 10.1038/ngeo391, 2008.
- Wollschläger, U., Attinger, S., Borchardt, D., Brauns, M., Cuntz, M., Dietrich, P., Fleckenstein, J. H., Friese, K., Friesen, J., Harpke, A., Hildebrandt, A., Jäckel, G., Kamjunke, N., Knöller, K., Kögler, S., Kolditz, O., Krieg, R., Kumar, R., Lausch, A., Liess, M., Marx, A., Merz, R., Mueller, C., Musolff, A., Norf, H., Oswald, S. E., Rebmann, C., Reinstorf, F., Rode, M., Rink, K., Rinke, K., Samaniego, L., Vieweg, M., Vogel, H.-J., Weitere, M., Werban, U., Zink, M., and Zacharias, S.: The Bode hydrological observatory: a platform for integrated, interdisciplinary hydro-ecological research within the TERENO Harz/Central German Lowland Observatory, *Environmental Earth Sciences*, 76, 29, 10.1007/s12665-016-6327-5, 2016.
- Worrall, F., Burt, T., and Shedden, R.: Long term records of riverine dissolved organic matter, *Biogeochemistry*, 64, 165-178, 10.1023/A:1024924216148, 2003.

*Supplement of***Modelling dissolved organic carbon export from a temperate headwater catchment using a complexity-reduced, mechanistic approach**

Benedikt J. Werner et al.

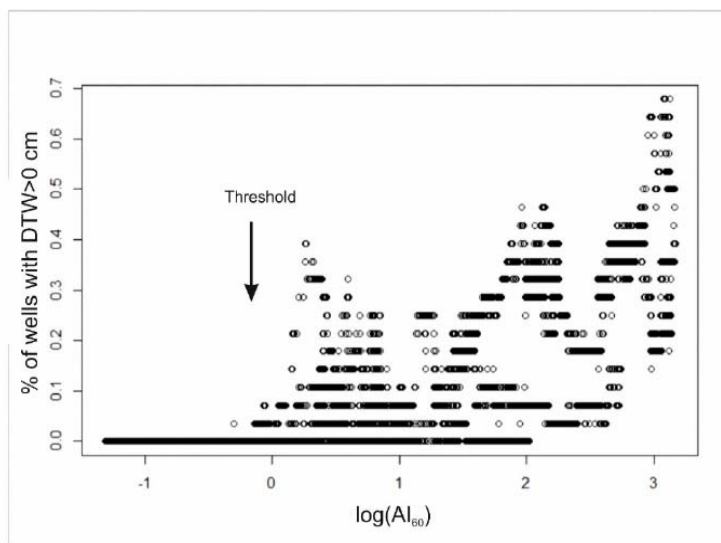


Figure S 1. X-axis: 60 day antecedent aridity index (AI_{60} ; representative of soil moisture), on the y-axis: number of wells with groundwater level at or above the surface ($DTW > 0$ cm) inducing surface runoff. At $\log(AI_{60})$ values around 0 (AI_{60} of 1 means that the sum of evapotranspiration equaled the sum of precipitation within the last 60 days), increasing numbers of wells within the study site (cf. Werner et al., 2021) start to provide surface runoff.

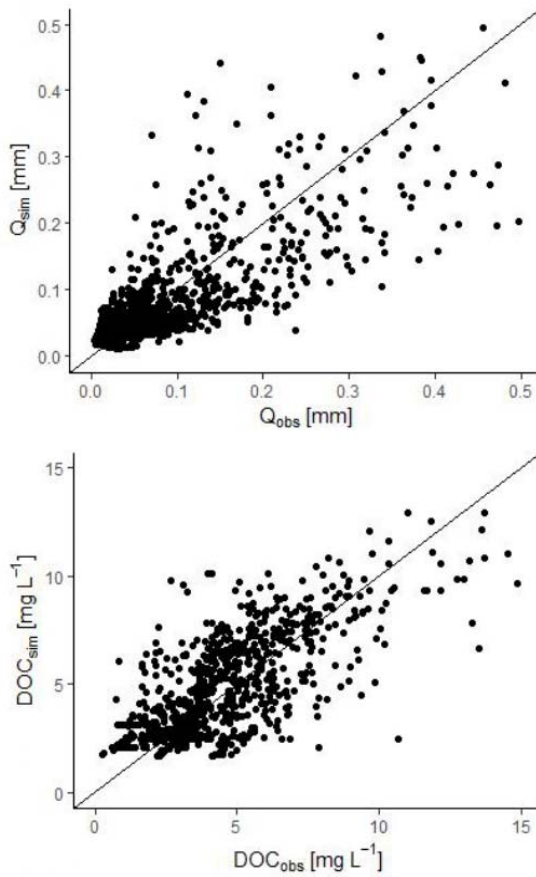


Figure S2. Relationship between observed and simulated runoff ($R^2 = 0.65$) and DOC concentration values ($R^2 = 0.57$). Black line indicates 1:1 relationship.

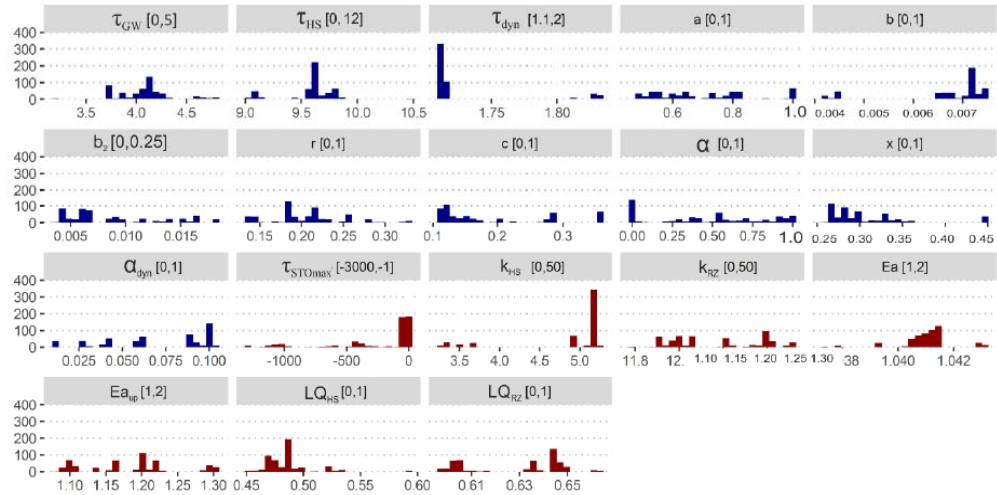


Figure S3. Histograms of the 500 best parameter sets and KGE values from the multi-objective calibration. Numbers in brackets indicate initial calibration range for every parameter. Histogram colors indicate if a parameter belongs to the hydrological (blue) or biogeochemical (red) module.

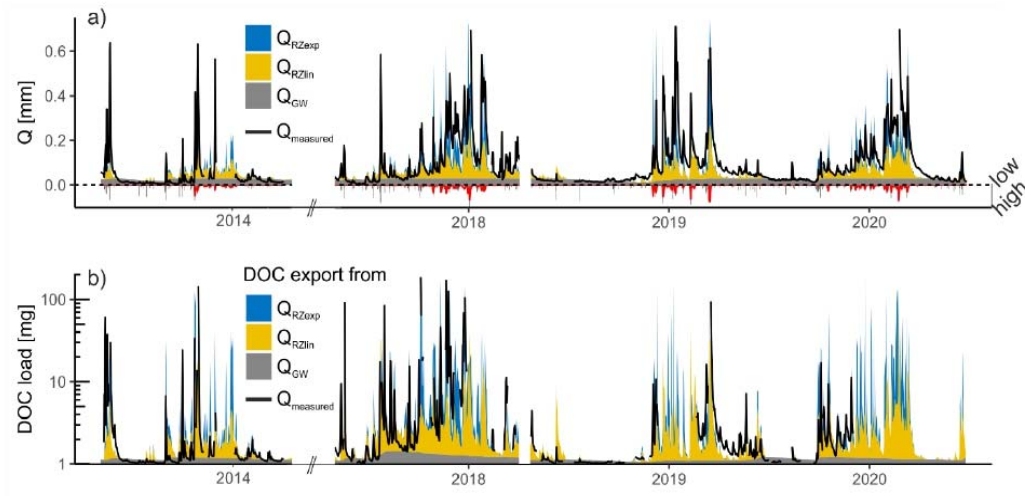


Figure S4. a) Simulated versus measured stream runoff. Colored areas indicate partitions of runoff generation from the groundwater storage (Q_{GW} ; grey) the riparian zone via exponential surface flow (Q_{RZexp} ; blue) and linear subsurface flow (Q_{RZlin} ; yellow) runoff generation. Black line indicates measured discharge of the Rappbode stream. b) Simulated versus calculated DOC export. Colored areas indicate partitions of exported DOC from the groundwater storage (Q_{GW} ; grey) the riparian zone via exponential surface flow (Q_{RZexp} ; blue) and linear subsurface flow (Q_{RZlin} ; yellow) runoff generation. Black line indicates calculated runoff of the Rappbode stream (from measured stream runoff and respective measured DOC concentrations).

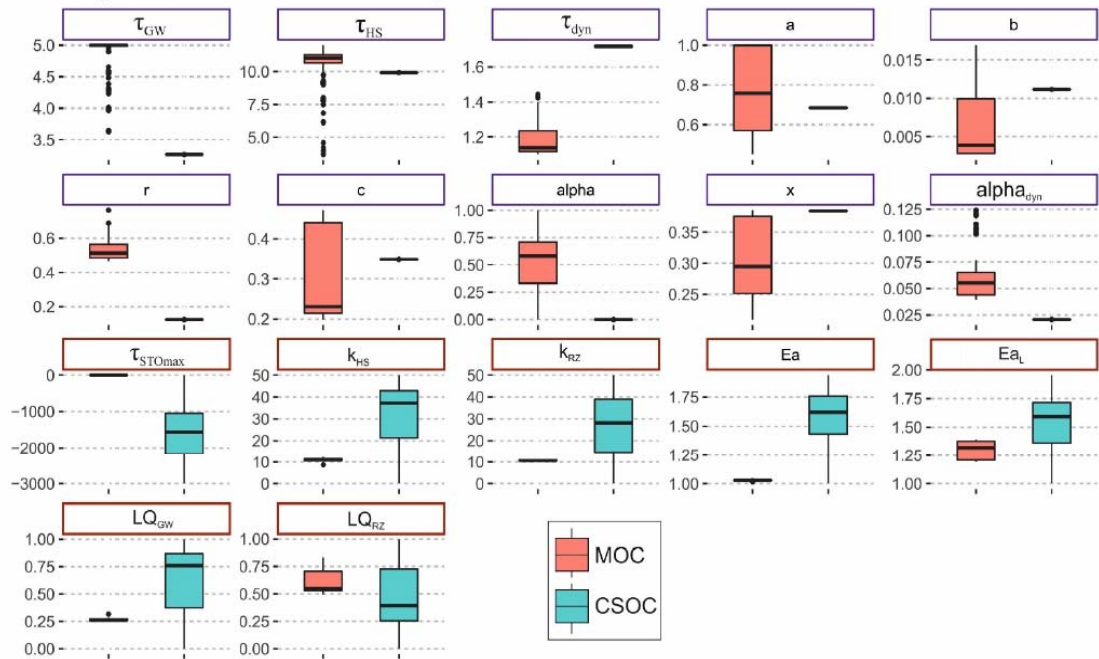


Figure S5: Comparison of the 500 best parameter sets of the TACHyB model when calibrated with the multi objective approach (MOC, red) against the consecutive single objective approach (CSOC, green). Initial calibration range for every parameter according to Table 1. Colored frames around the parameters indicates whether the parameter belongs to the hydrological (blue) or biogeochemical (red) calibration. Note that the 500 best biogeochemical parameter sets of the CSOC were based on the single best hydrological parameter set of the CSOC. Kolmogorov-Smirnov test statistics further suggest that MOC and CSOC parameter sets are not from the same distribution ($p < 0.001$ for every parameter).

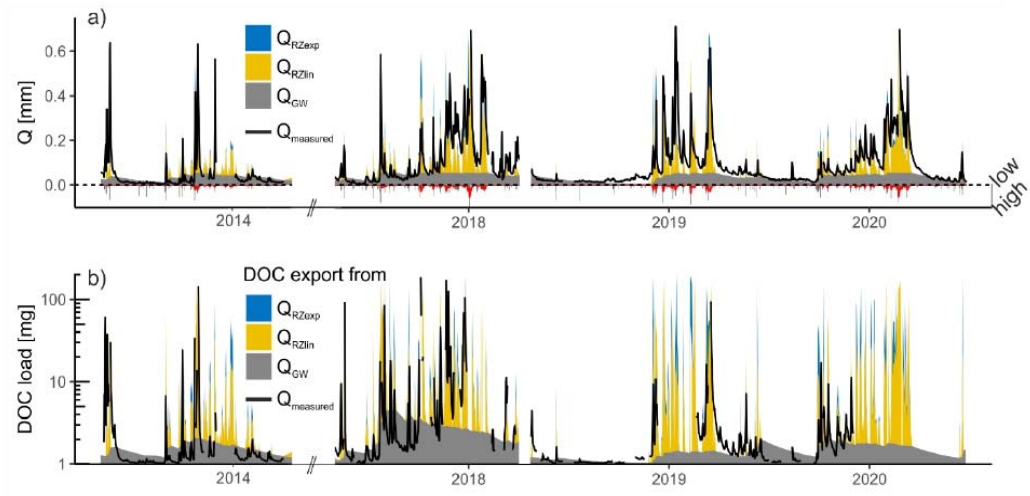


Figure S6. a) Simulated versus measured stream runoff for the consecutive single objective calibration. Colored areas indicate partitions of runoff generation from the groundwater storage (Q_{GW} ; grey) the riparian zone via exponential surface flow (Q_{RZexp} ; blue) and linear subsurface flow (Q_{RZlin} ; yellow) runoff generation. Black line indicates measured discharge of the Rappbode stream. b) Simulated versus calculated DOC export for the consecutive single objective calibration. Colored areas indicate partitions of exported DOC from the groundwater storage (Q_{GW} ; grey) the riparian zone via exponential surface flow (Q_{RZexp} ; blue) and linear subsurface flow (Q_{RZlin} ; yellow) runoff generation. Black line indicates calculated runoff of the Rappbode stream (from measured stream runoff and respective measured DOC concentrations).

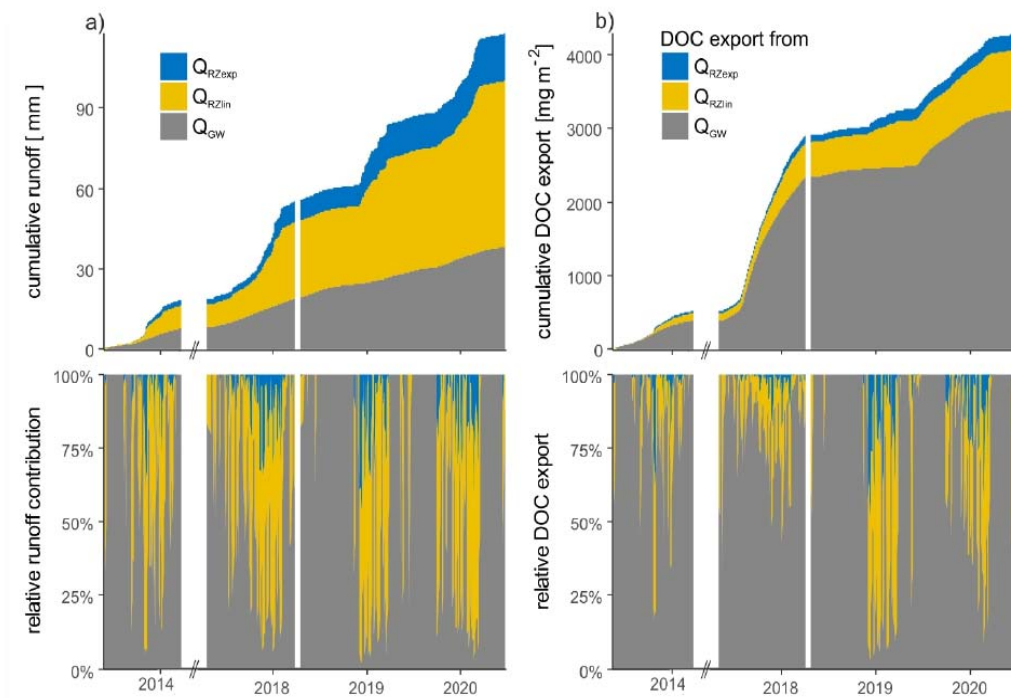


Figure S7: Comparison of CSOC modeled storage time series with actual measured groundwater samples near the outlet. Grey line indicates DOC concentration in the GW flux (Q_{GW}), yellow line indicates DOC concentration in the linear riparian flux (Q_{RZlin}) and blue line indicates DOC concentration in the exponential riparian flux (Q_{RZexp}). Red dots indicate actual measured groundwater samples at different dates.

Table S1. Comparison of mean performance of the multi-objective calibration (MOC) vs consecutive single objective calibration (CSOC) model performance for June 2013 - May 2014 & May 2017 - May 2018 calibration. Validation for May 2018 - June 2020 period. Performance metrics that differ by more than 0.2 between multiobjective and single objective calibration are printed in bold. VE: Volumetric efficiency (Eq. 5), KGE: Kling-Gupta-Efficiency of the discharge/DOC model (Eq. 4); r_p (pearson correlation) γ (variance) and β (bias) are the single components of the KGE equation (Eq. 4).

	MOC	CSOC	MOC	CSOC
	<i>calibration</i>		<i>validation</i>	
KGE _Q	0.79	0.82	0.71	0.69
r_{spear}	0.18	0.16	0.20	0.17
γ	0.10	0.08	0.18	0.24
β	0.07	0.04	0.11	0.10
KGE _{DOC}	0.73	-677.09 ^a	0.52	-896.01 ^a
r_{spear}	0.23	0.71 ^a	0.30	1.26 ^a
γ	0.14	677.97 ^a	0.10	896.89 ^a
β	0.02	12.61 ^a	0.36	14.32 ^a

^a based on the single best parameter set of the hydrological calibration.

List of peer-reviewed publications

- **Werner, B. J.**, Musolff, A., Lechtenfeld, O. J., de Rooij, G. H., Oosterwoud, M. R., and Fleckenstein, J. H.: High-frequency measurements explain quantity and quality of dissolved organic carbon mobilization in a headwater catchment, *Biogeosciences*, 16, 4497–4516, <https://doi.org/10.5194/bg-16-4497-2019>, 2019.
- **Werner, B. J.**, Lechtenfeld, O. J., Musolff, A., de Rooij, G. H., Yang, J., Gründling, R., Werban, U., and Fleckenstein, J. H.: Small-scale topography explains patterns and dynamics of dissolved organic carbon exports from the riparian zone of a temperate, forested catchment, *Hydrol. Earth Syst. Sci.*, 25, 6067–6086, <https://doi.org/10.5194/hess-25-6067-2021>, 2021.

(Eidesstattliche) Versicherungen und Erklärungen

(§ 8 Satz 2 Nr. 3 PromO Fakultät)

Hiermit versichere ich eidesstattlich, dass ich die Arbeit selbstständig verfasst und keine anderen als die von mir angegebenen Quellen und Hilfsmittel benutzt habe (vgl. Art. 64 Abs. 1 Satz 6 BayHSchG).

(§ 8 Satz 2 Nr. 3 PromO Fakultät)

Hiermit erkläre ich, dass ich die Dissertation nicht bereits zur Erlangung eines akademischen Grades eingereicht habe und dass ich nicht bereits diese oder eine gleichartige Doktorprüfung endgültig nicht bestanden habe.

(§ 8 Satz 2 Nr. 4 PromO Fakultät)

Hiermit erkläre ich, dass ich Hilfe von gewerblichen Promotionsberatern bzw. –vermittlern oder ähnlichen Dienstleistern weder bisher in Anspruch genommen habe noch künftig in Anspruch nehmen werde.

(§ 8 Satz 2 Nr. 7 PromO Fakultät)

Hiermit erkläre ich mein Einverständnis, dass die elektronische Fassung der Dissertation unter Wahrung meiner Urheberrechte und des Datenschutzes einer gesonderten Überprüfung unterzogen werden kann.

(§ 8 Satz 2 Nr. 8 PromO Fakultät)

Hiermit erkläre ich mein Einverständnis, dass bei Verdacht wissenschaftlichen Fehlverhaltens Ermittlungen durch universitätsinterne Organe der wissenschaftlichen Selbstkontrolle stattfinden können.

.....
Ort, Datum, Unterschrift

